PARTIAL OXIDATION OF α-OLEFINS OVER IRON ANTIMONY OXIDE CATALYSTS

By

Diplom-Ingenieur

Michael Schnobel

Thesis Presented for the Degree of

DOCTOR OF PHILOSOPHY

in the Department of Chemical Engineering

UNIVERSITY OF CAPE TOWN

September 1997

It is the glory of God to conceal a matter;
to search out a matter is the glory of the wise

- Proverbs 25:2

ACKNOWLEDGEMENTS

I would like to thank my supervisor Dr. Eric van Steen for his help and guidance without which this work would not have been accomplished. I would also like to thank Dr. Berry Southward for initially supervising this work as well as Professor Cyril O'Connor for making it possible to do my PhD in Cape Town.

I am grateful to the departmental staff for their invaluable help. Leslie thanks for your help with the XRD. I gratefully acknowledge the help of Mohammed Jaffer from the Electon Microscope Unit for his help with the TEM work and Katharina and Suzanna for their help with the BET surface area work. Thanks to the guys in the workshop Peter Dobias, Joachim Macke and James Daniels for building and maintaining my rig. Thanks to the guys in the electronic workshop Bill Randell and Granville de la Cruz for building the electronic appliances. Thanks goes also to Pam Linck for her help with ordering equipment and chemicals. Thanks to Craig Balfour, who was in charge of the computer network. Thanks to Klaus Moeller for his help with many equipment related things. Special thanks to Richard Walsh, Ashley Scheepers and Thomas Riedel who helped me with the experimental work.

I am grateful for the financial support from the Catalysis Research Unit, FRD and University of Cape Town. Thanks to Lorna van Bassow and Jill Stevenson for handling the administrative side.

I would also like to thank the other postgraduate students who made my stay so pleasant. A special thank you to Chamu and Stefan, my laboratory partners for their encouragement and friendship. Thanks to my friends outside the Department for keeping me sane when the research was taking its toll on me. Thanks to my digs mates for enduring me. I am also thankful to Pastor Paul Daniel and all members of the His People Christian Church for their spiritual input.

Last but not least to my parents, Johann and Stefanie, and my brothers and sisters, thank you for your love and support.

SYNOPSIS

Iron antimony oxide has been known to be an active and selective catalyst for the partial oxidation of propene to acrolein and the oxidative dehydrogenation of 1-butene to 1,3-butadiene. It has become the preferred catalyst for the industrial acrolein formation from propene.

The main purpose of this work was to investigate the influence of catalyst parameters such as calcination temperature, Sb:Fe ratio, type of pre-treatment, absence or presence of gaseous oxygen on the activity and selectivity in the partial oxidation of propene. Furthermore the influence of the reaction parameters temperature, space time, partial pressure, time on stream and the carbon chain length of the olefin have been studied in partial oxidation reactions using a fixed bed U-tube glass reactor. Various models have been tested for the rate of formation of products in the range of C_2 to C_6 α-olefins.

Increasing the calcination temperature from 500°C to 900°C resulted in an increase of the crystallite diameter and a simultaneous decrease of the surface area which might be ascribed to high temperature sintering of the catalyst. The activity decreased proportional to the decrease of surface area. At the same time the selectivity to acrolein increased with increasing calcination temperature.

Changing the Sb:Fe ratio of the catalyst revealed that highest conversions are obtained near a ratio of one, because of a maximum surface area in this region. The selectivity to acrolein was drastically enhanced with excess antimony. This can be attributed to the site isolation effect, whereby antimony inhibits the reducibility of the catalyst and therefore decreases the amount of electrophilic oxygen species on the catalyst surface which is mainly responsible for the formation of total oxidation products.

Pre-treatment of the catalyst with oxygen instead of nitrogen enhanced the initial yield to acrolein in the partial oxidation of propene showing the importance of keeping the catalyst in a high oxidation state. Comparing the partial oxidation of propene over iron antimonate

in the presence of gaseous oxygen and in the absence of gaseous oxygen showed that the activity is directly proportional to the amount of oxygen available. Time on stream experiments revealed that the selectivity to acrolein decreased strongly because of electrophilic oxygen species formed during the reoxidation of the catalyst, which increases the formation of total oxidation products. In the absence of gaseous oxygen the reoxidation of the catalyst was inhibited and the selectivity to acrolein remained somewhat constant with time on stream.

The partial oxidation of α-olefins in the range of ethene to 1-nonene have been studied over an iron antimony oxide catalyst. The temperatures studied were between 450 to 475°C for ethene and between 350 and 400°C for the other olefins. The primary reactions can be classified into five distinct classes, viz. double bond isomerisation, partial oxidation, oxidative dehydrogenation, cracking, and total oxidation. Ethene was unreactive and only total oxidation products were formed. Only propene and 1-butene formed conjugative aldehydes. The only other olefin that formed oxygenate was 1-pentene. Small amounts of 2-methyl-furan could be detected in the product stream during the selective oxidation of 1-pentene. Severe cracking was observed for olefins with a carbon number $C > 6$ at reaction temperatures $T \geq 375°C$. The rate of formation of cracking and total oxidation products was found to increase with increasing carbon number which can be explained by a shielding of the allylic hydrogen and therefore inhibiting the formation of a π-allylic intermediate which is necessary for the formation of partial oxidation and double bond isomerisation products. The rates of formation to these product groups are therefore decreasing with increasing carbon number. Changing the space time in the partial oxidation of C_2 to C_9 α-olefins revealed that cracking and total oxidation products can also be formed in a secondary reaction step from the other product groups.

The kinetics of the selective oxidation of α-olefins can be described in terms of an oxidation mechanism. It could be shown that the rate of formation of a product group can be described as:

$$r_i = \frac{a_i \cdot p_{olefin} \cdot p_{O2}^{\frac{1}{2}}}{1 + K_6 \cdot p_{olefin}}$$

The activation energies for the formation of the various product groups showed a dependency of the carbon number of the olefin. The activation energy for the formation of total oxidation and cracking products was higher than for the rest of the products.

TABLE OF CONTENTS

Page

LIST OF FIGURES

Page

TABLE OF CONTENTS

LIST OF FIGURES

Page

LIST OF TABLES

LIST OF PUBLICATIONS

Posters: "Catalytic oxidation of propene - an investigation of the kinetics over iron antimony oxide"
Environmental Catalysis, Conference of the South African Catalysis Society, Pretoria, South Africa, October, 1994.

"Partial oxidation of aliphatics over iron antimony oxide - influence of cofeeding hydrogen and water"
Conference of the South African Catalysis Society, Rustenburg, South Africa, June, 1995.

Papers: "Selective partial oxidation of α-olefins over iron antimony oxide"
in "Heterogeneous Hydrocarbon Oxidation", (Warren, B. K., and Oyama, S. T., Eds.); ACS Symposium Series 638, Washington, D. C., 1996, 276-291.

"Kinetics of selective partial oxidation of C_2-C_6 α-olefins over an iron antimony oxide catalyst"
Industrial Engineering Chemistry Research, 36(9), 1997, 3569-3575.

"Time on stream behaviour in the partial oxidation of propene over iron antimony oxide"
Applied Catalysis A: General, 165(1-2), 1997, 349-356.

NOMENCLATURE

a	kinetical constant, mmol/bar$^{1.5}$ g_{cat}
A_i	pre-exponential factor for component i, mmol/(g_{cat} · min · bar$^{-(m+n)}$)
$A_{i,ox}$	pre-exponential factor of oxidation step in the consumption of olefin i, mmol/ (g_{cat} · min · bar^{-m})
$A_{i,red}$	pre-exponential factor of reduction step in the consumption of olefin i, mmol/ (g_{cat} · min · bar^{-n})
b	kinetical constant, mmol/bar^2 g_{cat}
B	width of a diffraction line, rad
C	number of carbon atoms
d	diameter, mm
E_{ai}	activation energy to form product i, kJ/mol
$E_{ai,ox}$	activation energy of oxidation step in the consumption of olefin i, kJ/mol
$E_{ai,red}$	activation energy of reduction step in the consumption of olefin i, kJ/mol
f	response factor
F	volume flow, ml (NTP)/min
ΔH_{olefin}	enthalpy of adsorption of olefins, kJ/mol
k_i	rate constant for formation for product i, mmol/ (g_{cat} · min · bar$^{-0.5}$)
k_{ox}	rate constant of oxidation step, mmol/ (g_{cat} · min · bar^{-m})
k_{red}	rate constant of reduction step, mmol/ (g_{cat} · min · bar^{-n})
K	adsorption equilibrium constant
m	mass, g
$\dot{n}$	molar flow, mol/min
N	number of observations
OS	oxidized site
p_i	partial pressure of component i, bar
$r_{red,i}$	rate of consumption of olefin i, mmol/(g_{cat} · min)
r_i	rate of formation of product i, mmol/(g_{cat} · min)
R	universal gas constant, 8.314 J/(mol · K)

RS reduced site

S selectivity, C-%

S_i adsorption site

ΔS_{olefin} entropy of adsorption of olefins, J/(mol · K)

t time, h

T absolute temperature, K

WHSV weight hourly space velocity, 1/h

x molar fraction

X conversion, C-%

Y yield, C-%

Greek Letters

α stoichiometric number, moles oxygen required/mole olefin reacted

β X-ray diffraction broadening

β stoichiometric number

λ radiation wavelength in X-ray diffraction, Å

θ fraction of catalyst sites on catalyst surface

ρ density, kg/m^3

τ space time, s

Sub- and Superscripts

calc calcination

cryst crystallite

exp experimental

m order of reaction with respect to oxygen

meas measured

n order of reaction with respect to olefin

ox oxidation step

red reduction step

ref reference gas

List of Abbreviations

Cr	cracking
ODH	oxidative dehydrogenation
PO	partial oxidation
SSR	sum of squares of residuals
TEM	transmission electron microscopy
TO	total oxidation
TPR	temperature programmed reduction
XRD	X-ray diffraction

CHAPTER 1

INTRODUCTION

1. INTRODUCTION

Partial oxidation reactions play an important role in world-wide production of organic chemicals as illustrated in Figure 1-1. It shows that in the USA the use of selective oxidation processes is the highest with almost a third of the organic chemical production falling under selective oxidation (products of oil companies excluded (Reisch, 1992)).

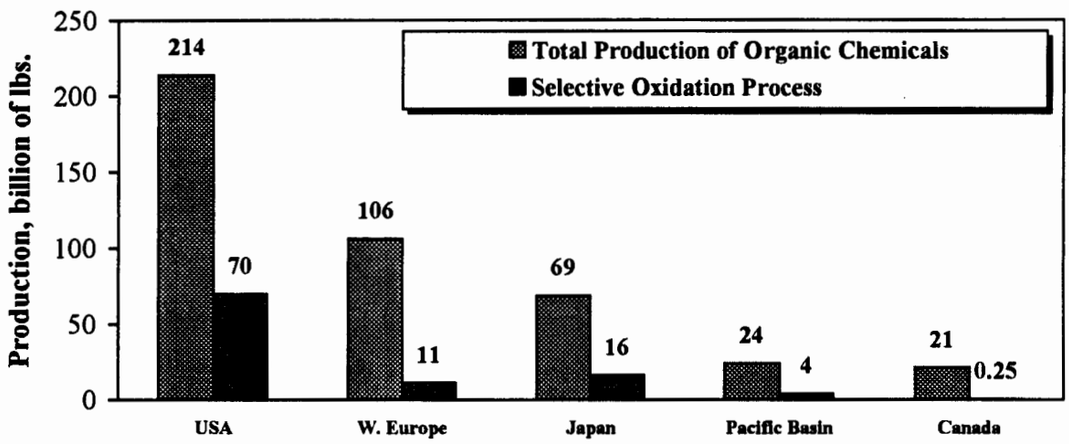

Figure 1-1 World-wide organic chemical production in 1991 (Oyama *et al.*, 1993)

Considering catalysis alone, the value of oxidation catalysts produced in the USA represents approximately 18% of sales, second only to polymerisation catalysts (Figure 1-2).

There is generally a trend in the partial oxidation of hydrocarbons to substitute olefins with paraffins as raw material because of their lower price (Cavani and Trifiró, 1992, Seshan, 1990), however, there are still countries where olefins are in greater excess available. South Africa, for example, produces large amounts of mostly α-olefins from syngas by the Fischer Tropsch process. These α-olefins are directly sold as chemicals or even converted into gasoline and diesel. The process would become more profitable if the α-olefins would be converted into higher value chemicals, e.g. aldehydes, alcoholes and ketones. Partial oxidation α-olefins is one route to produce these chemicals.

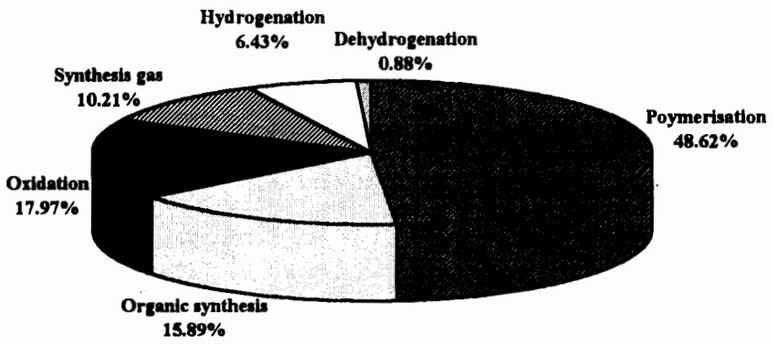

Figure 1-2 Sales of catalysts for the production of chemicals in the USA in 1991 (Weng, L.T., Delmon, B., 1992)

According to van Hooff (1979), the essence of partial oxidation reactions is a fast introduction of only a few oxygen atoms into a hydrocarbon molecule, while a further introduction should be slow. 'Fast' and 'slow' might be translated into 'low activation energy' and 'high activation energy'.
Combustion products, compared to partial oxidation products, are thermodynamically the most stable products under the usual experimental range of conditions. It is therefore of importance to intercept kinetically the valuable intermediate products.

Partial oxidation reactions have been studied extensively over bismuth molybdate and only to a lesser extend over iron antimonate catalysts. According to Allen *et al.* (1991) iron antimony oxide has become a preferred industrial catalyst.

The influence of chain length and branching of the olefins on their behaviour in the partial oxidation reaction has been studied by Adams (1965) over bismuth molybdate at 460°C. As yet, no detailed study of the influence of chain length of the olefins in the partial oxidation over iron antimony oxide catalyst has been done.

1.1 INDUSTRIAL PARTIAL OXIDATION PROCESSES

1.1.1 General overview

The most important partial oxidation process in terms of mass output is the production of ethylene oxide from ethene and oxygen. The commercial catalyst is based on silver with minor amounts of promoters and is commonly supported on alundum (α-alumina) and silicon carbide (Dever *et al.*, 1994). In 1995, the production of ethylene oxide in the United States reached $3.4 \cdot 10^6$ t/yr., which is approximately a third of the world wide production (Kirschner, 1996). The most important derivative of ethylene oxide is the manufacture of ethylene glycols for antifreeze or for polyester.

Another very important partial oxidation reaction is the production of maleic anhydride from benzene and more importantly from n-butane. The catalyst used in the benzene route is vanadium oxide supported on kieselguhr, alumina or silica. In the n-butane route vanadium-phosphorus-oxide (VPO) is used as the catalyst, sometimes with promoters added.

In 1993, the world maleic anhydride capacity was $0.86 \cdot 10^6$ t/yr., with 60% based on n-butane as feedstock. Maleic anhydride is used in the manufacture of polyester resins, surface coatings, lubricant additives, plasticisers, copolymers and agricultural chemicals (Felthouse *et al.*, 1995).

1.1.2 Production of acrolein

One of the most important industrial partial oxidation reactions which involves an α-olefin as feedstock is the production of acrolein from propene with oxygen:

$$CH_2{=}CH\text{-}CH_3 + O_2 \rightarrow CH_2{=}CH\text{-}CHO + H_2O \qquad (1\text{-}1)$$

Acrolein has been produced commercially since 1938. The first commercial processes were based on the vapour-phase condensation of acetaldehyde and formaldehyde (Schulz and Wagner, 1950). In the 1940s a series of catalyst developments based on cuprous oxide and cupric selenites led to a vapour-phase propene oxidation route to acrolein (Clark and Shutt, 1945). In 1959 Shell was the first to commercialise this propene to acrolein oxidation process. These early propene oxidation catalysts were capable of only low propene

conversions (ca. 15%) per pass and therefore required significant recycle of unreacted propene.

In 1957 Standard Oil of Ohio (Sohio) discovered bismuth molybdate catalysts capable of producing high yields of acrolein at low pressures (Callahan *et al.*, 1960).

According to Etzkorn *et al.* (1991), the most efficient catalysts are complex mixed metal oxides that consist of Bi, Mo, Fe, Ni, and/or Co, K, and either P, B, W, or Sb. Propene conversions are generally better than 93%, with typical acrolein selectivities of 80 to 90%.

The catalytic vapour-phase oxidation of propene is generally carried out in a fixed-bed multitube reactor at near atmospheric pressures and elevated temperatures (ca. 350°C); molten salt is used for temperature control. Air is commonly used as the oxygen source and steam is added to suppress the formation of flammable gas mixtures. The reaction is very exothermic. The heat of reaction of propene oxidation to acrolein is 340.8 kJ/mol. The principle side products are carbon dioxide, carbon monoxide, acrylic acid, acetaldehyde, and acetic acid.

A typical process flow diagram is given in Figure 1-3. The reactor effluent gases are cooled to condense and separate the acrolein from unreacted propene, oxygen, and other low-boiling components. Subsequent distillation refining steps separate water and acetaldehyde from the crude acrolein. In another distillation column, refined acrolein is recovered as an azeotrope with water (3 wt-%).

The major use of acrolein is in the direct oxidation to acrylic acid, which is used for the esterfication and subsequent polymerisation to emulsion and solution polymers and have applications as coatings, finishes, and binders for leathers, textiles, and paper. In the acrylic acid production, acrolein is not isolated from the intermediate production stream. The 1990 acrylic acid production demand in the United States alone accounted for more than 450 000 t/yr. (Chem. Mark. Rep., 1990a), with world-wide capacity approaching 1,470,000 t/yr. (Chem. Mark. Rep., 1990b).

More than 80% of the refined acrolein that is produced today goes into the synthesis of methionine, an important chicken feed supplement. The methionine production process involves the reaction of acrolein with methyl mercaptan. World-wide methionine production was estimated at about 170,000 t/yr. in 1990 (Chem. Mark. Rep., 1990c).

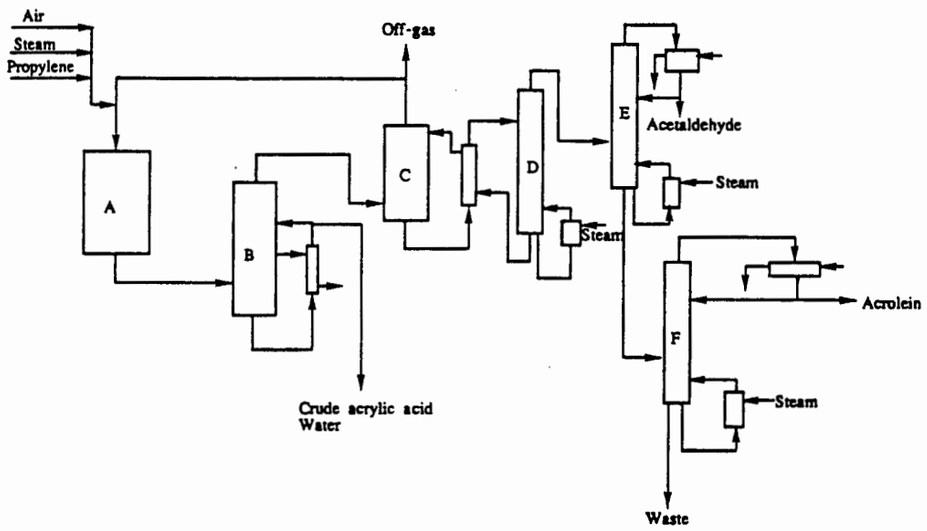

Figure 1-3 Typical process flowsheet for acrolein manufacture. A: fixed-bed or fluidised-bed reactor; B: quench cooler; C: absorber; D: stripper; E, F: fractionation stills (Etzkorn *et al.*, 1991).

1.2 THERMODYNAMICS OF HYDROCARBON OXIDATION

A thermodynamic investigation of a variety of reaction pathways of α-olefins will show which reactions are thermodynamically favoured. Table 1-1 shows the standard Gibbs energy for the formation of some products which might be formed during the partial oxidation of α-olefins at typical reaction conditions (327°C to 527°C and 1 bar).

Generally the complete combustion, or total oxidation products (reaction I and II) are thermodynamically more favourable than the formation of any other products. Double bond isomerisation reactions (reaction III) are thermodynamically the least favourable reactions. Partial oxidation reactions (reaction V) are expected to occur more likely than oxidative dehydrogenation reactions (reaction IV).

Temperature favours the formation of most of the listed reactions except for the double bond isomerisation reactions, the total oxidation of ethene to CO_2 and the partial oxidation of ethene to ethene oxide and of propene to acrylic acid.
With increasing chain length the equilibrium is shifted more towards the products.

Table 1-1 Standard Gibbs energy ΔG_R^0 for possible reactions during partial oxidation of α-olefins (using data from Stull *et al.*, 1969 and Reid *et al.*, 1987)

	Reaction	ΔG_R^0, kJ/mol		
		327°C	427°C	527°C
I	Ethene + 3 O_2 = 2 CO_2 + 2 H_2O	-1307	-1304	-1301
	Propene + 4.5 O_2 = 3 CO_2 + 3 H_2O	-1939	-1942	-1944
	1-Butene + 6 O_2 = 4 CO_2 + 4 H_2O	-2588	-2596	-2604
	1-Pentene + 7.5 O_2 = 5 CO_2 + 5 H_2O	-3236	-3250	-3263
	1-Hexene + 9 O_2 = 6 CO_2 + 6 H_2O	-3885	-3904	-3922
	1-Heptene + 10.5 O_2 = 7 CO_2 + 7 H_2O	-4534	-4558	-4582
	1-Octene + 12 O_2 = 8 CO_2 + 8 H_2O	-5182	-5213	-5242
	1-Nonene + 13.5 O_2 = 9 CO_2 + 9 H_2O	-5831	-5867	-5902
II	Ethene + 2 O_2 = 2 CO + 2 H_2O	-845	-861	-876
	Propene + 3 O_2 = 3 CO + 3 H_2O	-1248	-1277	-1305
	1-Butene + 4 O_2 = 4 CO + 4 H_2O	-1666	-1709	-1753
	1-Pentene + 5 O_2 = 5 CO + 5 H_2O	-2083	-2141	-2198
	1-Hexene + 6 O_2 = 6 CO + 6 H_2O	-2501	-2574	-2645
	1-Heptene + 7 O_2 = 7 CO + 7 H_2O	-2919	-3006	-3092
	1-Octene + 8 O_2 = 8 CO + 8 H_2O	-3338	-3439	-3539
	1-Nonene + 9 O_2 = 9 CO + 9 H_2O	-3756	-3871	-3986
III	1-Butene = cis-2-Butene	-3	-2	-1
	1-Butene = trans-2-Butene	-6	-5	-4
	1-Pentene = cis-2-Pentene	-7	-6	-6
	1-Pentene = trans-2-Pentene	-7	-7	-6
	1-Hexene = cis-2-Hexene	-11	-11	-11
	1-Hexene = trans-2-Hexene	-10	-9	-9
	1-Hexene = cis-3-Hexene	-2	-1	0
	1-Hexene = trans-3-Hexene	-7	-6	-5
IV	Propene + 0.5 O_2 = Allene + H_2O	-109	-117	-124
	1-Butene + 0.5 O_2 = 1,3-Butadiene + H_2O	-169	-175	-182
	1-Pentene + 0.5 O_2 = cis-1,3-Pentadiene +H_2O	-182	-189	-195
	1-Pentene + 0.5 O_2 = trans-1,3-Pentadiene + H_2O	-181	-187	-194
	1-Hexene + 0.5 O_2 = Cyclohexene + H_2O	-213	-214	-215
	1-Hexene + 1.5 O_2 = Benzene + H_2O	-687	-702	-716
V	Ethene + 0.5 O_2 = Ethene oxide	-56	-48	-40
	Propene + O_2 = Acrolein + H_2O	-399	-418	-439
	Propene + 1.5 O_2 = Acrylic acid + H_2O	-557	-550	-543
	1-Butene + 1.5 O_2 = Furan + 2 H_2O	-538	-541	-544

1.3 PARTIAL OXIDATION CATALYSTS

The key elements in oxidation catalyst according to Vedrine *et al.* (1997) are V or Mo but also cations of variable oxidation states as Fe^{3+}/Fe^{2+}, V^{5+}/V^{3+}, Mo^{6+}/Mo^{5+}, Cr^{6+}/Cr^{3+}, Cu^{2+}/Cu^{+}, Sb^{3+}/Sb^{5+}, etc. Some metals (mainly Ag for ethylene epoxidation), zeolites (TS-1 for phenol oxidation) and heteropolyoxometallates ($H_4PMo_{11}VO_{40}$ for isobutene oxidation to methacrolein) may also be used. In the following the iron antimony oxide is described in a more comprehensive way. However, uranium antimony oxide and bismuth molybdenum oxide shall also be briefly described due to their utmost importance in the partial oxidation of propene to acrolein.

1.3.1 Iron Antimony Oxide

1.3.1.1 Synthesis

Common synthesis methods include precipitation from slurry, solid state reaction, and impregnation. Examples for all three methods are presented.

1.3.1.1.1 Precipitation

Allen *et al.* (1991) prepared iron antimonate by heating $Fe(NO_3)_3 \cdot 9H_2O$ to 60°C, at which temperature a solution of iron nitrate in the water of crystallisation is formed. Sb_2O_3 is added and the temperature raised to 80°C and the pH of the solution is adjusted to pH 3 using aqueous ammonia. The solid is then dried overnight and calcined. Alternatively, Carbucicchio *et al.* (1985) used $FeCl_3 \cdot 6H_2O$ as the iron source and $SbCl_5$ as the antimony source. After mixing, the solution is neutralised with ammonia to pH 8.

1.3.1.1.2 Solid state reaction

Straguzzi *et al.* (1987a) mixed 2% of Sb_2O_3 to the iron antimonate precursor, followed by calcination in helium for 16h at 750°C. In comparison Fattore *et al.* (1975a) mixed $FeSbO_4$ and Sb_2O_4, which were calcined separately at 800°C for 2 hours or for a separate sample calcined the mixture at 800°C for 2 hours.

1.3.1.1.3 Impregnation

For Fe impregnation a solution of iron nitrate was formed by heating the salt. For Sb

impregnation, a solution of Sb_2O_3 in tartaric acid and distilled water was prepared and neutralised with aqueous ammonia (Straguzzi *et al.*, 1987a). The sample was dried and calcined at 50°C below the calcination temperature used for the original catalyst, at otherwise same conditions. The solutions (Fe or Sb) were then added to the iron antimonate, whereby the volume of the impregnating solution was close to the pore volume of the iron antimonate.

Yamazoe *et al.* (1981) used measured amounts of antimonic acid solution to impregnate on $FeSbO_4$ and calcined at 800°C for 2 hours.

1.3.1.2 Structure of iron antimonate

Iron antimonates have been known since the end of nineteen's century (Hussak and Prior, 1897). However, nothing has been known about their crystallography until Mason and Vitaliano (1955) investigated various antimony oxides and antimonates. They suggested the ideal formula to be $FeSbO_4$, rather than $Fe_3Sb_3O_{12}$, $Fe_2Sb_2O_7$ or $Fe_2Sb_2O_8$. The rutile structure for $FeSbO_4$ has been well established (Wells, 1975).

Most authors favour a unit cell $FeSbO_4$ as shown in Figure 1-4 with a random distribution of the cations over the oxygen octahedra and with the following unit cell diameters (JCPDS, 1990):

- $a = b = 4.6351$ Å
- $c = 3.0734$ Å
- $V = 66.03$ Å^3.

Using electon-diffraction techniques, Berry *et al.* (1987) claim that $c \approx 9.23$ Å as opposed to 3.07 Å determined by X-ray diffraction and that the extent of cationic ordering appears to be influenced by the nature of the cationic oxidation state. However, it seems that this structure is basically a trirutile structure with three unit cells on top of each other and therefore a height of the unit cell of $c \approx 3 \cdot 3.07$ Å.

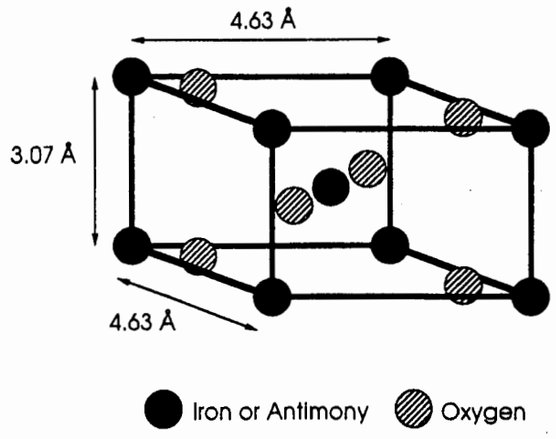

Figure 1-4 Unit cell of the rutile $FeSbO_4$ structure (Allen *et al.*, 1996)

1.3.1.3 Influence of Calcination Temperature

Intensive studies of the influence of calcination temperature have been undertaken by Carbucicchio *et al.* (1985). Iron antimonate containing Sb:Fe ratios of 1:1 (SbFe1) and 2:1 (SbFe2), synthesised according to the method described in Section 1.3.1.1.1, were investigated. Figure 1-5 shows the influence of calcination temperature, which was varied between 350 and 1000°C. Only the $FeSbO_4$ phase was detected for SbFe1, whereas the phases $FeSbO_4$ and β-Sb_2O_4 were detected for SbFe2.

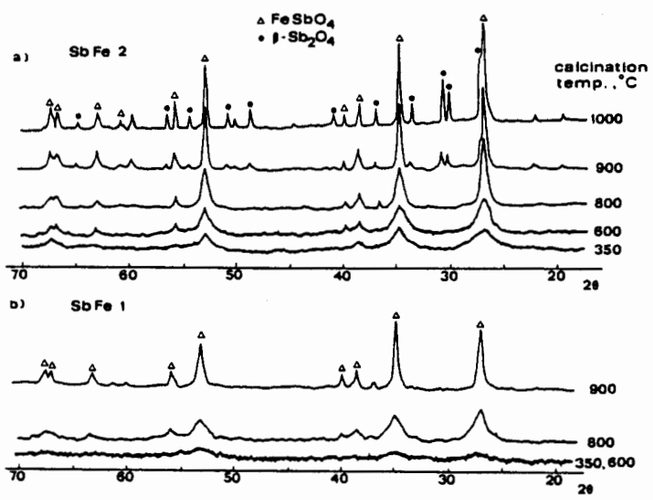

Figure 1-5 X-ray diffraction patterns of SbFe1 and SbFe2 as a function of calcination temperature (Carbucicchio *et al.*, 1985).

An increase in calcination temperature resulted in a decrease of peakwidth due to sintering of the catalyst. The most striking result was that the cell volumes of the unit cell for SbFe1 and SbFe2 were larger than the unit cell of $FeSbO_4$ for calcination temperatures of 800 and 900°C. However, SbFe2 calcined at 1000°C showed the same cell volume as the unit cell of $FeSbO_4$. The authors conclude that the excess antimony is held within the nonstoichiometic rutile structure of the catalyst for calcination temperatures up to 900°C. At a calcination temperature of 1000°C, the excess antimony is held in the β-Sb_2O_4 phase.

In contrast Teller *et al.* (1985) who investigated iron antimonate with Sb:Fe ratios between 1 and 5, which were calcined at 800 and 900°C found that the cell volumes of $FeSbO_4$ were literally identical to each other.

Burriesci *et al.* (1982) investigated the influence of calcination temperature between 300 and 900°C for iron antimonate having Sb:Fe ratios of 1 and 2, which were synthesised from Sb_2O_3 and iron nitrate. Figure 1-6 shows the detected phases as a function of calcination temperature.

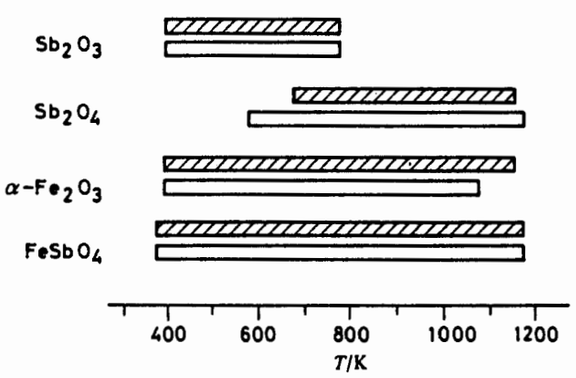

Figure 1-6 Occurrence of different phases as a function of calcination temperature for SbFe1 (dashed bars) and SbFe2 (empty bars); (Burriesci *et al.*, 1982).

There are significant differences to the findings of Carbucicchio *et al.* (1985). The main differences are the presence of Sb_2O_3 for calcination temperatures up to 500°C and of α-

Fe_2O_3 up to 850°C for SbFe2 and up to 900°C for SbFe1. Another difference is the presence of Sb_2O_4 for SbFe1. One explanation might be that the reaction during the synthesis was not complete.

1.3.1.4 Iron to Antimony Ratio

There is a general agreement that an excess of antimony is beneficiary for good catalytic oxidative activity and selectivity. However, the nature of the active site and the structure changes by the Sb-excess are not well understood. In this chapter various viewpoints from the literature are given which deal with the question why a Sb excess improves the catalytic properties of iron antimonate.

Boreskov *et al.* (1969) and Shchukin *et al.* (1970) explain an increased selectivity of the catalyst with excess antimony with the reaction of free Fe_2O_3 to $FeSbO_4$, because Fe_2O_3 is responsible for total oxidation reactions. However, this explanation is only valid for a Sb to Fe ratio up to 1.0 and cannot explain a further increase of the selectivity for iron antimonate with Sb to Fe ratios larger than 1.0, where no Fe_2O_3 is present.

Sala and Trifirò (1976) ascribe the increase selectivity in 1-butene oxidation over iron antimonates with a ratio of Sb to Fe of 2:1 to the formation of $FeSb_2O_6$, showing a trirutile structure or $FeSb_2O_7$. They suggest that the active oxidation site is tied somehow to Sb^{5+}. The role of Fe is to catalyse the reoxidation of the antimony ions, which were reduced during the interaction with the olefin, it is also responsible for the activation of gaseous oxygen, a property that is lacking in Sb_2O_5, where Sb^{5+} is present, but it is completely inactive for olefin oxidation. The authors point out that $Fe^{2+}Sb_2{}^{5+}O_6$ shows the following structure:

- Fe^{2+} - Sb^{5+} - Sb^{5+} - Fe^{2+} - Sb^{5+} - Sb^{5+} - Fe^{2+},

which presents a higher selectivity than a structure of the type

- Fe - Sb - Fe - Sb.

The IR spectra led to the interpretation of the presence of two Sb^{5+}=O groups. These double bonds, presented by two connected Sb^{5+} ions, can play an important role in the hydrogen allylic abstraction from olefins. The second Sb^{5+}=0 group makes a second

hydrogen abstraction possible, without movement of the hydrocarbon molecule on the catalyst surface.

Other workers could not confirm the presence of $FeSb_2O_6$ or $FeSb_2O_7$, however the synthesis methods were different.

Teller *et al.* (1985) used powder neutron-diffraction analysis for the investigation of iron antimonate and pointed out that in the case of excess antimony the only phases detected were $FeSbO_4$ and Sb_2O_4. Their neutron-diffraction analysis demonstrated that there is no evidence for the incorporation of an excess of Sb (or Fe) into the $FeSbO_4$ phase, the Fe/Sb ratio in $FeSbO_4$ was found to be 1, even in the presence of Sb_2O_4. This result proved that the presence of Sb_2O_4 has no effect on the bulk structure of iron antimonate. Scanning electron micrographs of iron antimonate gave evidence that larger crystals of $FeSbO_4$ are coated with smaller crystals of Sb_2O_4. Comparing the atomic positions in planes for the two phases led to the schematic diagram of a possible active catalyst as shown in Figure 1-7.

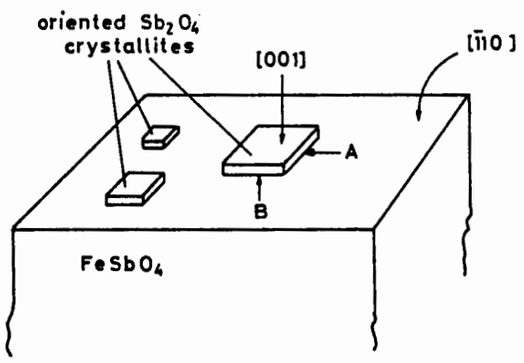

Figure 1-7 Scheme of the coating of small Sb_2O_4 crystallites on large $FeSbO_4$ crystallites and the orientation of the crystalline faces (Teller *et al.*, 1985).

The authors ascribe the high selectivities of iron antimonate to the interaction of Sb_2O_4 and $FeSbO_4$ crystallites. One function of the $FeSbO_4$ crystal may be in active-site reconstruction (catalyst reoxidation). The Fe redox couple ($Fe^{3+} + e^- \rightarrow Fe^{2+}$) would facilitate O_2

chemisorption with the $FeSbO_4$ acting as the oxidant for the reduced Sb_2O_4. Faces that contain Sb^{5+} and Sb^{3+} are the [100] and [010] faces (indicated by A and B in Figure 1-7). These crystal faces would then contain the sites of catalytic activity. Another possibility for the active sites is the coherent interface between [110] of $FeSbO_4$ and [001] of Sb_2O_4, where Sb^{5+}, Sb^{3+}, Fe^{3+} and Fe^{2+} are present which are all the necessary elements for olefin oxidation.

Fattore *et al.* (1975b) also believe that the active and selective species are formed at the grain boundary between Sb_2O_4 and $FeSbO_4$. They found an enhanced selectivity to acrolein in the partial oxidation of propene, when mixing mechanically $FeSbO_4$ with Sb_2O_4 towards an Sb:Fe ratio of 2 compared with the single phases on its own. A further increase in selectivity was observed when they calcined the mixture at 800°C for 2 hours, however the selectivity was still lower than the synthesised iron antimonate with a Sb:Fe ratio of 2. Since they obtained products from the dimerisation of allyl radicals on Sb_2O_4 and only traces of allyl radical derivatives, they postulate that the allyl radical formation takes place on Sb_2O_4. Oxygen ions seem to migrate from $FeSbO_4$ to Sb_2O_4 rather than the migration of the allyl species from Sb_2O_4 to $FeSbO_4$, because of a high probability for an organic species to be oxidised to total oxidation products on $FeSbO_4$. The ability of $FeSbO_4$ to release oxygen was supported by X-ray analysis after reduction of $FeSbO_4$, showing the decomposition of $FeSbO_4$ and formation of Sb_2O_4 and the subsequent reduction of Sb^{5+}. With the formation of Sb_2O_4 the production of hexadiene increased, proofing the ability of Sb_2O_4 to form allylic species.

Aso *et al.* (1980) made a more comprehensive study of the influence of the antimony content in iron antimonate in the catalytic oxidation of propene. The antimony content was changed between 0% (pure Fe_2O_3) and 100% (pure Sb_2O_4). In the antimony rich region the phases of $FeSbO_4$ and Sb_2O_4 were detected by X-ray diffraction analysis. The influence of the antimony content on the specific rate of formation of products and on the selectivity to acrolein is shown in Figure 1-8.

Pure Fe_2O_3 is a highly active catalyst, but catalyses exclusively total oxidation products. Pure Sb_2O_4 is able to form acrolein and 1,5-hexadiene in high selectivities, however the

activity is very low. The selectivity to acrolein increased sharply at an antimony content of 50% ($FeSbO_4$), while a maximum specific rate for the formation of acrolein is reached at an antimony content of ca. 60%. The authors proposed that acrolein and CO_2 are formed by different kinds of surface oxygen. While $FeSbO_4$ contains both types of surface oxygen, the addition of excess Sb_2O_4 forms a particular surface structure on top of the $FeSbO_4$ phase and so suppressing the deep oxidation. It is suggested that $FeSb_2O_6$ might be formed, however it could not be detected by X-ray diffraction analysis, because of a similar crystal structure with $FeSbO_4$.

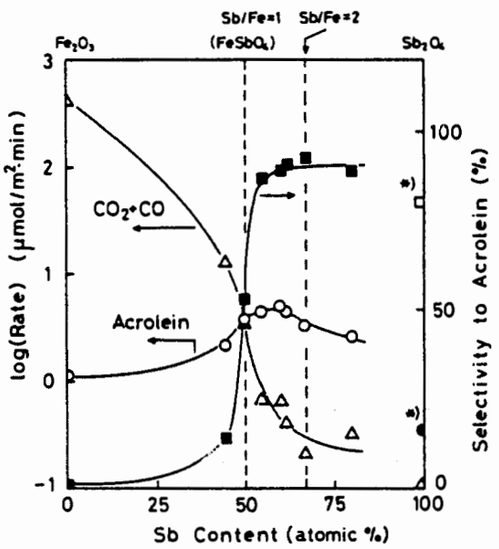

Figure 1-8 Specific rate of formation and selectivity to acrolein over iron antimonate for various antimony contents. T=400°C (500°C for Sb_2O_4), $p_{propene}$=0.05 atm, p_{O2}=0.20 atm, W/F=0.2 g·s/cm^3. *□, selectivity to acrolein (23%)+1,5hexadiene (57%); ●, rate of formation of acrolein+1,5 hexadiene (Aso *et al.*, 1980).

The same authors (Yamazoe *et al.*, 1981) continued their studies on iron antimonate, in order to obtain experimental evidence for their proposals, using TPD, XPS and SIMS. XPS studies suggested that iron antimonate with an excess of Sb consists of $FeSbO_4$ grains, which are covered with a Sb-rich layer, because of a sudden increase of the signal intensity ratios of Sb $3d_{3/2}$ to Fe $2p_{3/2}$ at a bulk ratio of Sb/Fe of 1. The thickness of the layer was estimated using depth profiling by SIMS and was found to be less than 6 Å.

By impregnating the $FeSbO_4$ grains with antimonic acid, Yamazoe *et al.* (1981) obtained catalyst with different amounts of excess surface antimony. Catalytic studies with propene oxidation revealed that the rate of formation of acrolein goes through a maximum at a surface coverage with Sb ions of 1.5, the rate of formation of CO_2 + CO decreased monotonously with increasing amount of impregnated Sb. The authors concluded using SIMS measurements combined with $^{18}O_2$ adsorption that adsorbed oxygen is preferentially bonded to Sb ions rather than to Fe ions. Two types of adsorbed oxygen were found, α and β, the former dominating in non-selective catalysts and corresponding to weakly bound oxygen. The role of the Fe ions is hypothesised to stabilise the oxidation state of $Sb^{(V)}$.

Carbucicchio *et al.* (1985) observed the presence of β-Sb_2O_4 in iron antimonate with a Sb to Fe ratio of 2 only for calcination temperatures $T \geq 900°C$. At lower calcination temperatures, but same Sb to Fe ratio, only $FeSbO_4$ was detected by X-ray diffraction analysis. At the same time the volume of a unit cell of $FeSbO_4$ decreased with increasing calcination temperature, which is contradictory to the observations of Teller *et al.* (1985), who didn't observe an influence of the calcination temperature and the Sb to Fe ratio on the volume of the unit cell of $FeSbO_4$. Carbucicchio *et al.* (1985) suggest that the excess antimony is held inside the rutile structure. Furthermore, using Mössbauer analysis, they found α-Fe_2O_3 being present in iron antimonate with a Sb to Fe ratio of 1 and suggested that even for this catalyst a non-stoichiometric (NS)-rutile structure with excess antimony is formed. However, the authors give no explanation, why the catalyst after catalytic tests didn't show the presence of α-Fe_2O_3 anymore. The antimony is probably situated in substitutional positions of $Fe^{(III)}$ and in interstitial positions. Figure 1-9 shows the deformed structure of the NS-rutile structure with excess antimony.

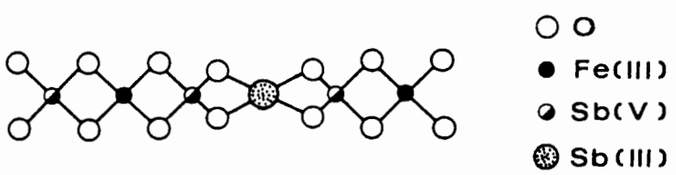

Figure 1-9 NS-rutile structure with incorporated $Sb^{(III)}$ ions (Carbucicchio *et al.*, 1985)

Infrared diffuse reflectance spectra indicated the presence of $Sb^{(V)}$=O groups on top layers of iron antimonate with a Sb to Fe ratio of 2. The fact that Sb_2O_4 was only present at calcination temperatures T≥900°C shows, that this $Sb^{(V)}$=O groups are strongly held in the NS-rutile structure.

A promoting effect by structurally distorted and defective $FeSbO_4$ is also claimed by Burriesci *et al.* (1982). However, they suggest the introduction of Fe(II) into the iron antimonate rutile structure near oxygen vacancies. Divalent iron was detected by Mössbauer spectroscopy for SbFe2, calcined at T ≥ 600°C and for SbFe1, calcined at T ≥ 800°C. The unit cell distortion was investigated using X-ray diffraction analysis. An increase in the unit cell parameters of $FeSbO_4$ was only found for those samples that showed the presence of $Fe^{(II)}$. The presence of $Fe^{(II)}$ accommodates β-oxygen, which is responsible for selective oxidation as suggested by Yamazoe *et al.* (1981).

Allen and Bowker (1995) investigated iron antimonate with a bulk Sb:Fe ratio of 1:1. X-ray diffraction data suggested the formation of $FeSbO_4$ with a rutile type structure. XPS analysis of the fresh catalyst revealed a surface ratio of Sb:Fe of 2:1. After reduction of the fresh catalyst in 1.5·10-4 Torr of ammonia at 550 K for 20 min, the XPS spectrum showed that $Sb^{(0)}$ metal was present on the catalyst surface, which was confirmed by TPD which showed antimony desorption with a peak at 690 K. The Sb:Fe ratio decreased after TPD to 1:2,6. The authors propose a structure as shown in Figure 1-10. The catalyst consists of a Sb enriched skin in the outer layers, presumably produced during the high temperature air calcination. The reason for the Sb enrichment on the surface must be that Sb oxide is of lower surface energy than either iron oxide or $FeSbO_4$.

The skin is stated to be greater than that proposed by Aso *et al.* (1980) and Teller *et al.* (1985). TPD spectra after dosing 4.5 Torr of propene, showed that large amounts of acrolein desorbing from the unreduced catalyst. However, the reduced catalyst which is rich in iron in the surface region showed a much increased yield in CO_2. The skin oxide left after reduction and Sb desorption might be Fe_2O_3, which is a low selectivity material.

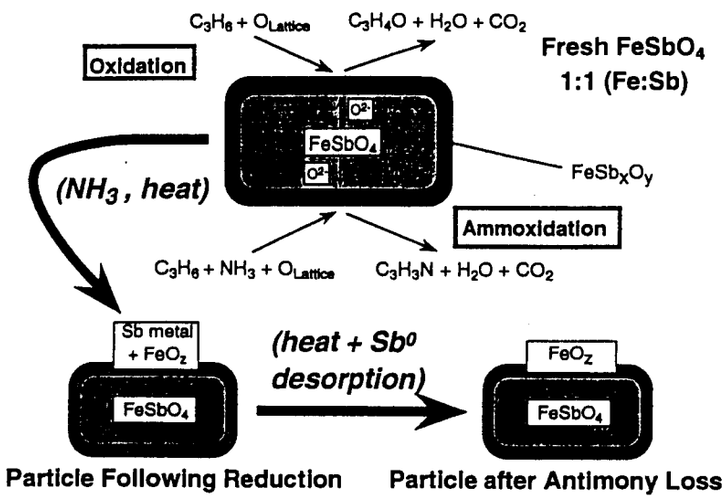

Figure 1-10 Schematic diagram of the structure of $FeSbO_4$ after different treatments (Allen *et al.*, 1996)

Bowker *et al.* (1996) who investigated iron antimonate for the propane ammoxidation stated that role if iron is primarily the Fe^{2+}/Fe^{3+} redox couple, facilitating oxygen adsorption and activation. Fe on the surface is beneficial, but too much leads to combustion. XPS studies showed a strong surface Sb enrichment of the catalyst, namely for a Sb:Fe bulk ratio of 1:1, a surface ratio of Sb:Fe = 4:1 was determined, while for a Sb:Fe bulk ratio of 2:1 a surface ratio of Sb:Fe = 8:1 was determined. Considering the Sb rich nature of the catalyst surface, they see Sb^{5+} species as the active species for selective (amm)oxidation.

1.3.2 Uranium antimony oxide

The uranium antimony oxide system has similar characteristics as the iron antimony oxide system and will be therefore briefly reviewed.

In 1966, a catalyst based on uranium antimony oxide has been brought into commercial use for the ammoxidation of propene (Callahan and Gertisser, 1965 and 1967). The synthesis method is similar to the synthesis of iron antimony oxide, with uranium nitrate replacing iron nitrate (Grasselli and Callahan, 1969). Grasselli and Callahan (1969) showed that the USb_3O_{10} phase is superior over the $USbO_5$ catalyst in terms of selectivity to acrylonitrile in the ammoxidation of propene. Grasselli and Suresh (1972) used the oxidation of propene to

acrolein as a test reaction and postulated that Sb^{5+} is the active site. The purpose of uranium is to stabilise Sb^{5+} by structural means and to provide a path via a redox reaction once Sb^{5+} has been reduced to a lower oxidation state.

Delobel *et al.* (1983) used Auger photoelectron spectra to show that the oxygen mobility through the uranium antimony oxide is low, since reoxidation only affects the surface antimony species.

1.3.3 Bismuth molybdenum oxide

Bismuth molybdate oxide catalysts are probably the most extensively studied selective oxidation catalysts and have been for many years the preferred commercial catalyst for the partial oxidation and ammoxidation of propene.

According to Keulks *et al.* (1978) Bi_2O_3 shows little activity and yields primarily total oxidation products, while MoO_3 has an even lower activity, but shows some selectivity to partial oxidation products. There are three important compounds formed from the combination of Bi_2O_3 and MoO_3: $Bi_2Mo_3O_{12}$, also called the α-phase, $Bi_2Mo_2O_9$ or β-phase, and Bi_2MoO_6 or γ-phase.

The α-phase is synthesised by a coprecipitation of molybdate trioxide dissolved in aqueous ammonia and bismuth nitrate in a 10% nitric acid solution. Bismuth nitrate solution is then added to ammonium molybdate solution under stirring (Brazdil *et al.*, 1980). In order to get the α-phase ($Bi_2Mo_3O_{12}$), the Bi:Mo ratio has to be adjusted to 2/3, whereas for the synthesis of the β-phase ($Bi_2Mo_2O_9$) and the γ-phase (Bi_2MoO_6) the same coprecipitation method as for the α-phase is used with the modification that the Bi:Mo ratios are 1 and 2, respectively. The formation of these phases have been identified by X-ray diffraction technique.

Grasselli *et al.* (1982), using pulse reduction and reoxidation studies revealed that the initial selectivity in the production of acrylonitrile in the propene ammoxidation in the absence of gaseous oxygen at 430°C decreases in the following order: $Bi_2Mo_2O_9$ (β) > $Bi_2Mo_3O_{12}$ (α) > Bi_2MoO_6 (γ). The β-phase possesses the surface structure and active-site configuration which is best suited for selective ammoxidation.

1.4 MECHANISM OF ALKENE OXIDATION

Most of the work in mechanistic studies, which are relevant to this study, has been concentrated on the partial oxidation of propene and to a much lesser extent on the oxidative dehydrogenation of 1-butene. The most common catalyst used for this studies in the literature has been bismuth-molybdate.

1.4.1 Redox (Mars-van Krevelen) mechanism

The research on the redox mechanism of metal oxide catalysts began with the concept of Lewis *et al.* (1949), who stated that the lattice oxygen of a reducible metal oxide would serve as a more useful oxidising agent for hydrocarbons than would gaseous oxygen. Mars and van Krevelen (1954) derived the rates for the reduction and reoxidation of the catalyst for the partial oxidation of aromatic hydrocarbons over vanadium oxide catalysts.

A scheme of the redox mechanism according to Mars and van Krevelen is shown in Figure 1-11.

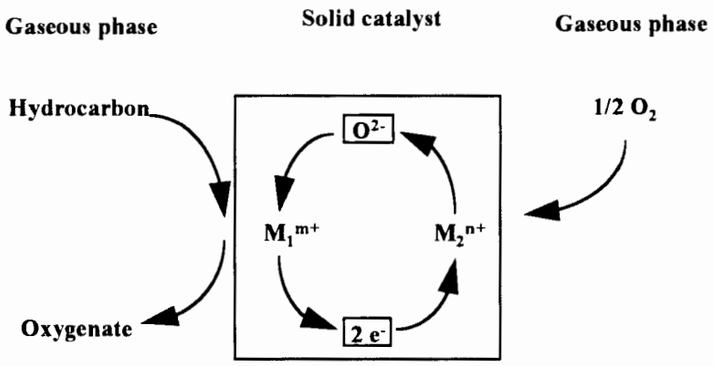

Figure 1-11 Scheme of the Mars and van Krevelen mechanism (Vedrine *et al.* 1997)

According to this mechanism the role of gaseous oxygen is to regenerate or maintain the oxidation state of the catalyst. The catalyst usually possesses two distinct active sites: an active cationic site which oxidises the hydrocarbon compound and another site active for the reduction of gaseous oxygen.

This redox concept let to the commercialisation of the oxidation and ammoxidation of

propene by the Standard Oil Company of Ohio (Sohio) (Callahan *et al.*, 1970).

1.4.1.1 Partial Oxidation of Propene to Acrolein

There is very little doubt from the literature (Grasselli and Burrington, 1981; Haber, 1985) that the first step in the partial oxidation of propene to acrolein is the abstraction of α-hydrogen in order to form a symmetric π-allylic species. This was shown by Sachtler and de Boer (1965) using labelled 1-^{14}C-prop-1-ene, 2-^{14}C-prop-1-ene, and 1-^{14}C-prop-2-ene. Acrolein formed as a result of propene oxidation over bismuth molybdate was decomposed photochemically with ultraviolet light:

$$H_2C{=}CH{-}CHO \xrightarrow{h\upsilon} H_2C{=}CH_2 + CO \qquad (1\text{-}2)$$

and the radioactivity of the products was determined. When feeding $^{14}CH_2{=}CH{-}CH_3$ and $CH_2{=}CH{-}^{14}CH_3$ the radioactivity was evenly distributed between $H_2C{=}CH_2$ and CO, whereas after oxidation of $CH_2{=}^{14}CH{-}CH_3$, radioactivity was only found in the unreacted propene and in $H_2C{=}CH_2$. This shows that dissociative chemisorption takes place in the first step, resulting in the formation of symmetric allyl species, with both terminal carbon atoms having an equal chance of forming a C=O bond. Confirmation of this mechanism was obtained by the work of Adams and Jennings (1964) using propene labelled with deuterium in various positions.

The reaction path of propene to acrolein can be summarised as follows (Bettahar *et al.*, 1996):

$$CH_2{=}CH_2{-}CH_3 \rightarrow \underset{\pi\text{-allyl}}{CH_2{\cdots}CH{\cdots}CH_2} \rightarrow \underset{\sigma\text{-allyl}}{CH_2{=}CH{-}CH_2{-}O} \rightarrow$$

$$\rightarrow CH_2{=}CH{-}CH{=}O$$

Burrington *et al.* (1984) investigated the reversibility of the insertion reaction (i.e. the $\pi \Leftrightarrow \sigma$ transformation) over molybdate and antimonate catalysts. Using deuterated 1,1-d_2-propene, it could be shown that although 1,1-d_2 and 3,3-d_2 allyl alcohol molecules were formed in a ratio of 1:1, the ratio of 3,3-d_2 acrolein to 1-d_1 acrolein was 1.63 over the molybdate catalyst, which reflects the value of the isotopic effect k_H/k_D = 1.5-2.5, because

the abstraction of H being easier than the abstraction of D. When using an antimonate catalyst the ratio of 3,3-d_2 acrolein to 1-d_1 acrolein was almost 1 (0.96), which reflects the value for the initially formed distribution of 1,1-d_2 and 3,3-d_2 allyl alcohol molecules, since the insertion of oxygen on either side of the π-allyl is equally likely. These results suggest the reversible O insertion for the molybdate catalysts, but an irreversible insertion for the antimonate catalysts.

Another difference between the mechanism of the partial oxidation of propene to acrolein over bismuth molybdate from antimony based catalysts is the sequence of the second hydrogen abstraction and the oxygen insertion step. Adams and Jennings (1963, 1964) showed by using deuterated propene that the second hydrogen abstraction takes place prior to the oxygen insertion step over bismuth molybdate. It was shown by Keulks and Lo (1986) that over iron antimony oxide the addition of oxygen takes place prior to the second hydrogen abstraction. This observation is consistent with results reported by Keulks *et al.* (1983) for uranium antimony oxide catalysts, by Portefaix *et al.* (1980) for tin-antimony oxide catalysts, and by Burrington *et al.* (1984) for iron antimony oxide catalysts.

1.4.1.2 Oxidation of 1-Butene

1-Butene, like propene, contains hydrogen atoms in the α-position with respect to the double bond. However, in the case of 1-butene it is a secondary hydrogen, which is more reactive than a primary hydrogen, as in the case of propene (Adams, 1965). 1-Butene is therefore readily transformed by hydrogen abstraction into an allylic compound.

As Bielanski and Haber (1991) pointed out, compared to propene, this allylic compound may react with oxygen along several different reaction pathways. In the presence of acid centres, which are present on many oxide surfaces, isomerisation of 1-butene to 2-butene takes place. The α-hydrogen of 2-butene can also be abstracted at basic centres of the oxide surface to form an allylic species. Adams (1965) showed that the reactivity per allylic hydrogen atom is similar for propene and for trans- and cis-2-butene. The allyl species have several possibilities of further transformation. The simplest is the repetition of the hydrogen abstraction from the α-position, but now with respect to the allylic bond, i.e. at the C-4 atom. The resulting 1,3-butadiene may desorb or react further.

The allyl species may also undergo a nucleophilic attack by lattice oxygen ions. Depending

on the properties of the catalyst, the nucleophilic addition of the O^{2-} ion may take place either at the C-3 position to form methyl vinyl ketone, or at the C-1 position, leading to the formation of 2-butenal (crotonaldehyde).

When electrophilic oxygen species are simultaneously present at the catalyst surface, they may react with butadiene to form furan, which reacts further to form maleic anhydride. When only electrophilic oxygen species are present at the catalyst surface, an electrophilic attack on the double bond of 2-butene may take place, resulting in the oxygenolysis of this bond and formation of acetaldehyde or acetic acid. The possible reaction pathways are shown in Figure 1-12. In the presence of electrophilic oxygen all compounds can combust to CO, CO_2 and H_2O. The steps leading to combustion products were omitted from Figure 1-12 in order to avoid unnecessary complication of the reaction network.

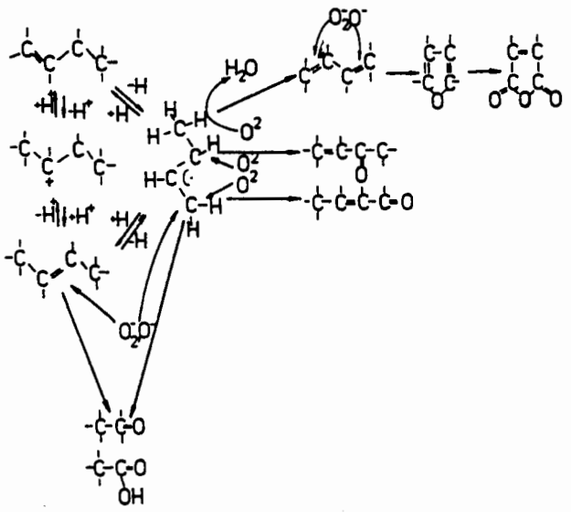

Figure 1-12 Reaction network of 1-butene at oxide surfaces (Bielanski and Haber, 1991).

In the following sections the oxidative dehydrogenation of 1-butene to butadiene and the allylic oxidation of 1-butene are investigated in more detail.

Oxidative dehydrogenation of 1-butene to butadiene

The selectivity to butadiene for the oxidative dehydrogenation of 1-butene over iron antimonate at 400°C ranged between 84% (Straguzzi *et al.*, 1987b) for iron antimonate and

86% (Sala and Trifirò, 1976) for iron antimony oxide containing a ratio Sb:Fe of 4:1. The conversion ranged between 44% and 48 %, respectively. Batist *et al.* (1966) proposed that the reaction of 1-butene over bismuth molybdate starts by abstraction of the α-hydrogen and formation of a π-allyl complex:

$$C_4H_8 + O^{2-} \rightarrow C_4H_7^- + OH^- \quad (1\text{-}3)$$

After further abstraction of a hydrogen, butadiene desorbs, whereas the remaining two OH^- groups on the catalyst surface recombine and desorb as water:

$$C_4H_7^- + O^{2-} + Mo^{6+} \rightarrow Mo^{4+} + OH^- + C_4H_6 \quad (1\text{-}4)$$

$$2OH^- \longleftrightarrow O^{2-} + \square + H_2O \quad (1\text{-}5)$$

where □ denotes an anion vacancy. The catalyst vacancies then become filled by gaseous oxygen and the reduced Mo ions are simultaneously reoxidised. According to Straguzzi *et al.* (1987b), when using the iron antimonate system, the ions Sb^{5+}/Sb^{3+} would replace the Mo^{6+}/Mo^{4+} ions from the previous equations.

The reaction in Equation 1-3 simultaneously provides a pathway for isomerisation, although the latter may also proceed by the carbonium ion mechanism if Brönsted acid sites are present at the catalyst surface (Alkhazov *et al.*, 1971).

Allylic oxidation of 1-butene

None of the reviewed papers about the oxidation of 1-butene over iron antimonate or bismuth molybdate reported the formation of partial oxidation products.

Haber (1982) investigated the partial oxidation of 1-butene over $Cu_2Mo_3O_{10}$ and $Cu_6Mo_4O_{10}$ catalysts at 370°C. In the case of $Cu_2Mo_3O_{10}$ the main products were cis- and trans-2-butene, with trans-2-butene having a slightly higher selectivity. The formation of butadiene indicated that allyl species appeared as intermediates. In the case of $Cu_6Mo_4O_{10}$ the main product was 2-butenal with a selectivity of 70 %, butadiene was only formed in trace amounts and isomerisation products were totally absent. The reason for this

behaviour might be that as different redox and phase equilibria may be established at the surface, different active centres may be generated which can selectively direct the transformation of butene molecules either to oxidative dehydrogenation or to partial oxidation.

1.4.1.3 Complete Combustion

The complete combustion or total oxidation products CO, CO_2 and H_2O are unwanted side products and their formation must therefore be kept at a minimum. In order to do so, it is of utmost importance to understand how and where on the catalyst surface complete combustion takes place.

The work of Saleh-Alhamed (1996) showed by cofeeding water to propene and oxygen, that there must be active sites for total oxidation reactions on the Sb/Sn/V oxide surface, which can be blocked by water and by doing so increase the selectivity to partial oxidation products.

In the oxidation of propene, carbon dioxide can be formed by a parallel reaction (direct oxidation of propene) or by a consecutive reaction (further oxidation of acrolein).
Keulks and Lo (1986) investigated the partial oxidation of propene over iron antimonate (atomic ratio Sb/Fe = 4). Propene labelled selectively with D or ^{13}C in a variety of positions and oxygen-18 were used as tracers to probe the mechanistic details of the reaction. They suggested that carbon dioxide is exclusively formed from acrolein because of similar apparent activation energies for the formation of each compound, similar reaction orders with respect to propene partial pressure, similar isotopic effects and a similar amount of oxygen layers participating in the formation of each compound as determined by the use of ^{18}O.
In contrast Davidov *et al.* (1978) who investigated surface complexes of propene and their role in catalytic oxidation over various oxide catalysts favours a parallel reaction for the formation of acrolein and CO_2. Using infrared spectroscopy and thermodesorption studies, they suggest the mechanism shown in Figure 1-13.
According to their scheme, acrolein is formed via π-allyl and σ-allyl complexes, while CO_2 is formed via π-complexes, carboxylates, carbonates and formates. The latter route may

occur either by a stepwise mechanism involving catalyst oxygen or by a concerted mechanism with the participation of molecular oxygen.

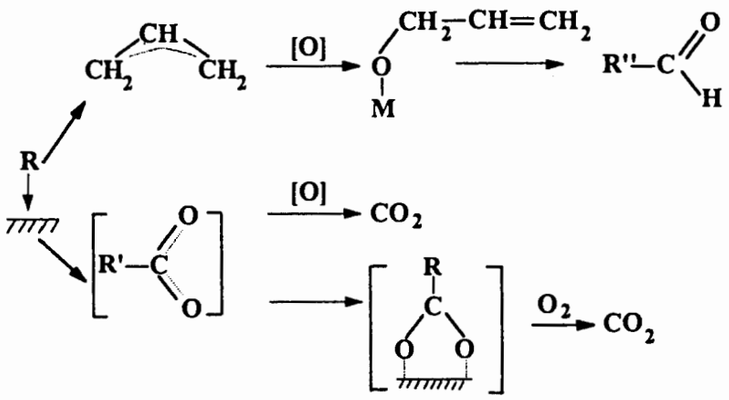

Figure 1-13 Scheme for the reaction mechanism of propene oxidation over oxide catalysts ([O]= catalyst lattice oxygen) (Davidov *et al.*, 1978)

The third option which is the formation of carbon dioxide through parallel and consecutive pathways is favoured by Keulks *et al.* (1983) who studied the catalytic oxidation of propene over USb_3O_{10}. The oxidation of 2,3,3,3-d_4-propene yielded an isotopic effect for the formation of acrolein, whereas for the formation of carbon dioxide only a partial isotopic effect was observed. This was interpreted by assuming that in the consecutive pathway the carbon dioxide is produced by the consecutive oxidation of acrolein, in which a full isotopic effect is observed, while in the parallel pathway the carbon dioxide is produced by oxygen attack at the double bond of propene. Since no C-H bond is involved in this process, no isotope effect is observed. Therefore a partial isotope effect suggests that both pathways are involved in the formation of carbon dioxide.

Adams *et al.* (1964) suggested as well a combination of parallel and consecutive reactions for the formation of CO_2 from propene over bismuth molybdate, because in the conversion-selectivity plot the selectivity to acrolein did not extrapolate to 100% at zero conversion, but to 90 %.

1.4.2 Oxygen species on oxide catalysts

From the mechanistic studies of partial oxidation reactions it is clear that both gaseous and lattice oxygen play a vital role for the functioning of the metal oxide catalyst. In this chapter the role of both kinds of oxygen will be investigated. While lattice oxygen can be associated with nucleophilic oxygen species, the gaseous of adsorbed species are associated with electrophilic oxygen species (Bilanski and Haber, 1991).

1.4.2.1 Role of lattice oxygen in the oxidation of hydrocarbons

One of the most interesting features in catalytic selective oxidation is the participation of lattice oxygen. Mars and van Krevelen (1954) were the first to propose a redox mechanism for the oxidation of aromatics over V_2O_5. This mechanism introduced the concept that lattice oxygen of a reducible metal oxide could serve as an useful oxidising agent for hydrocarbons. Since then there have been many reports which support the redox concept.

Reduction with propene

The role of lattice oxygen is best studied by simply operating the catalyst in an reduction atmosphere with the exclusion of any gaseous oxygen. Aso *et al.* (1980) investigated the reduction of Sb_2O_4 and iron antimonate with an antimony to iron ratio of 1 (SbFe1) and 2 (SbFe2) at 550°C.

In a previous study Aso *et al.* (1979) studied the reduction of Fe_2O_3 with propene at 400°C, which produced almost exclusively CO_2. In the case of Sb_2O_4, propene was converted selectively to 1,5-hexadiene and acrolein at low but nearly constant rates over the whole reduction period. X-ray diffraction analysis showed that in this case the reduction of the catalyst propagated into the bulk to form Sb_2O_3. In contrast the reduction of SbFe1 (Figure 1-14a) and SbFe2 (Figure 1-14b) is very active at its onset but declines sharply before reaching slow stationary rates, resulting in the appearance of sharp breaking points in the reduction curves.

The authors approximated that the amount of oxygen consumption up to the breaking points are roughly comparable to the surface monolayer, which contains approximately 15 μmol of oxygen atoms/m². The steady state oxygen consumption after the breaking points

apparently corresponded to the reduction into the bulk of the catalyst. X-ray diffraction analysis after reduction showed the formation of Fe_3O_4 and Sb_2O_4 from $FeSbO_4$. The breaking points are seen as the transition from surface reduction to bulk reduction. This suggests that surface oxygen is much more active than bulk oxygen.

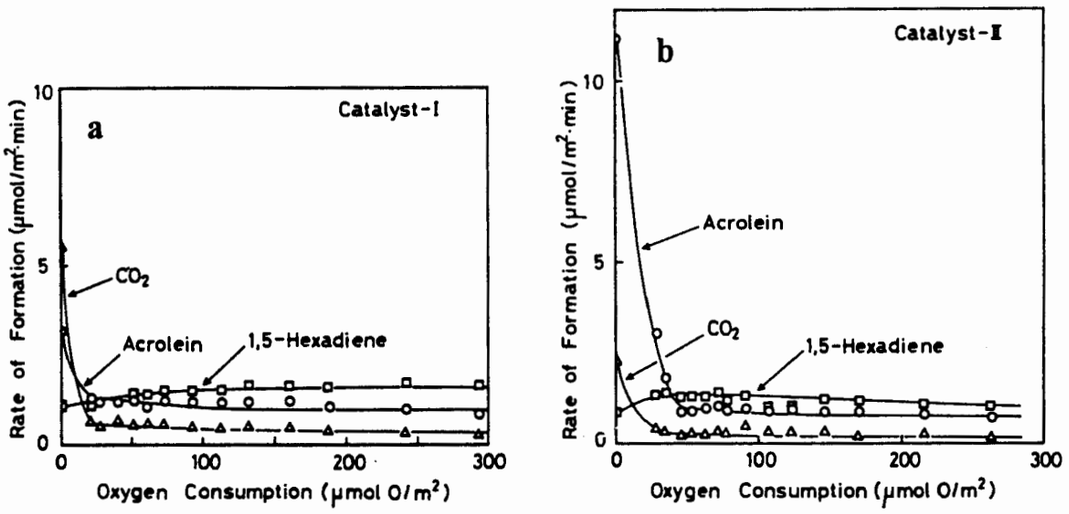

Figure 1-14 Reduction of (a) SbFe1 and (b) SbFe2 with propene. (T=550°C, $P_{propene}$ = 0.10 atm. W/F=2.0 g·s/cm³) (Aso *et al.*, 1980).

Figure 1-14 shows that during the surface reduction, like for the catalytic oxidation, the formation of CO_2 is favoured over catalyst SbFe1, whereas the formation of acrolein is favoured over SbFe2, suggesting that it is the surface oxygen that takes part in the catalytic oxidation of propene.

Fattore *et al.* (1975b) who studied the reduction of Fe_2O_3 and Sb_2O_4 with propene at 550°C as a function of reduction time confirmed the findings of Aso *et al.* (1980) that the reduction of Fe_2O_3 was greatly dependent on reduction time, while Sb_2O_4 was independent on reduction time. In addition the authors compared the oxygen consumption with the oxygen availability on the catalyst surface, which is for these oxides according to Adamiya *et al.* (1970) and Tsailingol'd *et al.* (1973) on average 9.38 μmol $(O_2)\cdot m^{-2}$.

In the case of Sb_2O_4 the oxygen consumed during the considered reaction time was less

than the oxygen available on the surface. This explains the independence of conversion from the reduction time, because no bulk oxygen from the catalyst is involved in the reaction and the oxidation may be ascribed to the surface oxygen which reacts according to a single mechanism. The authors ascribed the change of selectivities to acrolein, 1,5-hexadiene and benzene with reduction time over Fe_2O_3 and Sb_2O_4 to the different oxygen availability on the surface. A high density of oxygen atoms on the catalyst surface is present which leads to total oxidation of propene. The subsequent formation of anion vacancies and the lower probability of finding contiguous sites occupied by oxygen facilitate the oxidative dehydrogenation to an allylic intermediate. When the surface is further depleted, the probability of the interaction of two allyls increases in comparison to the probability of the oxidation of a single allyl to acrolein.

1.4.2.2 Chemical nature of lattice oxygen

The relationship between the metal-oxygen bond strength and the catalytic activity and selectivity for metal oxide catalysts has been studied by a number of workers. Sachtler and de Boer (1965) postulated that the tendency of an oxide to donate its oxygen should be of major importance in determining whether it is a selective oxidation catalyst. If reduction of the oxide is facile, i.e., if the free energy of oxygen dissociation is small, then oxygen could be donated to a hydrocarbon molecule, and the catalyst should be active but not necessarily selective. On the other hand, if it is difficult to dissociate oxygen because the metal-oxygen bond is strong, then the oxide should have low activity. In the intermediate range, oxides might be moderately active and selective.

Aso *et al.* (1979) correlated the initial rate of oxygen consumption for the reduction with propene with the heat of oxide formation per mol oxygen ($-\Delta H_f°$). The correlation indicated that the stronger the metal-oxygen bond is, the slower the rate of reduction becomes. They further correlated the reduction reaction with the catalytic oxidation, which not only confirmed the participation of lattice oxygen in the catalytic reaction, but also indicated that the cleavage of metal-oxygen bonds might be rate determining in the catalytic reaction.

Unfortunately, the absolute value of the metal-oxygen bond energy does not necessarily define the level of selectivity in the partial oxidation process. The importance of the

character of the metal-oxygen bond was investigated by Trifiró *et al.* (1968a, 1968b, 1970, 1971). A covalent metal-oxygen double bond was identified using infrared spectroscopy and was found in a great majority of the selective oxidation catalysts. However, this bond was systematically absent from total oxidation catalysts such as the oxides of iron, nickel and cobalt. It has also been reported that there is a direct interaction between adsorbed propene or acrolein and this double-bonded oxygen species. On the basis of this observations, Trifiró suggested that this type of surface lattice oxygen is directly involved in the selective oxidation of olefins.

1.4.2.3 Role of adsorbed oxygen in the oxidation of hydrocarbons

Bielanski and Haber (1991) investigated the role of oxygen in catalysis on metal oxides and pointed out that the generally accepted forms of adsorbed oxygen are besides electrically neutral molecular oxygen (O_2), also negatively charged oxygen species (O^{2-}, O^-, O_2^-). No thermodynamic data are available concerning the energy of formation of surface oxygen species.

Che and Tench (1983) provided data of the enthalpy of formation of mono- and dioxygen species in the gas phase. The only negative oxygen species stable in the gas phase with respect to O_2 is superoxide ion O_2^-, which is formed according to the following equation:

$$O_2 + e^- \rightarrow O_2^- \qquad \Delta H = -42.47 \frac{kJ}{mol} \qquad (1\text{-}6)$$

This species is a commonly adsorbed oxygen species. All other negative oxygen species, with the exception of ozonide ion O_3^- are unstable in the gas phase.
However, as Haber and Bielanski (1991) pointed out, they might be stabilised by the Madelung potential in the bulk of solid oxides or as adsorbed species. Che and Tench (1982) suggested among others the following scheme of oxygen incorporation in the oxide layer:

$$O_{2(g)} \rightarrow O_{2\,(ads)}^- \rightarrow O_{(ads)}^- \rightarrow O_{(lattice)}^{2-}$$
$$\searrow \qquad \nearrow$$
$$O_{2\,(ads)}^{2-}$$

The transformation of $O_2^-{}_{(ads)}$ into $O^-{}_{(ads)}$ is energetically more favourable than via the $O_2^{2-}{}_{(ads)}$ intermediate.

Libre *et al.* (1983) correlated the presence of a specific oxygen species with the catalytic behaviour. It was found that whenever electrophilic oxygen species O_2^- or O^- were present at the surface, total oxidation was observed in the catalytic hydrocarbon oxidation. However at the presence of the nucleophilic O^{2-} species, selective oxidation products were formed.

Bielanski and Haber (1991) distinguish between extrafacial and interfacial reactions (Figure 1-15). In the electrophilic oxidation, when O_2, O_2^- or O^- are adsorbed on the surface of the catalyst, both reactants are located at the gas phase side of the gas-solid interface and the reaction is therefore called extrafacial. The nucleophilic oxidation, on the other side, is a reaction between the adsorbed reactant and the nucleophilic oxide ion of the catalyst lattice, which is transferred across the gas-solid interface and is therefore called interfacial reaction.

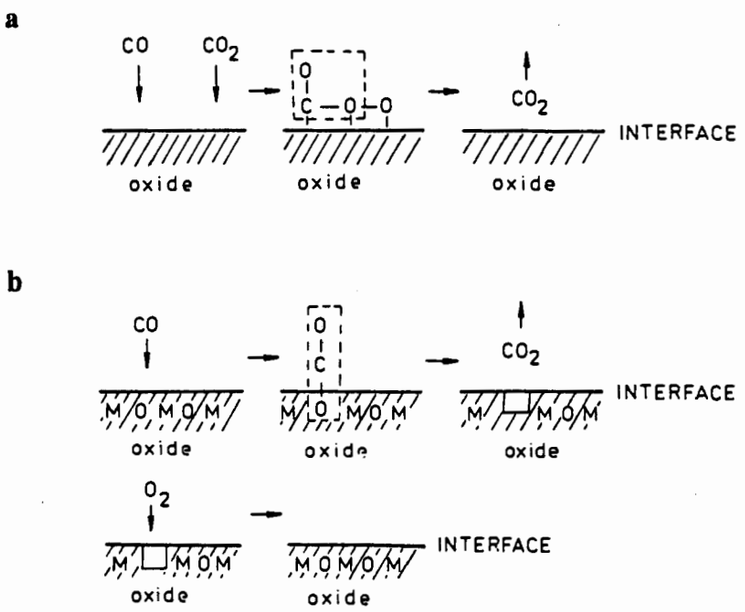

Figure 1-15 Extrafacial (a) and interfacial (b) reactions (Bielanski and Haber, 1991).

The isotopic exchange of oxygen, according to the reaction:

$$^{18}O_2 + {}^{16}O_2 \longleftrightarrow 2\,{}^{16}O^{18}O \qquad (1\text{-}7)$$

requires the activation of oxygen molecules at the surface of the catalyst; its rate may be thus taken as the measure of the ability of the catalyst surface to generate electrophilic oxygen species. In Table 1-2 the rates of isotopic oxygen exchange are given for double oxide systems, known to be selective in partial oxidation as well as their components, some of which are very active in total oxidation.

It can be seen that the very selective Bi-Mo catalysts show no activity in oxygen exchange, i.e., no adsorbed oxygen species are present on their surface. Direct adsorption measurements by Wragg *et al.* (1971) confirmed that no chemisorption of oxygen takes place at the surface of these catalysts. For the Co-Mo system it can be observed that the selective catalyst with a Co/Mo ratio of 1:1.7 shows a very slow exchange, while the much less selective catalyst with a Co/Mo ratio of 2:1 shows a higher rate of exchange and for Co_3O_4, which is a non-selective catalyst the value for the oxygen exchange is much higher. The same can be seen for the Fe-Mo and Fe-Sb systems. Bielanski and Haber therefore conclude that electrophilic oxygen attack in the catalytic oxidation of hydrocarbons result in the formation of total oxidation products.

Table 1-2 Activity of Oxides in Oxygen Isotopic Exchange (Bielanski and Haber, 1991).

Catalyst	T(°C)	Rate (g $O_2/m^2 \cdot h$)
MoO_3	580-601	9×10^{-4}
Bi/Mo = 2:1	250-500	No exchange
Bi/Mo = 1:1	474-500	No exchange
Co/Mo = 1:1.7	599-634	1.8×10^{-4}
Co/Mo = 2:1	401-462	2.9×10^{-2}
Co_3O_4	125-250	12.7
Fe/Mo = 1:1.7	511-551	7×10^{-3}
Fe/Mo = 1:1	508-552	1×10^{-3}
Fe_2O_3	350-450	4×10^{-1}
Fe/Sb = 1:2	530-598	1×10^{-5}
Fe/Sb = 1:1	548	1.7×10^{-7}
Sb_2O_5	538-600	1.7×10^{-6}

1.4.3 Acid-Base properties of oxide catalysts

The catalytic activity of transition metal oxides can also be considered in terms of their acid-base surface properties. Generally, oxides can have a basic, an amphoteric or an acidic character according to Cotton and Witkinson (1980) and Moeller (1982). Metal oxides are generally characterised as basic or amphoteric, while the oxides of non-metals (the highly electronegative elements) are characterised as acidic oxides or anhydrides. A summary of the acid -base properties of binary oxides is shown in Table 1-3.

Table 1-3 Tentative summary of the acid-base properties of binary metal oxides (Busca *et al.*, 1996)

Element	Oxidation state	Cation size (radius, Å)	M-O bond nature	Acidity type	Acidity strength	Basicity, nucleo-philicity	Examples
Semi-metal	≥ 3+	Small ≤ 0.4	Covalent	Brønsted	Medium to weak	None	B_2O_3, SiO_2, P_2O_5
Metal	High 5+ to 7+	Small to medium 0.3 to 0.7	Largely covalent	Brønsted Lewis	Medium to strong	None	WO_3, MoO_3, CrO_3, Ta_2O_5, Nb_2O_5, V_2O_5
Metal	Medium 3+ to 4+	Small 0.35 to 0.5	Ionic	Lewis	Strong	Weak	γ-Al_2O_3, β-Ga_2O_3
		Medium 0.5 to 0.6		Lewis	Medium	Medium to weak	TiO_2, Fe_2O_3, Cr_2O_3
		Large 0.7 to 1.2		Lewis	Medium to weak	Medium to strong	La_2O_3, SnO_2, ZrO_2, CeO_2, ThO_2, (Bi_2O_3, Sb_2O_3)
Metal	Low 1+ to 2+	Large to very large 0.7 to 1.5		Lewis	Medium to very weak	Strong to very strong	MgO, CaO, SrO, BaO, CoO, NiO, CuO, ZnO, (Cu_2O)

Since oxygen is one of the most electronegative elements, its bond with a metal is very ionic and gives rise to a basis nature of oxides and hydroxides. The bond of oxygen with non-metals, on the contrary is more or less covalent and gives rise to the acidic nature of anhydrides and oxo-acids. However, the actual electronegativity of an ion increases with its oxidation state (Sanderson, 1960) and therefore metal oxides in a high oxidation state are

characterised by covalent M-O bonds and behave also as anhydrides, in contrast to metal oxides in a lower oxidation state, which are typically 'basic' oxides.
For the surface of the catalyst similar considerations apply. The oxides of low oxidation state metals are highly ionic which leads to surface coordinatively unsaturated metal cations (Lewis acid sites) and oxide anions (basic sites and/or nucleophilic sites).

The oxides of high-oxidation state metals are also characterised by weak or no basicity. The association of cations with oxide ions leads to metal-oxygen double bonds, which have strong Lewis acidity. OH groups are covalently bonded to the metal and therefore give rise to medium to strong Brønsted acidity.
Busca *et al.* (1996) summarised the behaviour of transition metal oxides on the bases of results of Germain and Laugier (1972a, 1972b) and Germain and Perez (1972a, 1972b) for the oxidation of propene, toluene, benzene and ammonia. The results are shown in Table 1-4.

Table 1-4 Catalytic behaviour of binary oxides in hydrocarbon and ammonia oxidation (Busca *et al.*, 1996)

Group	Selectivity	Oxides	Cation reducibility	M-O character	Acidity type	Acidity strength	Nucleo-philicity
A	High to very high	Co_3O_4, Cr_2O_3, Fe_2O_3, MnO_2, NiO, CuO	Strong	Highly ionic	Lewis	Medium to weak	Strong to medium
B	Medium high	TiO_2, SnO_2, ZnO, ThO_2	Weak	Ionic	Lewis	Medium	Medium
C	Medium to low	V_2O_5, MoO_3, WO_3	Medium	Covalent	Brønsted + Lewis	Strong	Weak
D	Very low	Sb_2O_4, Nb_2O_5, Ta_2O5	Medium to weak	Partly covalent	Brønsted + Lewis	Strong	Weak
E	Very low	Bi_2O_3, ZrO_2	Very weak	Ionic	Lewis	Medium	Medium

Highly ionic metal oxides with highly reducible cations are generally good total oxidation catalysts, although some of them can have a selective behaviour in oxidative dehydrogenation reactions. Metal oxides applicable in selective oxidation reactions involve transition metals in a high oxidation state. Vedrine *et al.* (1996) pointed out that

hydrocarbons like alkanes and olefins can be considered as weak bases. Catalysts with strong acid cations are therefore more selective for propene partial oxidation than weak acids since the former cations result in weaker interaction with propene than the latter ions. A strong interaction of the cation with propene increases the probability of overoxidation and formation of total oxidation products.

1.4.4 Dynamics of the catalyst surface

Boreskov *et al.* (1971) postulated that for oxidation reactions which follow a redox mechanism, the oxygen coverage of a steady-state surface should depend on the oxygen-to-oxidisable substrate ratio in the feed stream as well as on the reaction temperature. Mamedov *et al.* (1979) studied the rate of diallyl and carbon dioxide production under the pulsing of a propene-oxygen mixture over Bi-Sn oxide. With increasing number of propene-oxygen pulses infected onto the catalyst, the catalyst reduction increased. At the same time the rate for the diallyl formation increased and the rate for the carbon dioxide formation decreased. The catalyst reached steady state after 75% of the surface oxygen had been removed. The steady-state surface of the Bi-Sn oxide had lost the weakly bound oxygen having a bond energy lower than 370 kJ/mol and is responsible for the total oxidation of a hydrocarbon.
Similar results have been obtained by Andrushkevich *et al.* (1977) for the oxidation of propene to acrolein over a Co-Mo oxide catalyst.

Boreskov *et al.* (1975) postulated that there is a correspondence between the steady-state extent of catalyst reduction and the mobility bulk oxygen. Catalysts with relatively immobile oxygen such as Fe-Sb and Bi-Sn oxides, display a rather high extend of surface reduction (60-70%), whereas a Fe-Mo catalyst with a high mobility of lattice oxygen, shows only a low steady-state reduction (10%). It was shown that the Fe-Mo catalyst didn't adsorb any oxygen at all in the oxidative dehydrogenation of 1-butene and the high selectivity is due to the absence of weakly bound oxygen on the surface.

1.4.4.1 Number of oxygen layers involved in oxidation reactions

Fattore et al (1975b) established the following order for oxygen mobility: Fe_2O_3 > MoBi > $FeSbO_4$ > Sb_2O_4. At 550° C they quantified the number of oxygen layers participating in

the reaction under reduction conditions as shown in Figure 1-16.

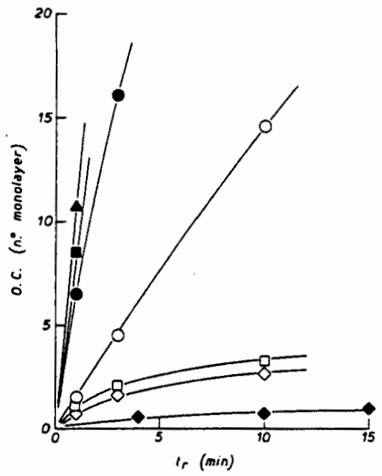

Figure 1-16 Number of oxygen layers consumed as a function of reduction time at 550° C with propene as reduction gas. (◊) FeSb1, (□) FeSb2, (O) MoBi, (●) Bi_2O_3, (■) MoO_3, (Δ) Fe_2O_3, (♦) Sb_2O_4 (Fattore *et al.* 1975b).

An increase in antimony content in iron antimonate resulted in a slight increase in the number of oxygen layers consumed.

Moro-oka *et al.* (1981) investigated the number of oxygen layers involved in the partial oxidation of propene over iron antimonate using ^{18}O tracers. The influence of Sb/Fe ration and the reaction temperature were investigated for a catalyst that was calcined at 750°C for eight hours. Assuming a surface lattice oxygen concentration of $1 \cdot 10^{19}$ oxygen atoms/m²-surface area, it was found that increase of antimony content results in an increase in oxygen layer participation: 4 for a Sb/Fe ratio of 1:1 and 6 to 7 for a Sb/Fe ratio of 4:1 at 450°C. An increase in reaction temperature from 350°C to 450°C at a constant Sb/Fe ratio of 2:1 resulted in an increase of oxygen layer participation from 3 to 5.

Compared to bismuth molybdate the oxygen layer participation in the formation of oxidation products is very low, e.g. Monnier and Keulks (1981) calculated for the oxidation of propene at 450°C over β-$Bi_2Mo_2O_9$ that 312 layers of oxygen are involved. These results show that the oxygen ions in iron antimonate are not very mobile compared

to bismuth molybdate. The mobility of oxygen ions could be increased slightly by increasing the reaction temperature and increasing the antimony content.

1.4.5 The remote control mechanism

Synergy effects between separate phases have been encountered by a number of workers, e.g. Carson *et al.* (1983) observed a synergy effect between the α and γ phases of bismuth molybdate with an enhancement in activity and selectivity for an intimate equimolar mixture.

However, it was basically the group of Delmon and co-workers (Delmon, 1979; Zhou *et al.*, 1987; Weng *et al.*, 1989; Baidikova *et al.*, 1992) who brought forward the concept of the remote control, where the mobile species, such as spillover oxygen, emitted by one phase creates or regenerates active and selective sites on another phase. They defined as the "Donor" the phase which produces oxygen species and as "Acceptor" the phase which receives the migrating species from the Donor.

Weng and Delmon (1992) see the role of mobile oxygen species as twofold: as a reactant and as an activating species for the remote control effects. The role of spillover oxygen as a reactant has been proved by the fact that ^{18}O originated from $Sb_2{}^{18}O_4$ was incorporated into oxygenated products in the oxidation of propene. The case of spillover oxygen acting as a reactant is shown in Figure 1-17.

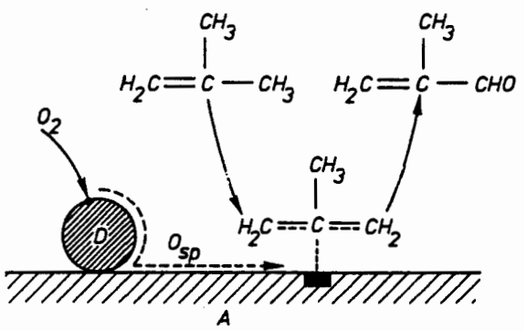

Figure 1-17 Schematic representation of spillover oxygen acting as a reactant in the oxidation of isobutene. A: Acceptor, D: Donator (Weng and Delmon, 1992).

The authors propose that the remote control effect is not only capable of the creation of new catalytic sites, but also capable of the regeneration of catalytic sites which are

deactivated during catalysis, which is shown in Figure 1-18 for the burning out of deposited coke.

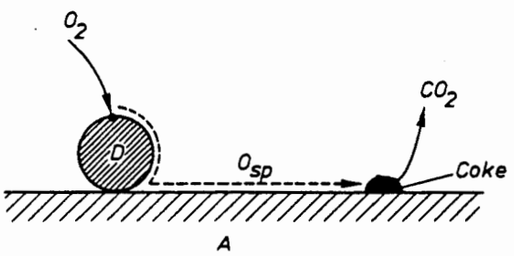

Figure 1-18 Schematic representation of spillover oxygen burning out deposited coke (Weng and Delmon, 1992).

1.5 INFLUENCE OF REACTION PARAMETERS

1.5.1 Influence of reaction temperature

All oxidation processes are strongly exothermic and the temperature of the catalyst bed usually rises downstream until high conversion into products has been attained. Towards the outlet of the reactor the reaction slows down, the heat evolution decreases and the temperature therefore decreases on approach of the outlet. Figure 1-19 shows a typical temperature profile in a fixed bed reactor.

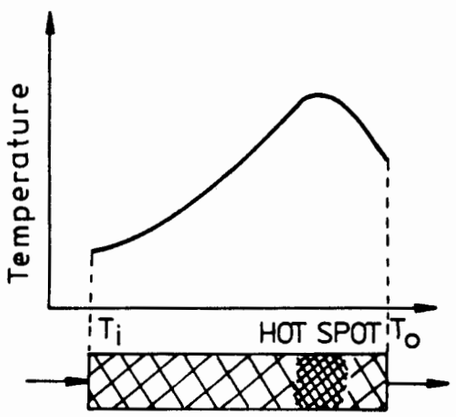

Figure 1-19 Axial temperature profile in a fixed-bed oxidation reactor (Bielanski and Haber, 1991).

The region of the high temperature is known as the hot spot. If the temperature in the hot spot rises above a certain critical value, combustion may start. The temperature might run away if the heat removal is not efficient enough. Therefore, the oxidation reaction is not only dependent on the properties of the catalyst, but also on the conditions under which the reaction is carried out: temperature, contact time, diffusional parameters, efficiency of heat transport, flow rate, etc.

There is also a possibility of secondary homogeneous reactions of the products of partial oxidation or reactions initiated by these products. This was elegantly shown by Cathala and Germain (1971), who investigated the ammoxidation of propene over bismuth molybdate catalyst at 460°C. Depending on whether the catalyst was situated near the inlet or the outlet of the reactor or whether it was mixed with a SiO_2 support, different conversions and yields to partial (amm)oxidation products were obtained, which proved the existence of secondary homogenous reactions behind the catalyst bed of the product.

1.5.2 Influence of partial pressures of the reactants

The influence of the partial pressure of the reactants on the rate of feed consumption or the rate of product formation has been studied by a number of authors who undertook kinetic studies. Tan *et al.* (1988) for example studied the kinetics of propene oxidation over bismuth molybdate catalyst. Figure 1-20 shows the influence of oxygen and propene concentration on the rate of propene consumption. Both, an increase of oxygen concentration and an increase in propene concentration leads to an increase in the rate of consumption of propene.

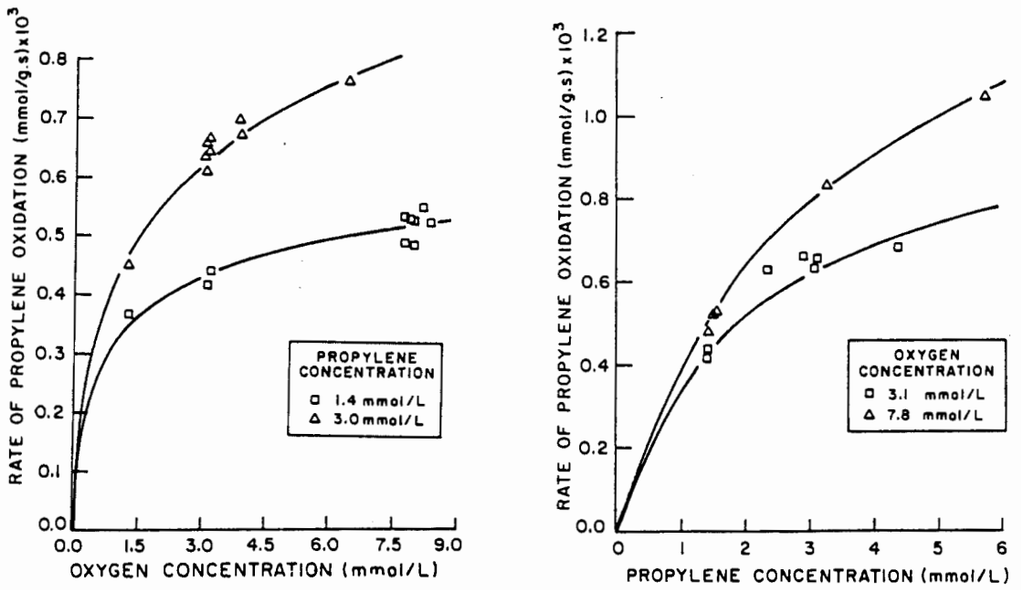

Figure 1-20 Rate of propene consumption as a function of oxygen concentration (a) and propene concentration (b) at 350°C over bismuth molybdate (Tan et al, 1988)

1.5.3 Influence of carbon number

Adams (1964) studied the influence of carbon number of several olefins on the partial oxidation over bismuth molybdate at 460°C, however he emphasised more on the different behaviour between linear and branched olefins.

Generally Adams found that a branched methyl group is necessary for aldehyde formation. The selectivity to aldehydes decreased rapidly with increasing C-number of the olefin. The main products except for propene and iso-butene were the conjugated dienes and products of total oxidation, especially in the case of higher conversions.

The relative reactivity per olefin molecule increased with increasing chain length for α-olefins in the range of C_3 to C_5. The selectivity to combustion products at constant conversion level increased with increasing chain length of the α-olefin in the range of C_4 to C_7. The author concluded that the initial reaction of these olefins seems to be very selective to conjugated dienes and hence the factors leading to faster initial reaction will result in a higher selectivity.

1.5.4 Influence of cofeeding water

Water plays an important role in the catalytic selective oxidation of hydrocarbons. It is produced during the reaction and influences its course as a reactant or/and the stability of the active phase of the catalyst or that of the active sites.

Konishi *et al.* (1982) showed that water can act as a nucleophilic reactant by increasing the hydroxyl species on the catalyst surface or it can directly act as an oxidising reactant as shown by Yokoyama *et al.* (1995) for the reaction of benzaldehyde to benzoic acid over zirconium oxide.

Saleh-Alhamed (1993, 1995, 1996) studied extensively the influence of water in the partial oxidation of propene over antimony-tin-vanadium oxide (Sb/Sn/V oxide) with 10 vol-% water concentration. Water suppressed the formation of CO/CO_2 by blocking the active sites which are responsible for CO/CO_2 formation by competitive adsorption on these sites. Experiments with $^{18}O_2$ in the presence and absence of water indicated a strong interaction between water and the catalyst surface, whereby water exchanged oxygen with the surface of the catalyst. Furthermore, water increased the activity of the catalyst. With the addition of water the reaction order with respect to oxygen for the formation of acrolein dropped from 0.62 to 0.21. A similar change was observed for other products. This indicates that water increases the catalyst activity by enhancing the rate of catalyst reoxidation.

Bettahar *et al.* (1996) suggested the scheme shown in Figure 1-21 for the chemical effect of water on the partial oxidation of propane and propene. It shows that the presence of water can be beneficial or detrimental or both to the desired products (propene, acrolein, acrylic acid). For propene as a reaction product, the presence (or addition) of water will be detrimental to its selectivity because its further oxidation to acetic acid and CO_x through the hydration step will be enhanced. This enhancement of acetic acid and CO_x will also be detrimental to the acrolein selectivity because propene is depleted. On the other hand, water addition increases the acrylic acid yield at the expense of the acrolein yield. For the acrylic acid formation, the addition of water is both beneficial and detrimental, because of an increased acrolein oxidation and increase in the competitive formation of acetic acid.

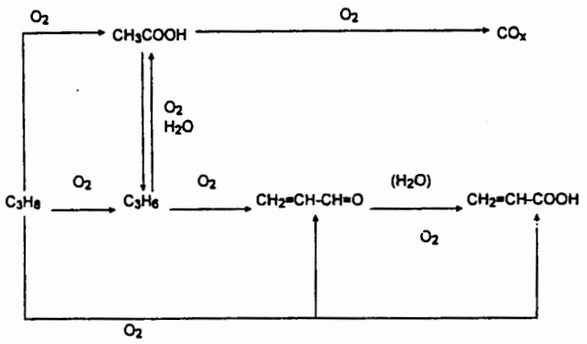

Figure 1-21 Scheme of the chemical effect of water on the partial oxidation of propane and propene (Bettahar *et al.*, 1996)

1.6 THE KINETICS OF ALKENE OXIDATION

1.6.1 Rate determining step

Keulks and Lo (1986) investigated whether the rate determining step for the conversion of propene over iron antimonate is the breakage of a C-H bond or the addition of an oxygen atom. If the rate determining step involves the breaking of a C-H bond, a primary kinetic isotope effect will be observed if the hydrogen in the C-H bond is replaced by deuterium. Two deuterated propenes were used:

- propene-1,1,2-d_3: CD_2=CD-CH_3 and
- propene-2,3,3,3-d_4: CH_2=CD-CD_3.

The rate constants for the oxidation for these deuterated propenes, k_D, were compared with those obtained for unlabeled propene, k_H. Table 1-5 shows the experimental and theoretical (in parentheses) k_H/k_D ratios for the formation of acrolein and carbon dioxide.

The kinetic isotope effect observed for the oxidation of propene-2,3,3,3-d_4 and not for propene-1,1,2-d_3 suggests that the abstraction of a hydrogen from the allylic carbon is the

rate determining step. This result was confirmed by Keulks *et al.* (1983) for the catalytic oxidation of propene over USb_3O_{10}.

Table 1-5: Oxidation of propene-1,1,2-d_3 and propene-2,3,3,3-d_4; k_H/k_D at 350, 400 and 450°C. (Keulks and Lo, 1986).

	Oxidation of propene-1,1,2-d_3		Oxidation of propene-2,3,3,3-d_4	
Temperature, °C	C_3H_4O	CO_2	C_3H_4O	CO_2
450	1.05 (1.0)	1.08 (1.0)	1.80 (1.8)	1.82 (1.8)
400	1.10 (1.0)	1.05 (1.0)	2.21 (2.0)	1.82 (2.0)
350	1.11 (1.0)	1.20 (1.0)	2.25 (2.2)	1.90 (2.2)

1.6.2 Power law model

Most kinetic studies have been performed for the partial oxidation of propene over mostly molybdate or antimonate catalysts.
Table 1-6 gives an overview on the results obtained from various investigators.

Bismuth molybdate catalysts

Krenzke and Keulks (1980b) explain the changing orders and activation energies for the formation of acrolein and CO_2 with a shift from a region where the rate of reoxidation of the catalyst controls the kinetics to a region where the rate of reduction of the catalyst controls the kinetics. In the transition region (e.g. 375°C), the observed kinetics would be a composite of both the reduction and reoxidation kinetics.

The kinetics for the reduction of Bi_2MoO_6 with propene and the subsequent reoxidation have been determined by Uda *et al.* (1980) using the microbalance technique. The reduction step was found to be first order in propene and had an activation energy of 58.6 kJ/mol and the reoxidation step had an order of 0.6 with respect to oxygen, with an activation energy of 192.6 kJ/mol.

Table 1-6 Overview of kinetic parameters obtained using the power-law model $r=k \cdot p_{propene}^{n} \cdot p_{O2}^{m}$

Catalyst	E_a (kJ/mol)		T (°C)	Acrolein formation		CO_2 formation		Reference
	acrolein	CO_2		n	m	n	m	
USb_3O_{10}	69.9 (T>425°C),	79.5 (T > 411°C),	350	0.4	0.3	0	0.8	Keulks *et al.* (1983)
	123.9(T<425°C)	144.4 (T < 411°C)	375	0.4	0.3	0.1	0.7	
			450	1	0	0.9	0.3	
Bi_2MoO_6	62.8 (T>420°C),	50.2 (T > 420°C),	350	0	0.4	0	0.4	Krenzke and Keulks
	180 (T < 420°C)	178 (T < 420°C)	375	0.2	0.4	0.2	0.4	(1980)
			450	1	0	1	0.4	
iron	82.1	81.6	350	0.5	0.4	0.4	0.6	Keulks and Lo (1986)
antimonate			375	0.5	0.3	0.6	0.7	
(Sb:Fe=4)			450	0.8	0.3	0.7	0.7	
iron	—	—	400	0.12	0.89	—	—	Aso *et al.* (1980)
antimonate								
(Sb:Fe=2)								
$FeSbO_4$	—	—	400	0.23	0.8	0.21	0.65	
(Sb:Fe=1)								

Comparison with the orders and activation energies determined by Krenzke and Keulks (1980b) show that the kinetic parameters for the reduction of Bi_2MoO_6 are very similar to those given for acrolein formation in the high temperature region; while the reoxidation kinetics are similar to the acrolein kinetics of the low temperature region. This suggests that propene oxidation is controlled primarily by catalyst reduction in the high temperature region and is reoxidation limited at lower temperatures. The only feature not accounted for, is the positive oxygen dependency for CO_2 formation in the high temperature (reduction limited) region. Krenzke and Keulks (1980a) suggested that the complete combustion region over bismuth molybdate was initiated by a charge transfer process which resulted in the activation of an oxide to an O^- ion.

Sancier *et al.* (1974) studied the kinetics of the charge transfer processes which occurred during the reduction and reoxidation of bismuth molybdate catalyst. It was found that during reoxidation, the charge transfer process exhibited an order of 0.5 with respect to oxygen. This is close to the order observed for the CO_2 formation in the high temperature region, where the redox reaction is no longer controlled by reoxidation. Krenzke and Keulks (1980b) therefore assume that the charge transfer process which occurs during reoxidation and the process which initiates carbon dioxide formation are closely related.

Antimonate catalysts

The results from Keulks *et al.* (1983) over USb_3O_{10} show that the reaction orders and the activation energies for the formation of acrolein and carbon dioxide change with temperature. The kinetic parameters are quite similar to those observed for bismuth molybdate and therefore it is suggested that propene oxidation is controlled primarily by catalyst reduction in the high temperature region and is reoxidation limited at lower temperatures. The authors attribute to fact of a much lower activation energy for the formation of acrolein at low temperatures compared to the one for the reaction over bismuth molybdate to two possibilities.

Firstly, it is possible that the lower activation energy indicates a strong inhibition by strong adsorption of acrolein at low temperatures. This is supported by the results of Godin *et al.*

(1971), Vinogradova *et al.* (1975) and Peacock *et al.* (1969), who measured the activation energy for the desorption of acrolein over various mixed metal oxide catalysts and reported values of 125 - 134 kJ/mol.

Secondly, it is possible that catalyst reoxidation is rate limiting at low temperatures. However, the difference in the activation energy can be explained by the fact, that much less catalyst oxygen layers participate in the reaction in the case of USb_3O_{10} than for bismuth molybdate.

The results for iron antimonate by Keulks and Lo (1986) and by Aso *et al.* (1980) show partial reaction orders in both reactants at all temperatures, indicating that the overall kinetics are a composite of the reoxidation and reduction kinetics.

1.6.3 Mechanistic models

Briefly, most mechanistic models for partial oxidation reactions are either based on a steady state redox mechanism (Mars-van-Krevelen) or a Langmuir Hinshelwood model.

Snyder and Hill (1989) developed kinetic models for the partial oxidation of propene to acrolein over bismuth molybdate. The first mechanism considered was a redox mechanism given in Equations 1-8 to 1-16.

Acrolein formation:

$$C_3H_6 + M \xleftrightarrow{K_1} C_3H_6\text{-}M \qquad (1\text{-}8)$$

$$C_3H_6\text{-}M + O\text{-}B \xrightarrow{k_1} C_3H_5\text{-}M + OH\text{-}B \qquad (1\text{-}9)$$

$$C_3H_5\text{-}M + O\text{-}M \xleftrightarrow{K_3} C_3H_5O\text{-}M + M \qquad (1\text{-}10)$$

$$C_3H_5O\text{-}M + OH\text{-}B \xrightarrow{k_4} C_3H_4O\text{-}M + H_2O\text{-}B \qquad (1\text{-}11)$$

$$C_3H_4O\text{-}M \xrightarrow{k_5} C_3H_4O + M \qquad (1\text{-}12)$$

$$H_2O\text{-}B \xrightarrow{k_6} H_2O + B \qquad (1\text{-}13)$$

Catalyst Reoxidation:

$$O_2 + M \xleftrightarrow{K_7} O_2\text{-}M \qquad (1\text{-}14)$$

$$O_2\text{-}M + M \xleftrightarrow{K_8} 2\ O\text{-}M \qquad (1\text{-}15)$$

$$O\text{-}M + B \xleftrightarrow{K_8} O\text{-}B + M \qquad (1\text{-}16)$$

The rate equations obtained for different rate determining steps are summarised in Equations 1-17 to 1-21.

Abstraction of an α-hydrogen:

$$\frac{d(C_3H_4O)}{dt} = \frac{k_2K_1K_9p_{C_3H_6}(K_7K_8p_{O_2})^{1/2}}{(1+K_1p_{C_3H_6}+(K_7K_8p_{O_2})^{1/2})(1+K_9(K_7K_8p_{O_2})^{1/2})} \qquad (1\text{-}17)$$

Abstraction of hydrogen from the allyl intermediate:

$$\frac{d(C_3H_4O)}{dt} = \frac{k_4K_1K_2K_3K_7K_8K_9p_{C_3H_6}p_{O_2}}{(1+(K_7K_8p_{O_2})^{1/2}+K_7p_{O_2}+K_1p_{C_3H_6})(1+K_9(K_7K_8p_{O_2})^{1/2})} \qquad (1\text{-}18)$$

Adsorption of gas-phase oxygen:

$$\frac{d(C_3H_4O)}{dt} = \frac{k_7p_{O_2}}{1+K_1p_{C_3H_6}} \qquad (1\text{-}19)$$

Dissociation of adsorbed oxygen:

$$\frac{d(C_3H_4O)}{dt} = \frac{K_7k_8p_{O_2}}{(1+K_7p_{O_2}+K_1p_{C_3H_6})^2} \qquad (1\text{-}20)$$

Transfer of oxygen from an M site to a B site:

$$\frac{d(C_3H_4O)}{dt} = \frac{0.5k_9(K_7K_8p_{O_2})^2}{1 + K_7p_{O_2} + K_1p_{C_3H_6} + (K_7K_8p_{O_2})^{1/2}} \quad (1\text{-}21)$$

In addition two hydroperoxide mechanisms have been suggested by the same authors. Mechanism I involves the direct use of gas-phase oxygen to form a hydroperoxide intermediate, while mechanism II involves adsorbed oxygen.

Hydroperoxide Mechanism I:

$$C_3H_6 + M \xleftrightarrow{K_1} C_3H_6\text{-}M \quad (1\text{-}22)$$

$$C_3H_6\text{-}M + O_2 \xrightarrow{k_2} C_2H_3CHOOH\text{-}M \quad (1\text{-}23)$$

$$C_2H_3CHOOH\text{-}M \xrightarrow{k_3} C_3H_4O\text{-}M + H_2O \quad (1\text{-}24)$$

$$C_3H_4O\text{-}M \xrightarrow{k_4} C_3H_4O + M \quad (1\text{-}25)$$

The rate equation derived from this mechanism assuming that the hydroperoxide formation from gas-phase oxygen is given in Equation 1-26.

$$\frac{d(C_3H_4O)}{dt} = \frac{k_2K_1p_{O_2}p_{C_3H_6}}{1 + K_1p_{C_3H_6}} \quad (1\text{-}26)$$

Hydroperoxide Mechanism II:

$$C_3H_6 + M \xleftrightarrow{K_1} C_3H_6\text{-}M \quad (1\text{-}27)$$

$$O_2 + M \xleftrightarrow{K_2} O_2\text{-}M \quad (1\text{-}28)$$

$$C_3H_6\text{-}M + O_2\text{-}M \xrightarrow{k_3} C_2H_3CHOOH\text{-}2M \quad (1\text{-}29)$$

$$C_2H_3CHOOH \xrightarrow{k_4} C_3H_4O\text{-}M + H_2O\text{-}M \quad (1\text{-}30)$$

$$C_3H_4O\text{-}M \xrightarrow{k_5} C_3H_4O + M \quad (1\text{-}31)$$

$$H_2O\text{-}M \xrightarrow{k_6} H_2O + M \quad (1\text{-}32)$$

Assuming that the hydroperoxide formation from adsorbed oxygen is the rate determining step, the following rate equation can be derived:

$$\frac{d(C_3H_4O)}{dt} = \frac{k_3K_1K_2p_{C_3H_6}p_{O_2}}{(1 + K_1p_{C_3H_6} + K_2p_{O_2})^2} \quad (1\text{-}33)$$

Comparison of the reaction orders for propene and oxygen from Krenzke and Keulks (1980) in Table 1-6 to the reaction orders predicted by the equations derived from the redox mechanism and the hydroperoxide mechanisms (Snyder and Hill, 1989) indicates that Equation (1-17) and (1-18) are the only equations which will predict the reaction orders observed above 400°C without making unreasonable assumptions. The possibility of either the second abstraction of hydrogen or a reoxidation step being rate limiting about 400°C can be eliminated on the basis of the results of kinetic isotope experiments by Krenzke and Keulks (1980a), where it was shown that the rate-limiting step is likely to be the abstraction of an α-hydrogen. According to Snyder and Hill (1989), the reaction orders with respect to propene and oxygen below 400°C can be most readily explained as being due to a rate-determining step involving transfer of oxygen between different functional groups within the catalyst.

Mars and van Krevelen (1954), who studied the partial oxidation of aromatic compounds over vanadium oxide catalyst modelled the rate of reduction of the hydrocarbon by assuming a steady state between the reduction and oxidation over one catalytic active site. The rate of consumption of the hydrocarbon R was derived to:

$$-r = \frac{1}{\frac{1}{k_1 p_R} + \frac{\beta}{k_2 p_{O_2}^{\ n}}}, \qquad (1\text{-}8)$$

where β is the stoichiometric number, k_1 and k_2 the rate constants for the rate of the reduction and the oxidation of the active site, respectively.

Tan *et al.* (1988) compared several models for the oxidation of propene over a silica supported bismuth molybdate catalyst over a temperature range of 350 to 390°C. The following seven models were considered for the description of the rate data:

- Model 1: a steady-state redox model with a first order oxygen concentration (n=1 in Equation 1-15),
- Model 2: a steady-state redox model based on a single site oxygen adsorption (n=0.5 in Equation 1-15),
- Model 3: a steady-state redox model with the additional assumption that the rate of oxygen desorption is not negligible.

$$-r = \frac{k_1 \cdot k_2 \cdot p_{O_2} \cdot p_R}{k_d + k_2 \cdot p_{O_2} + \beta \cdot k_1 \cdot p_R} \qquad (1\text{-}9)$$

- Model 4: a Langmuir-Hinshelwood model with the assumptions that equilibrium concentrations of oxygen and propene are established on the catalyst surface and that all sites have affinities for both oxygen and propene, whereby each adsorbed molecule occupies only one site:

$$-r = \frac{k_1 \cdot K_1 \cdot K_2 \cdot p_{O_2} \cdot p_R}{(1 + K_2 \cdot p_{O_2} + K_1 \cdot p_R)^2} \qquad (1\text{-}10)$$

- Model 5: a Langmuir-Hinshelwood model as model 4 with the modification that there are two types of sites, one with affinity for propene only and the other for oxygen only:

$$-r = \frac{k_1 \cdot K_1 \cdot K_2 \cdot p_{O_2} \cdot p_R}{(1 + K_2 \cdot p_{O_2})(1 + K_1 \cdot p_R)} \tag{1-11}$$

- Model 6: a Langmuir-Hinshelwood model as model 5 with the modification that each oxygen molecule is adsorbed on a pair of adjacent sites:

$$-r = \frac{k_1 \cdot K_1 \cdot K_2 \cdot p_{O_2}^{1/2} \cdot p_R}{(1 + K_1 \cdot p_{O_2}^{1/2})(1 + K_2 \cdot p_R)} \tag{1-12}$$

- Model 7: a steady-state redox model with the assumptions that propene is adsorbed on the catalyst surface and the adsorbed propene reacts with catalyst oxygen. Propene adsorption is assumed to follow the Langmuir-Hinshelwood adsorption equilibrium model:

$$-r = \frac{k_1 \cdot k_2 \cdot K_1 \cdot p_{O_2} \cdot p_R}{k_1 \cdot p_{O_2} + \beta \cdot k_1 \cdot K_1 \cdot p_R + k_2 \cdot K_1 \cdot p_{O_2} \cdot p_R} \tag{1-13}$$

It was found that rate data were satisfactorily described by the steady state redox model (Mars and van Krevelen model) with half-order oxygen concentration. The steady state redox model with first order oxygen concentration or with an oxygen desorption term, and the Langmuir-Hinshelwood models did not provide adequate fit. Model 7 fitted the rate data also well, however model 2 is the more adequate one because of having a lower mean square of residuals and one fewer parameter.

Adams (1965) did a comparative study of the partial oxidation of various linear and branched olefins over bismuth-molybdate catalyst. The rate of propene and butene oxidation was found to be first order with respect to oxygen and products, while the rate of reaction of higher olefins was severely inhibited be products and a positive oxygen dependency. However, the study was limited to one temperature (460°C) and therefore no activation energies were determined.

1.7 RESEARCH OBJECTIVES

Iron antimony oxide has already been investigated for the partial oxidation of propene to acrolein and the oxidative dehydrogenation of 1-butene to 1,3-butadiene. As yet, no comprehensive study of the partial oxidation of olefins over iron antimony oxide has been completed.

The aims and objectives of this study were:

(1) To synthesise and characterise iron antimony oxide containing different Sb:Fe ratios and calcined at different temperatures.

(2) To investigate the role of gaseous oxygen in the oxidation of propene over iron antimony oxide.

(3) To compare the partial oxidation of paraffins and olefins as feedstocks in the partial oxidation over iron antimonate.

(4) To investigate the influence of reaction conditions (reaction temperature, time on stream and cofeedstocks water or hydrogen) on the yields for propene partial oxidation.

(5) To investigate the influence of calcination temperature, Sb:Fe ratio, and pre-treatment of iron antimony oxide on the yields of propene partial oxidation as a function of time on stream.

(6) To investigate the influence of chain length of α-olefin feedstocks on conversion and selectivity for the partial oxidation over iron antimony oxide as a function of reaction temperature, space time and partial pressures of oxygen and olefin.

(7) To derive and test various models for the rate of consumption of olefin and for the rate of formation of products over iron antimony oxide.

CHAPTER 2

EXPERIMENTAL

2. EXPERIMENTAL

2.1 CATALYST SYNTHESIS

2.1.1 Iron Antimony Oxide

The catalysts were prepared using the method described by Allen *et al.* (1991). Briefly, iron nitrate $Fe(NO_3)_3 \cdot 9H_2O$ (Saarchem, 98%) was heated to 60°C at which temperature the iron salt dissolved in its crystal water. Subsequently, antimony trioxide Sb_2O_3 (Saarchem, 98%) was added under stirring with a glass rod to the desired iron to antimony ratio, after which aqueous ammonia (Saarchem, 25% NH_3) was added to adjust the pH to 3.0. The slurry was dried for 16 hours at 120 °C and then calcined in air at 500, 700, 800 or 900 °C for 7 hours using a high temperature furnace.

2.1.2 Iron Oxide and Antimony Oxide

Iron oxide (Fe_2O_3) was prepared using the same method as for iron antimony oxide (Section 2.1.1) with the exception that no antimony trioxide was added. Calcination in air was done at 600, 700, 800 or 900°C for 7 hours.

Antimony tetraoxide (Sb_2O_4) was prepared by calcining antimony trioxide (Sb_2O_3) in air at 600, 800 or 900°C for 7 hours.

2.1.3 Catalyst nomenclature

The catalysts synthesised and their nomenclature for the remainder of the thesis are outlined in Table 2-1.

Table 2-1 Catalysts synthesised and nomenclature

Catalyst	molar ratio Sb:Fe, mol/mol	Crystalline Phases	Nomenclature
Iron Oxide	0:1	100 mol-% Fe_2O_3	Fe_2O_3
Iron Antimony Oxide	0.25:1	60 mol-% Fe_2O_3, 40 mol-% $FeSbO_4$	SbFe025
Iron Antimony Oxide	0.5:1	33.3 mol-% Fe_2O_3, 66.7 mol-% $FeSbO_4$	SbFe05

Iron Antimony Oxide	0.75:1	14.3 mol-% Fe_2O_3, 85.7 mol-% $FeSbO_4$	SbFe075
Iron Antimony Oxide	0.9:1	5.3 mol-% Fe_2O_3, 94.7 mol-% $FeSbO_4$	SbFe09
Iron Antimony Oxide	1:1	$FeSbO_4$	SbFe1
Iron Antimony Oxide	1.1:1	4.8 mol-% Sb_2O_4, 95.2 mol-% $FeSbO_4$	SbFe11
Iron Antimony Oxide	1.25:1	11.1 mol-% Sb_2O_4, 88.9 mol-% $FeSbO_4$	SbFe125
Iron Antimony Oxide	1.5:1	20 mol-% Sb_2O_4, 80 mol-% $FeSbO_4$	SbFe15
Iron Antimony Oxide	1.75:1	27.3 mol-% Sb_2O_4, 72.7 mol-% $FeSbO_4$	SbFe175
Iron Antimony Oxide	2:1	33.3 mol-% Sb_2O_4, 66.7 mol-% $FeSbO_4$	SbFe2
Iron Antimony Oxide mixture	2:1	33.3 mol-% Sb_2O_4, 66.7 mol-% $FeSbO_4$	SbFe2mix
Antimony Oxide	1:0	100 mol-% Sb_2O_4	Sb_2O_4

2.2 CATALYST CHARACTERISATION

2.2.1 Catalyst structure

2.2.1.1 X-ray diffraction

The catalyst structures were determined by X-ray diffraction (XRD) using a Phillips X-ray diffractometer generating Cu-Kα radiation at 40 kV, 30 mA with a wavelength of 1.54 Å. Approximately 0.5 g of catalyst were placed onto the sample holder and the surface of carefully levelled out. A scan range of $20° < 2\theta < 70°$ with a step size of 0.1° and a step duration of 1s was applied. The XRD pattern were compared with values obtained from the literature (JCPDS, 1990).

2.2.1.2 Transmission electron microscopy

A JOEL 200CX transmission electron microscope was used to produce photographs of the catalyst samples. Magnifications between 50 000 and 270 000 were achieved operating at 200 kV.

Samples were prepared by ultrasonically dispersing small amounts of catalysts in methanol and allowing drops of the resulting suspension to dry on standard amorphous carbon film supported on copper specimen grids.

2.2.2 Catalyst surface area and pore volume

N_2-BET surface area measurements were determined using an Accelerated Surface Area and Porosimetry (ASAP) 2000 system obtained from Micromeritics®. Approximately 0.5 g of catalyst were placed into a glass tube. The sample was dried in situ at 120°C under vacuum. Nitrogen was used as adsorption gas at liquid nitrogen temperature applying different pressures.

2.2.3 Temperature Programmed Reduction (TPR)

2.2.3.1 Experimental Setup

Temperature programmed reaction studies were carried out in an upflow quartz glass tubular reactor (see Figure 2-1). The reactor was placed inside a furnace, which was able to heat the reactor to a maximum temperature of 1100 °C.

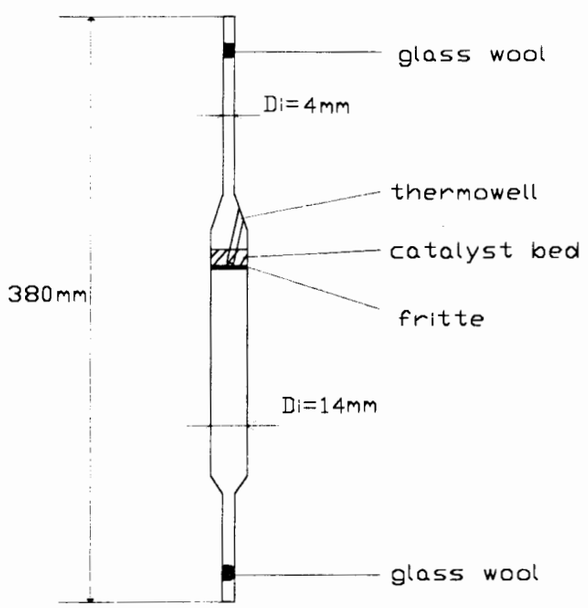

Figure 2-1 Quartz sample cell used for temperature programmed reaction studies

A flowsheet of the rig is shown in Figure 2-2. All gas flows were controlled using mass flow controllers (UNIT and Brooks). Propene was used as reduction gas. A Hewlett Packard 5971A GC-MS was used to monitor CO_2, water and the hydrocarbons in the effluent. The effluent was diluted with a constant He flow prior to its introduction in the GC-MS. The effluent line was heated to 150°C in order to prevent condensation in the line. The temperature of the catalyst bed was controlled by a thermocouple which was placed inside a thermowell in the catalyst bed in the centre of the cell.

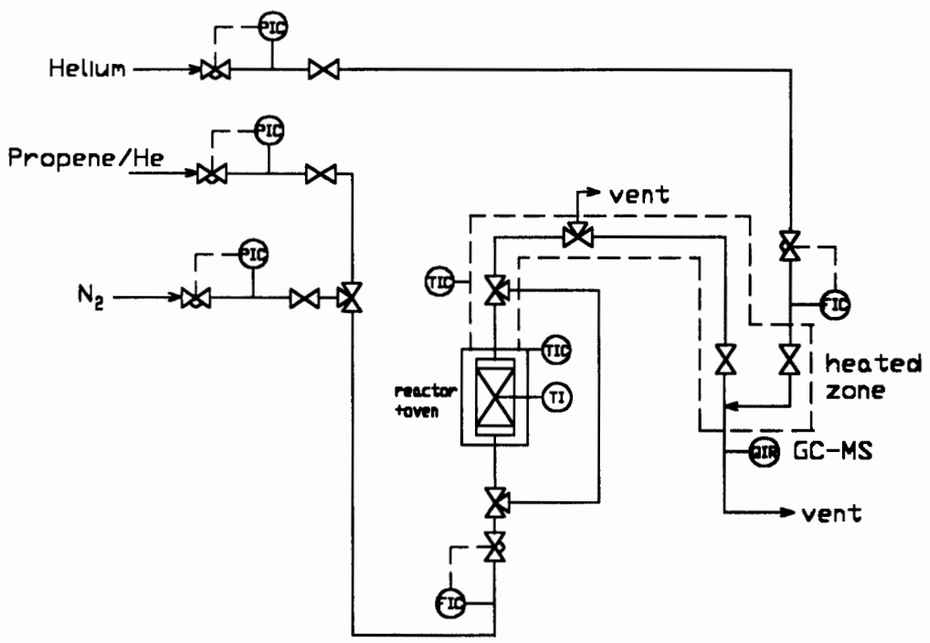

Figure 2-2 Flow diagram of the rig used for the temperature programmed reaction studies

The characteristic numbers for temperature programmed reduction with hydrogen, K and P, which are defined by Monti and Baiker (1983) and Malet and Caballero (1988) to facilitate selection of the most appropriate operating variables are shown in Appendix I for the propene reduction. The factor K contains the ratio between the amount of reducible species to the amount of reducing gas and is chosen in such a way that a noticeable

concentration change is guaranteed and at the same time the availability of the reducing gas is given. Propene availability during the temperature programmed reduction was granted, because the maximum conversion of propene was 25 mol-% and the change in propene concentration was sufficient in order to get reasonable sized product peaks. The factor P takes the heating rate into account in order to show if a good peak resolution is achieved. The reduction under isothermal conditions did not improve the peak resolution and therefore the heating rate didn't play a significant role during the temperature programmed reduction.

2.2.3.2 Experimental Procedure

The catalyst (m=0.15 g) was first dried in each experiment by heating it up in a nitrogen flow of 60 ml(NTP)/min with a heating rate of 10°C per minute up to 250°C and kept there for 120 minutes. Subsequently, the catalyst was cooled down to 100 °C.

After drying the catalyst, the nitrogen flow was switched off and 20 ml(NTP)/min of a 5 vol-% propene/helium gas mixture was allowed to flow through the bypass line to the mass spectrometer (MS). Before entering the mass spectrometer the stream had to be diluted with a helium flow of 150 ml(NPT)/min in order to not overload the MS-detector. The temperature from the reactor outlet to the MS was kept at 150 °C to prevent condensation. The stream through the bypass line was first analysed with the MS for 22 minutes after which the gas was allowed to flow through the reactor for 8 minutes. The temperature was then increased from 100°C to 650°C with a rate of 10 °C/min and kept at this temperature for 60 minutes.

The same experimental setup was also used to compare the partial oxidation of propene in the absence of gaseous oxygen with the partial oxidation of propene in the presence of oxygen. The catalyst (m=0.15g) was heated up in a flow of 60 ml(NTP)/min nitrogen to 375 °C with a heating rate of 10 °C/min, where the nitrogen flow was switched off and 20 ml(NTP)/min of a propene/helium gas mixture was allowed to flow through the bypass line and analysed by the MS. After 15 minutes the gas mixtures were allowed to flow through the reactor and the temperature was kept constant for 120 minutes.

The same procedure was applied for the partial oxidation of propene in the presence of gaseous oxygen, except that 1 ml(NTP)/min O_2 was added to the propene/helium gas

mixture. Preliminary experiments showed that this small change in total flow rate had negligible influence on the conversion and selectivities.

2.2.3.3 Product Analysis by mass spectrometry

The experimental setup shown in Figure 2-3 was used for the product analysis using mass spectrometry.

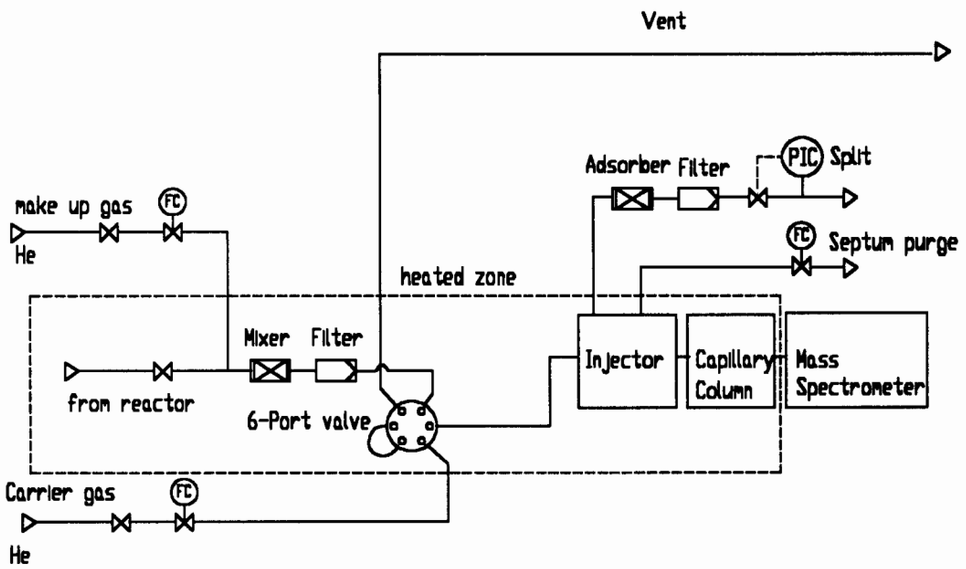

Figure 2-3 Flowsheet for the introduction of the sample into the gas chromatograph with mass spectrometer

As a sample passes through the gas chromatograph, it is separated into its various components. When entering the mass spectrometer, the components are bombarded by 70-eV electrons in the ion source causing molecules to fragment and ionise (see Figure 2-4). The mass spectrometer scanning process then filters the ions based on their mass/charge ratio.

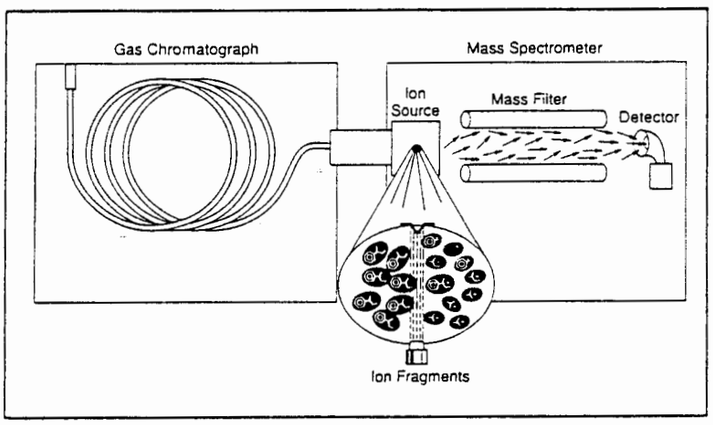

Figure 2-4 Simplified scheme of the working of the mass spectrometer (Hewlett Packard, 1989)

The identification or the molecule with a specific ion mass to electron ratio was done by comparing the ratios with values listed in tables in the literature (Eight Peak Index of Mass Spectra, 1991).

Table 2-2 shows the GC-MS settings used to analyse the products formed in the reduction using propene as a reduction gas.

Table 2-2 GC-MS settings

Oven Temperature	100°C, isotherm
split	1:100
column head pressure	7 psi
column	deactivated capillary column, l = 15m, d_i = 0.22mm
EM Volts	2400
Mode	Total Ion Chromatogram (TIC)
mass/charge range	1-200

Once the m/z values have been identified the corresponding abundances of the products and of propene have been used to calculate the conversion and the relative selectivities.

Absolute selectivities could not be calculated, because no calibration gas with the desired compounds could be obtained.

2.3 EXPERIMENTS IN FIXED BED REACTOR

2.3.1 Apparatus

Catalytic oxidation was carried out in a Pyrex U-reactor (Figure 2-5) mounted in a convection oven. The catalyst (0.5 g; $d_P < 0.1$ mm) was mixed with washed sand (4g; d_P = 0.2 - 0.3 mm) to minimise temperature gradients. The temperature of the catalyst bed was measured by a thermocouple which was placed inside a thermowell in the catalyst bed. The premixed gases were fed via a preheated zone consisting of washed sand heated to reaction temperature. The dead volume of the outlet of the reactor was minimised by a sand bed at the post reaction zone. The sand was kept in place by quartz wool in the inlet and outlet of the reactor.

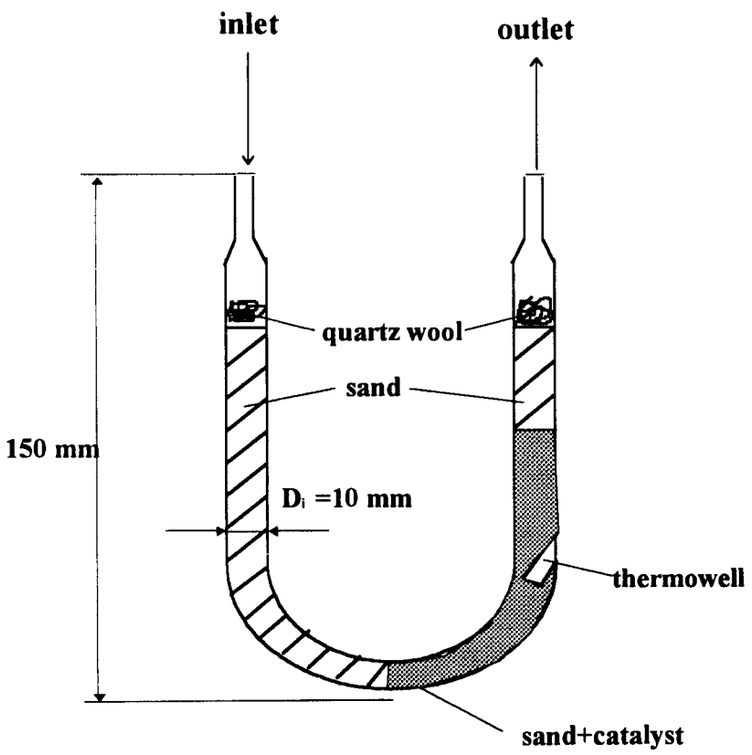

Figure 2-5 Pyrex U-reactor

Figure 2-6 shows the flowsheet of the partial oxidation rig. Flows of oxygen and nitrogen were controlled by mass flow controllers, the gaseous olefin (ethene, propene and 1-butene) and the gaseous paraffin (propane and n-butane) were controlled by keeping the pressure drop over an upstream deactivated silica capillary column (l=9cm, d_i=0.1 mm) constant (Figure 2-7). According to the Hagen-Poiseuille law the pressure drop is proportional to the flow through the capillary. Hydrogen could be added as a cofeedstock through a calibrated needle valve.

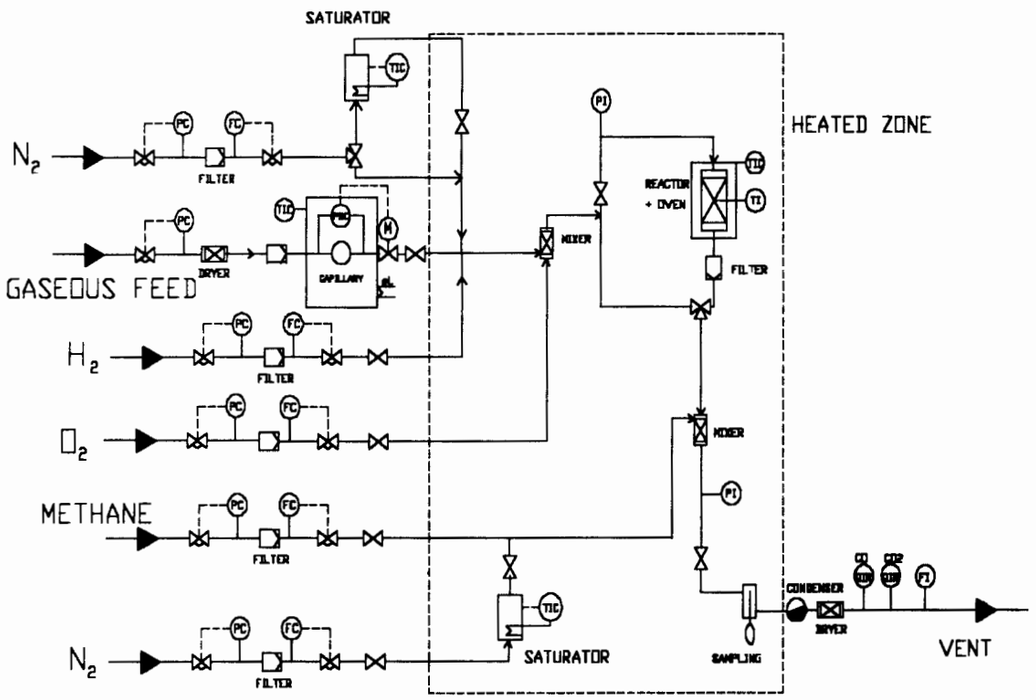

Figure 2-6 Flowsheet of the experimental rig

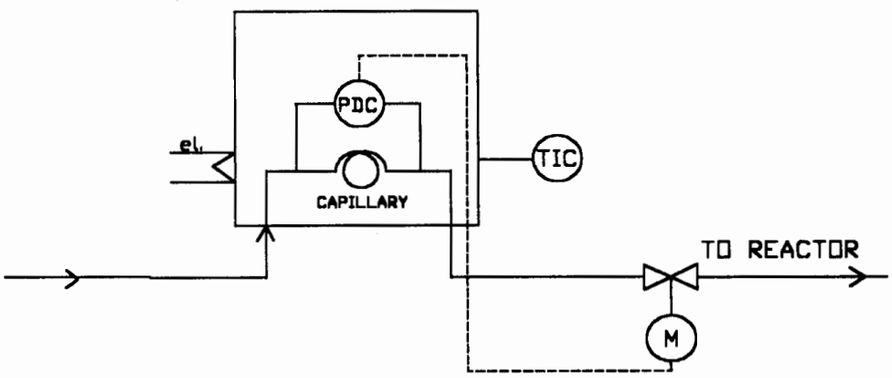

Figure 2-7 Capillary system to control flow of gaseous hydrocarbons

The liquid feedstocks (1-pentene, 1-hexene, 1-heptene, 1-octene and 1-nonene) and cofeedstocks (water) were fed by passing a known flow of nitrogen over acid washed macroporous Chromosorb®P (Sigma, 60-80 mesh, surface area 4 m^2/g) which served as a adsorbate for the liquid, using a fixed bed saturator (Figure 2-8).

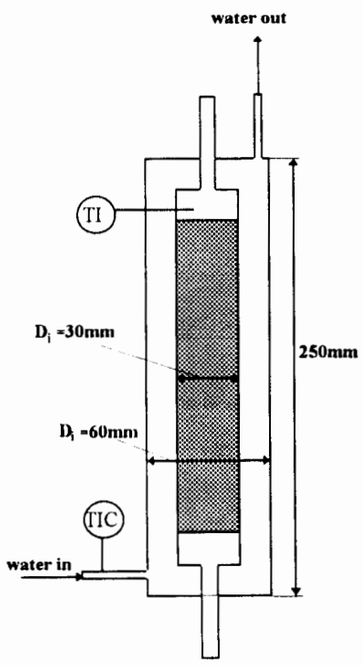

Figure 2-8 Fixed bed saturator filled

The catalyst was heated up in air, if not stated otherwise, with a heating rate of 5°C/min to the reaction temperature.

A constant flow of an internal standard was added through either a mass flow controller (Brooks) in the case for methane as internal standard or a double stage saturator in the case of iso-octane or cyclohexane to the effluent line of the reactor in order to obtain a quantitative momentary evaluation of the mass balance during the experiment

The organic compounds were detected by a flame ionisation detector using either a on-line GC sampling technique or an off line ampoule sampling technique (described in Section 2.3.2.1). The total oxidation products CO and CO_2 were monitored continuously using an on line IR-analyser. The flow of the dry effluent was determined using a soap bubble meter and was then vented.

2.3.2 Product analysis

2.3.2.1 Ampoule sampling technique

For the off gas sampling the ampoule sampling technique developed by Schulz *et al.* (1984) was used (Figure 2-9). Using this method, samples of the organic compounds in the effluent were collected by breaking pre-evacuated glass ampoules in the effluent line and sealing them off using a gas flame. Using this sampling technique, it was possible to take samples in very short time periods (about every 15 s) and it was possible to store the samples over long time periods. Furthermore, the sampling and analysis of complex product mixtures are completely decoupled. The ampoules were analysed by breaking them in a heated ampoule breaking device and flushing the content into the capillary column of a gas chromatograph.

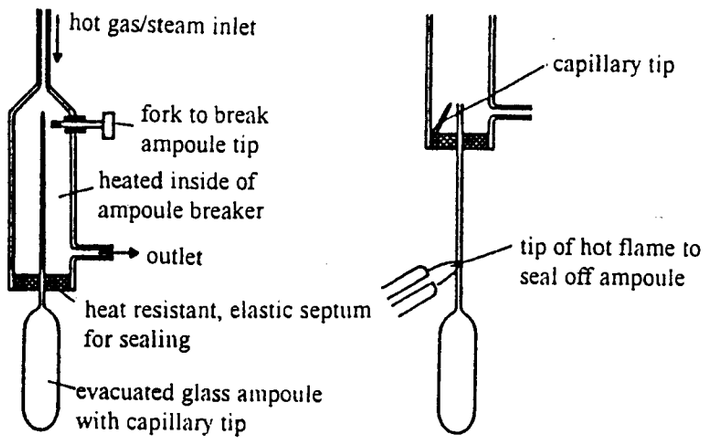

Figure 2-9 Ampoule sampling technique (Schulz *et al.*, 1984)

2.3.2.2 Gas chromatograph analysis

A Varian 3400 gas chromatograph was used for the analysis of organic products, except CO and CO_2. The GC was equipped with a flame ionisation detector (FID). Two different capillary columns were used for the separation of the products: SGE-BP5 and Hewlett Packard PONA. The PONA column was used for propane experiment, because there was a possibility that propene could be formed and this column was capable of separating propane/propene more easily. For all other experiments the BP5 column was used. Table 2-3 summarises the setup conditions of the GC.

Table 2-3 Overview of the GC setup conditions

Columns	SGE-BP5	Hewlett Packard-PONA
length [m]	25	50
inner diameter [mm]	0.32	0.2
stationary phase	phenyl dimethyl siloxan	methyl silicon
film thickness [μm]	0.5	0.5
column head pressure [psi]	10	20
split	1:100	1:100

Because of the wide variety of feedstocks used and to obtain optimal separation for each product spectrum, it was necessary to change the temperature program for the GC oven. Table 2-4 shows the temperature program used for the different feedstocks.

Table 2-4 Overview of different temperature programs used

Feed	Column	Temperature program
ethene, propene, butane	SGE-BP5	40°C, 6 min isotherm
propane	SGE-BP5	-40°C for 5min, heating rate 30°C/min to 100°C, 15 min isotherm
1-butene, 1-pentene	SGE-BP5	-8°C for 2min, heating rate 40°C/min to 40°C, 5min isotherm
1-hexene	SGE-BP5	0°C for 4min, heating rate 40°C/min to 40°C, 5min isotherm
1-heptene	SGE-BP5	-10°C for 5 min, heating rate of 40°C/min to 100°, isotherm for 10 min
1-octene,1-nonene	SGE-BP5	-5°C for 5 min, heating rate of 40°C/min to 100°, isotherm for 10 min

The inlet line of the gas chromatograph had to be altered in order to facilitate the analysis of glass ampoules. Figure 2-10 shows the flowsheet of the modified GC-system with an ampoule breaker. The ampoule breaker basically replaced the sample loop. After breaking the ampoule, the carrier gas (hydrogen) would carry the sample to the injector port of the GC. After an ampoule analysis a nitrogen stream would flush the ampoule breaker. The lines and the ampoule breaker were heated to 200° in order to prevent condensation.

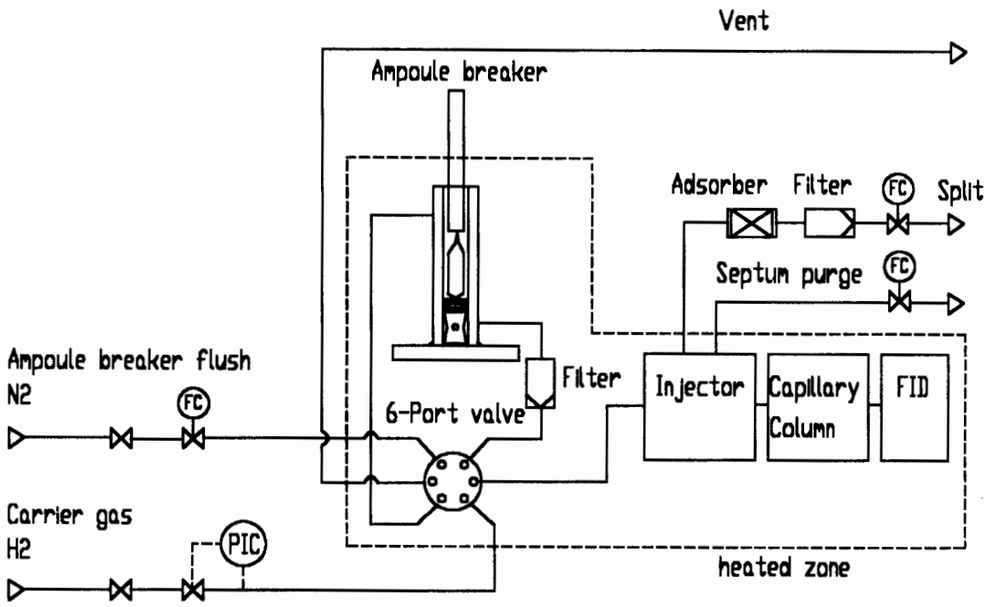

Figure 2-10 Flowsheet of the ampoule breaker device for the introduction of the sample into the gas chromatograph

2.3.3 Overview of experiments

2.3.3.1 Influence of gaseous oxygen on the partial oxidation of propene

The partial oxidation of propene in the absence of gaseous oxygen was investigated using the TPR apparatus described in Section 2.2.3.1. A GC-MS described in Section 2.2.3.3 was used for the product analysis. The catalysts that have been investigated are listed in Table 2-5.

Table 2-5 Experiments performed in the partial oxidation of propene in the absence of gaseous oxygen (T=350°C, m_{cat}=0.15g, $p_{propene}$=5 kPa, p_{He}=95 kPa)

Catalyst	T_{calc}, °C
Fe_2O_3	800
SbFe025	800
SbFe05	800
SbFe075	800
SbFe09	800

SbFe1	700
SbFe1	800
SbFe1	900
SbFe11	800
SbFe125	800
SbFe15	800
SbFe175	800
SbFe2	800
Sb_2O_4	800

In addition to the temperature programmed reduction studies time on stream behaviour of the partial oxidation of propene in the absence were performed using the catalyst SbFe1 (T_{calc}=800°C, t_{calc}=7h) at constant reaction temperature of 375°C. The time zero was defined as the time where the first products were detected by the GC-MS.

2.3.3.2 Investigation of temperature influence

Table 2-6 gives an overview over the feedstocks and the catalysts used in order to investigate the influence of the reaction temperature.

Table 2-6 Overview of experiments performed to study the influence of reaction temperature in the partial oxidation of olefins (300°C ≤ T ≤ 500°C, m_{cat}=0.5g, p=1.2 bar, F=110ml(NTP)/min, feed composition: 10 mol-% olefin, 20 mol-% O_2, balance N_2)

Feedstock	Catalyst	T_{calc}, °C
Ethene	SbFe15	900
Propene	SbFe15	900
Propene	Sb_2O_4	600
Propene	Fe_2O_3	600
Propene	SbFe2mix	600
Propene + 1.5 mol-% H_2	SbFe15	900
Propene + 1.5 mol-% water	SbFe15	900
1-Butene	SbFe15	900
1-Pentene	SbFe15	900
1-Hexene	SbFe15	900

2.3.3.3 Investigation of time on stream dependency

The ampoule sampling technique was used for the time on stream dependency, because the samples could be collected with high frequency (Chapter 2.3.2.2). This investigation was done for the partial oxidation of propene over iron antimony oxide containing various antimony contents, for the influence of the calcination temperature at constant iron to antimony ratio and for the influence of the pre-treatment in air or nitrogen for the above mentioned reaction over iron antimony oxide with a constant iron to antimony ratio. The catalyst was heated up in air or nitrogen with a heating rate of 5 K/min to reaction temperature. The gases were then switched to the bypass line and the propene line was opened. Time zero was defined as the time when the valve was switched from bypass to the reactor line. After 15 s the first ampoule sample was taken, which was approximately 3 s after the first traces of products were passing the ampoule sampling device. The internal standard was in all cases methane. Table 2-7 summarises the experiments performed. Table 2-8 shows the frequency of samples taken.

Table 2-7 Experiments performed to investigate the time-on-stream dependency in the partial oxidation of propene (T=350°C, m_{cat}=0.5g, p=1.2 bar, F=110ml(NTP)/min, feed composition: 10 mol-% propene, 20 mol-% O_2, balance N_2)

Catalyst	Tcalc, °C
Fe_2O_3	800
SbFe025	800
SbFe05	800
SbFe075	800
SbFe09	800
SbFe1	700
SbFe1	800
SbFe1	900
SbFe11	800
SbFe125	800
SbFe15	800
SbFe175	800
SbFe2	800
Sb_2O_4	800

Table 2-8 Frequencies of samples taken for the dependency of time on stream

time period	samples taken
0 - 30 s	every 15 s
30 - 5 min	every 30 s
5 - 10 min	every 60 s
10 - 30 min	every 5 min
30 - 60 min	every 10 min
60 - 120 min	every 15 min
120- 240 min	every 30 min

2.3.3.4 Investigation of space time at steady state

Table 2-9 gives an overview of feedstocks used and temperatures applied when varying the space time. On-line sampling technique was used for each experiment. Space time was calculated from the ratio of the total volumetric feed rate at reaction conditions to the volume of the catalyst bed which was kept constant at 2.2 ml.

Table 2-9 Experiments performed to investigate the influence of space time (Catalyst SbFe1, T_{calc}=900°C, t_{calc}=7h, m_{cat}=0.5g)

Feedstock	$T_{reaction}$, °C	τ,s	Internal standard
Propene	350, 375, 400	0.29...1.25	iso-Octane
1-Butene	350, 375, 400	0.45...1.03	iso-Octane
1-Pentene	350, 375, 400	0.29...1.25	iso-Octane
1-Hexene	350, 375, 400	0.29...1.25	iso-Octane
1-Heptene	350, 375, 400	0.29...1.25	Cyclohexane
1-Octene	325, 350, 375	0.33...1.31	Cyclohexane
1-Nonene	350, 375	0.36...1.25	Cyclohexane

The space time range for 1-butene was limited by the used capillary flow meter described in Section 2.3.1 because of the low partial pressure of butene at room temperature (p=2.56

kPa at T=20°C). For the feedstocks 1-octene and 1-nonene the maximum reaction temperature had to be limited to 375°C, because thermal cracking, as determined by carbon balance, became severe.

2.3.3.5 Kinetic studies

Kinetic studies were performed for five different α-olefins, which are listed in Table 2-10 together with the temperatures and partial pressures applied. All rates of reaction were calculated on a carbon basis and were measured at low conversion levels (usually X <10%) in order to operate the reactor differentially. The formulae for the calculation of the rates of consumption and rates of formation are given in Appendix II. The concentrations of the feedstocks were calculated using average concentrations of inlet and outlet in the catalyst bed.

Table 2-10 Reaction conditions applied for kinetic studies (SbFe15, T_{calc}= 900°C, t_{calc}=7h, m_{cat}=0.5g)

Feedstock	Temperature, °C	τ, s	$P_{olefins}$, bar	P_{oxygen}, bar
Ethene	425, 450, 475	0.79	0.075 - 0.45	0.075 - 0.825
Propene	350, 375, 400	0.38	0.055 - 0.34	0.095 - 0.34
1-Butene	350, 375, 400	0.54	0.075 - 0.18	0.095 - 0.65
1-Pentene	350, 375, 400	0.47	0.085 - 0.34	0.085 - 0.525
1-Hexene	325, 350, 375	0.43	0.055 - 0.34	0.095 - 0.475

CHAPTER 3

RESULTS

3. RESULTS

Besides the characterisation of the catalyst this chapter contains basically the results of propene partial oxidation in the presence and absence of gaseous oxygen, which will give valuable insight into the purpose of different oxygen species. Furthermore, the influence of the chain length of the α-olefins has received considerable attention, by investigating their oxidation over iron antimony oxide.

3.1 CHARACTERISATION OF IRON ANTIMONY OXIDE CATALYSTS

The iron antimony oxide catalysts with various antimony contents which have been calcined at various temperatures were characterised using a variety of techniques. The main purposes were the identification of the different phases by X-ray diffraction, the determination of crystal size by Transmission Electron Microscopy (TEM) and the measurement of the BET-surface area.

3.1.1 Crystallinity

Two parameters have been changed which have a strong influence on the crystallinity: calcination temperature and the antimony to iron ratio, both will be investigated in more detail in the following sections.

3.1.1.1 Influence of antimony to iron ratio

X-ray diffraction (XRD) was used in order to investigate what happens to the excess metal in the catalyst containing different antimony to iron ratios, whether a separate phase was formed or whether the excess metal was incorporated into the lattice of the active phase.

Figure 3-1 shows the influence of the antimony to iron ratio on the X-ray diffraction pattern of iron antimony oxide for ratios between 0 and 1.

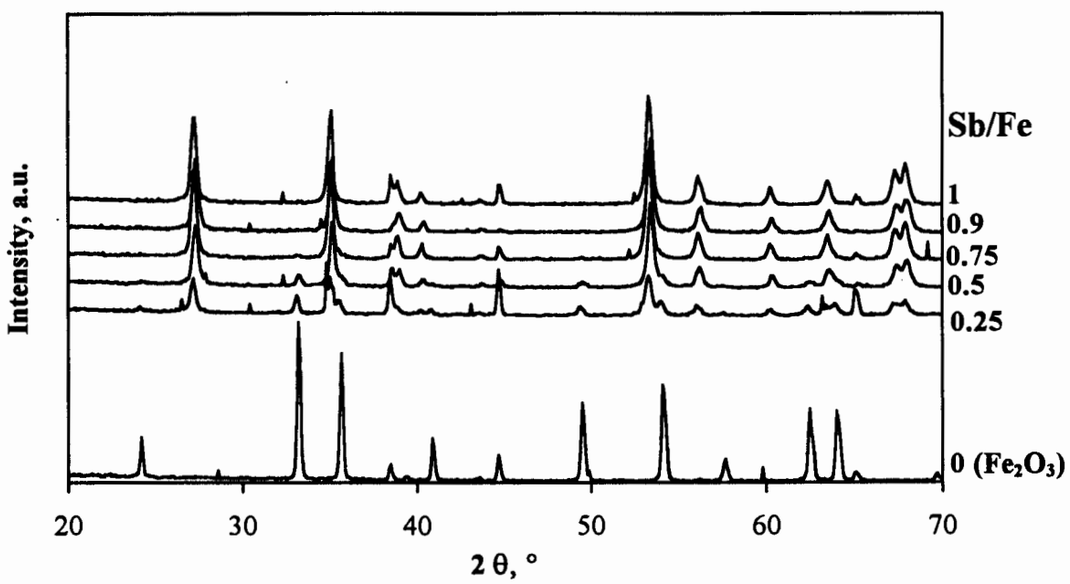

Figure 3-1 Influence of Sb: Fe ratio on X-ray diffraction pattern for ratios Sb:Fe≤1, calcined at 900°C in air for 7h.

With increasing ratios from Sb/Fe≥0.25 the peak intensities for the main peaks at 2θ=27.2°, 35.1° and 53.3° increase, while the peak intensities of the peaks at Sb/Fe=0 decrease with increasing Sb/Fe ratio. This clearly shows that different catalytic phases are prevalent when changing the Sb/Fe ratio.

The phases were identified by comparing the position of the main peaks with data from known phases. Table 3-1 shows that the material containing a Sb:Fe ratio of 0 was identified as Fe_2O_3. Although the peaks occurred at exactly the same 2θ values, the intensities are not exactly the same, which might indicate a preferential order of the crystals in the sample holder.

Table 3-1 D-space, 2θ, [h,k,l]-planes and peak intensities for phase containing a ratio of Sb:Fe=0 compared with data for Fe_2O_3 from JCPDS (1990).

Sample with ratio Sb:Fe=0			Data for Fe_2O_3	
2θ, °	D-space, Å	Intensity [%]	Intensity [%]	h k l
33.2	2.70	100	100	1 0 4
35.6	2.52	77.6	70	1 1 0
49.5	1.84	50.3	31	0 2 4
54.1	1.70	65	36	1 1 6
62.5	1.49	45	22	2 1 4
64.0	1.45	44	21	3 0 0

In Table 3-2, the X-ray diffraction pattern of the catalyst containing a Sb:Fe ratio of 1 is compared with those of $FeSbO_4$ and $FeSb_2O_6$. The position of the peaks in the sample corresponds to a $FeSbO_4$, since the peak at 2θ=21°, which exists for a $FeSb_2O_6$ phase, is missing.

Table 3-2 D-space, 2θ, [h,k,l]-planes and peak intensities for phase containing a ratio of Sb:Fe=1 compared with data for $FeSbO_4$ and for $FeSb_2O_6$ from JCPDS (1990).

Sample with ratio Sb:Fe=1			Data for $FeSbO_4$		Data for $FeSb_2O_6$	
2θ, °	D-space, Å	Intensity [%]	Intensity [%]	h k l	Intensity [%]	h k l
21.0	4.23	0	0	-	20	1 0 1
27.2	3.28	79.2	100	1 1 0	100	1 1 0
35.1	2.56	85.6	71	1 0 1	90	1 0 3
38.8	2.32	22.5	17	2 0 0	40	2 0 0
53.3	1.72	100	56	2 1 1	90	2 1 3
56.3	1.64	21.4	14	2 2 0	50	2 2 0
67.3	1.39	27.2	12	1 1 2	20	3 1 2
67.9	1.38	33.6	14	3 0 1	30	1 1 6

The X-ray diffraction pattern of iron antimony oxide for ratios Sb:Fe≥1 are shown in Figure 3-2.

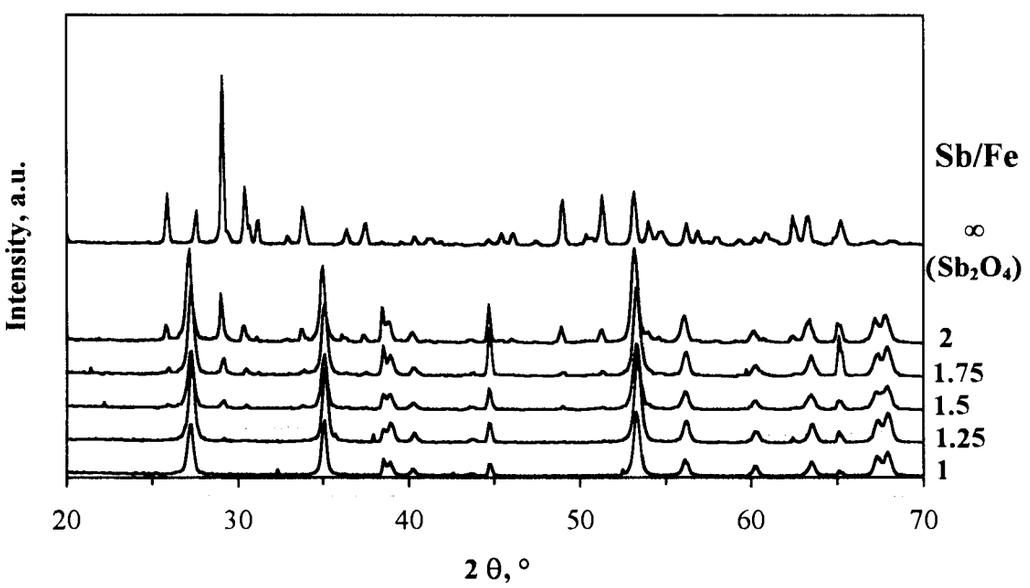

Figure 3-2 Influence of Sb: Fe ratio on X-ray diffraction pattern for ratios Sb:Fe≥1, calcined at 900°C in air for 7h.

Figure 3-2 shows that the intensities of the peaks which have been assigned to the $FeSbO_4$ phase further increase with increasing Sb/Fe ratios. The peak intensities at 2θ= 25.9°, 29.2°, 30.4°, 49° and 51.3° increase also with increasing Sb/Fe ratios and can be assigned to the material of a ratio Sb:Fe→∞ (contains no Fe). The phase for Sb:Fe→∞ has been compared with several antimony oxide phases and could be identified as Sb_2O_4, as shown in Table 3-3. Comparison with the work of Allen *et al.* (1996) revealed that the Sb_2O_4 consists mainly of α-Sb_2O_4, although there are traces of β-Sb_2O_4 present, due to small peaks at 2θ=30.5° (shoulder), 50.3° and 54.6°, which can be attributed to the β phase. Carbucicchio et al. (1985) detected besides $FeSbO_4$ only the β-Sb_2O_4 phase for a catalyst containing a Sb:Fe ratio of 2:1 (Figure 1-5). However, the X-ray diffraction pattern of their sample doesn't show a peak at 2θ= 29.2°, which is characteristic for both α-Sb_2O_4 and β-Sb_2O_4.

From Figures 3-1 and 3-2 it can be seen that for Sb:Fe ratios ≤ 1 the excess iron formed a Fe_2O_3 phase and for Sb:Fe ratios ≥ 1 the excess antimony formed the α and β-Sb_2O_4 phases. Apart from Fe_2O_3, $FeSbO_4$ and Sb_2O_4 no other crystalline phases could be detected.

Table 3-3 D-space, 2θ, [h,k,l]-planes and peak intensities for phase containing a ratio of Sb:Fe→∞ compared with data for Sb_2O_4 from JCPDS (1990).

Sample with ratio Sb:Fe→∞			Data for Sb_2O_4	
2θ, °	D-space, Å	Intensity [%]	Intensity [%]	h k l
25.9	3.44	29.4	30	1 1 1
29.1	3.07	100	100	1 1 2
30.4	2.94	33.5	45	0 0 4
49.0	1.86	25.6	25	0 2 4
51.3	1.78	28.7	20	2 2 1
52.9	1.73	30.7	20	2 2 2

In order to check whether the phases exist separately or whether atoms were incorporated into the $FeSbO_4$ structure, the unit cell dimensions of $FeSbO_4$ were calculated as a function of the Sb to Fe ratios. Following relation between the d-space of a h,k,l-plane and the unit cell dimensions applies (Mc Kie, 1980):

$$\frac{1}{d_{hkl}^2} = \frac{h^2}{a^2} + \frac{k^2}{b^2} + \frac{l^2}{c^2} + \frac{2 \cdot k \cdot l}{b \cdot c \cdot \cos\alpha} + \frac{2 \cdot l \cdot h}{c \cdot a \cdot \cos\beta} + \frac{2 \cdot h \cdot k}{a \cdot b \cdot \cos\gamma} \qquad (3\text{-}1)$$

For the tetragonal system $FeSbO_4$ Equation 3-1 can be simplified to

$$\frac{1}{d_{hkl}^2} = \frac{h^2 + k^2}{a^2} + \frac{l^2}{c^2} \qquad (3\text{-}2)$$

because of a=b and α=β=γ=90°. The values for a and c were calculated using the d-spaces of 9 different planes, which are listed in Table 3-4.

Table 3-4 Peaks and crystalline planes used to calculate unit cell dimension

2θ	27.2°	35.1°	38.8°	40.2°	53.3°	56.3°	60.2°	63.4°	67.3°
h,k,l	1,1,0	1,0,1	2,0,0	1,1,1	2,1,1	2,2,0	0,0,2	3,1,0	1,1,2

The cell unit parameters a and c of $FeSbO_4$ are shown as a function of the Sb/Fe ratio in Figure 3-3 for a calcination temperature of 800°C and 900°C. The values obtained were a = 4.639±0.011 Å and c = 3.076±0.036 Å for the calcination temperature of 800°C and a = 4.637±0.014 Å and c = 3.082±0.055 Å for a calcination temperature of 900°C. These results compare well with the parameters reported by Wyckhoff (1963) for $FeSbO_4$, which are a=4.623 Å and c=3.011 Å.

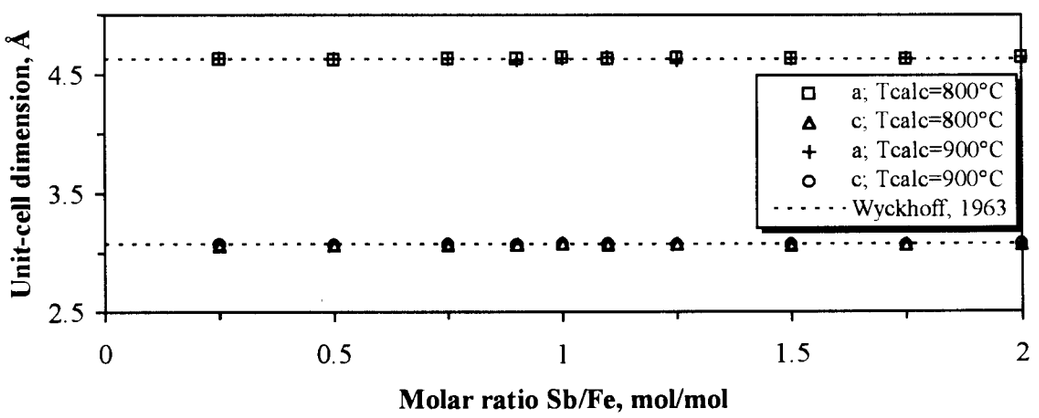

Figure 3-3 Unit cell dimensions of $FeSbO_4$, calcined at 800°C and at 900°C as a function of Sb/Fe ratio.

The unit cell dimensions from Figure 3-3 were used to calculate the unit cell volume of $FeSbO_4$ as a function of the Sb/Fe ratio for the calcination temperatures of 800°C and 900°C. The calculated unit cell volumes are compared with the values from Wyckhoff (1963) in Figure 3-4 . A good agreement was observed with these values, since a deviation of only 0.5 % was observed. It can therefore be concluded that no atoms were incorporated

in the $FeSbO_4$ lattice by changing the Sb/Fe ratio and the calcination temperature in the investigated range.

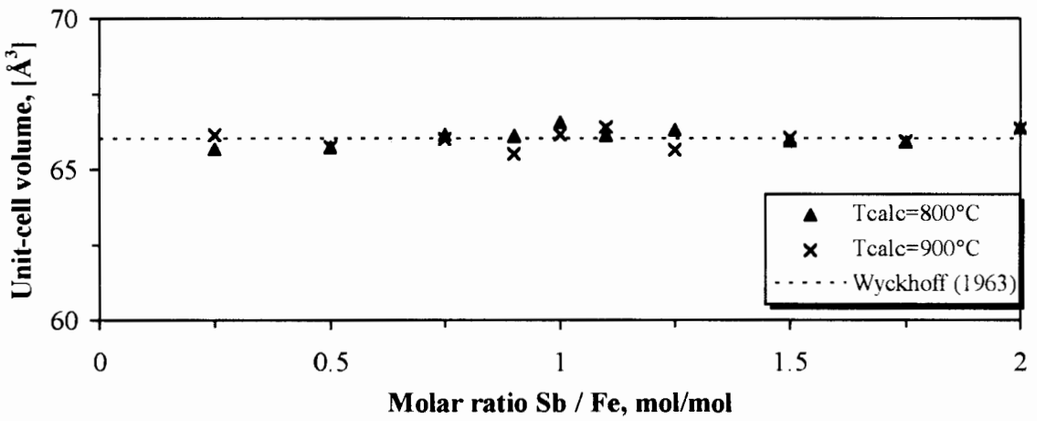

Figure 3-4 Unit cell volume of $FeSbO_4$, calcined at 800°C and 900°C as a function of the Sb/Fe ratio.

This result is a contradiction of the result of Carbucicchio *et al.* (1985), who concluded that antimony is incorporated into the $FeSbO_4$ lattice. However, they used $FeCl_3 \cdot 6H_2O$ and $SbCl_5$ as sources for the $FeSbO_4$ synthesis and used a pH of 8 for the precursor solution. Teller *et al.* (1985) who used $Fe(NO_3)_3 \cdot 9H_2O$ and Sb_2O_3 as sources for $FeSbO_4$ and a pH of 3 for the precipitation out of the solution did not observe an incorporation of any atom into the $FeSbO_4$ lattice. This might indicate that the method of the catalyst synthesis influences antimony incorporation into the $FeSbO_4$.

3.1.1.2 Influence of calcination temperature

The influence of the calcination temperature on the crystalline structure is shown in Figure 3-5 for the example of iron antimonate (Sb:Fe=1). The main peaks which occur at 2θ = 27.2°, 35.1° and 53.3° can already be observed at a calcination temperature of 500°C, indicating that iron antimonate is already formed at a calcination temperature of 500°C. Minor peaks at 2θ = 38.8° and 40.2° occur at a calcination temperature of 800°C. With increasing calcination temperature the peak intensity increases and the peak width decreases. The increase in the peak intensity indicates that more crystals are formed and the catalyst is of a higher crystallinity. The decrease in peak width with increasing calcination

temperature indicates a growth of the crystals, which might be attributed to sintering processes.

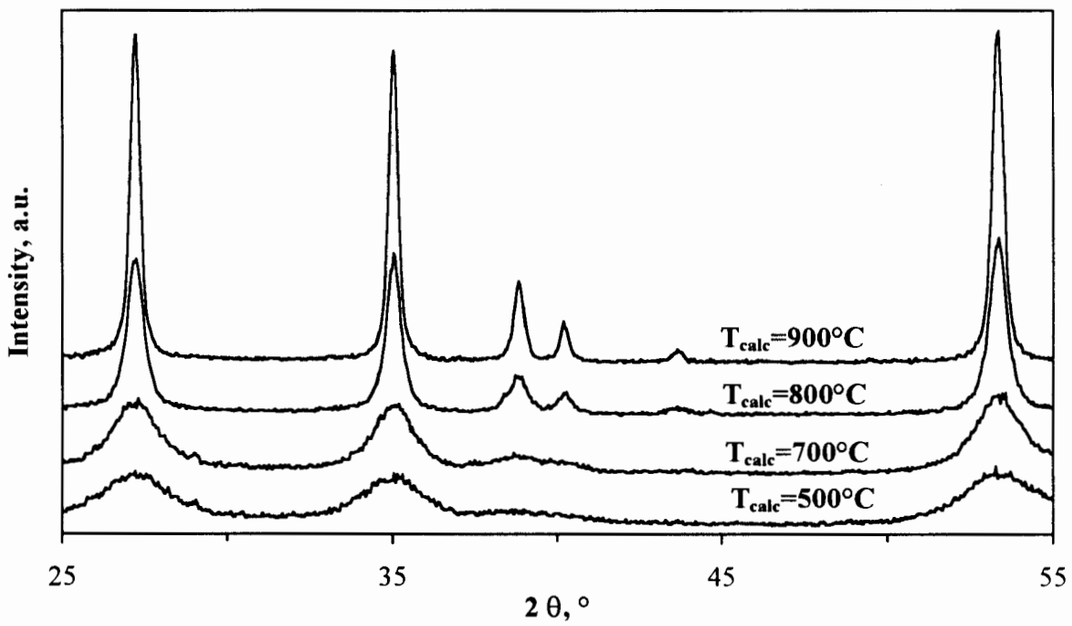

Figure 3-5 Influence of calcination temperature on the crystallinity of iron antimonate (Sb:Fe = 1) determined by X-ray diffraction.

The influence of calcination temperature for catalysts containing a Sb:Fe ratio of 0.5 and 2 are shown in Figures 3-6 and 3-7 respectively. From Figure 3-6 it can be observed that the intensities for peaks which are typical for Fe_2O_3 are much lower than the intensities of the $FeSbO_4$ peaks. This is expected since X-rays are scattered by the electrons associated with the atoms in a crystal (Ladd and Palmer, 1994). Antimony which has a higher atomic number than iron provides a greater concentration of electrons. The catalyst, which was calcined at 700°C shows mostly amorphous material, with no Fe_2O_3 peaks visible.

Sb_2O_4 peaks show a much higher intensity compared to Fe_2O_3, which can be seen in Figure 3-7 for a catalyst containing an excess of antimony (Sb:Fe=2). The Sb_2O_4 peaks can already be observed for the sample which was calcined at 700°C, meaning that Sb_2O_4 is already to a great extent in a crystalline form, since it is readily formed by oxidation from Sb_2O_3.

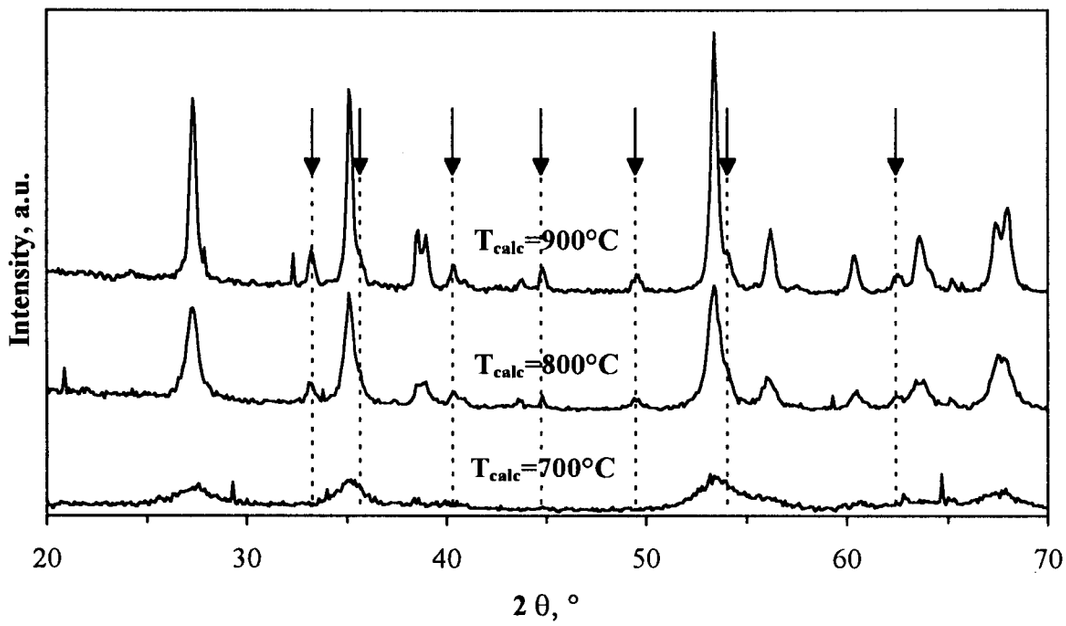

Figure 3-6 Influence of calcination temperature on the crystallinity of iron antimony oxide with an excess of iron (Sb:Fe=0.5) determined by X-ray diffraction; ↓ indicating typical peaks for Fe_2O_3.

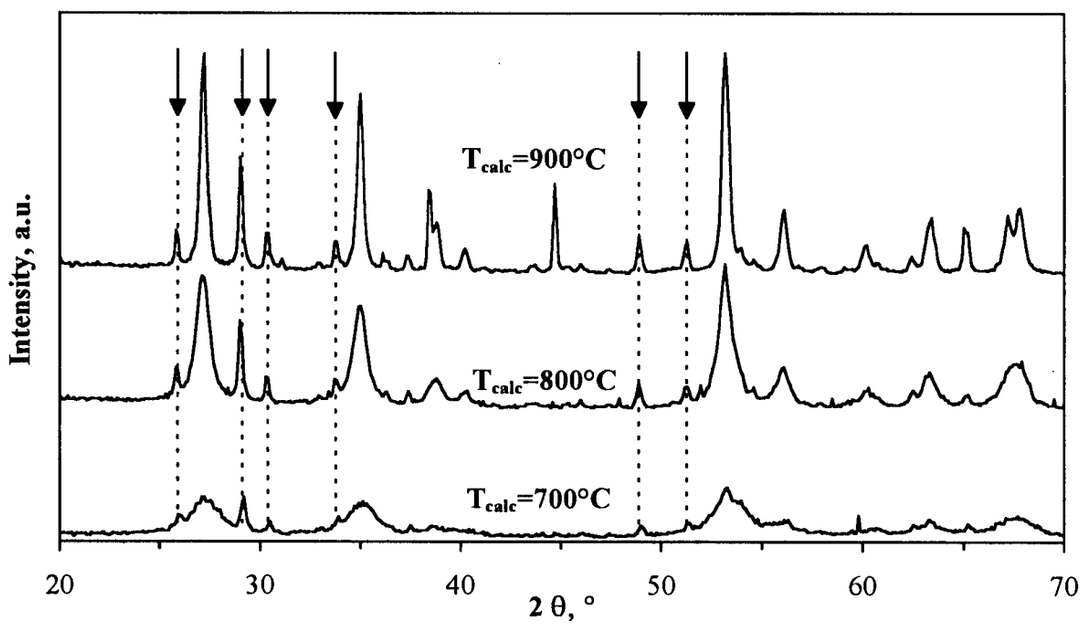

Figure 3-7 Influence of calcination temperature on the crystallinity of iron antimony oxide with an excess of antimony (Sb:Fe=2) determined by X-ray diffraction; ↓ indicating typical peaks for Sb_2O_4.

The influence of calcination temperature on the crystal structure, determined by X-ray diffraction, for iron antimony oxide containing the following Sb:Fe ratios: 0 (Fe_2O_3), 0.25, 0.75, 0.9, 1.25, 1.5, 1.75 and ∞ (Sb_2O_4) are shown in Appendix III.

3.1.2 Transmission Electron Microscopy (TEM)

The purpose for doing the TEM images was to visualise and measure the crystal size for iron antimony oxide as a function of calcination temperature and Sb:Fe ratio.

3.1.2.1 Influence of calcination temperature

The influence of the calcination temperature on the crystal size is visualised in Figure 3-8 for iron antimonate ($FeSbO_4$) calcined at 700°C and in Figure 3-9 for 800 and 900°C.

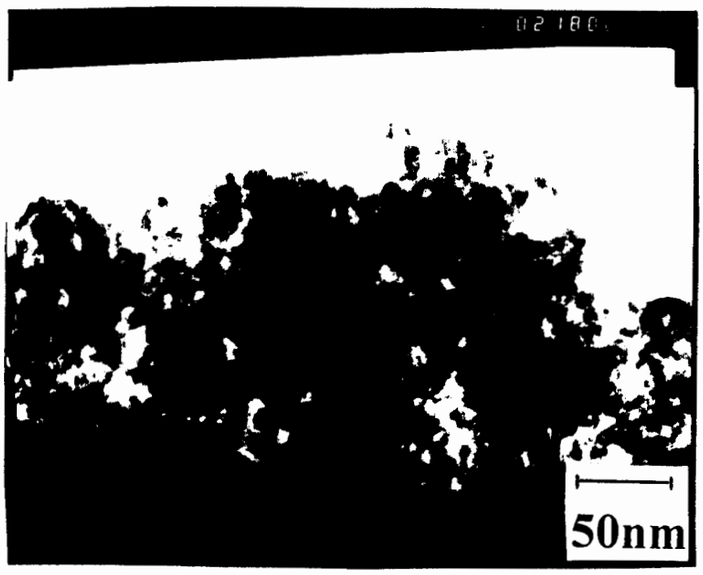

Figure 3-8 TEM image for $FeSbO_4$, calcined at 700°C.

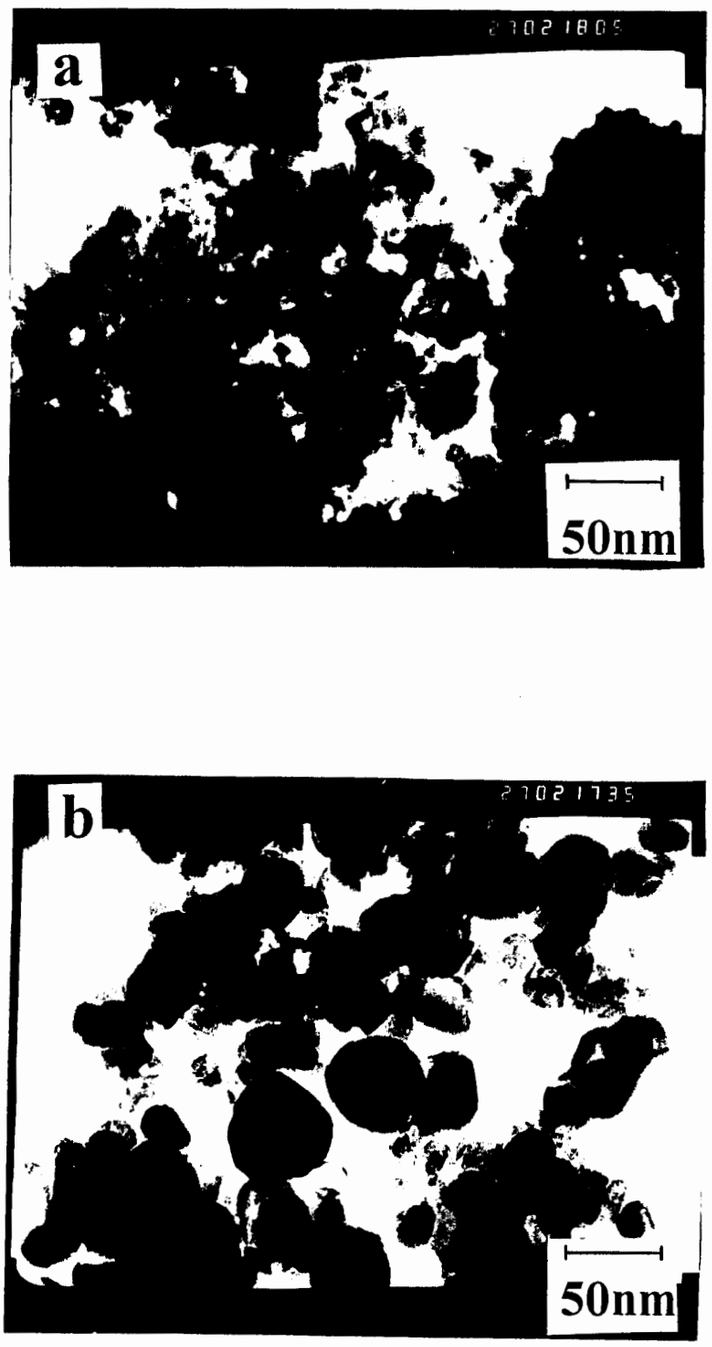

Figure 3-9 TEM images of $FeSbO_4$ calcined at 800°C (a) and 900°C (b).

The crystallites are different in shape, but can be best approximated as spheres. The mean diameter of the crystallites (Table 3-5) have been obtained by measurement from the TEM images.

Table 3-5 Influence of calcination temperature on mean crystallite diameter of $FeSbO_4$ as determined by TEM

T_{calc}, °C	700	800	900
$\overline{d_{cryst}}$, nm	7.8±1.7	11.9±3.3	26.9±5.8

An increase of the mean crystallite diameter with increasing calcination temperature can be observed, which is due to high temperature sintering.

3.1.2.2 Influence of Sb:Fe ratio

The images of iron antimony oxide samples containing different Sb:Fe ratios together with the frequency distribution of the crystal diameters are shown in Appendix IV. The mean crystallite diameters of $FeSbO_4$ crystals together with their deviation are summarised in Table 3-6.

Table 3-6 Influence of Sb:Fe ratio on the mean crystallite diameter of $FeSbO_4$

T_{calc}, °C	Sb:Fe	$\overline{d_{cryst}}$, nm
700	0.9	5.8±0.8
	1.0	7.8±1.7
	1.1	6.9±1.8
800	0.5	16.7±5.3
	1.0	11.9±3.3
	1.75	19.6±4.3
900	0.75	26.4±5.6
	1.0	26.9±5.8
	2.0	26.5±6.0

The Sb:Fe ratio doesn't seem to influence the crystallite size of $FeSbO_4$ at a certain calcination temperature.

3.1.3 Pore Volume and BET-Surface Area

Figure 3-10 shows the pore volume as a function of the average pore diameter at the calcination temperatures 700, 800 and 900°C. The calcined iron antimonate catalyst with a Sb/Fe ratio of 1:1 (T_{calc}=700, 800, 900°C) possesses pores in the range between 20 and 1700 Å. The pores develop during crystal growth, which leaves void volumes where crystals meet.

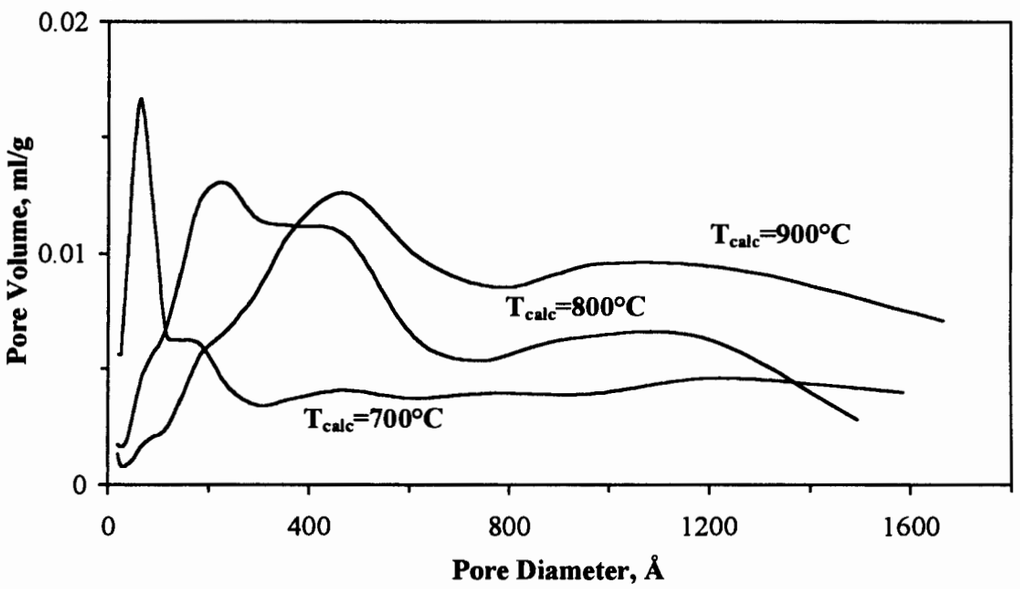

Figure 3-10 Pore Volume as a function of the average pore diameter and the calcination temperature for iron antimonate (Sb:Fe=1:1).

It can clearly be seen that the peak maximum shifts to higher average pore diameters with increasing calcination temperature. The influence of calcination temperature on the BET-surface, the pore volume and average pore diameter is summarised in Table 3-7. It has

already been shown with the TEM images (Section 3.1.2) that the crystal diameter increases with increasing calcination temperature. An increase in crystals size with increasing calcination temperature results in a decrease of the surface area and in an increase of the average pore diameter and a decrease in the pore volume. This is best explained by sintering of the crystals at high calcination temperatures, which was also observed by Carbucicchio *et al.* (1985) for the same catalyst.

Table 3-7 BET surface area, pore volume and average pore diameter as a function of calcination temperature for iron antimonate (Sb:Fe=1:1).

Calcination temperature, °C	only dried	700	800	900
BET-surface area, m^2/g	8.2	66.7	28.8	16.4
V_{pore}, ml/g	0.03	0.12	0.11	0.09
Average pore diameter, Å	157.4	69.9	158.2	226.0

The influence of the Sb:Fe ratio on the BET surface area is shown in Figure 3-11 for the range $0.25 \leq Sb:Fe \leq 2$.

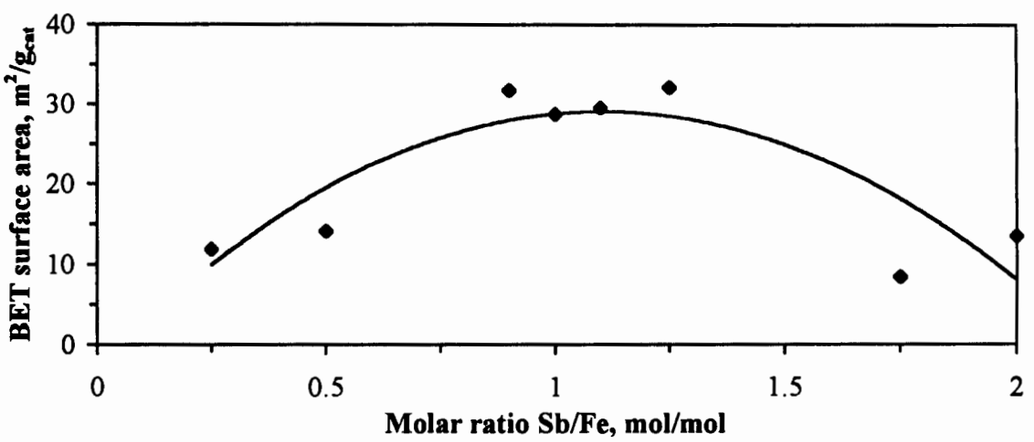

Figure 3-11 Influence of Sb:Fe ratio on the BET surface area (T_{calc}=800°C, t_{calc}=7h).

The BET surface areas show a maximum close to a Sb:Fe ratio of 1 and decrease when the content of Fe_2O_3 or Sb_2O_4 increase. The BET surface area, the pore volume and average pore diameter of Fe_2O_3 and Sb_2O_4 are shown in Table 3-8. The BET surface areas are much smaller than for $FeSbO_4$, which explains why the BET surface areas for iron antimony oxide containing different Sb:Fe ratios are highest at a ratio of 1 and decrease when the content of Fe_2O_3 or Sb_2O_4 is increased.

Table 3-8 BET surface area, pore volume and average pore diameter for the compounds Fe_2O_3 and Sb_2O_4 (T_{calc}=800°C, t_{calc}=7h).

Compound	Fe_2O_3	Sb_2O_4
BET-surface area, m^2/g	2.5	0.5
V_{pore}, ml/g	0.23	0.002
Average pore diameter, Å	3675.7	158.8

3.2 PARTIAL OXIDATION OF PROPENE OVER SINGLE METAL OXIDES IN A FIXED BED REACTOR

In order to show the exceptional ability of iron antimony oxide to oxidise propene to acrolein with high selectivities, experiments were performed with the single metal oxides Fe_2O_3 and Sb_2O_4. Those single metal oxides were either tested on their own or in a mixture of both components. The calculation method for the conversion, selectivity, yield and the mass balance are presented in Appendix II.

3.2.1 Iron oxide

Figure 3-12 shows the yields of acrolein, CO_2 and CO and the oxygen conversion for the partial oxidation of propene over Fe_2O_3 as a function of reaction temperature. The conversions of oxygen increases exponentially up to a reaction temperature of 400°C, where almost 100% oxygen conversion is achieved and the reaction becomes limited by the oxygen availability.

The yield of the main product CO_2 increases exponentially with increasing reaction temperature up to 400°C, where the yield remains constant for further increasing temperature, because of a lack of oxygen. The yields of acrolein and CO increase linearly with reaction temperature, but they stay well below 5 C-%. Acrolein is formed with the lowest yield.

The selectivity to acrolein decreases with increasing temperature from 30.6 C-% at 275°C to 2 C-% at 500°C. The selectivity to CO decreases with increasing temperature from 15.4 C-% at 275°C to 5.2 C-%, while the selectivity to CO_2 increases with increasing temperature from 54 C-% at 275°C to 92.8 C-% at 500°C.

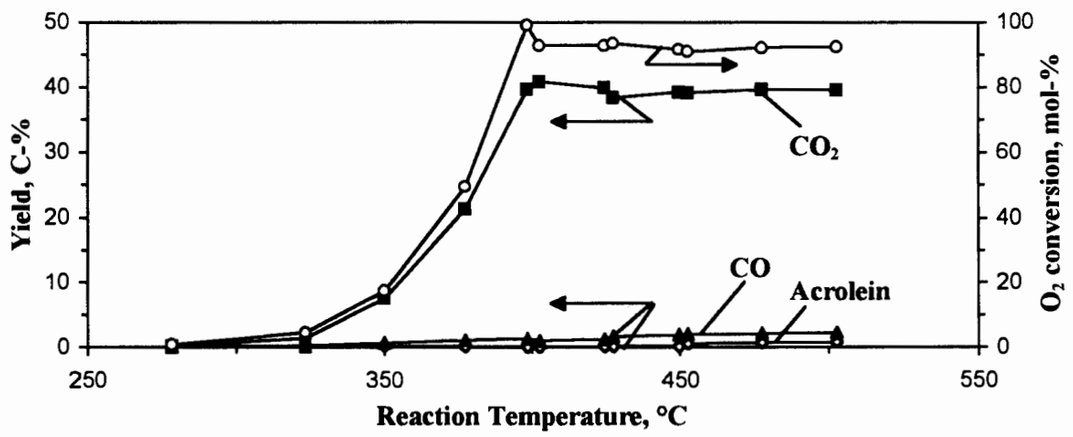

Figure 3-12 Influence of reaction temperature on yields of acrolein, CO_2 and CO in the partial oxidation of propene over Fe_2O_3 (T_{calc} = 600°C, t_{calc} = 7h), (p = 1.2 bar, WHSV = 2 $g_{propene}/g_{catalyst}$ h, $m_{catalyst}$=0.5g; feed composition: 10 mol-% propene, 20 mol-% O_2, balance N_2).

Fe_2O_3 is very active in the partial oxidation of propene, however, the selectivity to carbon oxides is dominant and makes it therefore not suitable as a partial oxidation catalyst.

3.2.2 Antimony Oxide

Figure 3-13 shows the yields of acrolein, CO_2 and CO in the partial oxidation of propene over Sb_2O_4 as a function of the reaction temperature. The catalyst shows for the whole range of reaction temperatures a very low activity (X < 10 mol-%). CO_2 was found to be the main reaction product, with acrolein being formed with higher yields than CO. The

yields of acrolein, CO_2 and CO increase with a relative low slope with increasing reaction temperature. The selectivity to acrolein decreases with increasing temperature from 36 C-% at 375°C to 17.3 C-% at 500°C. The selectivity to CO decreases with increasing temperature from 7.1 C-% at 375°C to 18.2 C-%, while the selectivity to CO_2 increases with increasing temperature from 56.9 C-% at 375°C to 64.5 C-% at 500°C.

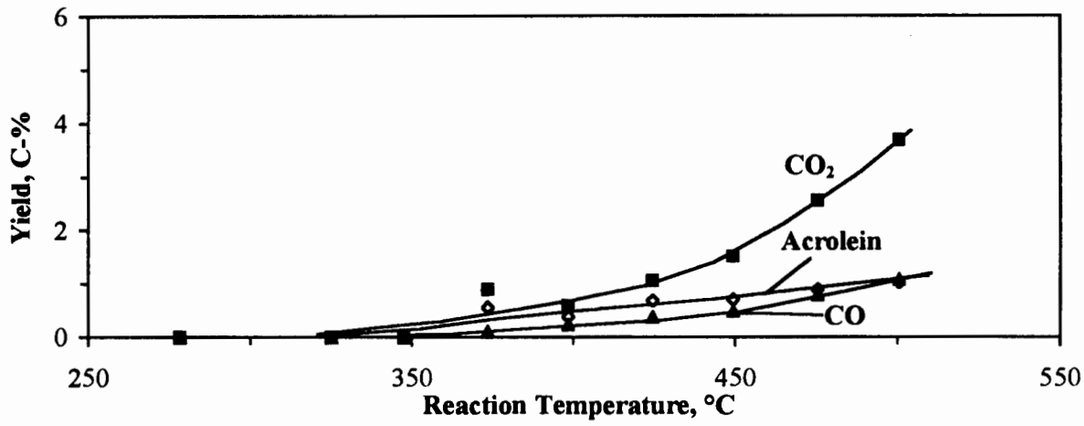

Figure 3-13 Influence of reaction temperature on yields of acrolein, CO_2 and CO in the partial oxidation of propene over Sb_2O_4 (T_{calc} = 600°C, t_{calc} = 7h), (p = 1.2 bar, WHSV = 2 $g_{propene}/g_{catalyst}$ h, $m_{catalyst}$ = 0.5 g; feed composition: 10 mol-% propene, 20 mol-% O_2, balance N_2).

Sb_2O_4 is not suitable as a partial oxidation catalyst, because the yields of acrolein are very low.

3.2.3 Fe_2O_3/Sb_2O_4 mechanical mixture

Figure 3-14 shows the yields of acrolein, CO_2 and CO as a function of reaction temperature over a mechanical mixture of Fe_2O_3 and Sb_2O_4 with a Sb:Fe ratio of 2. The yields increase slowly with increasing reaction temperature, with CO_2 being the main product. The reaction is not limited by oxygen availability, because the yield of CO_2 is remarkably lower than in the case of using Fe_2O_3.

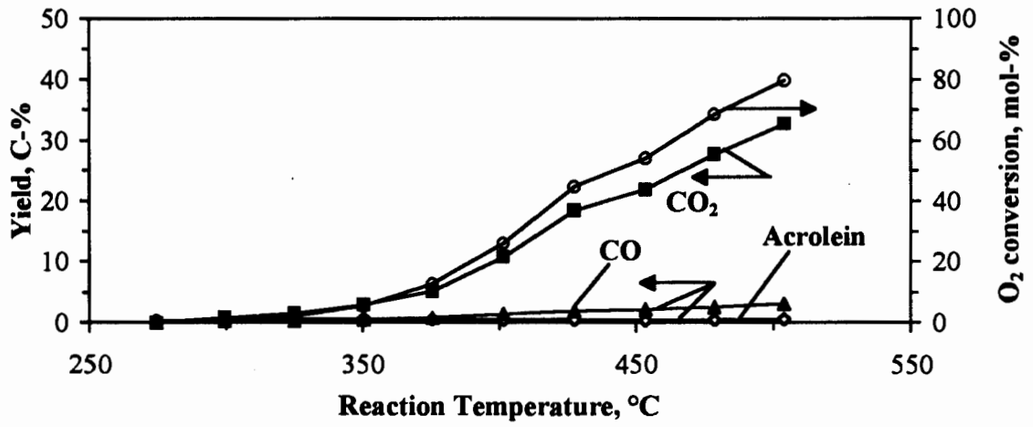

Figure 3-14 Influence of reaction temperature on yields of acrolein, CO_2 and CO in the partial oxidation of propene over a mechanical mixture of Fe_2O_3 and Sb_2O_4 (T_{calc} = 600°C, t_{calc} = 7h), (p = 1.2 bar, WHSV = 2 $g_{propene}/g_{catalyst}$ h, $m_{Fe2O3+Sb2O4}$ = 0.5 g, Sb:Fe=2; feed composition: 10 mol-% propene, 20 mol-% O_2, balance N_2)

A mixture of Fe_2O_3 and Sb_2O_4 with a Sb:Fe ratio of 2 shows a decrease in activity in proportion to the decrease of the mass of Fe_2O_3. The activity of the mixture with the single compounds was compared in a temperature region, where the reaction is not limited by the oxygen availability, e.g. at 375°C. The results are shown in Figure 3-15.

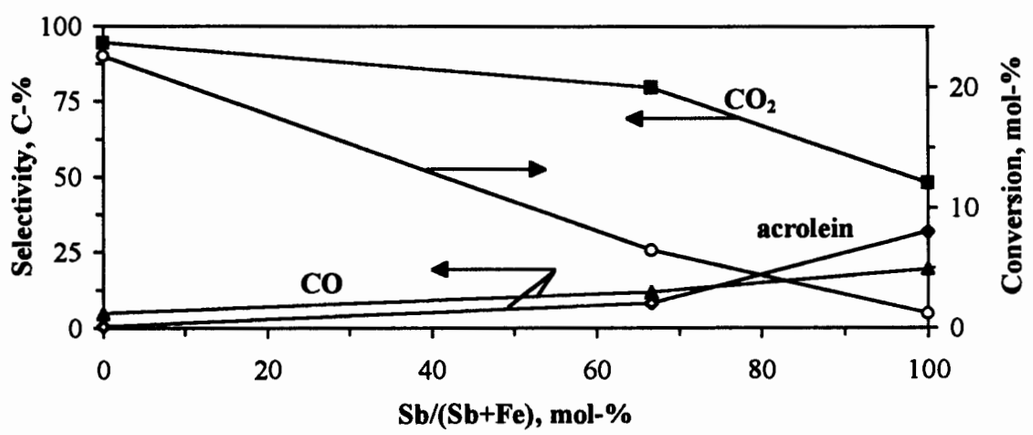

Figure 3-15 Propene conversion and selectivities to acrolein, CO_2 and CO in the partial oxidation of propene over Fe_2O_3, Sb_2O_4 and a mechanical mixture of Fe_2O_3 and Sb_2O_4 (Sb:Fe=2) (T_{calc} = 600°C, t_{calc} = 7h), (T=375°C, p = 1.2 bar, WHSV = 2 $g_{propene}/g_{catalyst}$ h, $m_{catalyst}$ = 0.5 g; feed composition: 10 mol-% propene, 20 mol-% O_2, balance N_2).

No catalytic synergy of the mixture of the two phases was observed, since by definition synergy is indicated when the catalytic performance exhibited by a mixture of oxide phases is higher than the averaged sum of the activities observed when the pure oxides are tested alone (Gaigneaux *et al.*, 1997).

3.3 ROLE OF LATTICE OXYGEN IN THE OXIDATION OF PROPENE

Partial oxidation of propene in the absence of gaseous oxygen will yield valuable insight in the role of lattice oxygen in the partial oxidation of hydrocarbons. Special interest was placed into the influence of the Sb:Fe ratio and calcination temperature.

3.3.1 Propene partial oxidation products and catalyst reduction products

Table 3-9 gives an overview of the products observed during the reduction of iron antimony oxide in propene.

Table 3-9 Mass to charge of ions detected as products in the reduction of iron antimony oxide with propene and the molecules assigned (Eight Peak Index of Mass Spectra, 1991)

m/e	product assigned
18	H_2O
44	CO_2
56	acrolein
67	1,5-hexadiene
78	benzene

A typical TPR spectrum of iron antimonate with Sb:Fe=1 with propene as the reduction agent is shown in Figure 3-16. Generally four phases of the temperature programmed reduction of iron antimony oxide catalysts can be observed: reduction between 250 and 350°C with the simultaneous formation of CO_2 and acrolein, reduction between 500 and 600°C with the formation of CO_2, reduction during the isothermal phase at 650°C between 55 and 95 min reduction time with the formation of CO_2, acrolein and the dehydrogenated

oligomerisation products hexadiene and benzene, finally a reduction during the isothermal phase at 650°C between 95 and 115 min reduction time with the formation of CO_2 and with a decreasing rate of formation the products acrolein, hexadiene and benzene.

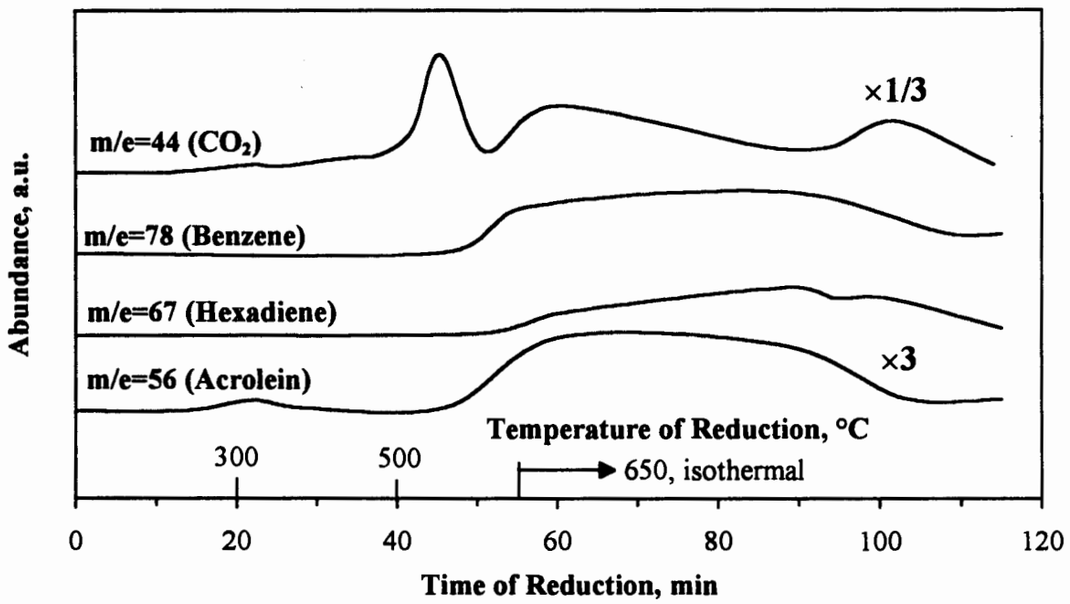

Figure 3-16 Evolution of various species during the temperature programmed partial oxidation of propene over iron antimonate (Sb:Fe=1, T_{calc} = 800°C, t_{calc} = 7 h) (feed: 5% propene in helium; F=20 ml (NTP)/min; temperature program: 10°C/min from 100°C to 650°C, then isothermally for 1 h).

The TPR experiment with propene was interrupted at certain stages of the reduction and the sample was investigated by X-ray diffraction, in order to identify the reduction products of the catalyst. Figure 3-17 shows the XRD pattern of a sample of $FeSbO_4$ before the reduction, in addition the same sample, which has been reduced for 85 min and one where the reduction has been completed (reduction time 115 min).

During the first two reduction steps no phase transition of $FeSbO_4$ using XRD could be detected. The formation of the oxidation products during the first two reduction step can be explained by the utilisation of lattice oxygen without destruction of the $FeSbO_4$ crystallite structure. The MS signals at the first reduction step between 250 and 350°C, where CO_2 and acrolein are formed, are very low and it is therefore likely that it only involves the creation of oxygen vacancies on the catalyst surface. This is supported by

Keulks and Lo (1986), who observed a participation of lattice oxygen of less than a monolayer in the partial oxidation of propene over iron antimony oxide (Sb:Fe=4) at the presence of gaseous oxygen at 350°C. The MS signal showing CO_2 during the second reduction step between 500 and 600°C is quite substantial. Therefore, it is very likely that the reduction at this stage involves oxygen of several oxygen layers of the catalyst lattice, without the destruction of the catalyst structure. An indication about the number oxygen layers involved might be given by the work of Moro-oka *et al.* (1981), who stated that four layers of lattice oxygen participate in the partial oxidation of propene over $FeSbO_4$ at 450°C.

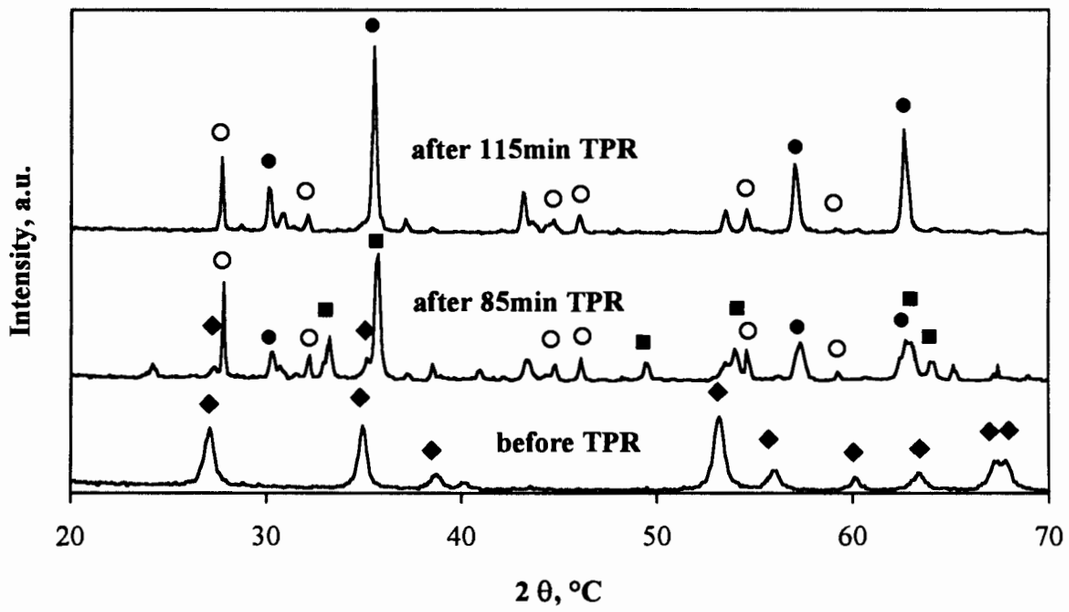

Figure 3-17 X-ray diffraction patterns of iron antimonate (Sb:Fe=1, T_{calc}=800°C, t_{calc}=7 h) at different stages of the reduction with propene. Phases: $FeSbO_4$ (◆), Fe_2O_3 (■), Fe_3O_4 (●) and Sb_2O_3 (○).

The XRD pattern of the freshly calcined sample shows only the existence of the $FeSbO_4$ crystal phase. The same sample which has been reduced for 85 min consists of mainly Sb_2O_3, Fe_2O_3 and Fe_3O_4. The main diffraction peaks of the $FeSbO_4$ phase are only present with low intensities. After completion of the TPR experiment the crystalline phases of Sb_2O_3 and Fe_3O_4 could be detected. From this result it is evident that the crystal structure

of $FeSbO_4$ is completely destroyed during the isothermal reduction at 650°C. Upon release of lattice oxygen $FeSbO_4$ decomposes to Fe_2O_3 and Sb_2O_3, during which partial oxidation products appear to be formed more selectively (Figure 3-16). Subsequently Fe_2O_3 is reduced to Fe_3O_4 and more of the total oxidation product CO_2 is formed. This was expected since iron oxide is well known for its activity for total oxidation of hydrocarbons (Fattore, 1975).

3.3.2 Influence of calcination temperature

Figure 3-18 shows the influence of the calcination temperature on the evolution of CO_2 in the temperature programmed partial oxidation of propene in the absence of gas phase oxygen over iron antimonate (Sb:Fe=1). The area of the low temperature reduction peak (at 550°C) decreases with increasing calcination temperature. Increasing the calcination temperature increases the crystallinity and the crystal size of the samples and decreases the exposed area of the $FeSbO_4$ crystals.

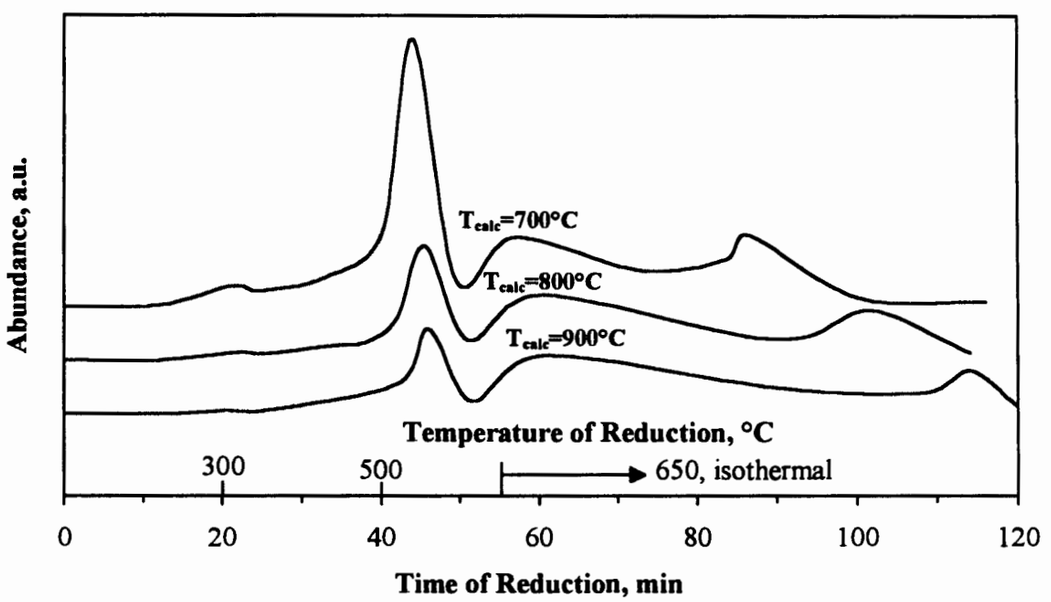

Figure 3-18 Influence of the calcination temperature on the evolution of CO_2 during the temperature programmed partial oxidation of propene in the absence of gas phase oxygen (feed: 5% propene in helium; F_{total}=20ml (NTP)/min; temperature programme: 10°C/min from 100°C to 650°C, then isothermally for 1 h).

At the same time it can be seen that the calcination temperature hardly influences the position of the first two reduction peaks, but does shift the third reduction peak with increasing calcination temperature to higher reduction times in the isothermal section of the reduction.

Upon reduction of iron antimonate the product with the lowest surface energy will be exposed to the gas phase. If this is Sb_2O_3 then the subsequent reduction of Fe_2O_3 will be inhibited. The mobility of Sb_2O_3 is expected to relatively high at 650°C, because this is close to its melting point, which is 656°C, and therefore the phase segregation will be observed in a measurable time span. If the phases are separated, the reduction of iron oxide will start taking place.

Table 3-10 shows the amount of propene converted for the surface reduction, which is the reduction between a reduction time of 0 to 50 minutes (see Section 3.3.1), and during the bulk reduction, which takes place between a reduction time of 50 minutes to the end (120 minutes). The propene conversion during the surface reduction decreases with increasing calcination temperature. Comparison with Table 3-7 shows that there is a relationship between the propene converted and the surface area, i. e. both decrease with increasing calcination temperature. The propene conversion during the bulk reduction doesn't change much and is not a function of the surface area, which was expected.

Table 3-10 Propene conversion during surface reduction (0-50 minutes) and during bulk reduction (50-120 minutes) of iron antimonate as a function of calcination temperature, determined by the area of the ion 42 (propene) signal from GC-MS.

$T_{calc.}$ °C	Propene Conversion, %	
	surface reduction	bulk reduction
700	3.9	9.2
800	1.8	11.3
900	1.5	10.6

Table 3-11 shows the peak ratio of acrolein:CO_2 during certain stages of the reduction, which is equivalent to the acrolein selectivity relative to the selectivity to CO_2. The relative selectivity to acrolein increases strongly during the reduction between 250 and 350°C and increases slightly during the bulk reduction with increasing calcination temperature, however, it is zero during the reduction between 500 and 600°C.

Table 3-11 Influence of calcination temperature on the peak ratio of acrolein to CO_2 during TPR using propene as reducing agent over iron antimonate. (feed 5% propene in helium; F_{total}=20ml (NTP)/min; temperature programme: 10°C/min from 100°C to 650°C, then isothermally for 1 h).

T_{calc}, °C	Peak ratio of acrolein:CO_2		
	$T_{reduction}$ =250-350 °C	$T_{reduction}$ =500-600 °C	$T_{reduction}$ =650 °C (isothermal)
700	0.06	0	0.13
800	0.14	0	0.15
900	0.29	0	0.18

The conversion of propene over iron antimonate (Sb:Fe=1) increases with decreasing calcination temperature in the absence of gaseous oxygen, which is probably due to the increasing surface area. A high reduction state of the catalyst is not desired since the partial oxidation product acrolein is absent. From the results of the partial oxidation of propene in the absence of gaseous oxygen over iron antimonate calcined at different temperatures, it is expected that in the presence of gaseous oxygen the selectivity to acrolein will also increase with increasing calcination temperature, since the catalyst will not reach a high degree of reduction.

3.3.3 Influence of Sb:Fe ratio

Figure 3-19 shows the evolution of the ion 44 (CO_2) and ion 56 (acrolein) peaks in the temperature programmed partial oxidation of propene in the absence of gas phase oxygen over iron antimony oxide containing different Sb:Fe ratios. It is interesting to note that while the position of the first three reduction peaks hardly changes with the Sb:Fe ratios,

the position for the fourth reduction peak, which represents the reduction to Fe_2O_3 to Fe_3O_4, does change. For high Sb:Fe ratios (≥1.75) the third reduction peak doesn't appear under the reduction conditions applied, indicating that the reduction of Fe_2O_3 to Fe_3O_4 only starts once the reduction of $FeSbO_4$ has been completed.

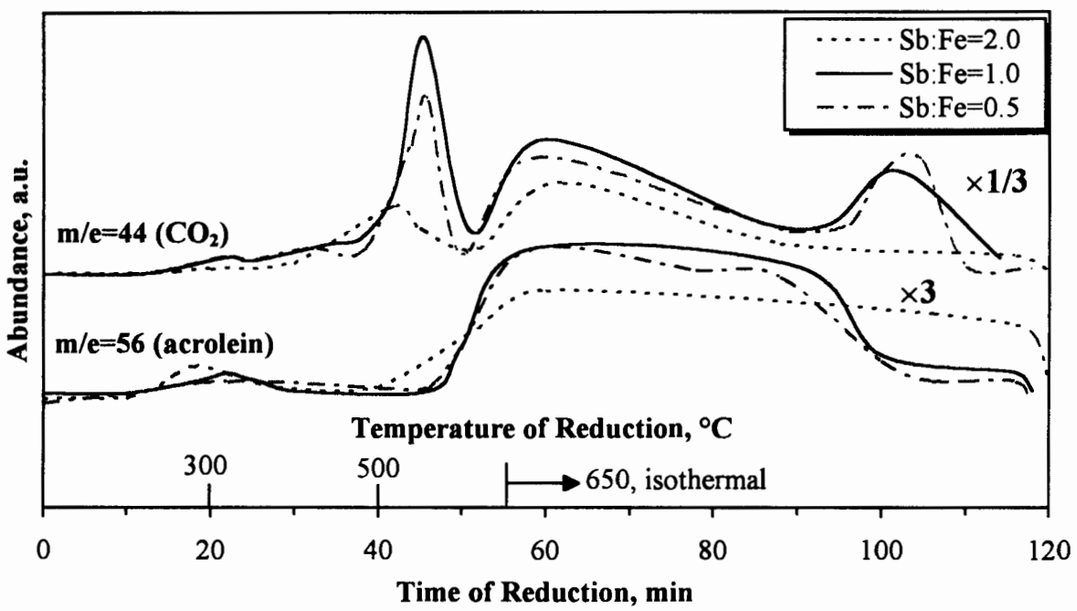

Figure 3-19 Influence of the Sb:Fe ratio on the evolution of the ion 44 (CO_2) and ion 56 (acrolein) peak during the temperature programmed partial oxidation of propene in the absence of gas phase oxygen (T_{calc}=800°C, t_{calc}=7h), (feed: 5% propene in helium; F_{total}=20ml (NTP)/min; temperature programme: 10°C/min from 100°C to 650°C, then isothermally for 1 h).

The conversion (see Figure 3-20) was determined during the surface reduction between T=250 and 600°C and during the bulk reduction from T=600°C to the end of the reduction, where the destruction of the bulk of the catalyst is taking place. The amount of propene converted during the bulk reduction is constant for catalysts containing a Sb:Fe ratio between 0.25 and 1.25 and then decreases for higher ratios. The decrease for higher Sb:Fe ratios is probably due to the fact that the reduction was not complete for the given temperature program, which can be observed in Figure 3-19, where the last reduction peak

for a ratio Sb:Fe=2 at t=100 min doesn't appear anymore. The maximum conversion of propene occured at a Sb:Fe ratio of 1.25.

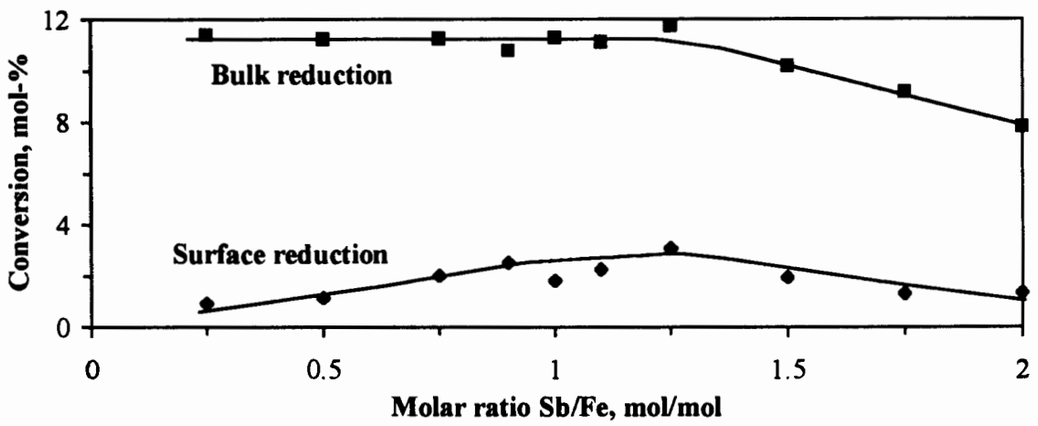

Figure 3-20 Propene conversion during the temperature programmed partial oxidation of propene in the absence of gas phase oxygen (T_{calc}=800°C, t_{calc}=7h), (feed: 5% propene in helium; F_{total}=20ml (NTP)/min; temperature programme: 10°C/min from 100°C to 650°C, then isothermally for 1 h).

The change in the selectivity to acrolein relative to the selectivity to CO_2 has been determined by the change of the ratios of the respective peak areas during the various reduction steps. Figure 3-21 shows the influence of changing the Sb/Fe ratio in the samples on the ratios of the peak areas of acrolein to CO_2. Figure 3-21 indicates that the selectivity to acrolein relative to CO_2 during the first reduction step between 250 and 350°C increases with increasing antimony content, especially for Sb:Fe>1. CO_2 is the sole product independent of the antimony to iron ratio during the reduction between 500 and 600°C, the relative selectivity to acrolein is therefore zero. The relative selectivity to acrolein during the bulk reduction of the catalyst ($T_{reduction}$=650°C isothermal) increases only slightly with increasing antimony to iron ratio, which is similar to the result of Aso *et al.* (1980), who observed that the bulk reduction of SbFe1 and SbFe2 is independent of the Sb:Fe ratio.

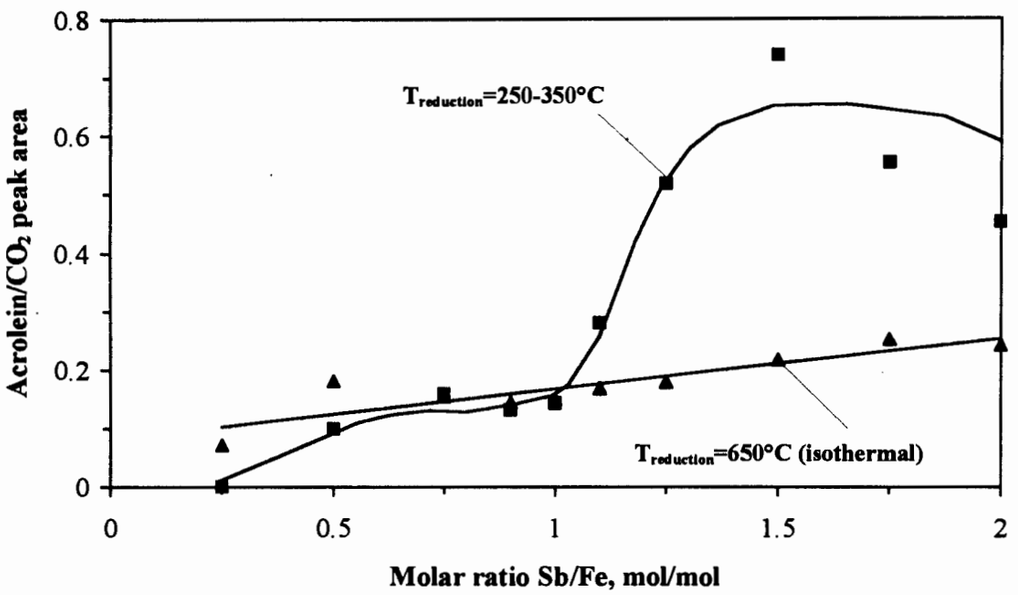

Figure 3-21 Influence of antimony to iron ratio in iron antimony oxide catalysts (T_{calc}=800°C, t_{calc}=7 hrs) on the relative selectivity of acrolein to CO_2 during TPR using propene as reducing agent. (feed 5% propene in helium; F_{total}=20ml (NTP)/min; temperature programme: 10°C/min from 100°C to 650°C, then isothermally for 1 h).

3.3.4 Isothermal Propene Oxidation in the Presence and Absence of Gas Phase Oxygen

The isothermal propene oxidation in the presence of gas phase oxygen was compared with the experiment performed in the absence of gas phase oxygen as a function of time on stream. Figure 3-22a shows the conversion of propene over iron antimony oxide (Sb:Fe=1) at 375°C both in the presence and in the absence of gas phase oxygen. The conversion in the absence of gaseous oxygen drops within 5 minutes time on stream to below 5 mol-%, which shows that the activity is dependent on the amount of available oxygen and that the depleted surface lattice oxygen is not readily regenerated by bulk lattice oxygen.

Even in the case of propene oxidation in the presence of gaseous oxygen the catalyst loses its initial high activity, showing that the initial high oxidation state cannot be maintained by the gaseous oxygen. Like the U-Sb-oxide system (Grasselli and Suresh, 1972), the Fe-Sb-oxide system needs to be in a high oxidation state.

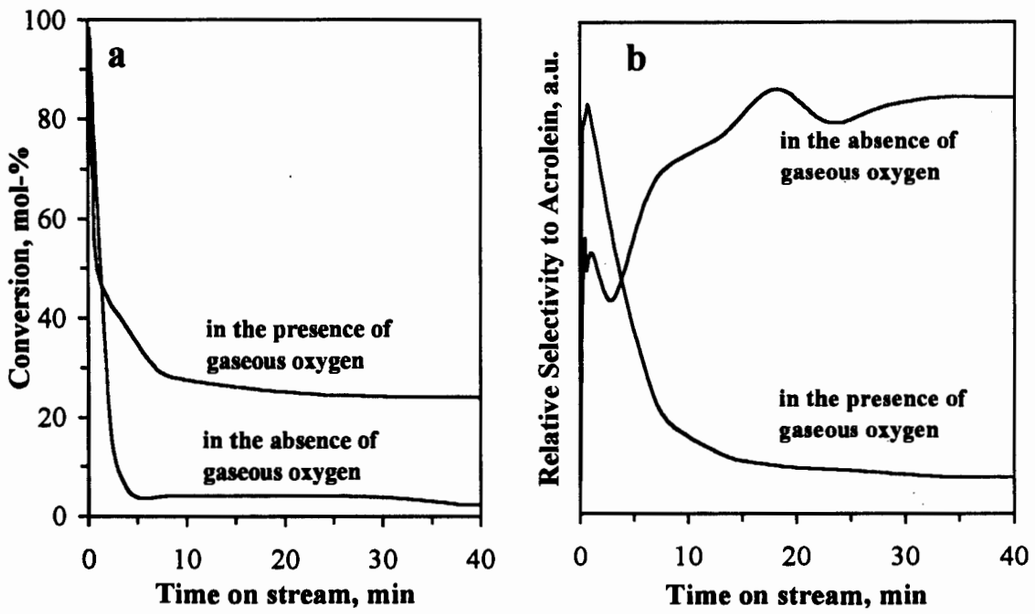

Figure 3-22 Formation of CO_2 and acrolein during propene oxidation in the presence and absence of gaseous oxygen over iron antimonate (Sb:Fe=1; T_{calc}=800°C, t_{calc}=7 h) at 375°C (feed: 5% propene in helium, F_{total}=20 ml (NTP)/min (absence of O_2); 5% propene in helium, F_{total}=21 ml (NTP)/min, F_{O2}=1 ml(NTP)/min (presence of O_2).

The relative selectivity to acrolein was determined by the ratio of the MS-signal of acrolein to the MS-signal of CO_2. The relative selectivity to acrolein (Figure 3-22b) in the presence of gaseous oxygen shows an initial maximum, but decreases thereafter to the steady state value, which is reached after about 20 minutes time on stream. The relative selectivity to acrolein in the absence of gaseous oxygen increases slightly with time on stream until steady state is reached.

3.4 PARTIAL OXIDATION OF PROPENE OVER IRON ANTIMONY OXIDE

In this section the partial oxidation between propene and propane will be compared. The influence of the cofeedstocks hydrogen and water has been investigated in order to explain the different behaviour of alkanes and alkenes in partial oxidation reactions. Furthermore the reaction parameters, temperature and time on stream, and the catalyst parameters,

calcination temperature and Sb:Fe ratio, have been investigated in more detail. This will complete the work, which was done in the absence of gaseous oxygen and offer a comparison between the two reaction conditions (absence of gaseous oxygen vs. presence of gaseous oxygen).

3.4.1 Comparison of the partial oxidation of propene with propane

There is a strong economic incentive to substitute olefins with paraffins as feedstock for partial oxidation reactions because of the considerable price difference (Kim and Woo, 1994). Since no results of the partial oxidation of paraffins over iron antimony oxide are reported in the literature, the partial oxidation of propane has been compared with propene.

In Figure 3-23 the yields of acrolein and carbon oxides ($CO+CO_2$) are compared for the two feedstocks propane and propene as a function of the reaction temperature over iron antimony oxide at same reaction conditions.

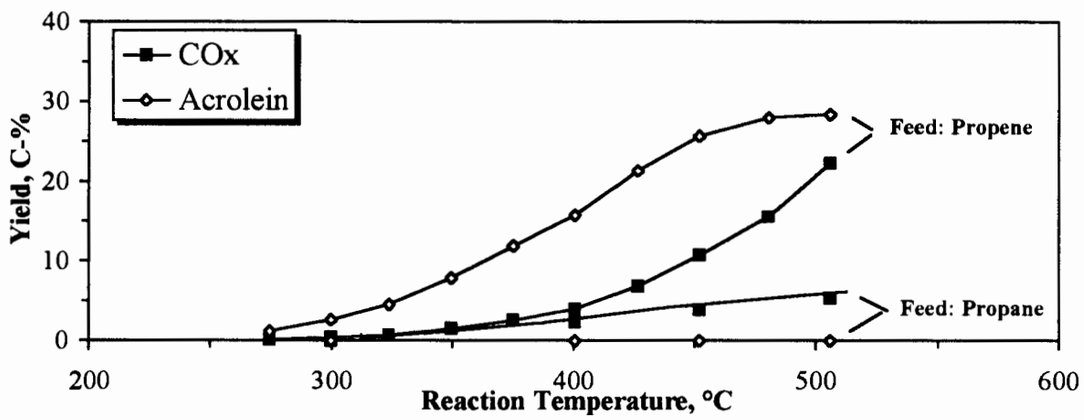

Figure 3-23 Yields of acrolein and carbon oxides ($CO+CO_2$) in the partial oxidation of propene and propane over iron antimony oxide (Sb:Fe=1.5, T_{calc} = 900°C, t_{calc} = 7h) as a function of reaction temperature (p = 1.2 bar, WHSV = 2 $g_{hydrocarbon}/g_{catalyst}$ h, $m_{catalyst}$ = 0.5 g; feed composition: 10 mol-% hydrocarbon, 20 mol-% O_2, balance N_2).

Propane is much less reactive than propene which is expected since it is known that alkanes in general are less reactive than alkenes (Kim and Woo, 1994).

For propene as feedstock the yield of acrolein increases from 1.2 C-% at 275°C in a S-shaped curve to 28.5 C-% at 505°C while the yield of carbon oxides increases exponentially from 0.2 C-% at 275°C to 22.3 C-% at 505°C. The stronger increase in the yield of carbon oxides indicates a higher activation energy to these products. The only detectable carbon products in the partial oxidation of propane were carbon oxides, which were produced with a maximum yield of 5.4 C-% at 505°C. This experiment showed that iron antimony oxide is not suitable to catalyse a reaction path of propane that leads to useful products, e.g. acrolein or propene, under the chosen experimental conditions.

In the partial oxidation of propene acrolein is formed with a selectivity of 88.5 C-% at 275°C, which drops to 53.1 C-% at 505°C. The selectivity to the carbon oxides increases with increasing reaction temperature, indicating a higher activation energy for the formation of carbon oxides than for the formation of acrolein.

3.4.2 Effect of cofeeding hydrogen and cofeeding water

A set of experiments was performed in order to test whether propane reacts via a surface alkyl species which leads to total combustion products while propene reacts via a surface allyl species. By cofeeding hydrogen to propene it was expected that an alkyl species can be formed more readily, which would lead to an increase in combustion products. The results were compared with partial oxidation of propene in the presence of water, which might also be formed when cofeeding hydrogen and might affect the selectivity of the reaction (Saleh-Alhamed *et al.*, 1993,1995,1996).

Figure 3-24 shows the conversion of propene and the selectivity to acrolein in the partial oxidation of propene over iron antimony oxide, compared with the cases of water (1.5 mol-%) or hydrogen (1.5 mol-%) being added to the feed.

The conversions (Figure 3-24a) in all three cases increase from 12 C-% at 350°C to 47 C-% at 500°C. The three curves are almost identical for the temperature range investigated, showing that there is very little effect of the co-feedstock on the conversion of propene.

The selectivity to acrolein (Figure 3-24b) decreases in the three investigated cases from between 84 - 87 C-% at 350°C to between 49-52 C-% at 500°C. The selectivity to acrolein in the case of water being co-fed is equal or higher than in the two other cases. It is known

from the work of Saleh-Alhamed (1993,1995,1996) that cofeeding water in the propene partial oxidation increases the selectivity to acrolein, when using Sb/Sn/V oxide catalysts.

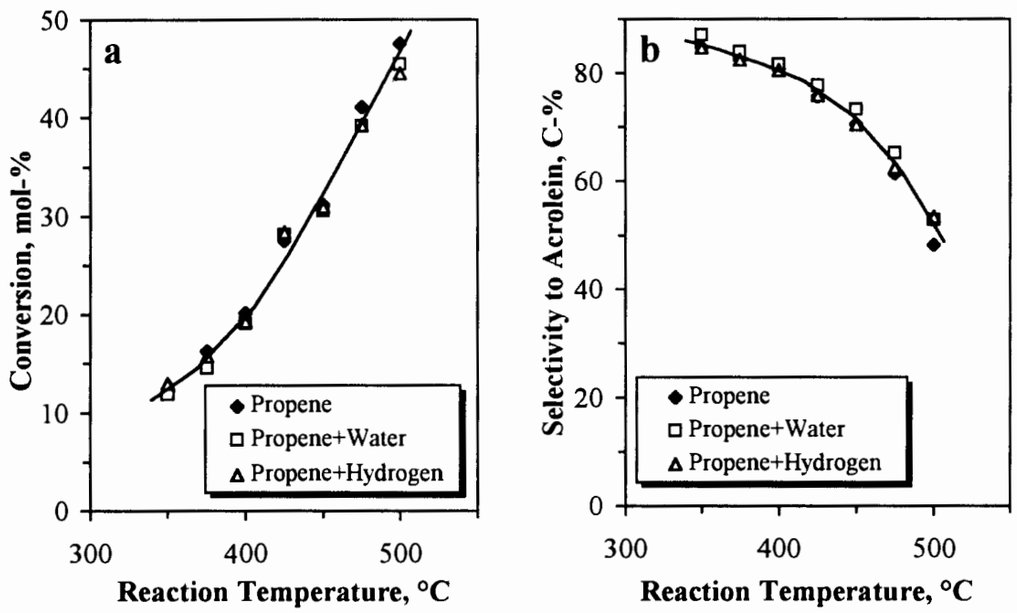

Figure 3-24 Conversion of propene (a) and selectivity to acrolein in the partial oxidation of propene over iron antimony oxide as a function of reaction temperature for cofeeding hydrogen and water (Sb:Fe=1.5, T_{calc}=900°C, t_{calc}=7h), (p = 1.2 bar, WHSV = 2 $g_{propene}/g_{catalyst}$ h, $m_{catalyst}$ = 0.5 g; feed composition: 10 mol-% hydrocarbon, 20 mol-% O_2, cofeedstock: 1.5 mol-% H_2 or H_2O, balance N_2).

Cofeeding hydrogen showed little effect, probably because of the small amount that was used (higher hydrogen partial pressures couldn't be used because of safety reasons) and because only a small fraction of hydrogen reacted: 8 % conversion of H_2 at 350°C, 19 % conversion of H_2 at 450°C. If water was formed when cofeeding hydrogen, the water concentration was much lower than in the water co-feeding experiments and no significant effect can be expected.

3.4.3 Influence of calcination temperature

3.4.3.1 Changing reaction temperature

The yields of the reaction products acrolein and carbon oxides for the partial oxidation of propene over iron antimony oxide (Sb:Fe=1.5) are shown in Figure 3-25 for the calcination temperatures 500°C, 700°C and 900°C as a function of the reaction temperature.
The yields of acrolein and carbon oxides increase with reaction temperatures because of an increase of reaction rate with increasing reaction temperature. The yields of carbon oxides increase stronger with increasing reaction temperature than the yields of acrolein, indicating that the activation energy for the formation of carbon oxides is higher than for the formation of acrolein.

The curves for the yields of acrolein and carbon oxides for calcination temperature 500 and 700°C start to flatten out above reaction temperatures of 400°C. A calculation of the oxygen conversion showed that limited oxygen availability might be the reason for this observation, while for the reaction over the third catalyst (T_{calc}=900°C) oxygen limitation has not yet been reached and therefore no flattening out of the curve is observed.

The activity of the catalysts decreases with increasing calcination temperature, especially above 700°C, which might be attributed to a decrease in surface area with increasing calcination temperature (see Table 3-7).

An increase in calcination temperature of iron antimonate from 500°C to 700° doesn't affect the yield of acrolein, the two curves are almost identical, which might be explained by the similar crystallinity of the two catalysts (see Figure 3-5). The yield of acrolein is the lowest for a calcination temperature of 900° up to a reaction temperature of 440°C, where the curve intercepts the two other curves and shows the highest yields with increasing reaction temperature. This fact can be attributed to the oxygen availability as discussed previously.

Increasing calcination temperatures results in decreasing yields of carbon oxides. However, the difference in the yields at the calcination temperatures of 500°C and 700°C is small,

while the yields drop strongly at a calcination temperature of 900°C. The selectivity to acrolein is highest for the catalyst calcined at 900°C, indicating that acrolein is more selectively formed over a more crystalline catalyst. Amorphous material at the same time is responsible for an increased formation of carbon oxides as indicated by the high yields of carbon oxides over iron antimony oxide calcined at 500 and 700°C.

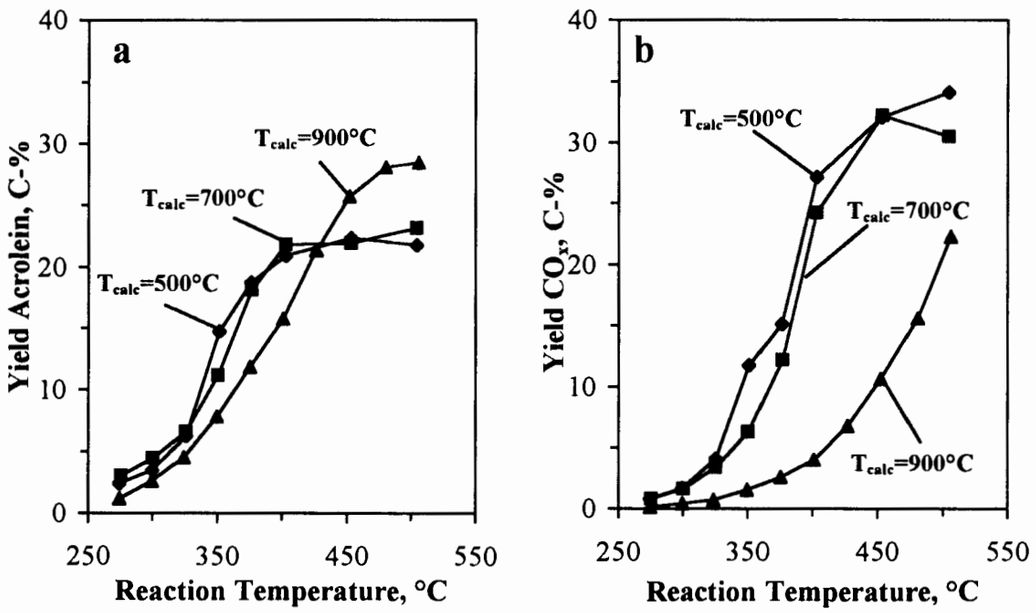

Figure 3-25 Yields of acrolein (a), carbon oxides (b) and oxygen conversion for the partial oxidation of propene over iron antimony oxide (Sb:Fe=1.5) as a function of reaction temperature and calcination temperature, p = 1.2 bar, WHSV = 2 $g_{propene}/g_{catalyst}$ h, $m_{catalyst}$ = 0.5 g; feed composition: 10 mol-% hydrocarbon, 20 mol-% O_2, balance N_2.

3.4.3.2 Influence of time on stream

The influence of time on stream on the partial oxidation of propene over iron antimonate was investigated at a constant reaction temperature of 350°C for the calcination temperature 700, 800 and 900°C, because it seems from the previous experiment that the calcination temperature of 500°C doesn't change the catalytic properties significantly compared to a calcination temperature of 700°C, because of their similar crystallinity.

Figure 3-26 shows the yields of acrolein, CO_2 and CO as a function of time on stream for the partial oxidation of propene over iron antimonate, calcined at three different temperatures (700°C, 800°C and 900°C).

The yield of acrolein (Figure 3-26a) goes through a maximum during the first minutes time on stream and decreases to its steady state value, which is reached after about 100 minutes time on stream. With decreasing calcination temperature the maximum yield is shifted to higher times on stream, but also to higher values. The steady state values of the yield of acrolein increases with decreasing calcination temperature, which indicates that the yields increase with increasing surface area of the catalyst (see Table 3-7).

Similar observations are made for the yield of CO_x (Figure 3-26b). The curves have a maximum during the first minutes time on stream, before decreasing to the steady state values. The yield of carbon oxides for T_{calc}=700°C decreases more drastically than for the other calcination temperatures. No explanation can be given for this. The decrease in yields of acrolein and carbon oxides with time on stream shows that the catalysts lose some of their activity within the first 100 minutes time on stream.

From the three investigated catalysts the one calcined at the lowest temperature (700°C) showed the highest activity, which coincides with the highest surface area obtained at this calcination temperature (see Table 3-7). The selectivities to acrolein were similar for the different calcination temperatures, but were difficult to determine due to the scatter in the data.

The different shape of the curves for the yields of acrolein compared to those curves which show the yield of carbon oxides indicated that different oxygen species are involved in the formation of partial oxidation and total oxidation products.

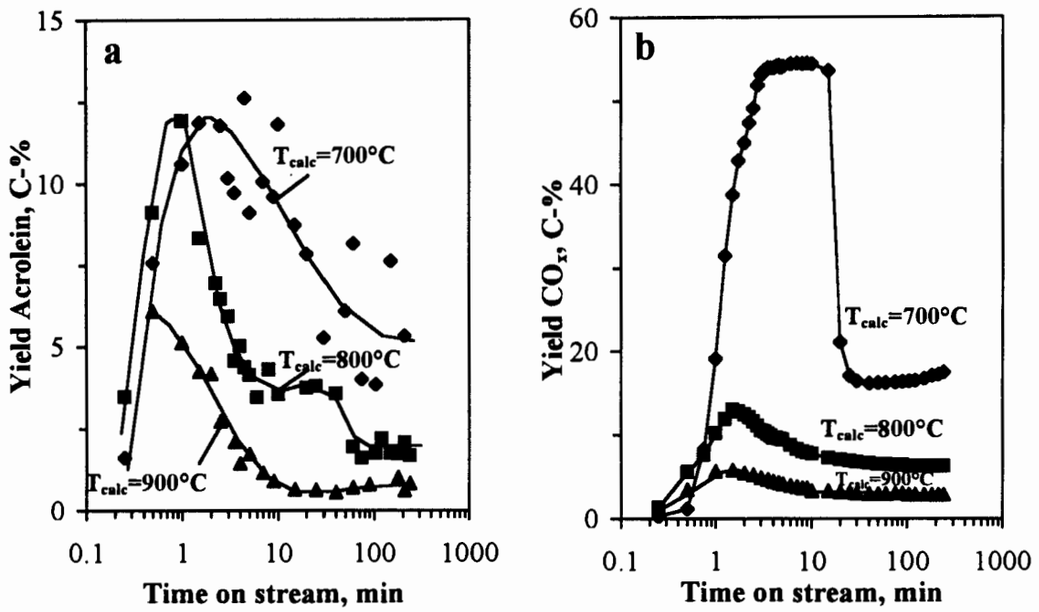

Figure 3-26 Yields of acrolein (a) and COx (b) during the partial oxidation of propene as a function of time on stream over iron antimonate (Sb:Fe=1.0), calcined at 700, 800 and 900°C, t_{calc}=7h, $T_{reaction}$ = 350°C, p = 1.2 bar, WHSV = 2 $g_{propene}/g_{catalyst}$; feed composition: 10% propene, 20 % O_2, balance N_2.

3.4.4 Influence of Sb:Fe ratio

The influence of the antimony content in the catalyst has been studied as a function of time on stream in a fixed bed reactor. This was done in order to be able to compare the results with those obtained in the isothermal runs in the absence of gaseous oxygen.

Figure 3-27 shows the yields of acrolein (Figure 3-27a) and of carbon oxides (Figure 3-27b) as a function of time on stream for the partial oxidation of propene over iron antimony oxide containing different Sb:Fe ratios.

The yield of acrolein passes through a maximum value after 0.5 to 5 minutes time on stream depending on the Sb:Fe ratio and reaches its steady state value after approximately 100 min, indicating a change of surface structure with time on stream. The maximum yield of acrolein doesn't change significantly for iron antimony oxide catalysts containing

Sb:Fe≥1. However, the highest yield of acrolein at steady state increases with increasing Sb:Fe ratio.

The maximum yields of carbon oxides occur after approximately 1 to 3 minutes time on stream, depending on the Sb:Fe ratio. The steady state values are reached between 60 and 200 minutes time on stream, the time until steady state is reached decreases with increasing Sb:Fe ratios. The maximum yield and the steady state value for the yield of carbon oxides decreases with increasing Sb:Fe ratio.

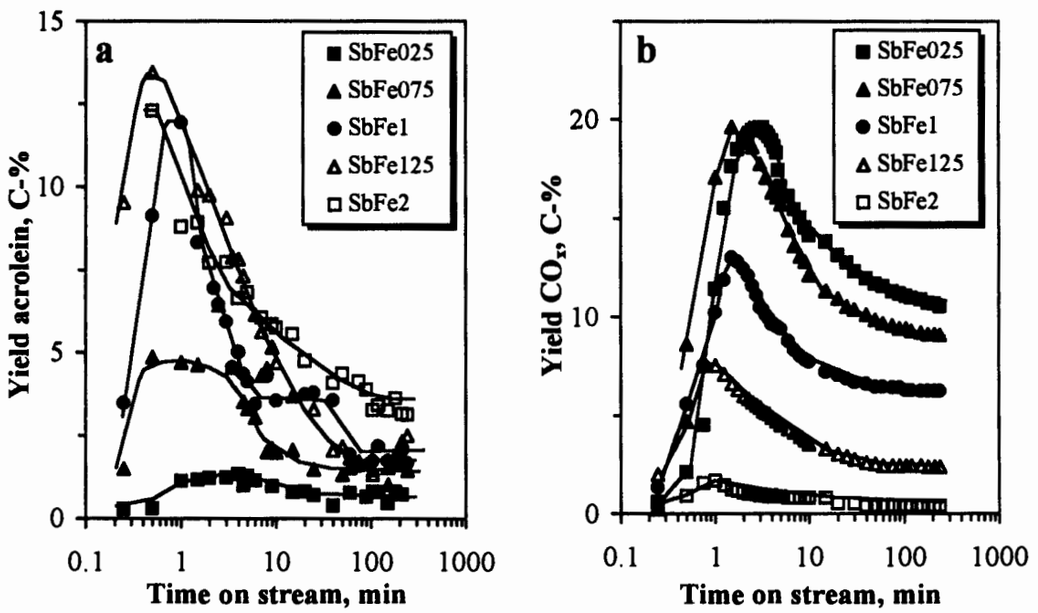

Figure 3-27 Yields of acrolein (a) and carbon oxides (b) during the partial oxidation of propene as a function of time on stream over iron antimony oxide containing various Sb:Fe ratios, T_{calc} = 800°C, t_{calc} = 7 h, $T_{reaction}$ = 350 °C, p = 1.2 bar, WHSV = 2 $g_{propene}/g_{catalyst}$; feed composition: 10% propene, 20 % O_2, balance N_2.

Figure 3-28 shows the selectivity to acrolein (Figure 3-28a) and the carbon monoxide content in the carbon oxides (Figure 3-28b) as a function of time on stream for various iron antimony oxides containing different Sb:Fe ratios.

The selectivity to acrolein for SbFe2 is almost constant at about 90 C-% with time on stream. For all other catalysts the selectivity drops from a initially higher value to the steady state value. Generally the selectivity to acrolein decreases with decreasing Sb:Fe ratio.

The carbon monoxide content in the carbon oxides increases within four minutes time on stream from the minimum value to the maximum value. With the exception of SbFe2, where the maximum value is constant with time on stream, the values decrease again with time on stream to a steady state value. The steady state value is the highest carbon monoxide content with 28% is reached for SbFe2. With decreasing antimony content in iron antimony oxide the steady state value of the carbon monoxide content decreases, which indicates a better total combustion capability of iron antimony oxide catalyst with low antimony content.

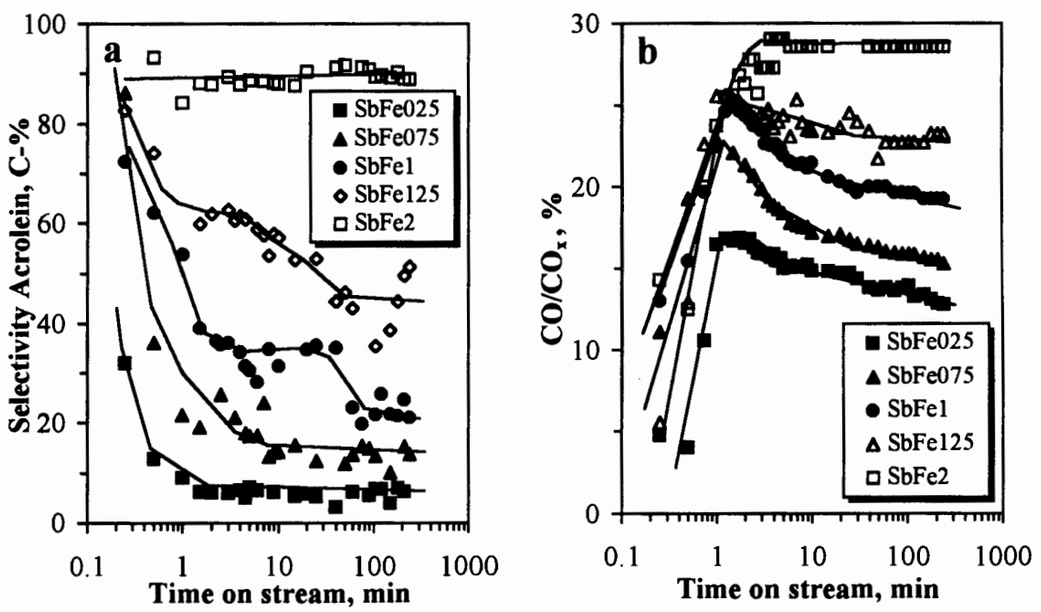

Figure 3-28 Selectivity to acrolein (a) and carbon monoxide content in carbon oxides (b) during the partial oxidation of propene as a function of time on stream over iron antimony oxide containing various Sb:Fe ratios, T_{calc} = 800°C, t_{calc} = 7 h, $T_{reaction}$ = 350 °C, p = 1.2 bar, WHSV = 2 $g_{propene}/g_{catalyst}$; feed composition: 10% propene, 20 % O_2, balance N_2.

Steady state values

The steady state values for the selectivities to acrolein, CO and CO_2 are shown in Figure 3-29a. The results are very similar to the findings of Aso *et al.* (1980), although the reaction parameters used by them were slightly different (T=400°C, $p_{propene}$=0.05 bar, W/F = 0.2 g·s/cm^3).

The selectivity to carbon oxides decreases with increasing Sb content from almost 100 C-% for Fe_2O_3 (Sb=0%) to about 10 C-% in the Sb-rich region. However, the selectivity to carbon oxides increases again to 62 C-% for Sb_2O_4 (Sb=100%),. The selectivity to acrolein on the contrary increases with increasing Sb content and decreases again for Sb_2O_4, showing that $FeSbO_4$ and Sb_2O_4 are both necessary for a high selectivities to acrolein in the partial oxidation of propene.

The steady state values for the propene conversion and the yields of acrolein, CO and CO_2 are shown in Figure 3-29b.

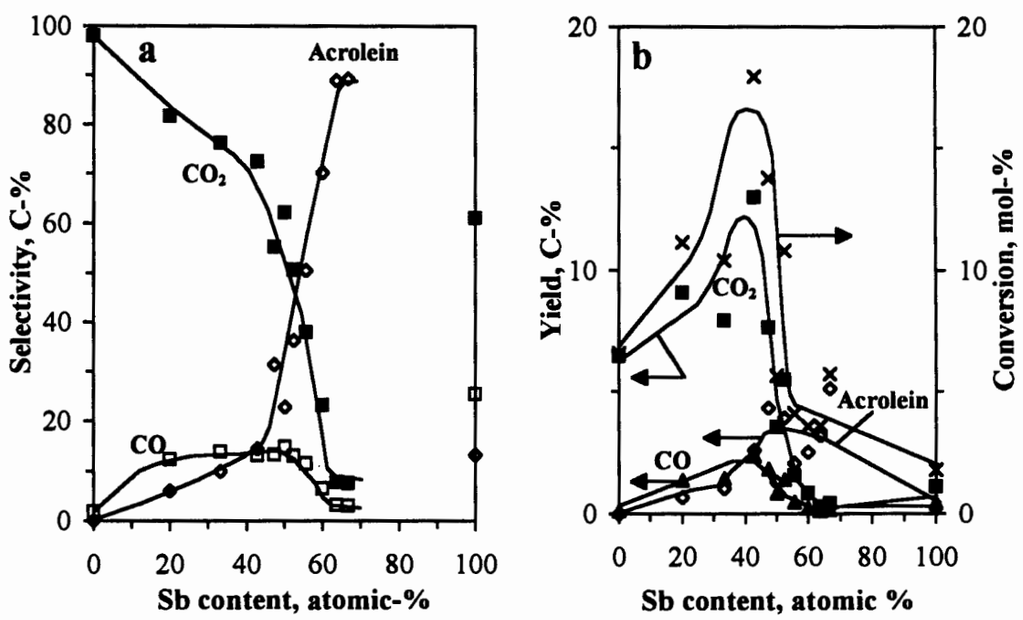

Figure 3-29 Selectivity to acrolein, CO and CO_2 (a) and conversion and yields of acrolein, CO and CO_2 (b) after 4h time on stream for the partial oxidation of propene over iron antimony oxide containing various Sb:Fe ratios; T_{calc} = 800°C, t_{calc} = 7 h, $T_{reaction}$ = 350 °C, p = 1.2 bar, WHSV = 2 $g_{propene}/g_{catalyst}$; feed composition: 10% propene, 20 % O_2, balance N_2.

The highest conversion (X=18 mol-%) of propene is found for a Sb content in the catalyst of 40%, where also the highest yield of 15 C-% of carbon oxides occurs. A further increase in the Sb-content results in a decrease in carbon oxide yields. The maximum yield of acrolein occurs at a Sb-content of close to 60%, which is similar to the result of Aso *et al.* (1980).

An excess of Sb in iron antimony oxide is therefore necessary in the partial oxidation of propene to obtain high selectivities to acrolein and more importantly high yields of acrolein.

3.4.5 Influence of pre-treatment of catalyst

Before the partial oxidation the catalyst has to be heated to the reaction temperature. There are several ways, how it can be done. Here the two cases of heating up in flowing air or flowing nitrogen shall be investigated.

During the initial stage of the reaction a difference in the yields of the various product compounds were observed between the partial oxidation of propene over iron antimonate heated in air (Figure 3-30a) and heated in nitrogen (Figure 3-30b). The steady state values of the yields of acrolein, CO and CO_2 are identical for the two cases within the experimental error.

The maximum values of the yields, which was reached within 0.5 and 2 minutes time on stream, was higher for the catalyst pre-treated in air, however, the yield of acrolein increases stronger than the yields of carbon dioxide and carbon monoxide.

This might be explained by a higher oxidation state of the catalyst when passing air over the catalyst, which results in higher initial selectivity to acrolein. By passing nitrogen over the catalyst, the catalyst might partially be reduced and the selectivity to acrolein is therefore lower.

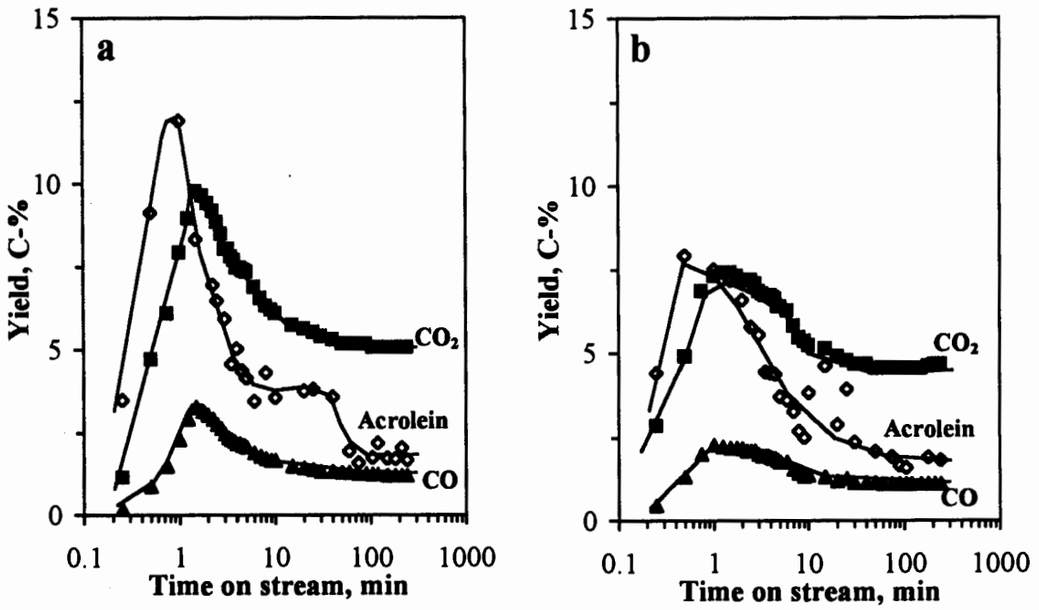

Figure 3-30 Yields of acrolein, CO and CO_2 during the partial oxidation of propene as a function of time on stream over iron antimony oxide (Sb:Fe=1.0, T_{calc} = 800°C, t_{calc} = 7 h) for different kinds of pre-treatments, a: catalyst pre-heated in flowing air (100 ml(NTP)/min),b: catalyst pre-heated in flowing nitrogen (100 ml(NTP)/min, $T_{reaction}$ = 350 °C, p = 1.2 bar, WHSV = 2 $g_{propene}/g_{catalyst}$; feed composition: 10% propene, 20 % O_2, balance N_2.

3.5 INFLUENCE OF ALKENE CHAIN LENGTH

The partial oxidation of α-olefins in the range of ethene to 1-nonene were studied in order to gain insight into the mechanism involved in α-olefin oxidation. The printouts of the GC together with the identified products are given in Appendix V.

The influence of the reaction parameters: temperature and space time were studied for the partial oxidation of α-olefins in the carbon number range two to nine.

3.5.1 Ethene Oxidation

The only products observed for the oxidation of ethene were the combustion products CO and CO_2.

3.5.1.1 Influence of reaction temperature

As a first reaction parameter the reaction temperature was changed between 325°C to 500°C. The only products observed were carbon oxides. Figure 3-31 shows the influence of the reaction temperature on the yields of CO and CO_2. The product yields increase exponentially with increasing reaction temperature, with the yield of CO_2 being higher than the yield of CO at all temperatures. The highest observed conversion of ethene was only 10 mol-% at a reaction temperature of 500°C.

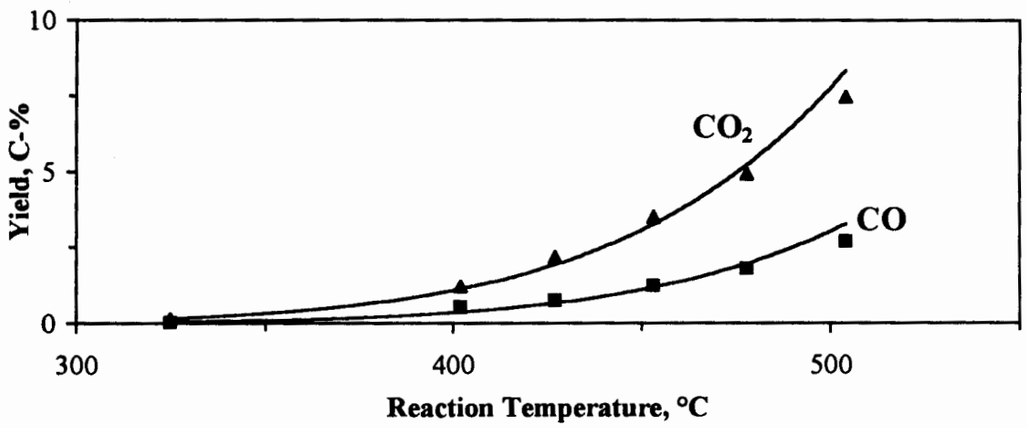

Figure 3-31 Influence of reaction temperature on yields of CO_2, CO and CO_x in the partial oxidation of ethene over iron antimony oxide; Sb:Fe=1.5, T_{calc} = 900°C, t_{calc} = 7h, p = 1.2 bar, F = 110 ml(NTP)/min, $m_{catalyst}$ = 0.5 g; feed composition: 10 mol-% ethene, 20 mol-% O_2, balance N_2.

The low reactivity and high selectivity to total oxidation products might be explained by the lack of stable C_2-intermediates on the catalyst surface (e.g. allylic species), which was shown by Dent and Kokes (1970) on the basis of IR studies, and the lack of stable C_2-oxygenates under the applied conditions.

3.5.2 Propene Oxidation

The reaction products observed were acrolein, carbon oxides (CO and CO_2) and water.

3.5.2.1 Influence of reaction temperature

The influence of reaction temperature for the partial oxidation of propene over iron antimony oxide was already shown in Figure 3-23 (Section 3.4.1), where propene and propane as feedstock were compared. The reaction temperature was changed between 275°C and 505°C. The yield of acrolein increases from 1.2 C-% at 275°C in an S-shaped curve to 28.5 C-% at 505°C while the yield of carbon oxides increases exponentially from 0.2 C-% at 275°C to 22.3 C-% at 505°C. Acrolein might be further oxidised in a consecutive reaction to carbon oxides at reaction temperatures above 450°C, this is indicated by a flattening out of the yield of acrolein in this temperature region.

3.5.2.2 Influence of space time

In order to decouple the formation of carbon oxides by the consecutive oxidation of acrolein from the direct combustion of propene, the space time of the reactants in the reactor was changed and the propene conversion and product selectivities monitored. Figure 3-32 shows the change in conversion (Figure 3-32a), in selectivity to acrolein (Figure 3-32b) and the CO-content in the carbon oxides (Figure 3-32c) with changing space time between 0.3 and 1.3 s for the reaction temperatures 350, 375 and 400°C.

The conversion increases with increasing space time and increasing temperature. The curves can be extrapolated to zero space time, where the conversion becomes zero.

The selectivity to acrolein increases with decreasing space times and flattens out at low space times for all three investigated temperatures. This indicates the consecutive reaction of acrolein to carbon oxides at high space times. The primary selectivity to acrolein decreases with increasing reaction temperature.

The selectivity to carbon oxides behaves contrary to acrolein, i. e. it increases with increasing space time and with increasing reaction temperature.

The fact the primary selectivity to acrolein decreases with increasing temperature, while the primary selectivity to carbon oxides increases with increasing temperature, indicates that the activation energy for total oxidation is higher than for partial oxidation.

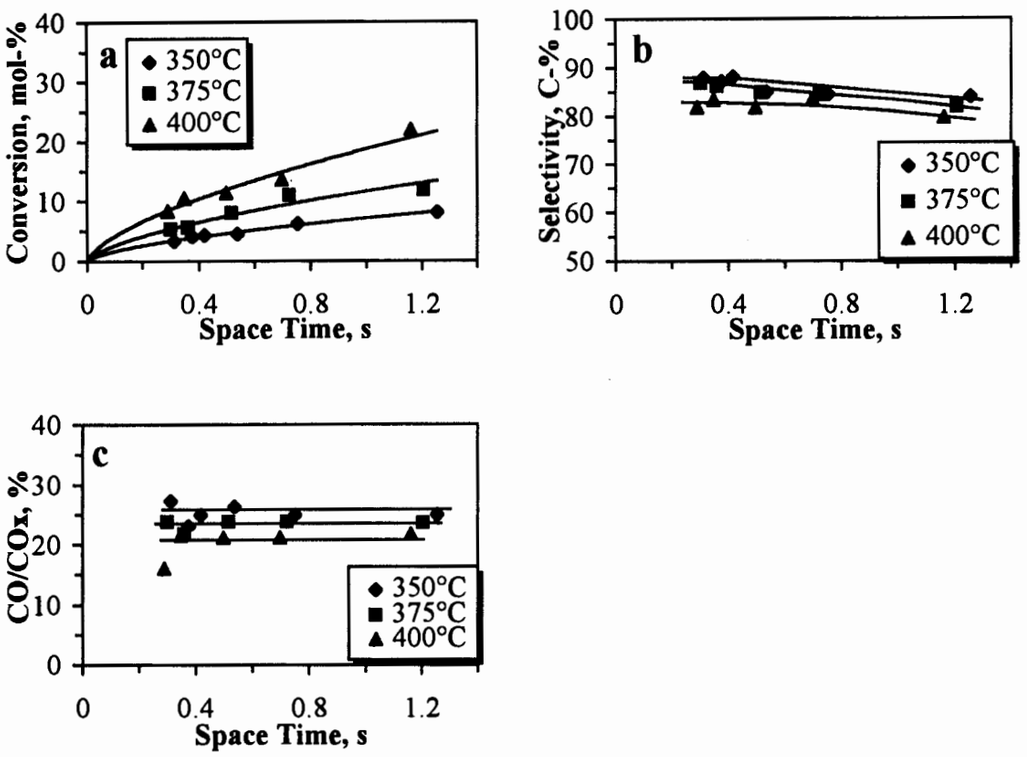

Figure 3-32 Influence of space time on the conversion (a), selectivity to acrolein (b) and on the CO content in the carbon oxides (c) for the partial oxidation of propene over iron antimony oxide at different reaction temperatures; Sb:Fe=1.5, T_{calc} = 900°C, t_{calc} = 7h, p = 1.2 bar, feed composition: 10 mol-% propene, 20 mol-% O_2, balance N_2, $m_{catalyst}$ = 0.5 g.

No change in the CO content of the total oxidation products was observed with changing space time, thus indicating the parallel formation of CO and CO_2. However, the CO content decreases with temperature, indicating that the activation energy for the CO_2 formation is higher than for the CO formation.

3.5.3 1-Butene Oxidation

In the 1-butene oxidation the formation of an aldehyde (2-butenal) and of total oxidation products, CO and CO_2, can be observed. In addition the double bond isomers trans- and cis-2-butene and the oxidative dehydrogenation product 1,3-butadiene were formed. Cracking products (C-number<3) can also be formed at high reaction temperatures. In the

following the reaction parameters temperature and partial pressures are investigated in greater detail.

3.5.3.1 Influence of reaction temperature

The influence of reaction temperature on the yields in the partial oxidation of 1-butene is shown in Figure 3-33. The temperature was varied between 300 and 500°C. The products which are produced with the highest yields over the investigated temperature range are 2-butenal and 1,3-butadiene, in almost the same amounts.

The shape of the curves for the yields of carbon oxides and the cracking products increase exponentially with temperature, while the curves for the yields of 2-butenal and 1,3-butadiene have a "S"-shape and the curve for the yield of 2-butene decreases for reaction temperatures above 450°C. This might indicate that for high reaction temperatures (T>450°C) a further reaction of butenal, 1,3-butadiene and 2-butene to the more stable products carbon oxides and cracking products occurs.

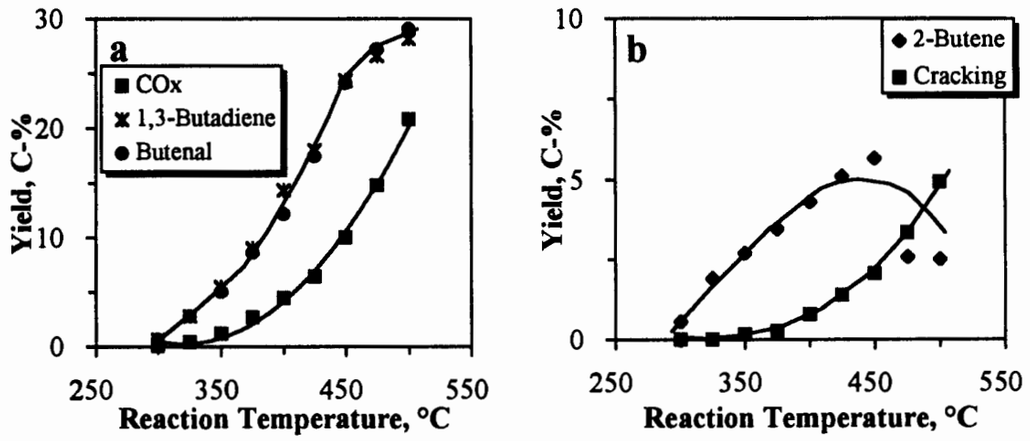

Figure 3-33 Influence of reaction temperature on the yields of CO_x, 1,3-butadiene and 2-butenal (a) 2-butene and cracking products (b) in the partial oxidation of 1-butene over iron antimony oxide; Sb:Fe=1.5, T_{calc} = 900°C, t_{calc} = 7h, p = 1.2 bar, F=110ml(NPT)/min, $m_{catalyst}$ = 0.5 g; feed composition: 10 mol-% butene, 20 mol-% O_2, balance N_2.

3.5.3.2 Influence of space time

Figure 3-34 shows the change in conversion of 1-butene (Figure 3-34a), in selectivity to 2-butenal and 2-butene (Figure 3-34b) and 1,3-butadiene and carbon oxides (Figure 3-34c) with changing space time between 0.3 and 1.3 s for the reaction temperatures 350, 375 and 400°C.

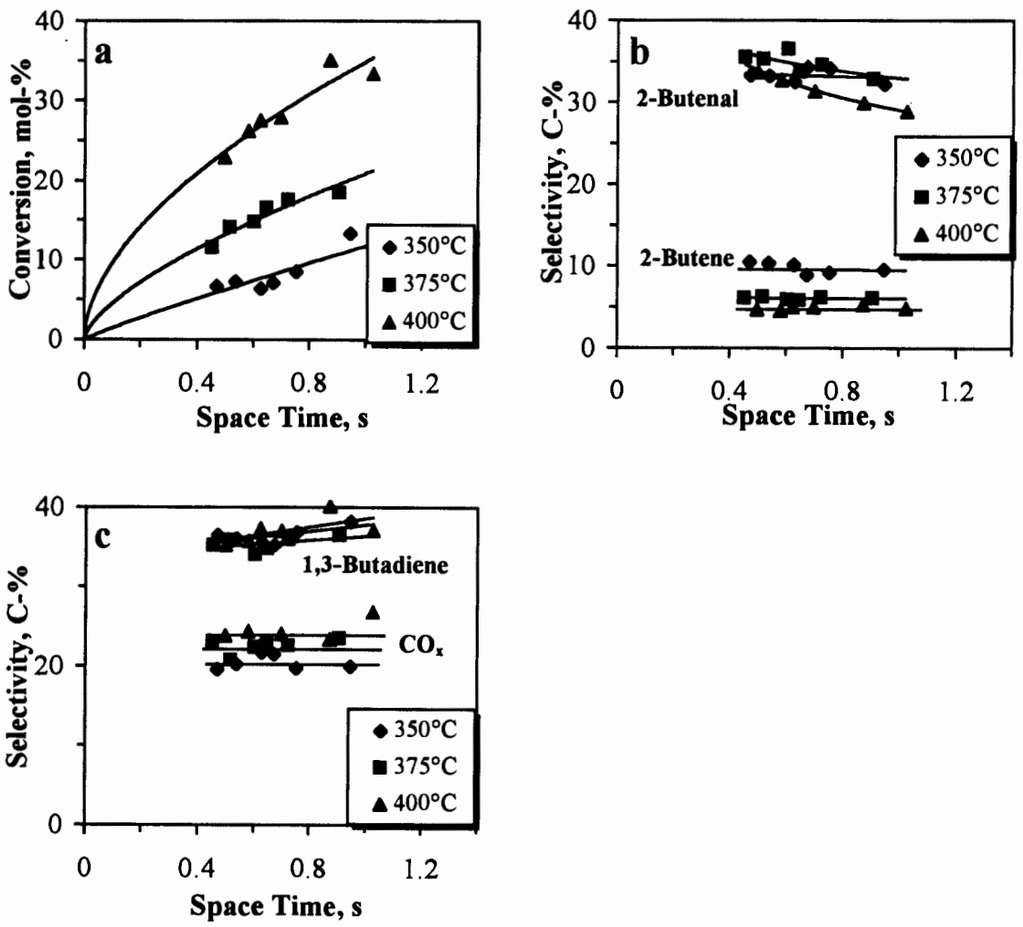

Figure 3-34 Influence of space time on the conversion (a), selectivities to 2-butenal and 2-butene (b) and 1,3-butadiene and carbon oxides (c) for the partial oxidation of butene over iron antimony oxide at different reaction temperatures; Sb:Fe=1.5, T_{calc} = 900°C, t_{calc} = 7h, p = 1.2 bar, feed composition: 10 mol-% butene, 20 mol-% O_2, balance N_2, $m_{catalyst}$ = 0.5 g.

The conversion of butene increases with increasing reaction temperature and with increasing space time. Space time has a slightly bigger influence on the butene conversion with increasing reaction temperature.

The selectivity to 2-butenal decreases slightly with increasing space time, while the selectivity to 1,3-butadiene increases with increasing space time. The selectivities to 2-butene and the carbon oxides remain constant with changing space time. This indicates that 2-butenal is a primary product, while 1,3-butadiene is a secondary product. Since the selectivities to the other products don't change with space time, it can be concluded that 2-butenal can be converted in a secondary reaction step to 1,3-butadiene. The selectivity to 2-butene remains totally unchanged during the space time study, which is to be expected on the basis of the findings of Adams (1965) who showed that β-olefins have a lower reactivity than α-olefins.

No specific trend in the influence of the reaction temperature on the selectivities to 1,3-butadiene and 2-butenal can be observed. However, the primary selectivity to the double bond isomers decreases with increasing temperature while, at the same time, the primary selectivity to the total oxidation products increases. This indicates a relative low activation energy for the double bond isomerisation and a relative high activation energy for total oxidation.

The amount of trans-2-butene in the fraction of 2-butene remains constant at 45% with both increasing space time and reaction temperature (Figure 3-35), compared with 61% at the thermodynamic equilibrium in this temperature range. This indicates that the more reactive and thermodynamically less stable cis-2-butene is preferentially formed from a common activated intermediate complex.

The CO content in the fraction of total oxidation products remains constant at 23 % with increasing space time, showing that no further reaction of CO to CO_2 takes place. The CO content is higher than the thermodynamic equilibrium which is at a CO content of 10 %, showing that preferential formation of the less stable CO. However, the CO content decreases slightly with increasing reaction temperature showing a slightly higher activation energy for the formation of CO_2 than for CO formation.

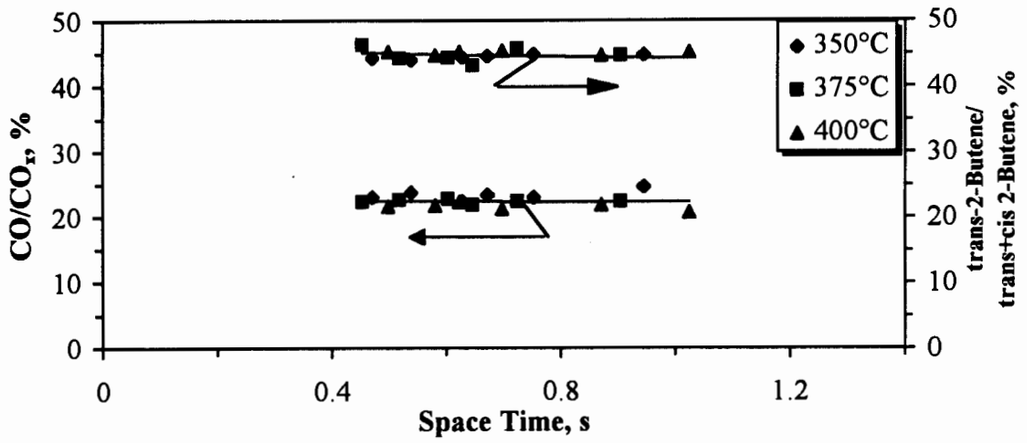

Figure 3-35 Influence of space time the CO content in the carbon oxides and the trans-2-butene content in the 2-butenes for the partial oxidation of butene over iron antimony oxide at different reaction temperatures; Sb:Fe=1.5, T_{calc} = 900°C, t_{calc} = 7h, p = 1.2 bar, feed composition: 10 mol-% butene, 20 mol-% O_2, balance N_2, $m_{catalyst}$ = 0.5 g.

It can be concluded that CO and CO_2 can be grouped together as total oxidation products (CO_x) and the cis/trans isomers can be grouped together because there is no change in selectivity in the space time experiments.

3.5.4 1-pentene

The main products observed in the 1-pentene oxidation were trans- and cis-1,3-pentadiene, 1,2-pentadiene, trans- and cis-2-pentene, CO and CO_2 and water. Only small amounts of C_5-oxygenates, viz. 2-methyl-furan was formed during the partial oxidation of 1-pentene.

3.5.4.1 Influence of reaction temperature

The influence of the reaction temperature on product yields is shown in Figure 3-36. The yield of carbon oxides increases most strongly with increasing temperature, indicating a relative high activation energy to carbon oxides. Up to 450°C 1,3-pentadiene is produced with highest yields, whereby for temperatures above 450°C carbon oxides are produced with highest yields. The curve for the yield of pentadiene is "S" shaped, which might indicate a further reaction of 1,3-pentadiene at higher temperatures to the more stable products carbon oxides and cracking products. The yield of 2-pentene increases only

slightly with increasing temperature, whereas cracking products are produced above 400°C in significant amounts. The oxygenate 2-methyl-furan is produced in only small amounts for all investigated temperatures and its yield decreases with increasing reaction temperature.

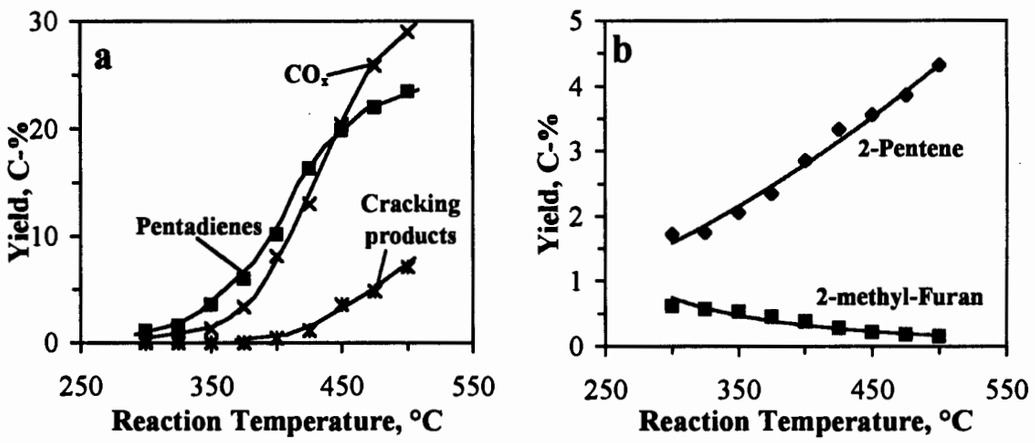

Figure 3-36 Influence of reaction temperature on the product yields of the partial oxidation of 1-pentene over iron antimony oxide; Sb:Fe=1.5, T_{calc} = 900°C, t_{calc} = 7h, p = 1.2 bar, F=110ml(NPT)/min, $m_{catalyst}$ = 0.5 g; feed composition: 10 mol-% pentene, 20 mol-% O_2, balance N_2.

3.5.4.2 Influence of space time

Figure 3-37 shows the change in conversion (Figure 3-37a), in selectivity to pentadiene and 2-pentene (Figure 3-37b) and carbon oxides (Figure 3-37c) with changing space time between 0.3 and 1.6 s for the reaction temperatures 350, 375 and 400°C.

The conversion of pentene increases with increasing reaction temperature and increases linearly with increasing space time. Space time has a slightly bigger influence on the butene conversion at 400°C than at 350 and 375°C.

The selectivity to 2-pentene remains unchanged during the space time study, showing that 2-pentene is relatively unreactive.

Decreasing space time showed a slight increase in the selectivity to dienes and 2-methyl-furan with a corresponding decrease in the selectivity to the carbon oxides, showing that

pentadiene and 2-methyl-furan are primary products, which can further react to carbon oxides.

The primary selectivity to the total oxidation products increases with increasing temperature, indicating a relative high activation energy for total oxidation.

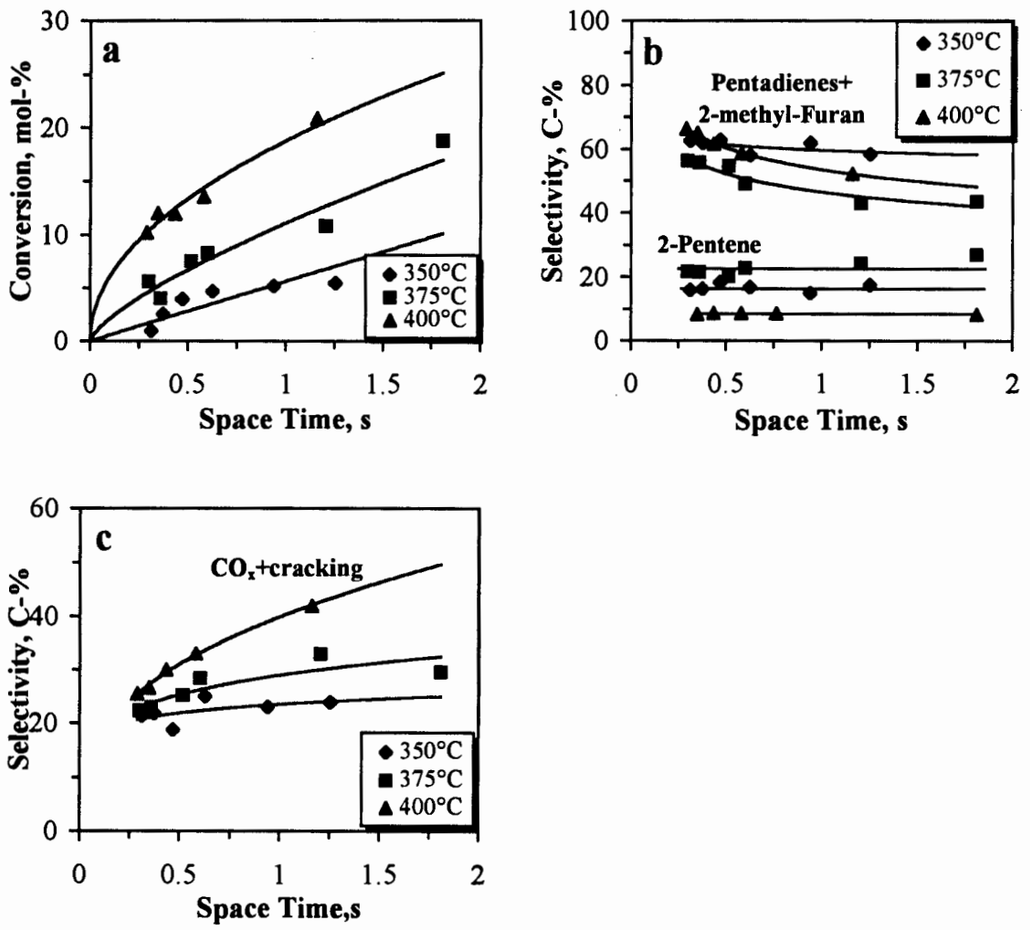

Figure 3-37 Influence of space time on the conversion (a), selectivities to pentadiene and 2-pentene (b) and carbon oxides (c) for the partial oxidation of butene over iron antimony oxide at different reaction temperatures; Sb:Fe=1.5, T_{calc} = 900°C, t_{calc} = 7h, p = 1.2 bar, feed composition: 10 mol-% pentene, 20 mol-% O_2, balance N_2, $m_{catalyst}$ = 0.5 g.

The amount of trans-2-pentene in the fraction of 2-pentene remains constant about 60% with both increasing space time and reaction temperature (see Figure 3-38a). The amount

of trans-1,3-pentadiene remains constant at about 50% with both increasing space time and reaction temperature.

The CO content in the fraction of total oxidation products remains constant at about 23% with increasing space time, showing that no further reaction of CO to CO_2 takes place. The reaction temperature doesn't affect the CO content in the investigated temperature range.

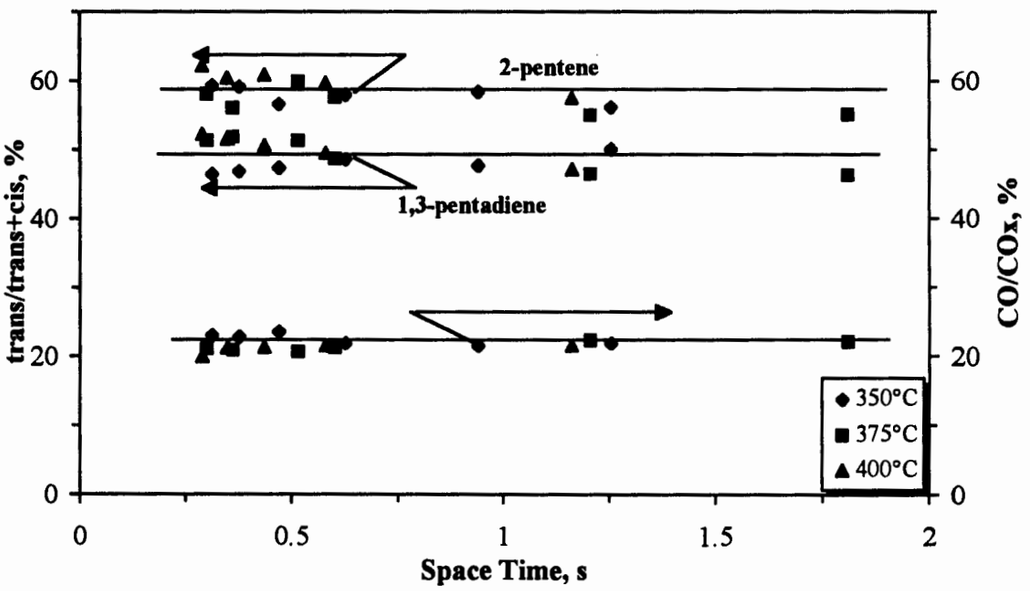

Figure 3-38 Influence of space time the CO content in the carbon oxides and the trans-2-pentene content in the 2-pentenes and the trans-1,3-pentadiene content in the 1,3-pentadienes for the partial oxidation of pentene over iron antimony oxide at different reaction temperatures; Sb:Fe=1.5, T_{calc} = 900°C, t_{calc} = 7h, p = 1.2 bar, feed composition: 10 mol-% pentene, 20 mol-% O_2, balance N_2, $m_{catalyst}$ = 0.5 g.

3.5.5 1-hexene

The products in the partial oxidation of 1-hexene were cis-and trans-2-hexene, cis and trans-3-hexene, which are summarised in the following as double bond isomerisation products. Furthermore cis-1,3 hexadiene, trans-1,3 hexadiene, 2,4-hexadienes, cyclohexene, cyclohexadiene and benzene, which are summarised in the following as

oxidative dehydrogenation products. The rest of the products were cracking products, carbon oxides and water.

3.5.5.1 Influence of reaction temperature

The influence of reaction temperature on product yields is shown in Figure 3-39. The oxidative dehydrogenation products show the highest yields, except for 500°C, where the yield of carbon oxides is the highest.

The curve for the yields of carbon oxides show the highest slope over the entire temperature range, indicating a higher activation energy to carbon oxides.

The curves for the yields of oxidative dehydrogenation products and cracking products flatten out at temperatures above 450°C, which might indicate the further oxidation to carbon oxides or a change in the activation energy.

The yield of the double bond isomerisation products increases only slightly with increasing temperature, indicating a relative low activation energy to these products.

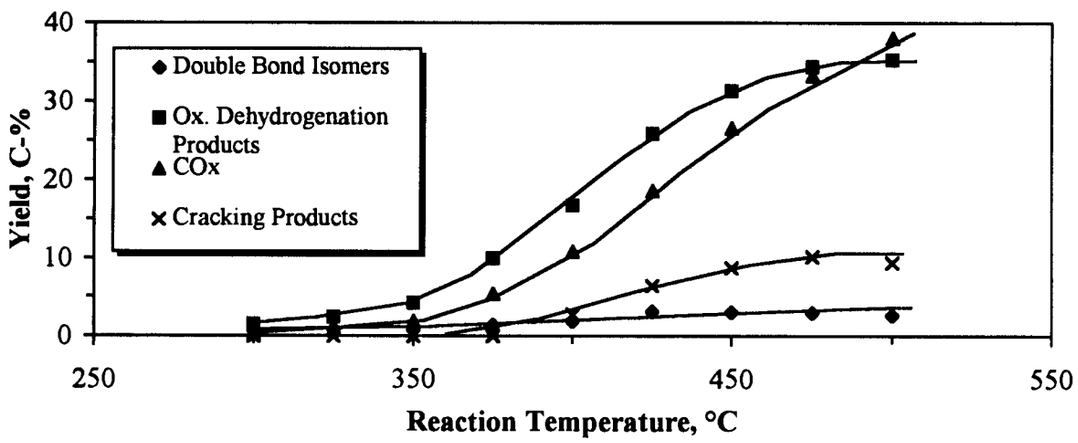

Figure 3-39 Influence of reaction temperature on the product yields of the partial oxidation of 1-hexene over iron antimony oxide; Sb:Fe=1.5, T_{calc} = 900°C, t_{calc} = 7h, p = 1.2 bar, F=110ml(NPT)/min, $m_{catalyst}$ = 0.5 g; feed composition: 10 mol-% hexene, 20 mol-% O_2, balance N_2.

3.5.5.2 Influence of space time

Figure 3-40 shows the change in conversion (Figure 3-40a), in selectivity to double bond isomers (Figure 3-40b), hexadienes plus cyclic products (Figure 3-40c), and cracking products plus carbon oxides (Figure 3-40d) with changing space time between 0.3 and 1.3 s for the reaction temperatures 350, 375 and 400°C.

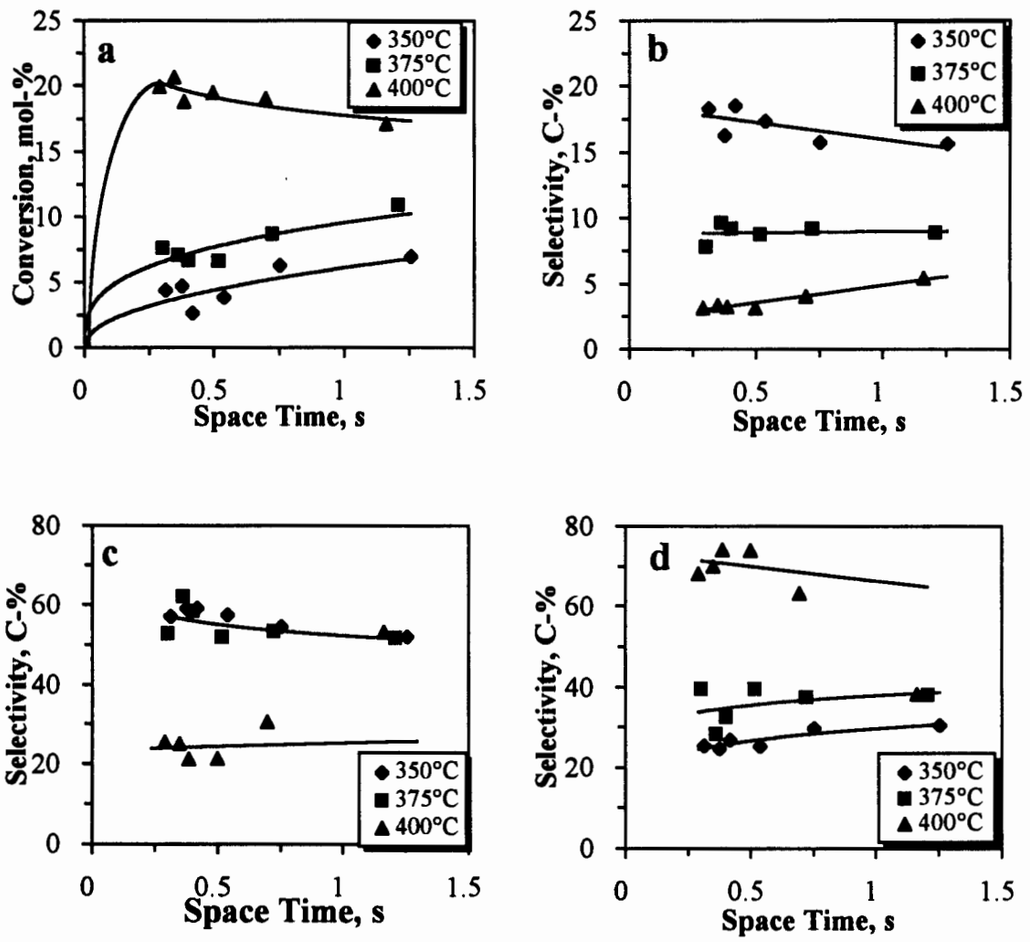

Figure 3-40 Influence of space time on the conversion (a), selectivities to double bond isomers (b), hexadiene plus cyclic products (c), and cracking products plus carbon oxides (d) for the partial oxidation of hexene over iron antimony oxide at different reaction temperatures; Sb:Fe=1.5, T_{calc} = 900°C, t_{calc} = 7h, p = 1.2 bar, feed composition: 10 mol-% hexene, 20 mol-% O_2, balance N_2, $m_{catalyst}$ = 0.5 g.

The conversion of hexene increases with increasing reaction temperature and increases linearly with increasing space time at 350 and 375°C, but decreases at 400°C.

Determination of trends for the space time runs is somehow difficult because they are not consistent for all temperatures. The selectivity to double bond isomers decreases with increasing space time at 350°C, but increases at 375 and 400° with increasing space time. The selectivity to hexadienes plus cyclic products decreases with increasing space time at 350 and 375°C, but increases with increasing space time at 400°C. The selectivities to

cracking products and carbon oxides increase with increasing space time at 350 and 375°C, but decrease with increasing space time at 400°C.

The selectivities to the double bond isomers and the hexadienes plus cyclic products decrease with increasing temperature while, at the same time, the selectivities to carbon oxides plus cracking products increase with increasing temperature. This indicates a lower activation energy for the formation of double bond isomers, hexadienes and cyclic products than for the formation of carbon oxides plus cracking products.

Figure 3-41 shows the content of cyclic products in the group of cyclic products plus oxidative dehydrogenation products (Figure 3-41a) and the content of cracking products in the group of cracking products plus total oxidation products (Figure 3-41b).
The content of cyclic products increases with increasing space time, indicating that cyclic products are secondary products, which are formed from hexadienes. No cracking products could be detected at 350°C. The content of cracking products doesn't change at 375°C, but decreases with increasing space time at 400°C, indicating that at high temperatures cracking products can be further oxidised to total oxidation products.

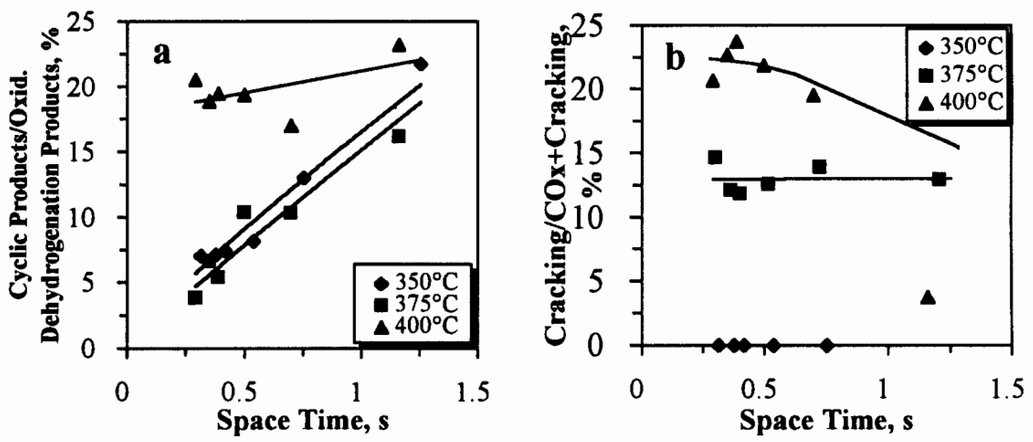

Figure 3-41 Influence of space time on the content of cyclic products in the oxidative dehydrogenation products (a) and on the content of cracking products in the group of cracking and total oxidation for the partial oxidation of hexene over iron antimony oxide at different reaction temperatures; Sb:Fe=1.5, T_{calc} = 900°C, t_{calc} = 7h, p = 1.2 bar, feed composition: 10 mol-% hexene, 20 mol-% O_2, balance N_2, $m_{catalyst}$ = 0.5 g.

3.5.6 1-heptene

The detected products of the partial oxidation of 1-heptene were cis- and trans-2-heptene, cis-and trans-3-heptene, which are summarised in the following as double bond isomers. Furthermore 1,4- and 1,5-heptadiene, cracking products, carbon oxides and water.

3.5.6.1 Influence of space time

Figure 3-42 shows the change in conversion (Figure 3-42a), in selectivity to double bond isomers (Figure 3-42b), hepatadienes (Figure 3-42c) and cracking products plus carbon oxides (Figure 3-42d) with changing space time between 0.3 and 1.3 s for the reaction temperatures 350, 375 and 400°C.

The conversion of heptene increases with increasing reaction temperature and increases with increasing space time.

The selectivity to double bond isomers decreases with increasing space time, showing that they are primary products. The same behaviour with space time is seen for the formation of hepatadienes. The selectivity to carbon oxides and cracking products increases with increasing space time showing that they can be formed in a secondary reaction step from the other products. The selectivities to carbon oxides and cracking products increase with increasing temperature, while the selectivities to double bond isomers and heptadienes decrease with increasing temperature, which indicates a higher activation energy for the formation of carbon oxides and cracking products than for the formation of double bond isomers and heptadienes.

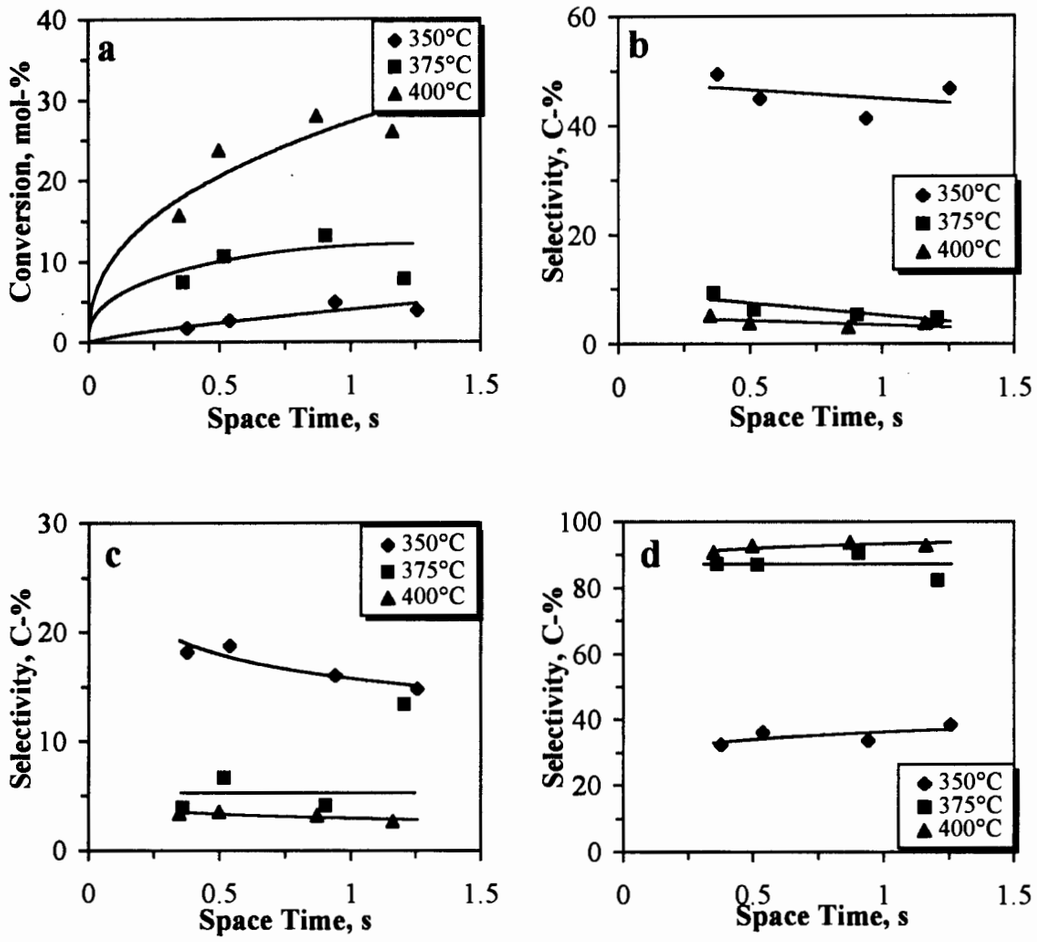

Figure 3-42 Influence of space time on the conversion (a), selectivities to double bond isomers (b), heptadienes (c), and cracking products plus carbon oxides (d) for the partial oxidation of heptene over iron antimony oxide at different reaction temperatures; Sb:Fe=1.5, T_{calc} = 900°C, t_{calc} = 7h, p = 1.2 bar, feed composition: 10 mol-% heptene, 20 mol-% O_2, balance N_2, $m_{catalyst}$ = 0.5 g.

3.5.7 1-octene

Products formed were cis- and trans-2-octene and cis- and trans-4-octene, which are summarised as double bond isomerisation products. Furthermore cracking products were formed, which consisted of alkenes and oxygenates with a carbon number smaller than eight. The rest of the products were carbon oxides and water. No oxidative dehydrogenation products could be detected.

3.5.7.1 Influence of space time

Figure 3-43 shows the change in conversion (Figure 3-43), in selectivity to double bond isomers (Figure 3-43b), and carbon oxides plus cracking products (Figure 3-43c) with changing space time between 0.3 and 1.3 s for the reaction temperatures 325, 350 and 375°C. Higher temperatures couldn't be applied, because of severe cracking taking place.

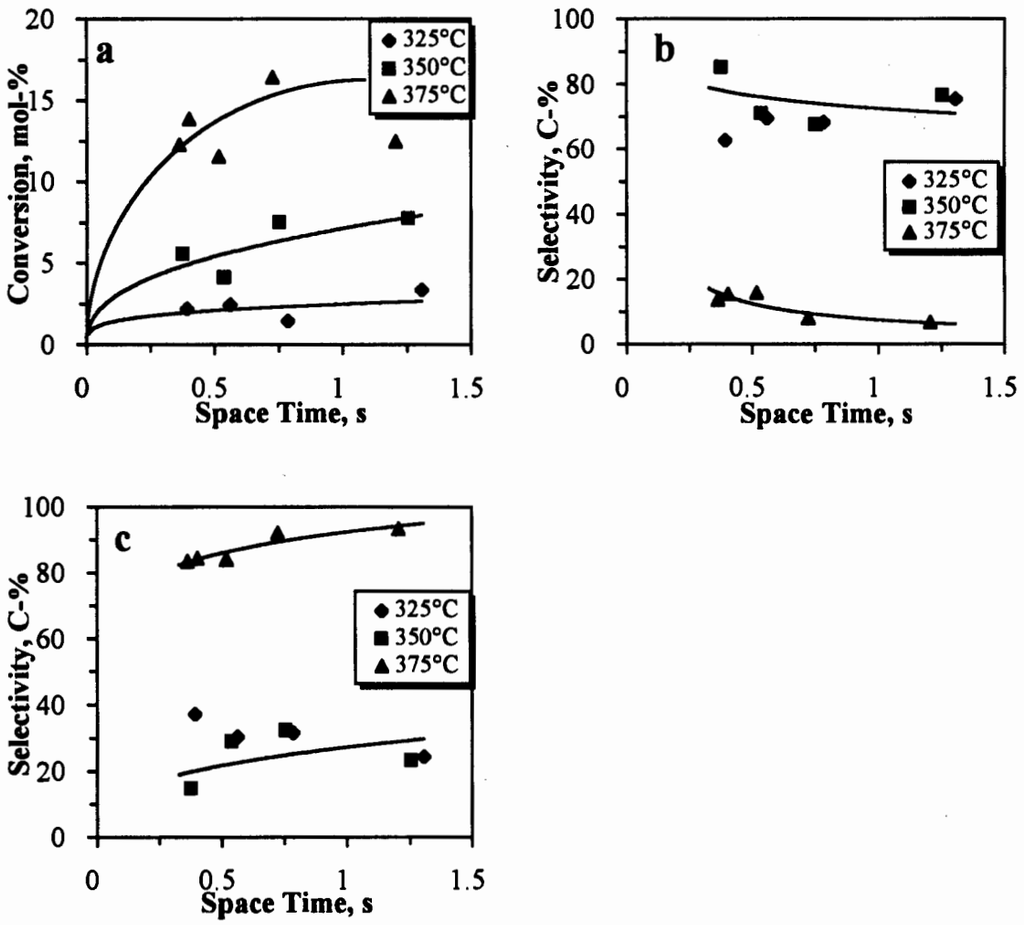

Figure 3-43 Influence of space time on the conversion (a), selectivities to double bond isomerisation products (b), carbon oxides and cracking products (c) for the partial oxidation of octene over iron antimony oxide at different reaction temperatures; Sb:Fe=1.5, T_{calc} = 900°C, t_{calc} = 7h, p = 1.2 bar, feed composition: 10 mol-% octene, 20 mol-% O_2, balance N_2, $m_{catalyst}$ = 0.5 g.

The conversion of octene increases with increasing reaction temperature and increases slightly with increasing space time. The selectivity to double bond isomers increases with decreasing space time, while the selectivities to cracking products and carbon decrease with decreasing space time. It can be concluded from this behaviour that double bond isomers are primary products, while carbon oxides and cracking products are secondary products, which can be formed from 1-octene and from the double bond isomers, viz. 2-octene and 4-octene.

The primary selectivity to the double bond isomers decreases with increasing temperature while, at the same time, the primary selectivities to the total oxidation products and cracking products increase. This indicates a lower activation energy for the formation of double bond isomerisation products than for the formation of total oxidation products and cracking products.

3.5.8 1-nonene

3.5.8.1 Influence of space time

The products detected were 2-nonene, CO, CO_2 and cracking products, no oxidative dehydrogenation products could be detected. The influence of space time and temperature on the conversion and selectivities are summarised in Table 3-12. Because of the high price of 1-nonene only few different space times were investigated. The reaction temperature was kept at 350 and 375°C, because of excessive cracking at higher temperatures.

The primary selectivity to cracking products increased most strongly with increasing temperature, viz. from 0 C-% at 350°C to 41 C-% at 375°C, whereas the primary selectivity to total oxidation products increased from 40 C-% at 350°C to 49 C-% at 375°C. The primary selectivity to double bond isomerisation products decreased with increasing temperature from 60 C-% at 350°C to 10 C-% at 375°C. This shows that the activation energy to form double bond isomerisation products is lower than for the formation of cracking products and total oxidation products.

Table 3-12 Influence of space time and reaction temperature on the conversion and selectivities of 1-nonene over iron antimony oxide. (Sb:Fe=1.5, T_{calc} = 900°C, t_{calc} = 7h; p = 1.2 bar, feed composition: 10 mol-% nonene, 20 mol-% O_2, balance N_2, $m_{catalyst}$ = 0.5 g).

T [°C]	τ [s]	X [mol-%]	S_{DI}[1)][C-%]	S_{TO}[1)][C-%]	S_{Cr}[1)][C-%]
350	1.25	8.4	73.5	26.5	0.0
	0.54	2.4	60.5	39.5	0.0
	0.38	2.1	59.8	40.2	0.0
375	0.52	13.4	5.8	44.4	49.8
	0.36	8.7	9.6	49.0	41.4

1) S_{DI} = Selectivity to double bond isomerisation products; S_{TO} = Selectivity to total oxidation products; S_{cr} = Selectivity to cracking products.

CHAPTER 4

DISCUSSION

4. DISCUSSION

The discussion of the results is divided into two main sections, one dealing with the iron antimony oxide catalyst and the other with partial oxidation reactions of α-olefins over an iron antimony oxide catalyst.

In the first section the most important properties of iron antimony oxide are discussed, which are crystallinity, effect of lattice oxygen and adsorbed oxygen, influence of calcination temperature and influence of the bulk Sb to Fe ratio in the catalyst. In the second section the partial oxidation of various linear α-olefins over iron antimony oxide is discussed. The influence of the chain length on the product selectivities, both at constant feed concentrations and for varying feed concentrations and the rates of product formation at constant feed concentrations are discussed.

4.1 IRON ANTIMONY OXIDE CHARACTERISATION

4.1.1 Crystallinity

Investigation of the crystal composition of iron antimony oxide using powder X-ray diffraction revealed that irrespective of the antimony to iron ratio in the range $0.25 \leq Sb/Fe \leq \infty$, there is always a $FeSbO_4$ phase formed. Excess Fe will lead to the formation of Fe_2O_3, while excess Sb leads to the formation of a Sb_2O_4 phase. The formation of a $FeSb_2O_6$ bulk phase in the presence of excess antimony, as suggested by Bryström *et al.* (1941) can be ruled out on the basis of the X-ray diffraction results (Section 3.1.1.1), which didn't show a characteristic peak for $FeSb_2O_6$ at $2\theta=21°$. This is in agreement with most of the publications in this field (Carbucicchio *et al.*, 1985, Teller *et al.*, 1985, Allen *et al.*, 1996). The absence of a low angle diffraction peak at $2\theta=21°$ also favours the existence of a unit cell of $FeSbO_4$ in a single rutile structure (Allen *et al.*, 1996) as opposed to the trirutile structure proposed by Berry *et al.* (1987).

The X-ray diffraction pattern for iron antimony oxide, calcined at 900°C in air showed decreasing diffraction peak heights for Fe_2O_3 and increasing diffraction peak heights for the peaks which can be associated with Sb_2O_4 and $FeSbO_4$ (Figures 3-1 and 3-2). This result is

expected for Fe_2O_3 and Sb_2O_4, because the volumetric fraction of Fe_2O_3 in the sample decreases with increasing Sb:Fe ratios up to a ratio of 1, where the volumetric fraction of Fe_2O_3 becomes zero. In contrast, the volumetric fraction of Sb_2O_4 increases with increasing Sb:Fe ratios above a ratio of Sb:Fe=1. An increase of the $FeSbO_4$ diffraction peak intensity is only expected up to a Sb:Fe ratio of 1:1, because the volumetric fraction of $FeSbO_4$ increases and should theoretically stagnate or even decrease for a further increase of the Fe:Sb ratio above 1, which is the stoichiometric ratio to form $FeSbO_4$. However, the intensities seem to increase further even for Sb:Fe ratios greater than 1.0. In this section this phenomena is discussed in more detail.

Figure 4-1 shows the peak height associated with the (1,1,0)-plane of $FeSbO_4$, which was obtained from the X-ray diffraction pattern at various Sb:Fe ratios and at calcination temperatures of 700°, 800° and 900°C together with their trendlines. For all three investigated calcination temperatures the peak height increases with increasing Sb/Fe ratio.

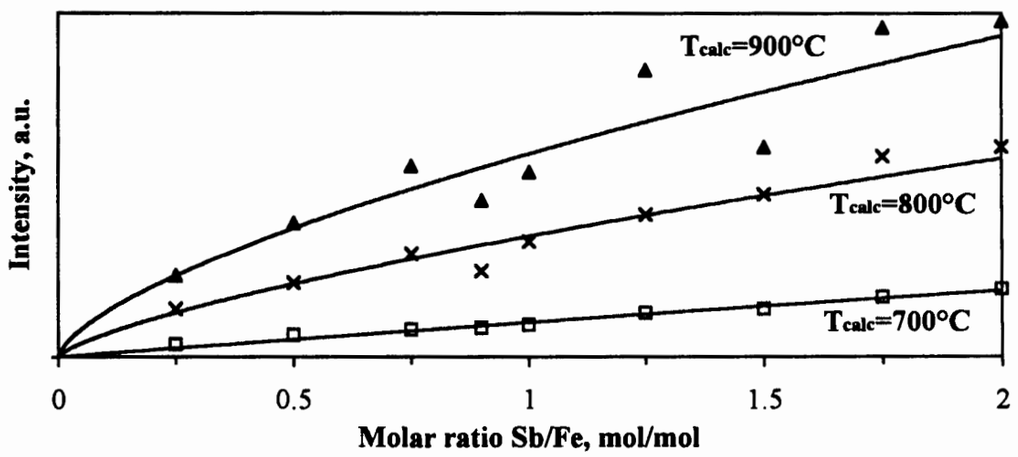

Figure 4-1 Peak height for the (1,1,0) $FeSbO_4$ plane from the X-ray diffraction pattern (Cu-Kα radiation) at 2θ=27.2°, as a function of Sb/Fe ratio and calcination temperature.

However, the diffraction peak intensity is better represented by their peak area than the peak height. Figure 4-2 shows the X-ray diffraction peak area of the (1,1,0) plane as a function of the Sb/Fe ratio and calcination temperature.

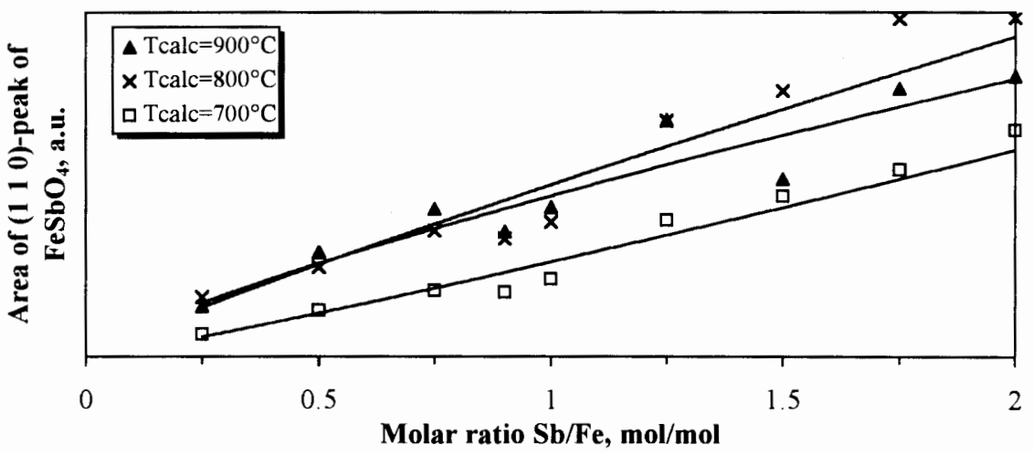

Figure 4-2 X-ray diffraction peak area pattern (Cu-Kα radiation) for the (1,1,0) $FeSbO_4$ plane as a function of Sb/Fe ratio and calcination temperature.

From Figure 4-2 it is evident that the percentage crystallinity of $FeSbO_4$, defined as the volumetric fraction of crystals present in the sample, increases with increasing calcination temperature from 700°C to 800°C and doesn't further increase with increasing calcination temperature to 900°C.

According to Klug and Alexander (1974), the diffraction peak area can be related to the volumetric fraction of a crystal phase in the sample. Since the density of the samples were approximately constant over the whole investigated Sb/Fe ratio range (see Appendix VI) and since the same volumetric amount of sample was used, the increase in the peak area corresponds to a proportional increase in the weight fraction of the particular crystals in the sample. The increase of the peak area of the (1,1,0) diffraction peak with increasing Sb/Fe ratio corresponds therefore to an increase in the weight fraction of crystalline $FeSbO_4$ in the sample. An increase of weight fraction of crystalline $FeSbO_4$ over the stoichiometric necessary ratio of 1:1 is unexpected, since the sample contains Sb_2O_4 when excess antimony is present. This indicates, that antimony facilitates the formation of $FeSbO_4$ crystals due to a closer interaction of antimony trioxide with iron nitrate during the catalyst

synthesis. At the same time excess antimony accelerates the formation of $FeSbO_4$ crystals leading to a reduction in the amount of amorphous material in the sample.

Increasing the calcination temperature from 700 to 800°C increases the fraction of iron antimonate crystals in the sample. A further increase in calcination temperature hardly influences the crystallinity of $FeSbO_4$.

The influence of Sb/Fe ratio and the calcination temperature on the crystal size of $FeSbO_4$ is shown in Figure 4-3.

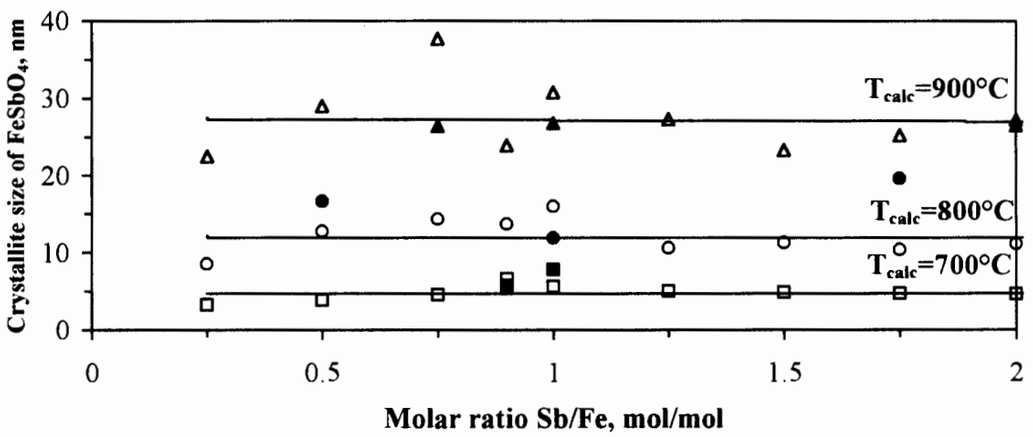

Figure 4-3 Crystal size of $FeSbO_4$ as a function of Sb/Fe ratio and calcination temperature as determined by peak broadening of the (1,1,0) diffraction peak at 2θ=27.3°(open symbols) and for comparison from TEM images (filled symbols).

With increasing calcination temperature, the crystal size of $FeSbO_4$ increases, which can be ascribed to high temperature sintering processes. Despite some scatter of the points, the crystal size does not show an influence of the Sb/Fe ratio. The mean diameter of $FeSbO_4$ crystallites from TEM measurements have been included in Figure 4-3, which confirms the findings by the peak broadening.

Although the Sb/Fe ratio has no significant influence on the crystal size, it shows a strong influence on the number of $FeSbO_4$ crystallites (Figure 4-4).

Increasing the calcination temperature severely reduces the number of crystallites due to sintering, which leads to formation of bigger crystals by fusion of several smaller crystals. The Sb/Fe ratio has a strong influence on the number of $FeSbO_4$ crystallites for Sb/Fe ratios > 1. Up to a Sb/Fe ratio of one, the number of $FeSbO_4$ doesn't change significantly, but

increases strongly for higher Sb/Fe ratios. This can again be ascribed to the synthesis method where a close interaction of antimony trioxide and iron nitrate is desirable.

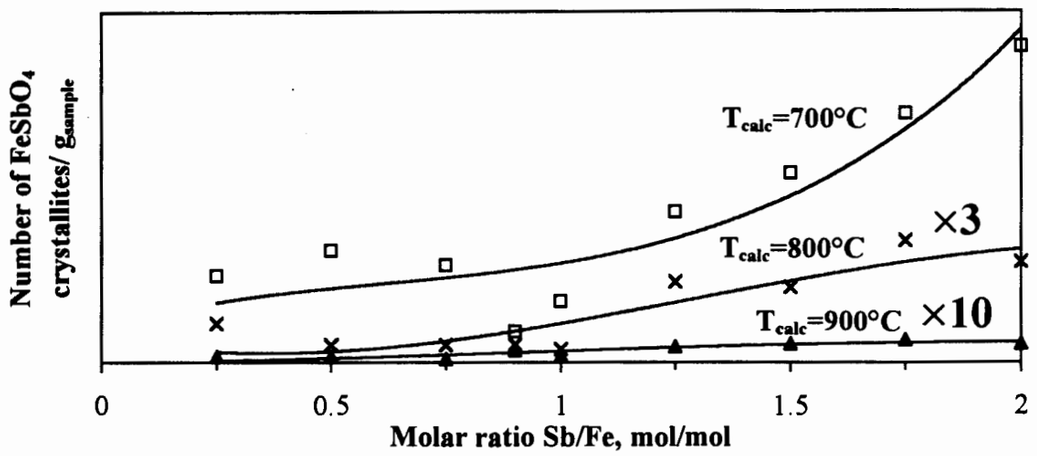

Figure 4-4 Relative number of $FeSbO_4$ crystals per gram of catalyst as a function of calcination temperature and Sb/Fe ratio.

Having established the number, size and shape of the $FeSbO_4$ crystals, the relative surface area of $FeSbO_4$ crystals can be derived, which is shown in Figure 4-5. The relative surface area of $FeSbO_4$ crystals reflects the trend of the number of crystals, viz. a strong increase for a Sb/Fe ratio > 1. The surface area decreases with increasing calcination temperature, because of sintering and a consequent increase in crystal size and at the same time a decrease in number of crystals.

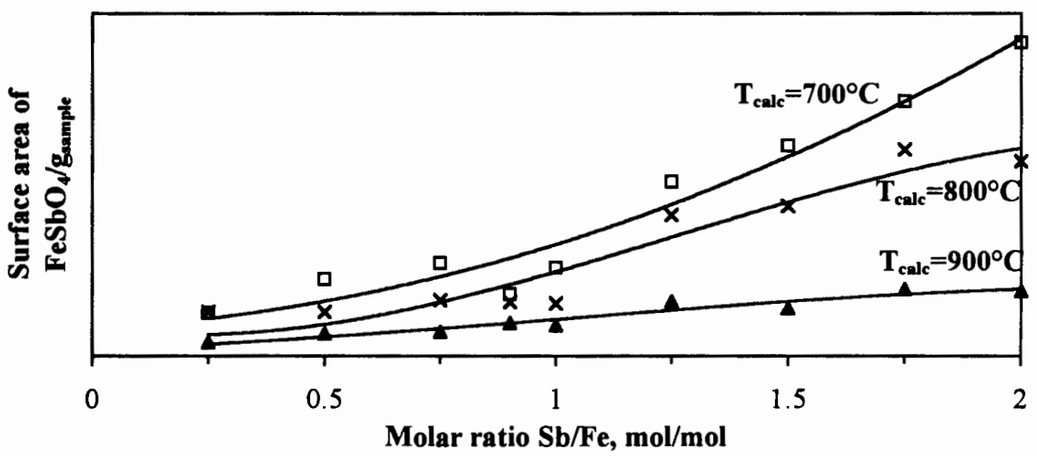

Figure 4-5 Surface area of $FeSbO_4$ crystallites per gram of catalyst as a function of calcination temperature and Sb/Fe ratio.

BET surface area measurements for iron antimony oxide (T_{calc}=800°C) containing different Sb:Fe ratios (Figure 3-11) showed a maximum surface area around Sb:Fe=1. It has been shown that amorphous $FeSbO_4$ has a higher surface area compared to Fe2O3 and Sb2O4 (Table 3-7 and 3-8). Figure 4-5 shows only the surface area of the $FeSbO_4$ crystallites and not amorphous material. In order to get a maximum surface area at a ratio Sb:Fe=1 their must be more amorphous material present than at a higher Sb:Fe ratio.

It can be concluded from the surface area that the effect of excess Sb is to increase the crystallinity of $FeSbO_4$. The higher crystallinity of $FeSbO_4$ can be correlated to the increase of the yield of acrolein (Figure 3-29b) over iron antimony oxide with excess Sb.

4.1.2 Role of gaseous and lattice oxygen

The results referred to in this part of the discussion can be found in Figure 3-22 in Section 3.3.4. The results showed that the activity of the catalyst is proportional to the amount of oxygen available. No significant difference in the initial activity was observed when gaseous oxygen was present compared to when gaseous oxygen was absent, however the activity drops drastically in the absence of gaseous oxygen. Brazdil *et al.* (1980) observed a similar behaviour for the propene ammoxidation in the absence of gaseous oxygen at 430°C over $Bi_3FeMo_2O_{12}$ and Bi_2MoO_6, however other catalytic systems like $Bi_2Mo_2O_9$ and $Bi_2Mo_3O_{12}$ regained some of the initial activity with further reduction, which was explained by the existence of two different sites of different oxygen coordination with the capability of the selective ammoxidation of propene.

Even in the case of propene oxidation in the presence of gaseous oxygen the catalyst loses its initial high activity, showing that the initial high oxidation state cannot be maintained by the gaseous oxygen. Like the U-Sb-oxide system, which has been investigated by Grasselli and Suresh (1972), the Fe-Sb-oxide system needs to be in a high oxidation state.
The relative selectivity to acrolein in the presence of gaseous oxygen shows an initial maximum, but decreases with time on stream. The relative selectivity to acrolein in the absence of gaseous oxygen increases slightly with time on stream.

selectivity to acrolein in the presence of gaseous oxygen can't be explained by a secondary reaction of acrolein to the combustion products because of the relative high stability of acrolein at this temperature which was shown in the experiments of changing space times (Figure 3-32b).

The decrease of the relative selectivity to acrolein in the presence of gaseous oxygen is an indirect effect. The formation of total oxidation products has been attributed to the reaction of adsorbed hydrocarbon species with electrophilic oxygen species, whereas the formation of partial oxidation products is attributed to a reaction with nucleophilic oxygen species (Bielanski and Haber, 1991). The electrophilic oxygen species are intermediates in the reoxidation of the catalyst with gaseous oxygen, therefore, the relative selectivity to acrolein decreases in the case where gaseous oxygen is present. However, the situation is different in the case where no gaseous oxygen is present. With the formation of oxygenated products oxygen vacancies on the catalyst surface are created, which can't be refilled from the gas phase and therefore fewer electrophilic oxygen species are present to form combustion products.

The importance of the oxidation state of the catalyst was also shown by heating the catalyst in flowing nitrogen and flowing air prior to the partial oxidation of propene.

The catalyst which has been heated up in flowing air showed a higher initial activity, confirming that the catalyst needs to be in a high oxidation state in order to show maximum activity. A decrease of the oxidation state when heating the catalyst in nitrogen might be explained by the autoreduction of the antimony on the catalyst surface, which is supported by the characteristic of antimony oxide to autoreduce at a relative low temperature of 380°C (Pietsch, 1949). The initial selectivity to acrolein is lower in the reaction over the reduced catalyst because of the increased formation of electrophilic oxygen species during the reoxidation which leads to an increase of the selectivity to combustion products.

Temperature Programmed Reduction (TPR) with propene as reduction gas revealed that iron antimony oxide catalysts are able to replenish oxygen vacancies from the bulk until the collapse and reduction of the bulk of the catalyst is taking place.

4.1.3 Influence of calcination temperature

The influence of the calcination temperature has been investigated for $FeSbO_4$ in the presence (Section 3.4.3) and absence of gaseous oxygen (Section 3.3.2). In the presence of

gaseous oxygen the influence of reaction temperature (Section 3.4.3.1) and the influence of time on stream (Section 3.4.3.2) has been studied.

The conversion of propene increases in the absence and in the presence of gaseous oxygen with decreasing calcination temperature. However, during the TPR experiments the conversion only increases with decreasing calcination temperature during the surface reduction, which shows that the increase in activity can be correlated to a higher surface area of the catalyst.

The relative selectivity to acrolein during the surface reduction (reduction temperature between 250 and 350°C) increases with increasing calcination temperature. The selectivity to acrolein increases with increasing calcination temperature in the presence of gaseous oxygen at different reaction temperatures (Figure 3-25). Due to scatter of the data the influence of the calcination temperature in the time on stream experiments was not so clear (Figure 3-26). This shows that acrolein is more selectively formed over more crystalline $FeSbO_4$. The reason why a higher crystallinity increases the selectivity to acrolein might be explained by more strongly bound oxygen on the catalyst surface. This will decrease the availability of oxygen on the catalyst surface, which will lead preferably to the formation of total oxidation products instead of total oxidation products, which require a high availability of oxygen on the surface (Callahan and Grasselli, 1963).

4.1.4 Influence of Sb:Fe ratio

The results referred to in this part of the discussion can be found in Section 3.3.3 and 3.4.4. The selectivity to acrolein increases with increasing Sb:Fe ratio in the presence and in the absence of gaseous oxygen.

In the presence of gaseous oxygen and in the absence of gaseous oxygen the conversion of propene decreases with increasing Sb:Fe ratio for Sb:Fe>1. Highest conversion was observed in both cases for iron antimony oxide close to Sb:Fe=1, which is the stoichiometric ratio of $FeSbO_4$. Excess antimony therefore has the effect that the conversion of propene decreases. Excess antimony inhibits the reduction of iron antimony oxide according to Allen *et al.* (1996) probably due to a stronger metal-oxygen bond strength (Sachtler and de Boer, 1965). Since a reduction step is involved in the redox mechanism the conversion has to decrease accordingly.

The influence of excess antimony on the selectivity to acrolein can be ascribed to the site isolation effect formulated by Callahan and Grasselli (1963). Due to the inhibition of the reduction the number of active oxygen for the oxidation of propene is limited and the formation of products which consume less oxygen is preferred. Since the stoichiometric oxygen requirement for the formation of acrolein is less than for total oxidation products, the formation of acrolein is preferred. In the presence of gaseous oxygen the effect of reoxidation is added which produces electrophilic oxygen species on the catalyst surface, which leads to a high selectivity to total oxidation products, when the reduction of the catalyst is high.

The second reduction peak during TPR of iron antimony oxide evolves between 500 and 600°, with CO_2 being the sole product independent of the antimony content in the catalyst. The formation of metallic Sb has been observed by Allen *et al.* (1995, 1996), at this temperature range. Although m/e=121 (antimony) was not observed in the product spectra, a metallic precipitation on the reactor outlet was observed when removing the reactor. Upon desorption of Sb the surface becomes Fe rich and total combustion products become the preferred products. An excess of Sb inhibits the formation of metallic Sb (Allen *et al.*, 1996) and the size of the second reduction peaks decreases accordingly (Figure 3-19).

A further reduction is not desirable because it leads to the distruction of the $FeSbO_4$ and Sb_2O_4 structure. In this range the Sb:Fe ratio has hardly any influence on the product selectivities.

4.2 INFLUENCE OF CHAIN LENGTH ON THE PARTIAL OXIDATION OF LINEAR α-OLEFINS

4.2.1 Effect on selectivities and rates

The number of products formed in the partial oxidation of C_2 to C_9-α-olefins increases drastically from 1-butene onwards to higher α-olefins. This is due to the formation of double bond isomers and oxidative dehydrogenation products and the formation of trans-cis isomers within these product groups. Therefore the following product groups were used: double bond isomerisation, partial oxidation, oxidative dehydrogenation, cracking and total oxidation products. All products containing hydrocarbons with a C-number smaller than

that of the feed were summarised as cracking products. CO and CO_2 were summarised as total oxidation products.

The major trends observed when changing the space time as shown in Section 3.5 are the following. The selectivity to partial oxidation products decreases with increasing space time, meaning that it is a primary product, which can be converted to the thermodynamical more stable carbon oxides at higher space times.

Carbon oxides can be formed in a secondary reaction, because their selectivity increases with increasing space time. Changing the space time had no effect on the ratio of CO within the carbon oxides.

The selectivity to oxidative dehydrogenation products decreases with increasing space time, indicating that they are primary products, which can be converted into the thermodynamically more stable carbon oxides. One exception from this rule is selectivity to 1,3-butadiene, which increases with increasing space time. This might indicate that 2-butenal can be converted to 1,3-butadiene at higher space times. Changing the space time didn't influence the selectivity to cis/trans-isomers. The fact that the concentration of the oxidative dehydrogenation products doesn't reach zero for high space times shows that they are relative stable products in comparison to the feed.

The selectivity to double bond isomerisation products is constant with changing space time in the region of C_4-C_6 α-olefins, showing that the double bond isomers are quite stable molecules, which is expected on the basis of the findings of Adams (1965) who showed that β-olefins have a lower reactivity than α-olefins. However, for α-olefins from a carbon number of C_7 onwards the selectivity to double bond isomers decreases with increasing space time, showing that they can be converted into carbon oxides. Changing the space time didn't influence the ratio of trans/cis isomers.

The selectivity to cracking products in the group of cracking plus total oxidation products decreases for α-olefins up to C_6 with increasing space time, showing that in this C-number range cracking products can be converted to the carbon oxides. For α-olefins longer than C_6 the selectivity to cracking products in the group of cracking plus total oxidation products increases with increasing space time, indicating that cracking products might be formed in a secondary step from either double bond isomers or oxidative dehydrogenation products.

Based on the results obtained in the space time experiments, where it was shown that the extrapolated selectivities to any of the product groups at zero space time are larger than zero, it can be concluded that all products in the various categories can be formed as primary products. Furthermore, the cracking products and total oxidation products can be formed in a secondary reaction from any of the other product groups. However, the double bond isomers have been found more stable than the partial oxidation products, which can be reacted more readily to cracking products or total oxidation products. The cracking products are also readily converted into total oxidation products. The scheme in Figure 4-6 summarises the findings of the space time experiments.

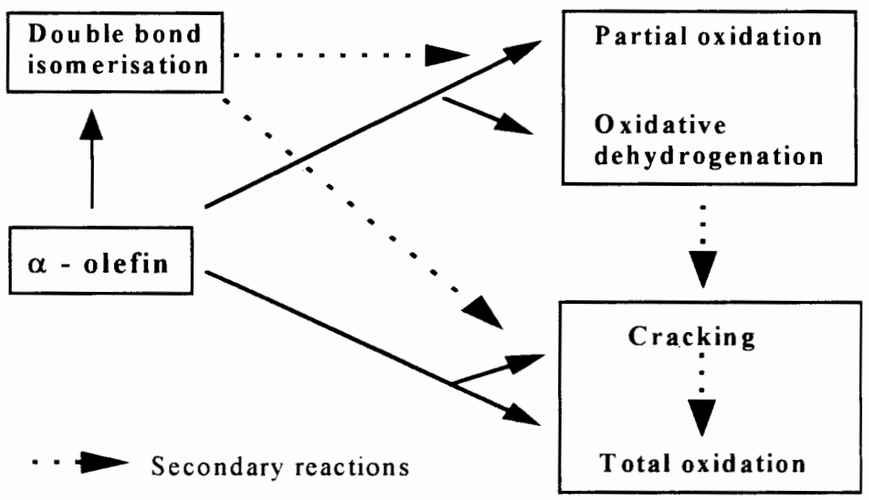

Figure 4-6 Proposed general scheme for the oxidative conversion of α-olefins over iron antimony oxide catalyst.

Cracking and total oxidation products can be further lumped together because they are the most stable products. Partial Oxidation and oxidative dehydrogenation products can be further lumped together, because of their similar reaction paths in their formation.

Figures 4-7a and 4-7b show the primary selectivities to the distinct product groups as a function of the chain length of the α-olefin for 350°C and 375°C, respectively. Higher temperatures could not be applied for the whole series of feedstocks (C_3-C_9 α-olefins), because thermal cracking, as determined by the carbon balance, becomes very severe for higher molar weight feedstocks, especially in the case of 1-octene and 1-nonene.

Ethene was almost nonreactive at 350 and 375°C and could therefore not be incorporated in the comparison of the influence of carbon number on the primary selectivity. However, at higher reaction temperatures (T≥450°C) ethene yields only total oxidation products.

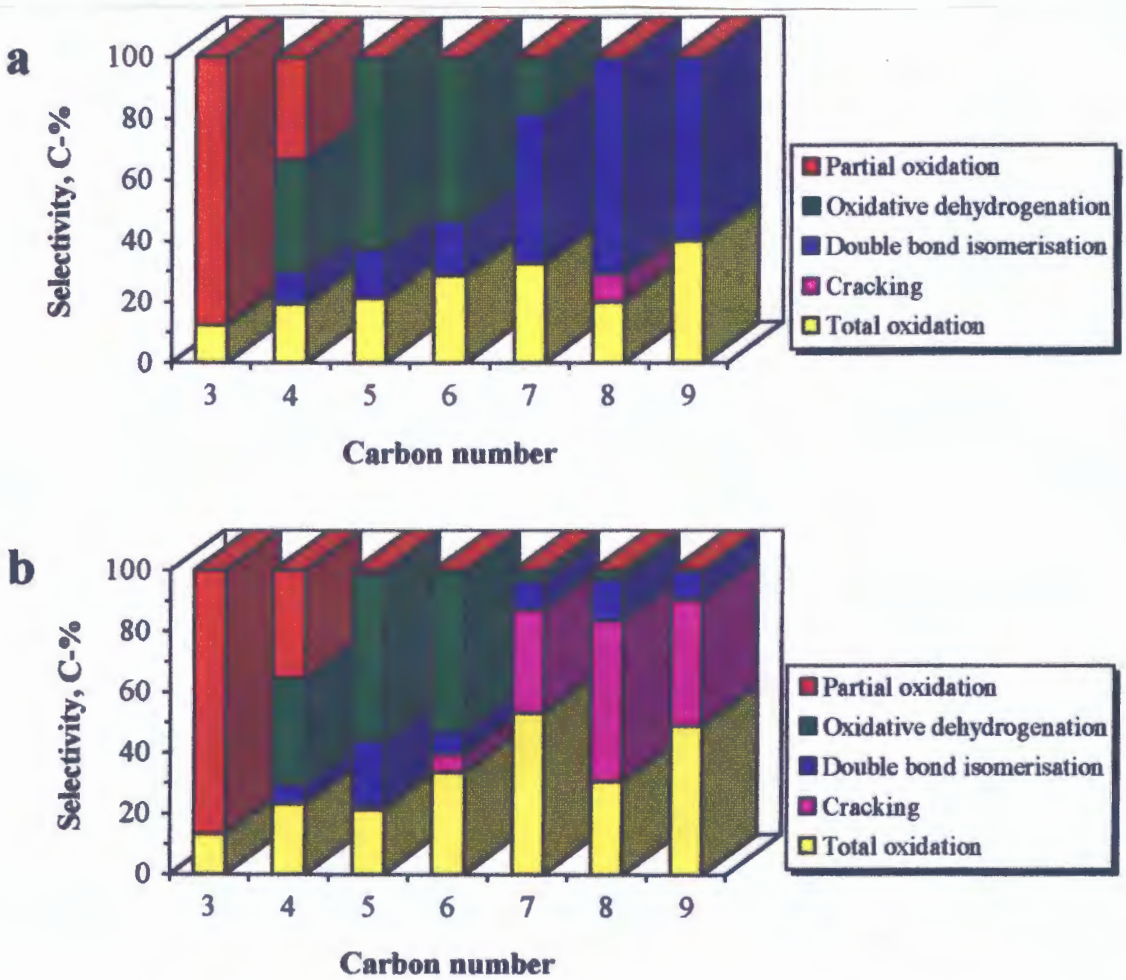

Figure 4-7 Influence of carbon number on the primary selectivity of α-olefin partial oxidation over iron antimony catalyst at 350°C (a) and 375°C (b) (Sb:Fe=1.5, T_{calc}=900°C for 7h in air; p=1.2 bar, feed composition: 10 mol-% hydrocarbon, 20 mol-% O_2, balance N_2, τ<0.5s; m_{cat}=0.5g diluted with 4g sand).

The formation of partial oxidation products appear only to a significant extend for propene and 1-butene as feedstocks and the primary selectivity to this product class drops dramatically with increasing carbon number.

At 350°C, the primary selectivity to double bond isomers increases steadily for carbon numbers of 4 and higher. The same applies to the primary selectivity to total oxidation

products, which increases steadily with carbon number. The primary selectivity to oxidative dehydrogenation products increases from C_4 to C_5 and decreases steadily with increasing carbon number to C_9, where no oxidative dehydrogenation products are detected anymore.

At 375°C, cracking products appear from a carbon number of 5 and the primary selectivity to those products increases steadily with increasing carbon number. The primary selectivity to total oxidation products increases with increasing temperature, whereas the primary selectivity to double bond isomers and oxidative dehydrogenation products decreases, especially when cracking products are formed, viz. from C_6 onwards.
The following conclusion can be drawn. The activation energy for the formation of cracking and total oxidation products is higher than for the formation of double bond isomers and oxidative dehydrogenation products.
The activation energy for the formation of total oxidation products increases with increasing carbon number because the primary selectivity to total oxidation products increases more strongly for higher carbon numbers of the feed. The same applies for the activation energy for the formation of cracking products. The activation energy for the formation of double bond isomers and oxidative dehydrogenation products decreases with increasing carbon number because the primary selectivities to those products decrease more strongly for higher carbon numbers of the feed.

The rate of consumption of olefins equals the sum of the rate of formation of the individual product compound. Since the rates were calculated on a C-basis and the inlet partial pressure of the olefins was kept constant for each olefin, therefore the molar flow of carbons increased with increasing carbon number of the olefin. The rates for the formation of partial oxidation products and oxidative dehydrogenation products show the same trend when increasing the carbon number of the olefin, indicating that they proceed along the same reaction pathway. Therefore they were investigated in one group. The same was observed for the rate of formation of cracking products and total oxidation products, both were therefore lumped together.

Figure 4-8 shows the carbon number dependency of the sum of the rates of formation of partial oxidation and oxidative dehydrogenation (Figure 4-8a) and the combined rate of cracking and of total oxidation (Figure 4-8b) at 350, 375 and 400°C.

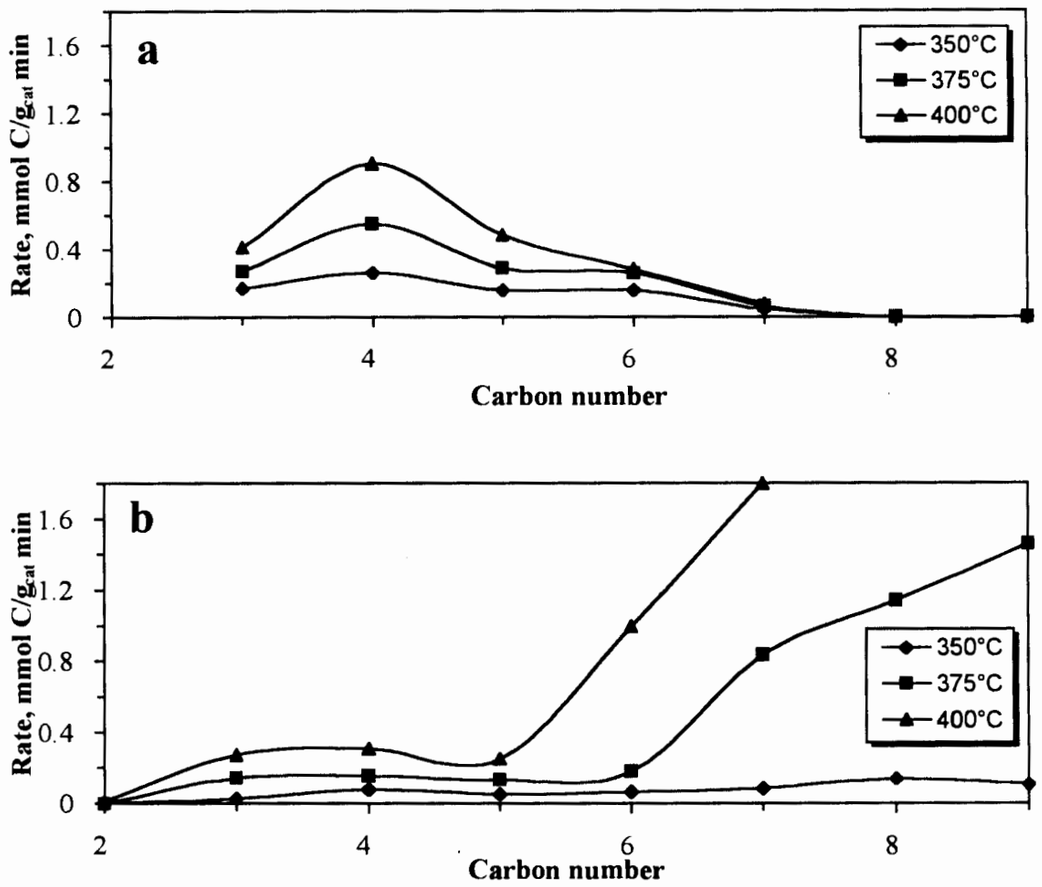

Figure 4-8 The rate of formation of some product groups as a function of carbon number at different temperatures over iron antimony oxide catalyst

a: rate of formation of partial oxidation and oxidative dehydrogenation products

b: rate of formation of cracking and total oxidation products

(p=1.2 bar, feed composition: 10 mol-% hydrocarbon, 20 mol-% O_2, balance N_2, τ=0.5s; m_{cat}=0.5g diluted with 4g sand).

The rate of formation of partial oxidation and oxidative dehydrogenation products show a maximum at C_4 and steadily decreases towards zero at C_8. Both the dienes and the conjugated aldehydes might be formed from a π-allylic intermediate. The existence of a maximum might be explained by a dual effect, viz. reduction of the electron density in the

π-allylic species by hyperconjugation, thereby stabilising this species on the catalyst surface, and shielding of both the allylic hydrogen atom thus inhibiting the formation of the π-allylic species but also inhibiting the initial olefin adsorption by shielding of the double bond.

The combined rate of formation of cracking and total oxidation products increases dramatically with increasing carbon number. The reaction pathway of the oxidative decomposition of α-olefins must involve the double bond via an adsorbed π-olefinic complex, because the oxidation of paraffins with the same catalyst and under identical reaction conditions is not feasible. This was shown for the example of propane (Chapter 3-4), proving that the activation of the paraffinic C-H bond is not possible under the reaction conditions applied.

The strong increase in the rate of formation of cracking and total oxidation products with increasing carbon number might be explained by the enhanced strength of adsorption of the olefin on the oxide surface. However, an electronic effect caused by the change in alkyl chain length is a short range effect which might well explain the observed increase from C_2 to C_3, but cannot explain the dramatic increase of these rates with carbon number. Increasing chain length causes a move effective shielding of the allylic hydrogen atom, which might therefore increase a direct attack on the double bond by a surface hydroxyl group thus yielding a surface alkyl species bonded to a lattice oxygen. According to Finocchio *et al.* (1994), this species results in a C-C bond cleavage and the formation of both cracked products and total oxidation products.

The rate of formation of double bond isomers on a carbon atom basis was hardly affected by both carbon number and temperature.

4.2.2 Effect of changing partial pressures

The effect of changing the partial pressures of the olefin and of oxygen on the selectivities for each individual olefin in the range C_2 to C_6 is shown in Appendix VII. In this section the influence of partial pressure on the selectivities is compared for changing the carbon number of the olefin.

Table 4.1 gives and overview of the influence of changing partial pressures of the olefin and oxygen on the selectivities.

Table 4-1 Effect of increasing partial pressures of the olefin and oxygen on the selectivities in the oxidative conversion of various α-olefins over iron antimony oxide. (Sb:Fe=1.5, T_{calc}=900°C, t_{calc}=7h). (p=1.2 bar, $m_{catalyst}$=0.5g)

α-olefin feed	product formed	p_{olefin} ↑	p_{O2} ↑
ethene	Sco	const.	↑ (high T)
	S_{CO2}	const.	↓ (high T)
propene	S_{PO}[1)]	↑ (high T)	const.
	S_{TO}[1)]	↓ (high T)	const.
1-butene	S_{DBI}[1)]	↑(low T)	↓
	S_{ODH}[1)]	↓(high T)	↑(high T)
	S_{PO}[1)]	↓(low T),↑(high T)	↑
	S_{TO}[1)]	const.	const.
1-pentene	S_{DBI}[1)]	↑	↓
	S_{ODH}[1)]	↓	↑
	S_{TO}[1)]	↑(high T)	const.
1-hexene	S_{DBI}[1)]	↑	↓(high T)
	S_{ODH}[1)]	↓	const.
	S_{TO}[1)]	↑(high T), ↓(low T)	↑(high T)
	S_{crack}[1)]	↑	const.

[1)] S_{PO}=Selectivity to partial oxidation products; S_{ODH}=Selectivity to oxidative dehydrogenation products; S_{DBI}=Selectivity to double bond isomers; S_{TO}=Selectivity to total oxidation products; S_{crack}=Selectivity to cracking products

Generally one can observe that the influence of increasing partial pressure of the olefin on the selectivities is countercurrent to the influence of the partial pressure of oxygen. In some cases there is only an influence at one specific temperature (indicated by high T or low T), where for other temperatures the selectivity remains constant.

Changing partial pressures has the least influence on the selectivity to total oxidation products, it remains constant in most of the cases. The selectivities to double bond isomers and oxidative dehydrogenation products behave concurrently with changing partial pressures of α-olefin and oxygen. While the selectivity to double bond isomers increases with increasing partial pressure of α-olefins, it decreases with increasing partial pressure of oxygen. The opposite happens to the selectivity to oxidative dehydrogenation products. With increasing partial pressure of α-olefins, the selectivity tends to decrease, while it increases with increasing partial pressure of oxygen. This is an indication that the double bond isomerisation reaction requires less oxygen than the oxidative dehydrogenation reaction and will therefore be preferentially be formed when less oxygen is made available, by either increasing the partial pressure of α-olefin or decreasing the partial pressure of oxygen.

It is difficult to make a statement about the influence of partial pressure on the selectivity to partial oxidation products in comparison to the other product groups, since the only time when it is formed in measurable amounts concurrently with double bond isomers and oxidative dehydrogenation products is in the case of 1-butene as feedstock.

Changing the partial pressure of oxygen doesn't change the selectivities in the case of propene as feedstock. In the case of butene, the selectivity to partial oxidation increases in comparison to the selectivity to total oxidation with increasing partial pressure of oxygen. This can be explained by increasing the oxidation state of the catalyst, which is favourable for the formation of partial oxidation products as shown when passing oxygen prior to the partial oxidation reaction of propene over the catalyst, which resulted in an increase of the initial activity and selectivity to acrolein (Section 3.4.5).

CHAPTER 5

MODELLING THE KINETICS OF THE PARTIAL OXIDATION OF α-OLEFINS

APPENDIX II

DATA WORK UP

5. MODELLING THE KINETICS OF THE PARTIAL OXIDATION OF α-OLEFINS

The modelling is divided into one section which deals with the kinetics of the olefin feed consumption and one which deals with the kinetics of the formation of products. The various models are compared by means of the average error between the calculated and measured rates and the accuracy of the determined parameters by means of the 95% confidence limits. The model development will be first introduced before the results are shown in a separate section.

5.1 MODEL DEVELOPMENT

In the following the development of four models is described. The first model is a redox model, which goes back to the findings of Mars and van Krevelen (1954) on the partial oxidation of aromatics over vanadium oxide catalysts. Furthermore a power law model, a single site Langmuir-Hinshelwood model and an oxidation model were considered.

5.1.1 Redox (Mars-van Krevelen) mechanism

Mars and van Krevelen (1954) were the first to suggest a redox mechanism in partial oxidation reactions, which assumes a steady state between the reduction of the catalyst by an hydrocarbon feed and the reoxidation by gaseous oxygen. As a consequence this model emphasises strongly on the role of lattice oxygen and the degree of reduction of the catalyst. It immediately follows that a change in the product spectrum by varying the partial pressures of the reactants can only be related to the extent of reduction of the catalyst or to the difference in the rate constants of the active sites yielding the different product compounds.

The rate of reduction and rate of oxidation of the catalyst can be expressed following:

$$r_{reduction} = k_{reduction} \cdot p_{olefin}^{n} \cdot \theta_{ox} \qquad (5\text{-}1)$$

$$r_{oxidation} = k_{oxidation} \cdot p_{O_2}^{m} \cdot (1-\theta_{ox}) \qquad (5\text{-}2)$$

with θ_{ox} being the fraction of the oxidised active sites of the catalyst. At steady-state the rate of oxidation equals the rate of reduction. If β moles of oxygen are required to oxidise 1 mole of olefin feed then the rate of olefin consumption can be brought into the form:

$$-r_{olefin} = \frac{k_{reduction} \cdot p_{olefin}^{n} \cdot k_{oxidation} \cdot p_{O_2}^{m}}{\beta \cdot k_{reduction} \cdot p_{olefin}^{n} + k_{oxidation} \cdot p_{O_2}^{m}} \qquad (5\text{-}3)$$

The stoichiometric number β is strongly dependent on the type of product formed, e.g. total oxidation or double bond isomers etc., but to a lesser extent on the partial pressures of the reactants oxygen and olefin and on the temperature.

The rate constants $k_{reduction}$ and $k_{oxidation}$ and the orders n and m were obtained by minimising the sum of squares of residuals (SSR), which is defined as

$$SSR = \sum_{J=1}^{N} \left(r_{measured,J} - r_{model,J} \right)^2 \qquad (5\text{-}4)$$

where N is the number of observations, using the downhill simplex method (Press et al., 1989). The sum of squares of residuals (SSR) was calculated at three different reaction temperatures for each feed. The PASCAL programme which has been used to make the optimisation is included in Appendix VIII.

The average orders with respect to oxygen and with respect to the olefin were determined for the olefins in the carbon number range from C_2 to C_6, for each olefin at three different temperatures. The average order with respect to oxygen was determined as 1.0 ± 0.4 and the average order with respect to the olefin as 1.1 ± 0.4. This shows that the observed kinetics over iron antimony oxide are a composite of both the reduction and the reoxidation kinetics, which confirms the findings of Keulks and Lo (1986), who stated that the partial oxidation of olefins over iron antimony oxide takes place over a partially reduced surface with a relatively slow rate of reoxidation.

For the next stage of the kinetic investigation, which is the calculation of activation energies and pre-exponential factors, the reaction orders m and n in Equation 5-3 were

fixed at a value of 1 and the rate constants optimised for different temperatures and the different olefins. The rate of olefin consumption in its final form is shown in Equation 5-5:

$$-r_{olefin} = \frac{k_{reduction} \cdot k_{oxidation} \cdot p_{olefin} \cdot p_{O_2}}{\beta \cdot k_{reduction} \cdot p_{olefin} + k_{oxidation} \cdot p_{O_2}} \qquad (5\text{-}5)$$

5.1.2 Power law model

A power law model was applied in order to give an indication on the effect of partial pressures and temperature on the rate of formation of the different product groups, i.e. partial oxidation plus oxidative dehydrogenation, total oxidation plus cracking and double bond isomerisation. The rate of consumption of the olefin is simply the sum of the rate of formation of all product groups.

Assuming an Arrhenius relationship between the rate constant and temperature, then the reaction orders with respect to the partial pressure of the olefin and of oxygen and the activation energy can be estimated using:

$$r_i = A_i \cdot e^{-\frac{E_{a,i}}{R \cdot T}} \cdot p_{olefin}^{n} \cdot p_{O_2}^{m} \qquad (5\text{-}6)$$

The parameters A_i, $E_{a,i}$, n and m were optimised by minimising the sum of squares of residuals (SSR) in Equation 5-4.

5.1.3 Single site Langmuir-Hinshelwood model

If the rate determining step is known, then the rate of formation of the products can be modelled using the Langmuir-Hinshelwood model.

For this model the assumptions were made that all catalytic sites are energetically equal and all sites have affinities for both olefin and oxygen and each molecule occupies only one site. If both the adsorption of the olefin and of oxygen are assumed to be at equilibrium and the rate determining step is the reaction between the adsorbed olefin and an adjacent oxygen species, then following rate equation can be derived:

$$\text{olefin} + * \overset{K_1}{\longleftrightarrow} \text{olefin}*$$

$$O_2 + 2^* \xleftrightarrow{K_2} 2\,O^*$$

$$\text{olefin}^* + O^* \rightarrow \ldots \quad \text{(rds)}$$

The rate equation for the formation of product i according to the single site mechanism can be derived to:

$$r_i = k_i \frac{K_1 \cdot K_2 \cdot p_{olefin} \cdot p_{O_2}^{\frac{1}{2}}}{(1 + K_1 \cdot p_{olefin} + K_2 \cdot p_{O_2}^{\frac{1}{2}})^2} \qquad (5\text{-}7)$$

When optimising the parameters k_i, K_1 and K_2 by minimising Equation 5-4, the oxygen inhibition term was generally found to be negligible. In order to minimise the number of parameters Equation 5-7 was brought into the form:

$$r_i = k_i \frac{K_1 \cdot K_2 \cdot p_{olefin} \cdot p_{O_2}^{\frac{1}{2}}}{(1 + K_1 \cdot p_{olefin})^2} \qquad (5\text{-}8)$$

5.1.4 Oxidation model

Oxygen is situated either as a multiple bonded terminal oxygen or as a bridging oxygen between two metal atoms. This concept is similar to the one described by Mitchell and Trifirò (1970) for a bismuth molibdate catalyst.

$$Sb + O_2 \xleftrightarrow{K_1} Sb\text{-}O\text{-}O \qquad (5\text{-}9)$$

$$Sb\text{-}O\text{-}O + * \xleftrightarrow{K_2} Sb{=}O + O^* \qquad (5\text{-}10)$$

$$Sb{=}O + * \xleftrightarrow{K_3} Sb + O^* \qquad (5\text{-}11)$$

$$Sb\text{-}O\text{-}O + \text{olefin} \longrightarrow Sb\text{-}O\text{-}O\text{-olefin} \qquad (5\text{-}12)$$

Sb-O-O-olefin	+	*	$\longrightarrow$	$CO+CO_2$	(5-12a)
Sb=O	+	olefin	$\overset{K_5}{\longleftrightarrow}$	Sb-O-olefin	(5-13)
Sb-O-olefin	+	O*	$\longrightarrow$	PO/ODH	(5-13a)
Sb-O-olefin	+	O*	$\longrightarrow$	Double bond isomers	(5-13b)
Sb	+	olefin	$\overset{K_6}{\longleftrightarrow}$	Sb-olefin	(5-14)
Sb-olefin	+	O*	$\longrightarrow$	CO+CO2	(5-14a)
Sb-olefin	+	O*	$\longrightarrow$	Double bond isomers	(5-14b)

with * and O* being the bridging positions between two metal atoms in the crystallite lattice surface. It is assumed that at steady state there is no net flux of lattice oxygen to the surface of the catalyst.

The formation of the various products can be thought to arise from the various olefin surface species:

It can be assumed, that the reactions (5-9), (5-10), (5-11), (5-13) and (5-14) are at equilibrium and reactions (5-12), (5-12a), (5-13a), (5-13b), (5-14a) and (5-14b) are irreversible.

The derivation of the rate equations for the formation of the product groups is shown in detail in Appendix IX.

The rate equation for the formation of partial oxidation and oxidative dehydrogenation products according to the oxidation mechanism can be derived to:

$$r_i = \frac{a_i \cdot p_{olefin} \cdot p_{O2}^{\frac{1}{2}}}{(1+K_1 \cdot p_{O_2} + K_1^{\frac{1}{2}} \cdot K_2^{\frac{1}{2}} \cdot K_3^{\frac{1}{2}} \cdot p_{O_2}^{\frac{1}{2}} + \frac{k_4}{k_{4a}} \cdot K_1 \cdot p_{olefin} \cdot p_{O_2} + K_1^{\frac{1}{2}} \cdot K_2^{\frac{1}{2}} \cdot K_3^{\frac{1}{2}} \cdot K_5 \cdot p_{O_2}^{\frac{1}{2}} \cdot p_{olefin} + K_6 \cdot p_{olefin})} \quad (5\text{-}15)$$

with $a_i = n_{Sb,\,total} \cdot k_{5a} \cdot K_1^{1/2} \cdot K_2^{1/2} \cdot K_3^{-1/2} \cdot K_5$

for the rate of formation of double bond isomers the equation becomes:

$$r_i = \frac{a_i \cdot p_{olefin} \cdot p_{O2}^{\frac{1}{2}} + b_i \cdot p_{olefin}}{(1+K_1 \cdot p_{O_2} + K_1^{\frac{1}{2}} \cdot K_2^{\frac{1}{2}} \cdot K_3^{\frac{1}{2}} \cdot p_{O_2}^{\frac{1}{2}} + \frac{k_4}{k_{4a}} \cdot K_1 \cdot p_{olefin} \cdot p_{O_2} + K_1^{\frac{1}{2}} \cdot K_2^{\frac{1}{2}} \cdot K_3^{\frac{1}{2}} \cdot K_5 \cdot p_{O_2}^{\frac{1}{2}} \cdot p_{olefin} + K_6 \cdot p_{olefin})} \quad (5\text{-}16)$$

with $a_i = n_{Sb,total} \cdot k_{5b} \cdot K_1^{1/2} \cdot K_2^{1/2} \cdot K_3^{-1/2} \cdot K_5$

and $b_i = n_{Sb,total} \cdot k_{6b} \cdot K_6$

for the rate of formation of total oxidation and cracking products the equation becomes:

$$r_i = \frac{a_i \cdot p_{olefin} \cdot p_{O2}^{\frac{1}{2}} + b_i \cdot p_{olefin} \cdot p_{O_2}}{(1 + K_1 \cdot p_{O_2} + K_1^{\frac{1}{2}} \cdot K_2^{\frac{1}{2}} \cdot K_3^{\frac{1}{2}} \cdot p_{O_2}^{\frac{1}{2}} + \frac{k_4}{k_{4a}} \cdot K_1 \cdot p_{olefin} \cdot p_{O_2} + K_1^{\frac{1}{2}} \cdot K_2^{\frac{1}{2}} \cdot K_3^{\frac{1}{2}} \cdot K_5 \cdot p_{O_2}^{\frac{1}{2}} \cdot p_{olefin} + K_6 \cdot p_{olefin})} \quad (5\text{-}17)$$

with $a_i = n_{Sb,total} \cdot k_{6a} \cdot K_6 \cdot K_1^{1/2} \cdot K_2^{1/2} \cdot K_3^{-1/2}$

and $b_i = n_{Sb,total} \cdot k_4 \cdot K_1$.

Here, as already the case at the single site mechanism, the optimisation of the parameters a_i, b_i, k_i and K_i by minimising SSR in Equation 5-4 revealed that the oxygen inhibition terms are negligible. Furthermore the parameter b_i gave very small or even negative values, so that b_i in the Equations 5-16 and 5-17 can also be neglected. This shows that the formation total oxidation and cracking products from Sb-O-O-olefin species (Equation (5-12)) and the formation of double bond isomers from Sb-olefin species (Equation (5-14b)) are negligible. This is expected since it has been suggested that metal-bonded intermediates produce total oxidation products (Oyama, 1996).

Equations 5-15 to 5-17 were therefore brought into the simplified form:

$$r_i = \frac{a_i \cdot p_{olefin} \cdot p_{O2}^{\frac{1}{2}}}{1 + K_6 \cdot p_{olefin}} \quad (5\text{-}18)$$

5.2 MODELLING THE RATE OF CONSUMPTION OF OLEFINS

5.2.1 Redox (Mars-van Krevelen) mechanism

Table 5-1 shows the rate constants for the reoxidation and reduction step together with their 95% confidence limits and the sums of squares of the residuals. The accuracy of the estimated rate constants tends to decrease with increasing chain length of the α-olefins, especially for the rate constants of the reoxidation step.

Table 5-1 Rate constants for the rate of consumption of the α-olefins (C_2-C_6) according to the redox model together with their 95% confidence limits.

Feed	$T_{reaction}$, °C	$k_{reduction}$, $\frac{mmol}{g_{cat} \cdot min \cdot bar}$	$k_{oxidation}$, $\frac{mmol}{g_{cat} \cdot min \cdot bar}$	SSR, $10^{-4} \frac{mmol}{g_{cat} \cdot min \cdot bar}$
ethene	450	0.70 ± 0.04	0.41 ± 0.10	5.28
	460	0.84 ± 0.03	0.62 ± 0.09	3.95
	475	0.99 ± 0.04	1.25 ± 0.19	4.55
propene	350	0.76 ± 0.08	1.10 ± 0.09	4.13
	375	1.52 ± 0.10	1.41 ± 0.32	6.20
	400	1.94 ± 0.15	2.44 ± 0.57	10.61
1-butene	350	2.06 ± 0.09	0.78 ± 0.05	5.24
	375	3.98 ± 0.35	1.92 ± 0.17	30.74
	400	5.81 ± 0.47	3.91 ± 0.26	39.38
1-pentene	350	1.41 ± 0.07	0.46 ± 0.05	5.88
	375	1.45 ± 0.11	1.23 ± 0.33	14.32
	400	2.20 ± 0.17	4.03 ± 1.46	22.47
1-hexene	350	0.52 ± 0.14	1.74 ± 12.15	24.28
	375	1.58 ± 0.35	3.92 ± 7.26	72.13
	400	3.21 ± 0.52	19.79 ± 33.57	27.26

The rate constants for the reduction step increase with increasing temperature and show a maximum at C_4. The rate constants for the reoxidation step for 1-hexene as feedstock could not be determined accurately. For the C_3-C_5 olefins the rate constants for the reoxidation step show different trends for different temperatures, e. g. they decrease at 350°C and increase at 400°C.

The redox (Mars van Krevelen) model was evaluated using the parity plots (Figure 5-1) together with the average error (Table 5-2), which is defined as:

$$average\ error \equiv \frac{1}{N}\sum_{j=1}^{N}\frac{\left|r_{j,calculated} - r_{j,measured}\right|}{r_{j,measured}} \tag{5-19}$$

where N is the number of observations (Borman and Westerterp, 1995).

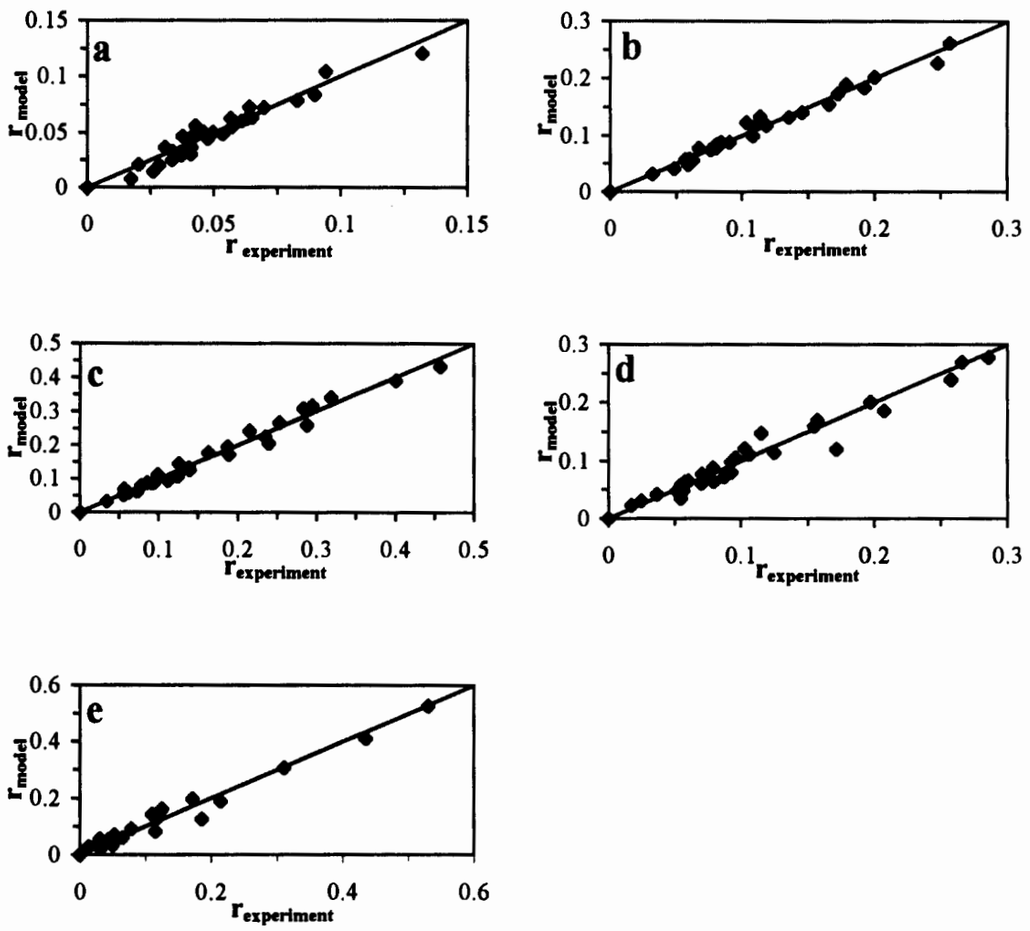

Figure 5-1 Parity between the experimental rates and the rates obtained by the redox (Mars van Krevelen) model for the consumption of ethene (a), propene (b), butene (c), pentene (d) and hexene (e) over iron antimony oxide (Sb:Fe=1.5, T_{calc}=900°C). T=350, 375 and 400°C (450, 460, 475°C for Ethene).

Table 5-2 Average error (%) in the prediction of the rate of consumption of α-olefins (C_2-C_6) in the partial oxidation over iron antimony oxide (Sb:Fe=1.5, T_{calc}=900°C).

feedstock	average error, %
ethene	13.31
propene	6.13
1-butene	8.47
1-pentene	12.88
1-hexene	28.16

Except for 1-hexene, the average error for the rate of consumption of α-olefin is below 15% and thus a reasonable description of the kinetics.

The activation energies of the reduction and reoxidation step as a function of the carbon number of the α-olefin are shown in Figure 5-2.

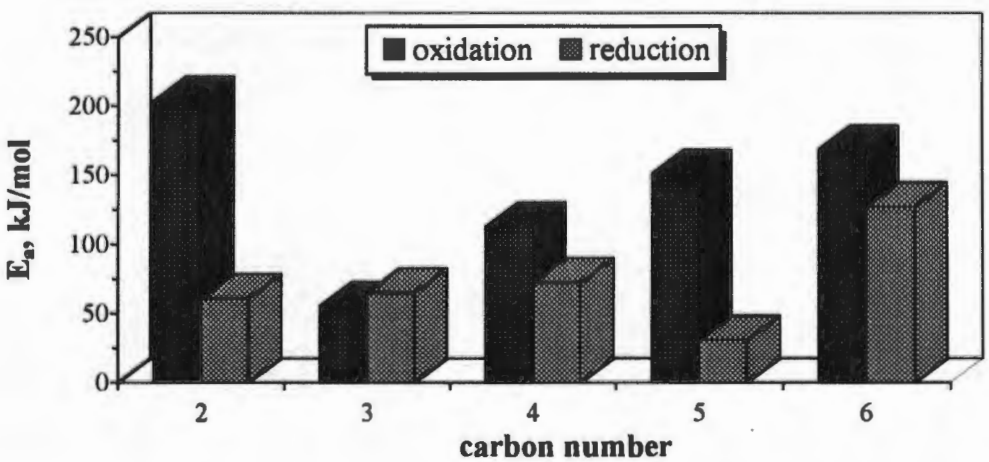

Figure 5-2 Activation energy for the reduction step and reoxidation step using the redox (Mars van Krevelen) model as a function of carbon number in the partial oxidation over iron antimony oxide (Sb:Fe=1.5, T_{calc}=900°C, t_{calc}=7h).

The activation energy for the reduction step is within the accuracy of the determination of the rate constants independent of the carbon number of the α-olefin, indicating that the step

leading to the reduction of the oxide catalyst has the same energy barrier for all the olefins. The activation energy for the reoxidation step is higher than for the reduction step and shows a carbon number dependency. The carbon number dependency of the activation energy of the reoxidation step is not expected since the activation energy should be independent of the way the partially reduced catalyst was created, i.e. independent of the used feed. The Mars-van Krevelen mechanistic description is therefore inadequate.

5.3 MODELLING THE RATE OF FORMATION OF PRODUCTS

The models considered to describe the rate of formation of the various product groups were a power law model, a Langmuir-Hinshelwood model and an oxidation model. The redox (Mars-van Krevelen) model was not considered for the rate of formation of products because the material balance over the catalytic site is valid for the consumption of the olefin but not necessarily for the rate of formation of products. It would only be valid if each product was formed at a different catalytic sire, however, there is no proof for such a behaviour.

Having calculated the rate of formation of the individual product groups, the rate of consumption of the feed can be calculated from the sum of the rate of formation of all products.

5.3.1 Power law model

A power law model was applied to give a first indication on the effect of partial pressures and temperature on the rate of formation of the different product groups, i.e. partial oxidation plus oxidative dehydrogenation, total oxidation plus cracking and double bond isomerisation (see Section 4.2.1). The rate of consumption of the α-olefin can then be calculated by the sum of the rates of formation of the individual product groups. The reaction orders with respect to the partial pressure of olefin and oxygen together with the activation energy were estimated using:

$$r_i = A_i \cdot e^{-\frac{E_{a,i}}{R \cdot T}} \cdot p_{olefin}^{n} \cdot p_{O_2}^{m} \qquad (5\text{-}20)$$

and optimised by minimising the sum of squares of residuals in Equation 5-4. Figure 5-3 shows the influence of olefin chain length on the orders with respect to oxygen and olefin partial pressures for the rate of formation of the various product groups.

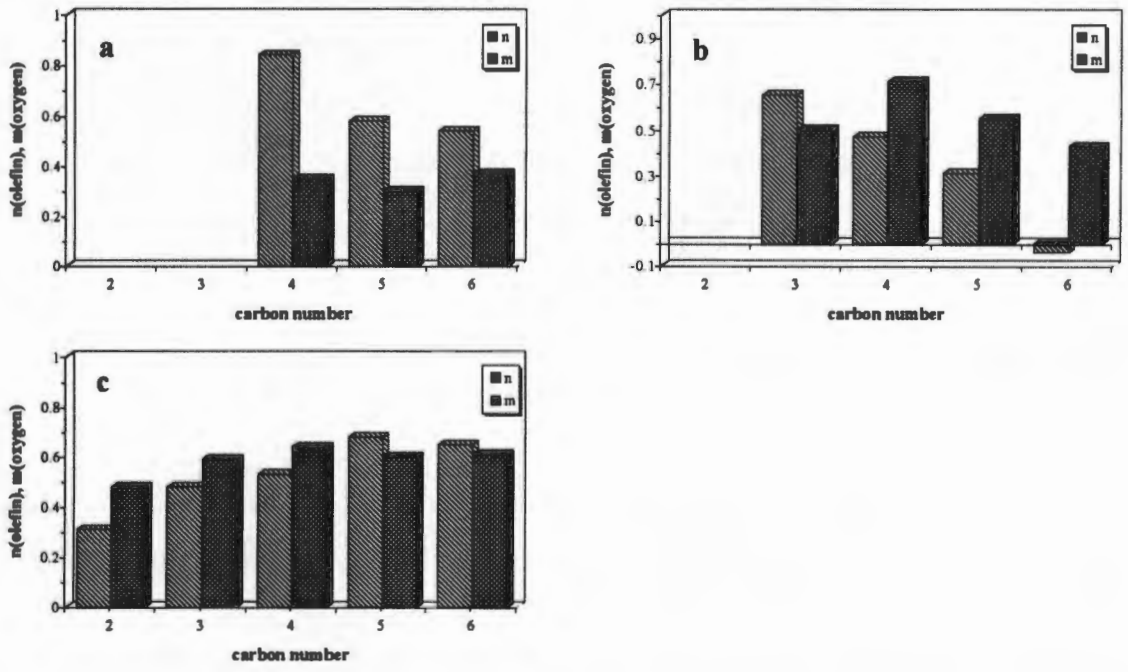

Figure 5-3 Influence of carbon number on the order m with respect to olefin partial pressure and n with respect to oxygen partial pressure for the rate of formation of double bond isomers (a), partial oxidation plus oxidative dehydrogenation (b) and total oxidation plus cracking products (c). (T=350, 375 and 400°C for C_3-C_6, T=450, 460 and 475°C for C_2)

Formation of double bond isomers (Figure 5-3a)

The rate of formation of double bond isomers is much stronger dependent on the partial pressure of the olefins than on the oxygen partial pressure, whereas for the other products groups the rates are stronger dependent on the oxygen partial pressure. A decrease of the order with respect to olefin with increasing carbon number is observed, indicating an increasing adsorption strength with increasing carbon number. The positive order with respect to the oxygen indicates an involvement of surface oxygen in the isomerisation reaction, possibly in a reversible hydrogen transfer.

Formation of partial oxidation and oxidative dehydrogenation products (Figure 5-3b)

The order with respect to olefin partial pressure decreases strongly with increasing carbon number and becomes even slightly negative for 1-hexene. The fact that olefin inhibits the oxidative olefin conversion for high carbon numbers indicates a increase in adsorption strength with increasing carbon number of the olefin feed. The order with respect to oxygen is positive and generally higher than the order with respect to olefin. The carbon number has no strong influence on the order with respect to oxygen, with the exception at C_4 which is slightly higher than for the rest of the investigated olefins.

Formation of total oxidation and cracking products (Figure 5-3 c)

The order with respect to the partial pressure of oxygen is again almost constant for different carbon numbers of the olefin feed. The order with respect to olefin partial pressure behaves differently from the formation of the other product groups, it increases with increasing carbon number. This suggests that the formation of total oxidation plus cracking products follow a different mechanism or have a different rate determining step. This behaviour might be attributed to the fact that the formation of total oxidation products results from the reaction of the adsorbed olefin with electrophilic oxygen species, while the partial oxidation products are formed by a reaction with nucleophilic oxygen species (Bielanski and Haber, 1991). The electrophilic oxygen species are intermediates in the reoxidation of the catalyst. Increasing the olefin partial pressure will yield a higher degree of reduction on the catalyst surface, which in turn will result in a relative higher content of the electrophilic oxygen species in the pool of oxygen species. The influence of the olefin partial pressure is therefore an indirect one.

The influence of the chain length of the α-olefin on the activation energy and pre-exponential factor, which was calculated by optimising Equation 5-20 for the formation of the various product groups is shown in Figure 5-4.

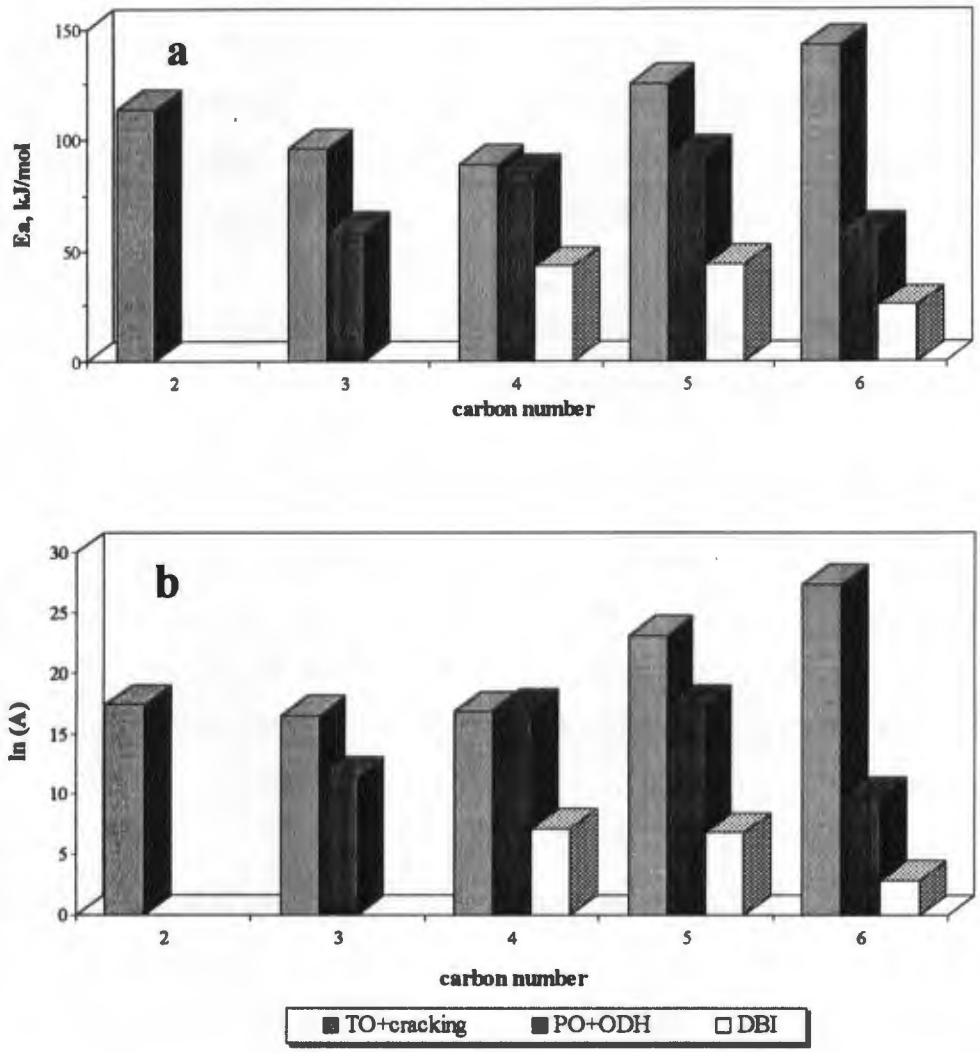

Figure 5-4 Influence of carbon number on the activation energy (a) and the pre-exponential factor (b) in the partial oxidation of α-olefins over iron antimony oxide (Sb:Fe=1.5, T_{calc}=900°C, t_{calc}=7h) for the formation of total oxidation plus cracking products (total ox.), partial oxidation plus oxidative dehydrogenation products (PO+ODH) and double bond isomers (DBI) as determined by the power law model.

The activation energy over the range of α-olefins from ethene to 1-hexene follow the order:

$$E_{a,\text{total oxidation+cracking}} > E_{a,\text{partial oxidation+oxidative dehydrogenation}} > E_{a,\text{double bond isomerisation}}$$

The pre-exponential factors A follow the same trend. A strong correlation between ln(A) and the activation energy can be observed.

The activation energy for the formation of total oxidation plus cracking products shows a minimum at C_4. This minimum might be caused by a dual effect of increasing heat of adsorption with increasing carbon number which leads to a decrease in activation energy and a decreasing reactivity and hence increase of activation energy with increasing carbon number due to steric effects. Increasing olefin chain length results in a shielding of the double bond, which inhibits the adsorption of the olefin and a shielding of the allylic hydrogen, which might lead to an enhanced probability of the direct attack of the double bond by electrophilic oxygen (Section 4.2.1).

The activation energy for the formation of partial oxidation products plus oxidative dehydrogenation products increases from C_3 to C_5 and seem to reach a maximum at C_5, but a significant drop was observed for the activation energy for the formation of partial oxidation plus oxidative dehydrogenation products in the partial oxidation of 1-hexene. The increase from C_3 to C_5 might be attributed to the influence of the alkyl chain on the stability of the intermediate π-allyl complex.

The activation energy for the formation of double bond isomers is hardly dependent on the carbon number of the α-olefin and is estimated to be 45 kJ/mol, however a drop in the activation energy at C_6 can be observed.
Figures 5-5 to 5-7 show the parity plots of the measured rates and the calculated rates for the formation of the different product groups.

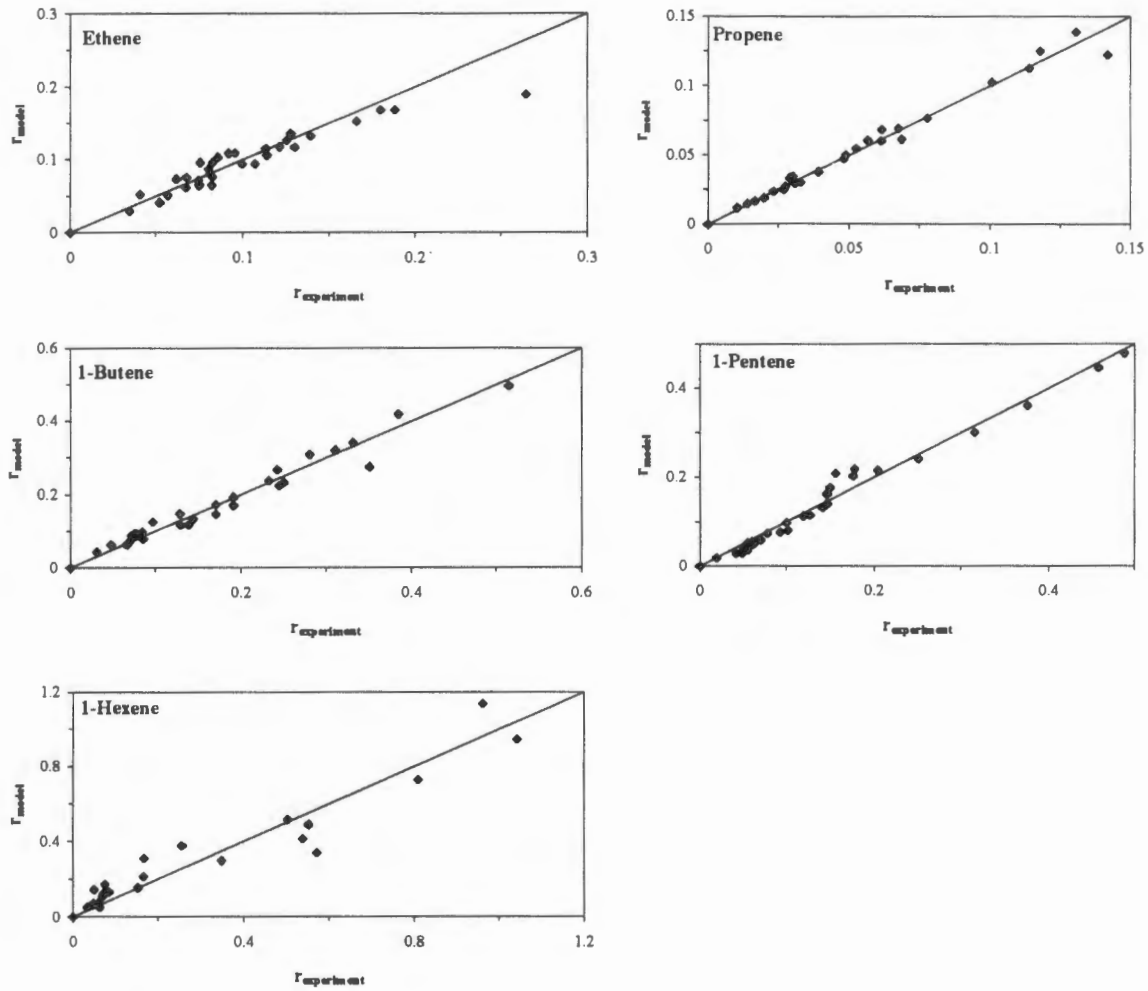

Figure 5-5 Parity between the calculated rates and experimental rates for the formation of total oxidation plus cracking products in the conversion of various α-olefins (C_2-C_6) over iron antimony oxide (Sb:Fe=1.5, T_{calc}=900°C, t_{calc}=7h) using the power-law model.

The measured rates lie close to the diagonal line, except for hexene, where the deviation is slightly higher.

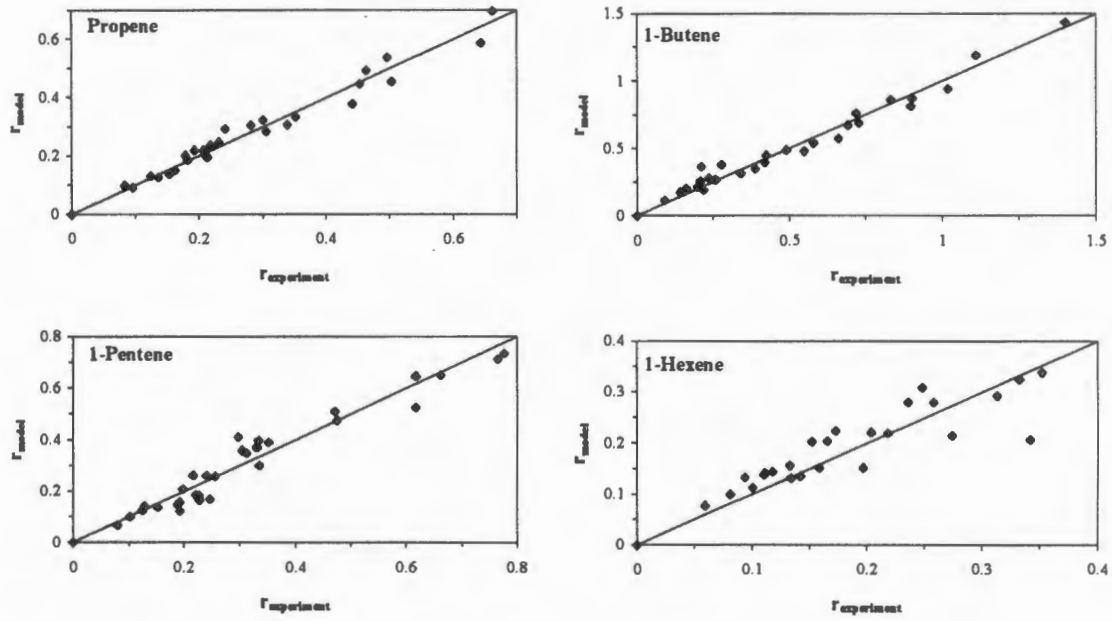

Figure 5-6 Parity between the calculated rates and experimental rates for the formation of partial oxidation plus oxidative dehydrogenation products in the conversion of various α-olefins (C_3-C_6) over iron antimony oxide (Sb:Fe=1.5, T_{calc}=900°C, t_{calc}=7h) using the power-law model.

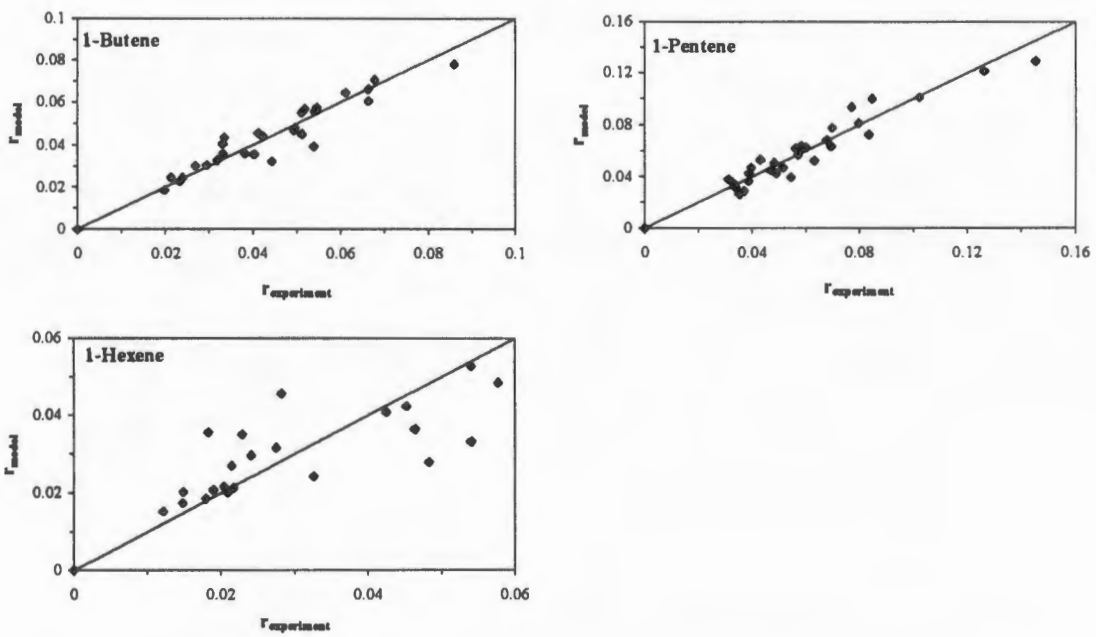

Figure 5-7 Parity between the calculated rates and experimental rates for the formation of double bond isomers in the conversion of various α-olefins (C_4-C_6) over iron antimony oxide (Sb:Fe=1.5, T_{calc}=900°C, t_{calc}=7h) using the power-law model.

A diagonal line describes satisfactory the relationship between measured and calculated rates for the feedstocks 1-butene and 1-pentene. However, for 1-hexene the model at low rates of formation are higher than the measured rates, while for high rates of formation the model gives values which are lower than the experimental rates.

Table 5-3 shows the average error calculated with Equation 5-19 for the rates of formation of the different product groups.

Table 5-3 Average error in the prediction of the rate of formation for the different product groups in the partial oxidation of α-olefins (C_2-C_6) over iron antimony oxide (Sb:Fe=1.5, T_{calc}=900°C, t_{calc}=7h) according to the power law model.

	Double bond isomerisation	Partial oxidation + oxidative dehydrogenation	Total oxidation + cracking
ethene			12.0
propene		8.4	5.6
1-butene	9.5	12.6	12.2
1-pentene	11.2	13.5	14.3
1-hexene	24.3	18.3	46.4

The power law model describes the rates of product formation well in the range C_2 to C_5, however the rate of product formation for 1-hexene as a feedstock can't be described accurately.

5.3.2 Langmuir-Hinshelwood model and oxidation model

The values of the optimised parameters together with their 95 % confidence limits and the sums of squares of the residuals (SSR) are given in Table 5-4 for the single site Langmuir-Hinshelwood model and in Table 5-5 for the oxidation model.

Table 5-4 Apparent rate constant k_iK_2 (in mmol C/g_{cat} min $bar^{0.5}$) and equilibrium constant K_1 (in bar^{-1}) together with their 95% confidence limits and the sum of squares of residuals (SRR in 10^{-3} (mmol C/g_{cat}min)^2) for the rate of formation of the various product groups in the partial oxidation of α-olefins (C_2-C_6) over iron antimony oxide according to the single site Langmuir-Hinshelwood model.

		Isomerisation			Partial Oxidation + Oxidative Dehydrogenation			Total Oxidation + Cracking		
Feed	$T_{reaction}$	$k_{iso}K_2$	K_1	SSR	$k_{PO+ODH}K_2$	K_1	SSR	$k_{TO}K_2$	K_1	SSR
ethene	450							0.53±0.11	4.01±2.57	1.06
	460							0.83±0.08	2.60±1.46	1.15
	475							1.76±0.23	1.37±0.57	1.74
propene	350				1.89±0.17	2.04±0.64	0.90	0.23±0.01	3.11±0.91	0.02
	375				4.21±0.61	1.39±0.47	2.34	0.54±0.08	2.05±1.09	0.20
	400				6.98±1.86	1.03±0.53	9.29	1.04±0.14	2.11±1.03	0.80
1-butene	350	2.43±3.4	0.22±0.37	0.42	1.90±0.34	6.28±3.68	11.46	0.62±0.07	6.02±2.40	0.56
	375	2.60±2.37	0.28±0.32	0.40	4.76±0.54	3.99±1.91	38.57	1.69±0.23	4.02±2.28	6.84
	400	4.63±3.49	0.22±0.19	0.30	7.68±0.90	4.20±1.93	99.66	3.10±0.23	3.08±0.96	6.07
1-pentene	350	0.59±0.16	1.54±1.09	0.27	1.62±0.17	3.23±2.11	7.30	0.57±0.07	2.28±1.17	0.37
	375	0.63±0.07	1.60±0.55	0.11	2.26±0.16	4.01±1.54	5.68	1.26±0.08	2.10±0.55	0.41
	400	1.33±0.49	1.02±0.68	0.40	5.80±0.66	2.17±0.92	14.70	5.91±3.05	0.68±0.52	3.55
1-hexene	350	0.28±0.15	2.11±4.11	0.78	0.91±0.20	7.78±4.63	2.29	0.51±0.11	8.02±4.58	0.65
	375	0.46±0.37	1.75±4.15	0.66	1.88±0.93	13.27±13.94	21.20	7.36±24.67	0.77±4.04	85.97
	400	0.41±0.27	2.34±5.08	0.41	2.52±0.51	10.58±5.44	11.70	9.79±4.38	1.80±1.94	29.80

Table 5-5 Apparent rate constant a_i (in mmol C/g_{cat} min $bar^{0.5}$) and equilibrium constant K_6 (in bar^{-1}) together with their 95% confidence limits and the sum of squares of residuals (SRR in 10^{-3} (mmol C/g_{cat}min)^2) for the rate of formation of the various product groups in the partial oxidation of α-olefins (C_2-C_6) over iron antimony oxide according to the oxidation model.

		Isomerisation			Partial Oxidation + Oxidative Dehydrogenation			Total Oxidation + Cracking		
Feed	$T_{reaction}$	a_i	K_6	SSR	a_i	K_6	SSR	a_i	K_6	SSR
ethene	450							0.14±0.03	34.1±67.9	0.83
	460							0.26±0.07	11.2±14.97	1.00
	475							0.66±0.16	4.03±2.53	1.49
propene	350				0.67±0.11	6.69±3.08	0.69	0.07±0.01	12.02±7.89	0.02
	375				1.65±0.37	3.82±1.80	2.21	0.19±0.05	7.12±5.79	0.17
	400				2.90±1.14	2.57±1.81	9.41	0.36±0.10	7.29±5.87	0.72
1-butene	350	1.09±1.64	0.50±0.88	0.42	0.57±0.15	34.41±71.90	11.33	0.19±0.03	30.31±39.80	0.55
	375	1.26±1.36	0.59±0.75	0.40	1.70±0.44	12.93±13.60	40.16	0.61±0.18	12.86±16.00	7.00
	400	2.12±1.74	0.48±0.46	0.30	2.73±0.66	13.90±14.30	102.41	1.17±0.21	9.11±5.49	6.02
1-pentene	350	0.23±0.11	4.43±4.95	0.42	0.48±0.14	17.92±27.96	6.57	0.19±0.05	8.69±7.85	0.32
	375	0.23±0.05	4.96±2.67	0.11	0.61±0.08	37.42±53.42	5.02	0.42±0.05	7.86±3.02	0.26
	400	0.54±0.26	2.66±2.31	0.39	1.95±0.44	8.01±5.62	13.64	2.57±1.67	1.59±1.51	3.61
1-hexene	350	0.10±0.12	6.54±21.36	0.78	0.22±0.04	234±2072	1.59	0.12±0.02	370±4540	0.40
	375	0.17±0.22	5.31±17.07	0.65	0.52±0.18	96±504	11.52	3.25±13.6	1.76±11.09	86.10
	400	0.15±0.17	7.23±21.70	0.41	0.59±0.12	172±861	9.0	3.91±2.93	4.69±7.30	35.07

The sums of squares of residuals for the single site Langmuir-Hinshelwood model and the oxidation model are the same for the rate of formation of double bond isomers, however for the product groups partial oxidation plus oxidative dehydrogenation and total oxidation plus cracking the oxidation model shows generally the lower sums of squares. On the other hand the parameters for the single site Langmuir-Hinshelwood model could be determined with a higher accuracy, which is reflected by the generally lower 95% confidence limits.

The adsorption equilibrium constants K_1 and K_6 for the olefin adsorption for both models are similar for the formation of the partial oxidation plus oxidative dehydrogenation products and of the total oxidation products, especially, when taking the 95 % confidence limits into account. For both models, K_1 and K_6 is generally lower in the double bond isomerisation reactions. This might indicate that the double bond isomerisation takes place on different sites.

Figures 5-8 to 5-10 show the parity plots of the measured rates and the rates calculated using both models.

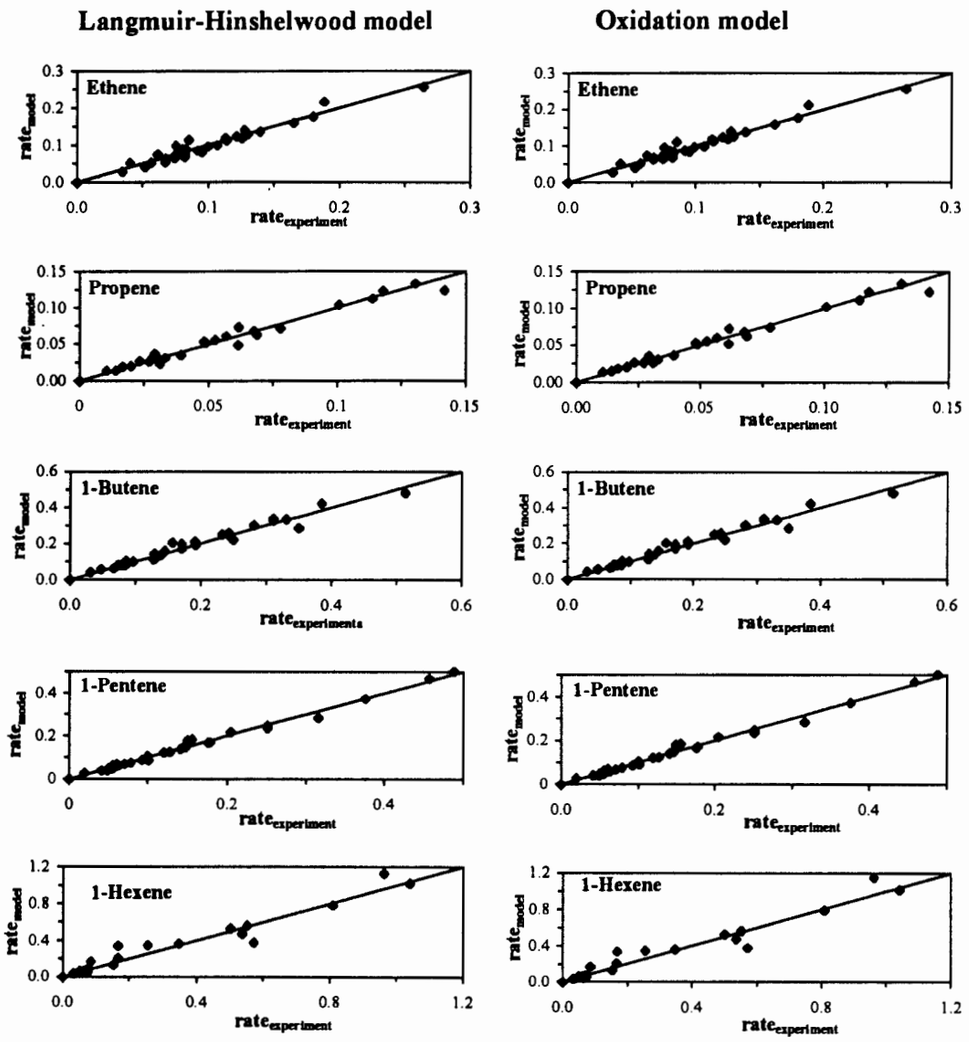

Figure 5-8 Parity between the calculated rates and experimental rates for the formation of total oxidation plus cracking products in the conversion of various α-olefins (C_2-C_6) over iron antimony oxide (Sb:Fe=1.5, T_{calc}=900°C, t_{calc}=7h) for the single site Langmuir-Hinshelwood model and the oxidation model.

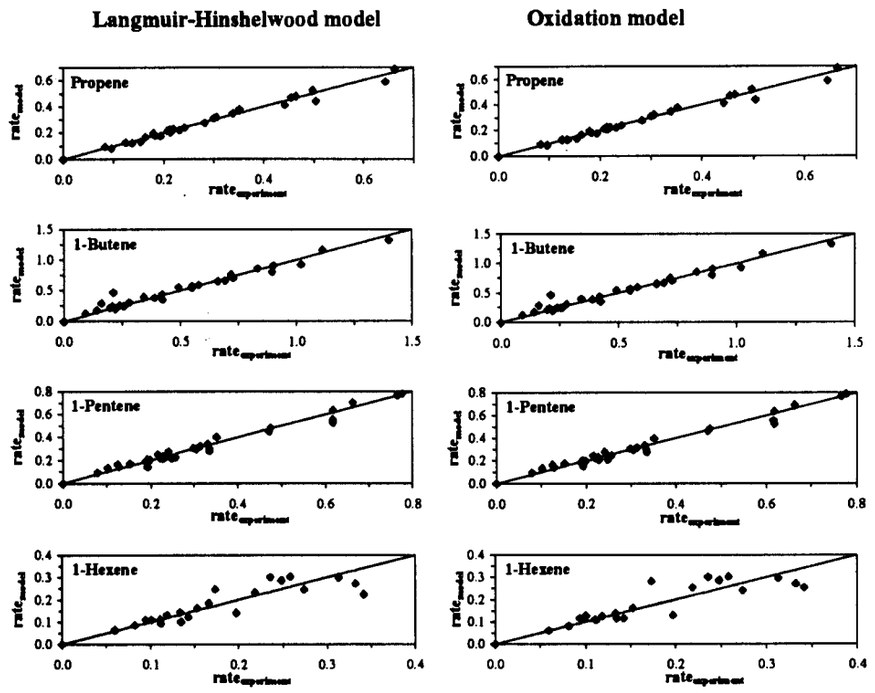

Figure 5-9 Parity between the calculated rates and experimental rates for the formation of partial oxidation plus oxidative dehydrogenation products in the conversion of various α-olefins (C_3-C_6) over iron antimony oxide (Sb:Fe=1.5, T_{calc}=900°C, t_{calc}=7h) for the single site Langmuir-Hinshelwood model and the oxidation model.

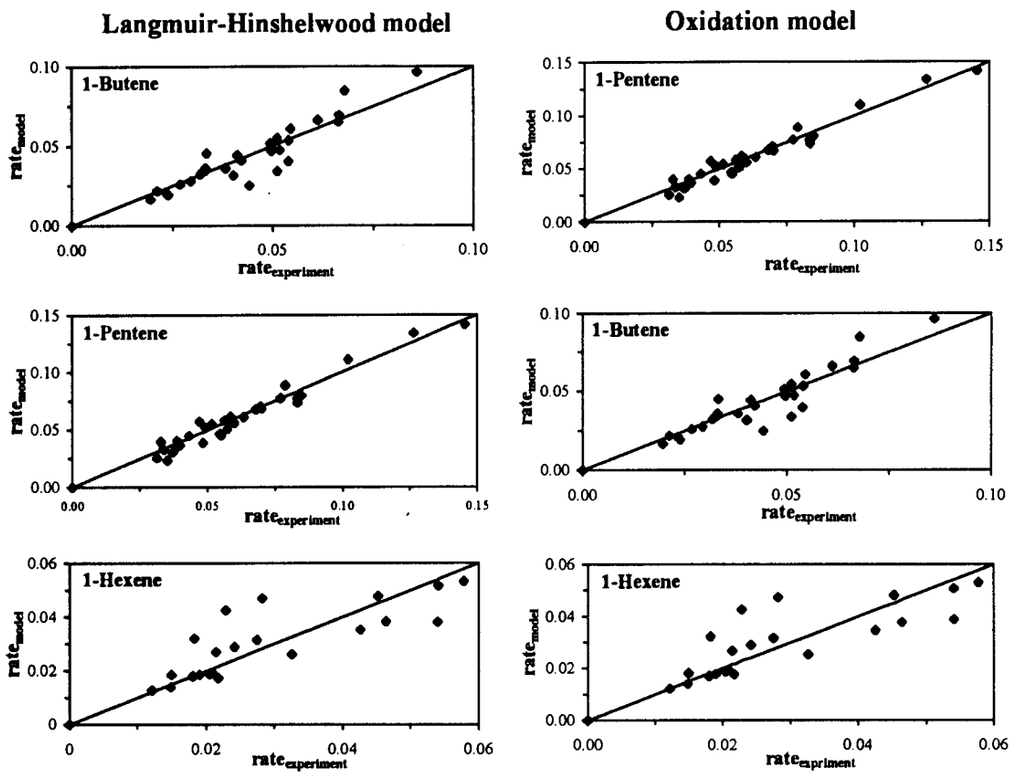

Figure 5-10 Parity between the calculated rates and experimental rates for the formation of double bond isomers in the conversion of various α-olefins (C_4-C_6) over iron antimony oxide (Sb:Fe=1.5, T_{calc}=900°C, t_{calc}=7h) for the single site Langmuir-Hinshelwood model and the oxidation model.

No difference between the Langmuir-Hinshelwood model and the oxidation model can be detected by using the parity plots. In order to be able to better distinguish between the two models the average error between the measured and calculated rates as defined by Equation 5-19 was calculated for the various product groups and is listed in Table 5-6.

Table 5-6 Average error (%) in the prediction of the rate of formation for the different product groups in the oxidative conversion of α-olefins (C_2-C_6) over iron antimony oxide (Sb:Fe=1.5, T_{calc}=900°C, t_{calc}=7h) according to the single site Langmuir-Hinshelwood model (LHM) and the oxidation model (OM).

	Isomerisation		Partial oxidation + oxidative dehydrogenation		Total oxidation + cracking	
	LHM	OM	LHM	OM	LHM	OM
ethene					10.4	9.5
propene			6.1	5.4	9.2	8.6
1-butene	11.5	11.5	15.1	15.0	9.5	9.3
1-pentene	9.3	9.2	9.7	9.0	7.4	7.1
1-hexene	22.4	22.1	15.6	13.4	20.6	19.5

The average error for the prediction of the rate of formation of isomers is for both models the same, while the average error for the remaining product groups is lower for the oxidation model than for the Langmuir-Hinshelwood model. The average error for the prediction of the rate of formation of products is highest for 1-hexene as feedstock, which might be explained by competitive adsorption of the cracking products, which are only formed to a greater extent when using 1-hexene in the range of C_2-C_6 α-olefins.

Since the parameter of the single site Langmuir-Hinshelwood model could be determined more accurately, the influence of chain length on the kinetics of the oxidative conversion of α-olefins was investigated using the single site Langmuir-Hinshelwood model.

Figure 5-11 shows the influence of chain length on the activation energies and the pre-exponential factors for the formation of the three product groups.

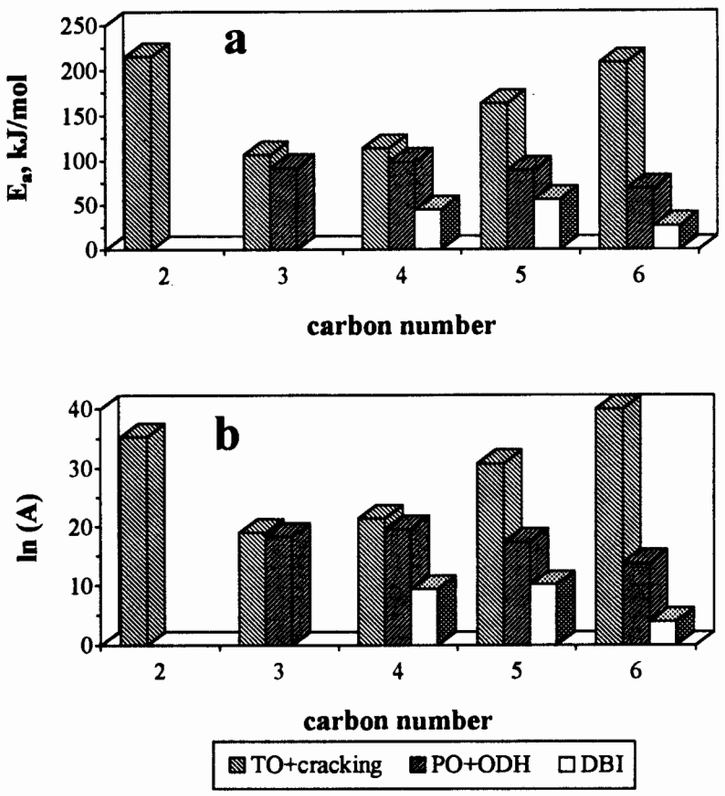

Figure 5-11 Influence of carbon number on the apparent activation energy (a) and the pre-exponential factor (b) for the formation of total oxidation plus cracking products (TO+cracking), partial oxidation plus oxidative dehydrogenation products (PO+ODH) and double bond isomers (DBI) in the oxidative dehydrogenation of α-olefins (C_2-C_6) over iron antimony oxide (Sb:Fe=1.5, T_{calc}=900°C, t_{calc}=7h) as determined by the single site Langmuir-Hinshelwood model.

The activation energy over the range of α-olefins from ethene to 1-hexene follow the same order as in the case of the power law model, viz.:

$$E_{a,\text{total oxidation+cracking}} > E_{a,\text{partial oxidation+oxidative dehydrogenation}} > E_{a,\text{double bond isomerisation}}$$

The pre-exponential factors A follow the same trend. A strong correlation between ln(A) and the activation energy can be noticed. The single site Langmuir-Hinshelwood model emphasises stronger the outsider role ethene plays in this series of C_2 to C_6 α-olefins. The

apparent activation energy for the oxidation of ethene is much higher (220 kJ/mol) than for the total oxidation of the C_3-olefin and in fact all other investigated α-olefins. This can be explained by the differences in the mechanism for the total oxidation of ethene and the higher olefins. The total oxidation of ethene requires the direct attack on the adsorbed olefin, whereas the higher olefins are able to form stable π-allylic intermediates which are attacked by the active site of the catalyst.

The apparent activation energy for the total oxidation increases with increasing carbon number from C_3. This might be attributed to the influence of the alkyl chain on the adsorbed olefinic intermediate. Due to the increasing length of the alkyl chain, it becomes more and more probable that the alkyl chain may be activated instead of the allylic hydrogen. It was shown that paraffinic species yield total oxidation products over this catalyst (Section 3.4).

With increasing carbon number the apparent activation energy for the partial oxidation plus oxidative dehydrogenation and for the double bond isomerisation reaction remains constant within the accuracy of their determination.

The heat of adsorption, which was calculated using the single site Langmuir-Hinshelwood model is shown in Table 5-7.

Table 5-7 Estimated heats of adsorption of the α-olefins as determined by the kinetics of the formation for the total oxidation products in the partial oxidation of α-olefins (C_2-C_6) over iron antimony oxide (Sb:Fe=1.5, T_{calc}=900°C, t_{calc}=7h) according to the single site Langmuir-Hinshelwood model.

Feed	$\Delta H_{ads,\ olefin,}$ kJ/mol
ethene	193
propene	28
1-butene	47
1-pentene	83
1-hexene	107

The heat of adsorption of ethene is much higher than for the other α-olefins, which might be attributed to the inability of ethene to form a stabile intermediate surface species. Increasing the chain length from C_3 onwards the heat of adsorption of the α-olefins increases.

5.4 COMPARISON OF THE VARIOUS MODELS

The following rate expressions have been derived :

a) Power law model: $$-r_{olefin} = A_i \cdot e^{-\frac{E_{a,i}}{R \cdot T}} p_{olefin}^{n} \cdot p_{O_2}^{m} \qquad (5\text{-}21)$$

b) Redox model: $$-r_{olefin} = \frac{k_{reduction} \cdot k_{oxidation} \cdot p_{olefin} \cdot p_{O_2}}{a \cdot k_{reduction} \cdot p_{olefin} + k_{oxidation} \cdot p_{O_2}} \qquad (5\text{-}22)$$

c) Langmuir-Hinshelwood model: $$-r_{olefin} = k_i \frac{K_1 \cdot K_2 \cdot p_{olefin} \cdot p_{O_2}^{\frac{1}{2}}}{(1 + K_1 \cdot p_{olefin})^2} \qquad (5\text{-}23)$$

d) Oxidation model: $$-r_{olefin} = \frac{a_i \cdot p_{olefin} \cdot p_{O2}^{\frac{1}{2}}}{1 + K_6 \cdot p_{olefin}} \qquad (5\text{-}24)$$

A comparative study of the influence of the different models on the prediction of the rate of consumption of propene is shown in Figure 5-12. For high partial pressures of propene the differences in the prediction of the rate of consumption of propene is quite substantial. The power law model predicts the highest rates because of the lack of an propene inhibition term. The redox model predicts a lower rate than the power law model because of its propene inhibition term. From Equation 5-22 it is clear that the for high propene partial pressures the rate of consumption becomes constant, which is also the case for the oxidation model (Equation 5-24). The Langmuir-Hinshelwood model predicts the lowest rates of consumption. For high partial pressures of the olefin the rate of consumption decreases because of the inhibition term in the denominator is in square.

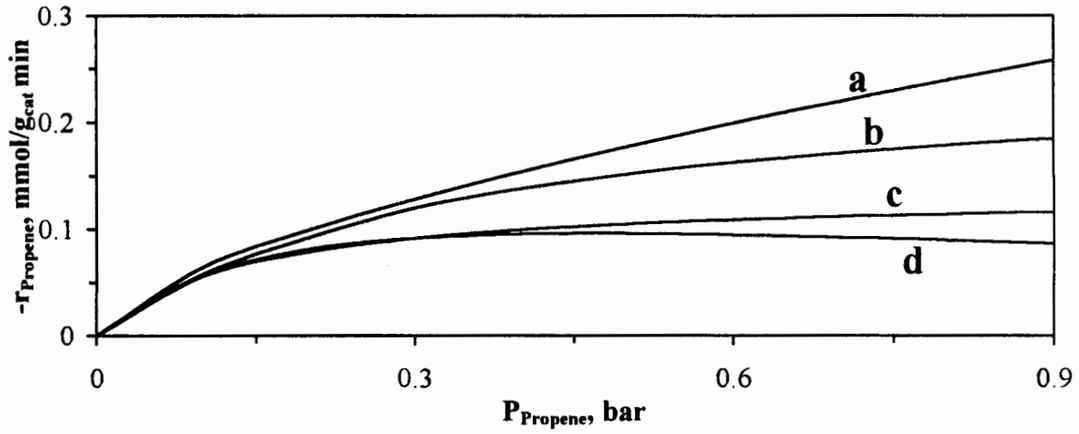

Figure 5-12 Prediction of the rate of consumption of propene as a function of propene partial pressure for the power law model (a), redox model (b), oxidation model (c) and the Langmuir-Hinshelwood model (d), (T=350°C, p_{O2}=0.3 bar, p_{total}=1.2 bar).

CHAPTER 6

CONCLUSIONS

6. CONCLUSIONS

The partial oxidation of α-olefins has been investigated over iron antimony oxide catalysts. This reaction utilises lattice oxygen of the iron antimonate.

Time on stream studies of the propene partial oxidation over $FeSbO_4$ in the absence of gaseous oxygen revealed that the activity of this catalyst is strongly dependent on the amount of oxygen species present on the catalyst surface. Although the initial activity is similar whether gaseous oxygen is present or not, activity drops rapidly when gaseous oxygen is absent. This condition must therefore be avoided. The importance of the oxidation state of the catalyst for higher acrolein yields was revealed when iron antimony oxide was heated up to reaction temperature in flowing air as compared to flowing nitrogen. Heating the catalyst in a flow of nitrogen resulted in a lower initial yield of acrolein. This can be ascribed to an autoreduction of the catalyst. It is therefore of greatest importance to keep iron antimony oxide in a high oxidation state.

The shape of the selectivity curves over time on stream for the selectivity to acrolein relative to CO_2 supports the hypothesis that mainly two different oxygen species are present on the catalyst surface, nucleophilic and electrophilic oxygen species. Electrophilic oxygen species are responsible for the formation of total oxidation products, while nucleophilic oxygen species are responsible for the formation of partial oxidation products (Libre *et al.*, 1983). Electrophilic oxygen species are intermediates during the reoxidation of the catalyst (Che and Tench, 1982). This explains the change in selectivity with time on stream which was observed. From this point of view reactor systems which separate the reduction and reoxidation of the catalyst by using different chambers (e.g. recirculating solids reactor) should eliminate nonselective pathways.

The Sb:Fe ratio in the iron antimony oxide catalyst has a strong influence on the conversion and selectivity in the partial oxidation of propene. BET surface area measurements revealed that the conversion is a function of the surface area of iron antimony oxide, which was highest at a Sb:Fe ratio of 1.

Time on stream experiments revealed that a high initial selectivity to acrolein can be achieved independently from the Sb content of the catalyst. However, an excess of antimony (Sb:Fe ≥ 1.5) is necessary to maintain the high initial selectivity to acrolein. The influence of excess antimony can be ascribed to the site isolation principle formulated by Callahan and Grasselli (1963), whereby Sb inhibits reduction of the catalyst and therefore decreases the amount of electrophilic oxygen species on the catalyst surface.

A strong influence of the chain length of the olefin on the reactivity and product distribution in the partial oxidation could be observed. Changing the space time in the oxidation of C_2 to C_9 α-olefins revealed the following scheme of possible reaction pathways:

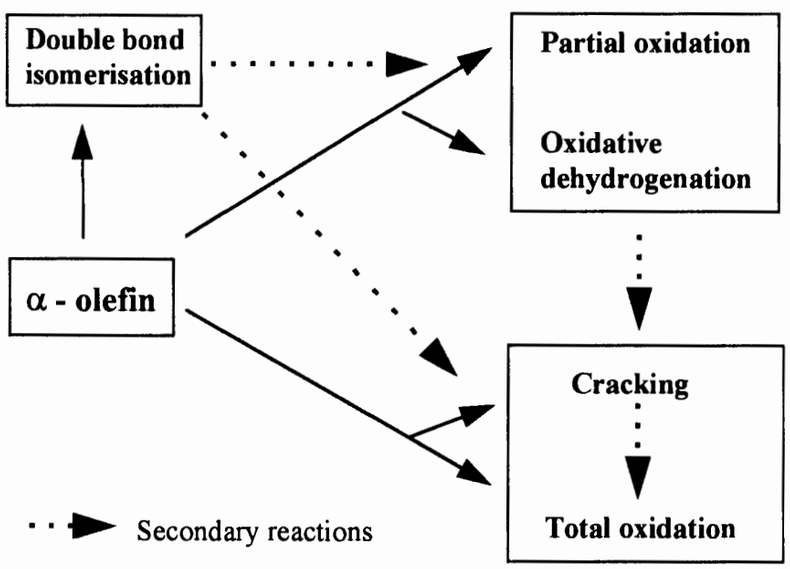

The products in the partial oxidation of C_2 to C_9 α-olefins will fall into at least one of the following product groups: double bond isomerisation, partial oxidation, oxidative dehydrogenation, cracking, total oxidation. Each of the product groups: double bond isomerisation, partial oxidation and oxidative dehydrogenation can be converted in a secondary step in the thermodynamically more stable product groups cracking and total

oxidation. Cracking products can also be converted into total oxidation products in a secondary step.

Ethene behaved totally different from the other investigated α-olefins. It showed a low reactivity and only total oxidation products were formed, which can be explained by a lack of stable C_2-intermediates (Dent and Kokes, 1970). Partial oxidation products were only detected in the conversion of C_3 to C_5 α-olefins. The rate of formation of partial oxidation plus oxidative dehydrogenation products showed a maximum at C_4 and decreased with increasing carbon number. The rate of formation of total oxidation plus cracking products increased with increasing carbon number. This can be explained by shielding of the allylic hydrogen and the double bond and therefore inhibiting the formation of the π-allylic intermediate, which is necessary for the formation of partial oxidation and oxidative dehydrogenation products. The rate of formation of double bond isomerisation products were hardly affected by the carbon number.

A redox (Mars-van Krevelen) model was inadequate to describe the kinetics of the partial oxidation of C_2 to C_6 α-olefins. The activation energy for the reoxidation of the catalyst showed a carbon number dependency although it should be independent of the way the catalyst was reduced. The redox model can not be applied for the rate of formation of products, because a steady state of reduction and reoxidation of the catalyst can be assumed for the consumption of olefins but not for the formation of a single product compound.

The rate of formation of products for the various α-olefins were modelled using a power law model, Langmuir-Hinshelwood model and an oxidation model.

The oxidation model showed a slightly lower error in the description of the experimental rates of formation of products than the Langmuir-Hinshelwood model and is therefore the preferred model.

The activation energies for the formation of the different product groups according to the power law model, Langmuir-Hinshelwood model and oxidation model followed the order:

$E_{a,total\ oxidation+cracking} > E_{a,partial\ oxidation+oxidative\ dehydrogenation} > E_{a,double\ bond\ isomerisation}$

It is therefore recommended that low reaction temperatures are applied to suppress the formation of unwanted total oxidation products.

REFERENCES

REFERENCES

Adamiya, T. V., Mishchenko, Y. A., Gel'bshtein, A. I., Kinet. Katal., **11**, 1970, 734.

Adams, C. R., In: *Proceedings of the 3rd International Congress on Catalysis, Amsterdam, 1964*, (Sachtler, W. M. H., Schuit, G. C. A., Zwietering, P., Eds.), North Holland Publishing Company, Amsterdam, Vol. 1, 1965, 240.

Adams, C. R., Jennings, J. T., J. Catal., **2**, 1963, 63.

Adams, C. R., Jennings, J. T., J. Catal., **3**, 1964, 549.

Adams, C. R., Voge, H. H., Morgan, C. Z., Armstrong, W. E., J. Catal., **3**, 1964, 379.

Alkhazov, T. G., Belenkii, M. S., Khiteva, W. M., Alekseeva, R. I., In: *Proceedings of the 4th International Congress on Catalysis, Moscow, 1968*, (Kazanskii, V. B., Ed.), Akademiai Kiado, Budapest, Vol. 1, 1971.

Allen, M., Betteley, R., Bowker, M., Hutchings, G. J., Catal. Today, **9**, 1991, 97.

Allen, M., Bowker, M., Catal. Letters, **33**, 1995, 269.

Allen, M. D., Poulston, S., Bithell, E. G., Goringe, M. J., Bowker, M., J. Catal., **163**, 1996, 204.

Andrushkevich, T. V., Boreskov, G. K., Pankratiev, Y. D., Pitayeva, A. N., Kinet. Katal., **16**,1975, 1442.

Aso, I., Nakao, M., Yamazoe, N., Seiyama, T., J. Catal., **57**, 1979, 287.

Aso, I., Furukawa, S., Yamazoe, N., Seiyama, T., J. Catal., **64**, 1980, 29.

Baidikova, I., Matralis, H., Naud, J., Papadopoulou, C., Mamedov, E. A., Delmon, B., Appl. Catal. A: General, **89**, 1992, 169.

Batist, P. A., Lippens, B. C., Schuit, G. C. A., J. Catal., **5**, 1966, 55.

Berry, F. J., Holden, J. G., Loretto, M. H., J. Chem. Soc., Faraday Trans. 1, **83**, 1987, 615.

Bettahar, M. M., Costentin, G., Savary, L., Lavalley, J. C., Appl. Catal. A: General, **145**, 1996, 1.

Bielanski, A., Haber, J., Oxygen in Catalysis, Marcel Dekker Inc., New York, 1991, 44.

Boreskov, G. K., Ven'yaminov, S. A., Dzis'ko, V. A., Tarasova, D. V., Dindoin, V. M., Sazonova, N. N., Olen'kova, I. P., Kefeli, L. M., Kinet. Katal., **10**, 1969, 1350.

Boreskov, G. K., Popovskii, V. V., Mamedov, E. A., Dokl. AN SSSR, **197**, 1971, 373.

Boreskov, G. K., Ven'yaminov, S. A., Sazonova, N. N., Pankratiev, Y. D., Pitayeva, A. N., Kinet. Katal., **16**, 1975, 1442.

Borman, P. C., Westerterp, K. R., Ind. Eng. Chem. Res., **34**, 1995, 49-58.

Bowker, M., Bicknell, C., R., Kerwin, P., Appl. Catal. A: General, **136**, 1996, 205.

Brazdil, J. F., Suresh, D. D., Grasselli, R. K., J. Catal., **66**, 1980, 347.

Bryström, A., Hök, B., Mason, B., Ark. Kemi Mineral. Geol., **15B(4)**, 1941, 34.

Burrington, J. D., Kartisek, C. T., Grasselli, R. K., J. Catal., **87**, 1984, 363.

Burriesci, N., Garbassi, F., Petrera, M., Petrini, G., J. Chem. Soc., Faraday Trans. 1, **78**, 1982, 817.

Busca, G., Finocchio, E., Ramis, G., Ricchiardi, G., Catal. Today, **32**, 1996, 133.

Callahan, J. L., Foreman, R. W., Veatch, F., U. S. Pat. 2,941,007, June 14, 1960.

Callahan, J. L., Gertisser, B., U. S. Pat. 3,198,750, August 3, 1965.

Callahan, J. L., Gertisser, B., U. S. Pat. 3,308,151, March 7, 1967.

Callahan, J. L., Grasselli, R. K., AIChE J., **9**, 1963, 755.

Callahan, J. L., Grasselli, R. K., Milberger, E. C., Strecker, H. A., Ind. Eng. Chem. Prod. Res. Dev., **9 (2)**, 1970, 134.

Carbucicchio, M., Centi, G., Trifirò, F., J. Catal., **91**, 1985, 85.

Carson, D., Coudurier, G., Forissier, M., Verdrine, J. C., J. Chem. Soc., Faraday Trans. 1, **79**, 1983, 1921.

Cathala, M., Germain, J. E., Bull. Soc. Chim. Fr., 1971, 2174.

Cavani, F., Trifiro, F., Appl. Catal. A: General, **88**, 1992, 115.

Centi, G., Trifiro, F., Catal. Rev.-Sci. Eng., **28** (2&3), 1986, 165.

Che, M., Tench, J., Adv. Catal., **31**, 1982, 77.

Che, M., Tench, J., Adv. Catal., **32**, 1983, 1.

Chem. Mark. Rep., **54**, 1990a.

Chem. Mark. Rep., **22**, 1990b.

Chem. Mark. Rep., **20**, 1990c.

Clark, A., Shutt, R. S., U. S. Pat. 2,383,711, Aug. 28, 1945.

Cotton, F. A., Wilkinson, G., Advanced Inorganic Chemistry, Fourth Edition, John Wiley and Sons, New York, 1980.

Davidov, A. A., Mikhaltchenko, V. G., Sokolovskii, V. D., Boreskov, G. K., J. Catal., **55**, 1978, 299.

Delmon, B., Bull. Soc. Chim. Belg., **88**, 1979, 979.

Delobel, R., Baussart, H., Leroy, J. M., Grimblot, J., Gengembre, L., J. Chem. Soc., Faraday Trans. 1, **79**, 1983, 879.

Dent, A., Kokes, R. J., J. Am. Chem. Soc., **92**, 1970, 6718.

Dever, J. R., George, K. F., Hoffman, W. C., Soo, H., In: *Kirk-Othmer, Encyclopedia of Chemical Technology*, Fourth Edition, (Kroschwitz, J. I., Howe-Grant, M., Eds.), Vol. 9, John Wiley and Sons, New York, 1994.

Dietz, W. A., J. Gas Chromatography, **2**, 1967, 68.

Dry, M. E., Appl. Catal. A: General, **138**, 1996, 319.

Eight Peak Index of Mass Spectra, Volume 1, Part 1, The Royal Society of Chemistry, Fourth edition, Cambridge, 1991.

Etzkorn, W. G., Kurland, J. J., Neilsen, W. D., In: *Kirk-Othmer, Encyclopedia of Chemical Technology,* Fourth Edition, (Kroschwitz, J. I., Howe-Grant, M., Eds.), Vol. 1, John Wiley and Sons, New York, 1991.

Fattore, V., Fuhrman, Z. A., Manara, G., Notari, B., J. Catal., **37**, 1975a, 223.

Fattore, V., Fuhrman, Z. A., Manara, G., Notari, B., J. Catal., **37**, 1975b, 215.

Felthouse, T. R., Burnett, J. C., Mitchell, S. F., Mummey, M. J., In: *Kirk-Othmer, Encyclopedia of Chemical Technology,* Fourth Edition, (Kroschwitz, J. I., Howe-Grant, M., Eds.), Vol. 15, John Wiley and Sons, New York, 1995, 903.

Gaigneaux, E. M., Tsiakaras, P. E., Herla, D., Ghenne L., Ruiz, P., Delmon, B., Catal. Today, **33**, 1997, 151.

Germain, J. E., Laugier, L., Bull. Soc. Chim. Fr., 1972a, 541.

Germain, J. E., Laugier, L., Bull. Soc. Chim. Fr., 1972b, 2910.

Germain, J. E., Perez, R., Bull. Soc. Chim. Fr., 1972a, 2042.

Germain, J. E., Perez, R., Bull. Soc. Chim. Fr., 1972b, 4683.

Godin, G. W., McCain, C. C., Porter, E. A., In: *Proceedings of the 4th International Congress on Catalysis, Moscow, 1968*, (Kazanskii, V. B., Ed.), Akademiai Kiado, Budapest, Vol. 1, 1971, 271.

Grasselli, R. K., Callahan, J. L., J. Catal., **14**, 1969, 93.

Grasselli, R. K., Suresh, D. D., J. Catal., **25**, 1972, 273.

Grasselli, R. K., Burrington, J. D., Adv. Catal., **30**, 1981, 133.

Grasselli, R. K., Burrington, J. D., Brazdil, J. F., Faraday Discuss. Chem. Soc., **72**, 1982, 203.

Haber, J., In: *Proceedings of the 4th International Conference of Chemistry and uses of Molybdenum, Golden Colorado, 1982,* (Barry, H. F., Mitchell, P. C. H., Eds.), Climax Molybdenum, 1982, 395.

Haber, J., In: *Solid State Chemistry in Catalysis*, (Grasselli, R. K., Brazdil, J. F., Eds.), ACS Symposium Series 279, Washington, D. C., 1985.

Hewlett Packard, Workbook, Publication No. G1030-90004, 1989.

Hurst, N. W., Gentry, J., Jones, A., McNicol, B. D., Catal. Rev.-Sci. Eng., **24(2)**, 1982, 233.

Hussak, E., Prior, G. T., Mineral. Mag. J. Mineral. Soc., **11**, 1897, 302.

JCPDS International Centre for Diffraction Data, Swarthmore, 1980.

Kaiser, R., Chromatograhie in der Gasphase, Vol. 3, Second edition, Bibliographisches Institut, Mannheim, 1969.

Keulks, G. W., J. Catal., **19**, 1970, 232.

Keulks, G. W., Krenzke, L. D., Notermann T. M., Adv. Catal., **27**, 1978, 183.

Keulks, G. W., Lo, M.-Y., J. Phys. Chem., **90**, 1986, 4768.

Keulks, G. W., Yu, Z., Krenzke, L. D., J. Catal., **84**, 1983, 38.

Kim, J. S., Woo, S. I., Appl. Catal. A: General **110**, 1994, 173-184.

Kirschner, E. M., Chem. & Eng. News, April 8, 1996.

Klug, H. P., Alexander, L. E., X-Ray Diffraction Procedures, Second edition, John Wiley and Sons, 1974, 533.

Kock, A. J. M. H., Fortuin, H. M., Geus, J. W., J. Catal., **96**, 1985, 261.

Krenzke, L. D., Keulks, G. W., J. Catal., **61**, 1980a, 316.

Krenzke, L. D., Keulks, G. W., J. Catal., **64**, 1980b, 295.

Konishi, Y., Sakata, K., Misono, M., Yoneda, Y., J. Catal., **77**, 1989, 169.

Ladd, M. F. C., Palmer, R. A., Structure Determination by X-ray Crystallography, Third edition, Plenum Press, New York, 1994.

Lemaitre, J. L., In: *Characterization of Heterogeneous Catalysts,* Chemical Industries, Vol. 15, (Delannay, F., Ed.), Macel Dekker Inc., 1984, New York, Basel, Chapter 2, 29.

Lewis, W. K., Gilliland, E. R., Reed, W. A., Ind. Eng. Chem., **41**, 1949, 1227.

Libre, J. M., Parbaux, Y., Grzybowska, P., Conflant, P., Bonnelle, J. P., Appl. Catal., **6**, 1983, 315.

Malet, P., Caballero, A., J. Chem. Soc., Faraday Trans. 1, **84**(7), 1988, 2369.

Mamedov, E. A., Gamid-Zade, E. G., Pankratiev, Y. D., Kuliev, A. R., Rizayev, R. G., React. Kinet. Catal. Lett., **10**, 1979, 19.

Mars, P., van Krevelen, D. W., Chem. Eng. Sci. Suppl., **3**, 1954, 41.

Mason, B., Vitaliano, J., Mineral. Mag. J. Mineral. Soc., **30**, 1955, 100.

Mc Kie, D., Mc Kie, C., Crystalline Solids, A. Wheaton and Co. Ltd., 1980.

Melander, L., Isotope Effect on Reaction Rate; Ronald Press, New York, 1960, 22.

Mitchell, P. C. H., Trifiró, F., J. Chem. Soc. (A), 1970, 3183-3188.

Moeller, T., Inorganic Chemistry, A Modern Introduction, John Wiley and Sons, New York, 1982.

Monnier, J. R., Keulks, G. W., J. Catal., **68**, 1981, 51.

Catalyst	K-value, s	P-value, K
Fe_2O_3	1263	211
SbFe025	1049	175
SbFe05	942	157
SbFe075	879	146
SbFe09	851	142
$FeSbO_4$	836	139
SbFe11	825	138
SbFe125	811	135
SbFe15	793	132
SbFe175	778	130
SbFe2	766	128
Sb_2O_4	657	109

$\beta = 0.17$ K/s

$C_0 = 2.23$ μmol/cm³

$F = 0.33$ cm³/s

TPR K and P-value determination

Monti and Baiker (1983) have proposed the use of a characteristic number, K, to assist in the selection of appropriate operating variable for TPR. They have suggested that for commonly used heating rates, between 6 and 18 K/s the limiting values of K are 55s < K < 140s.

$$K = \frac{S_0}{F \cdot C_0}$$

S_0 = amount of reducible species, μmol

F = total volumetric flowrate, cm^3(NTP)/s

C_0 = concentration of reducing gas, μmol/ cm^3

In addition Malet and Caballero (1988) defined a P-value, which incorporates the heating rate β into the formula. For good peak resolution a P-value of lower than 20 K is appropriate.

$$P = \frac{\beta \cdot S_0}{F \cdot C_0}$$

β = heating rate, K/s

In the following the K and P-values are summarised for the reducing gas propene and the various catalysts used in the TPR experiments.

APPENDIX I

TPR K AND P-VALUE DETERMINATION

Wragg, R. D., Ashmore, P. G., Hockey, J. A., J. Catal., **22**, 1971, 49.

Wyckhoff, R. W. G., Crystal Structures, Vol. 1, Second edition, John Wiley and Sons, New York, 1963.

Zhou, B., Ceckiewicz, S., Delmon, B., J. Phys. Chem., **91**, 1987, 5061.

Trifirò, F., Pasquon, I., J. Catal., **12**, 1968b, 412.

Trifirò, F., Kubelkova, L., Pasquo, I., J. Catal., **19**, 1970, 121.

Trifirò, F., Centola, P., Pascquon, I., Jirû, P., In: *Proceedings of the 4th International Congress on Catalysis, Moscow, 1968*, (Kazanskii, V. B., Ed.), Akademiai Kiado, Budapest, Vol. 1, 1971, 252.

Tsailingol'd, A. L., Komarovskii, N. A., Chekhov, E. E., Stepanov, G. A., Tuktarova, S., Pankrat'ev, Y. D., Slin'ko, M. G., Kinet. Katal., **13**, 1973, 1181.

Uda, T., Lin, T., Keulks, G. W., J. Catal., **62**, 1980, 26.

van Hooff, J. H. C., In: *"Chemistry and Chemical Engineering of Catalystic Processes", Proceedings of the NATO Advanced Study Institute, Noordwijkerhout, The Netherlands, 1979,* (Prins, R., Schuit, G. C. A., Eds.), Sijthoff & Noordhoff, Alphen aan den Rijn, The Netherlands, Germantown, Maryland, USA, 1980, 507.

Yamazoe, N., Aso, I., Amamoto, T., Seiyama, T., In: *"New Horizons in Catalysis", Proceedings of the 7th International Congress on Catalysis, Tokyo, 1980,* Studies in Surface Science and Catalysis 7B, (Seiyama T., Tanabe, K., Eds.), Kodansha-Elsevier, Tokyo-Amsterdam, 1980, 1239.

Yokoyama, T., Fujita, N., Make, T., Appl. Catal. A: General, **125**, 1995, 159.

Vedrine, J. C., Millet, J. M. M., Volta, J. C., Catal. Today, **32**, 1996, 115.

Vedrine J. C., Coudurier, G., Millet, J. M. M., Catal. Today, **33**, 1997, 3.

Vinogradova, O. M., Vytnov, G. Z., Luiksaar, I. V., Al'tahuler, O. V., Kinet. Katal., 16, 1975, 671.

Wells, A. F., Structural Inorganic Chemistry, Claredon Press, Oxford, 1975, 203.

Weng, L. T., Delmon, B., Appl. Catal. A: General, **81**, 1992, 141.

Weng, L. T., Ruiz, P., Delmon, B., Duprez, D., J. Mol. Catal., **52**, 1989, 349.

Saleh-Alhamed, Y. A., Hudgins, R.R., Silveston, P. L., Appl. Catal. A: General, **127**, 1995, 177.

Saleh-Alhamed, Y. A., Hudgins, R.R., Silveston, P. L., J. Catal., **161**, 1996, 430.

Sancier, K. M., Aoshima, A., Wise, H., J. Catal., **34**, 1974, 257.

Sancier, K. M., Wentrcek, P. R., Wise, H., J. Catal., **39**, 1975, 141-147.

Sanderson, R. T., Chemical Periodicity, Reinhold, New York, 1960.

Schulz, H., Wagner, H., Angew. Chem., **62**, 1950, 105.

Schulz, H., Böhringer, W., Kohl, C. P., Rahmann, N. M., Well, A., DGMK-Forschungsbericht 320, DGMK, Hamburg, 1984.

Seshan, K., Appl. Catal. A: General, **67**, 1990, N5.

Sêsták, J., Šavata, V., Wendlandt, W. W., Thermochim. Acta, 7, 1973, 333

Shchukin, V. P., Boreskov, G. K., Vent'yaminov, S. A., Tarasova, D. V., Kinet. Katal., **11**, 1970, 153.

Snyder, T. P., Hill, C. G., Catal. Rev.-Sci. Eng., **31**, 1989, 43.

Straguzzi, G. I., Bischoff, K. B., Koch, T. A., Schuit, G. C. A., J. Catal., **103**, 1987, 357.

Straguzzi, G. I., Bischoff, K. B., Koch, T. A., Schuit, G. C. A., J. Catal., **104**, 1987b, 47.

Stull, D. R., Westrum, E. F., Sinke, G. C., The Chemical Thermodynamics of Organic Compounds., John Wiley and Sons, New York, 1969.

Tan, H. S., Downie, J., Bacon, D.W., Can. J. Chem. Eng., **66**, 1988, 611.

Teller, R. G., Brazdil, J. F., Grasselli, R. K., J. Chem. Soc., Faraday Trans. 1, **1**, 1985, 1693.

Trifirò, F., Centola, P., Pasquon, I., J. Catal., **10**, 1968a, 68.

Monti, D. A., Baiker, A., J. Catal., **83**, 1983, 323.

Moro-oka, Y., Ueda, W., Tanaka, S., Ikawa, T., In: *New Horizons in Catalysis, Proceedings of the 7th International Congress on Catalysis, Tokyo, 1980,* Studies in Surface Science and Catalysis 7B, (Seiyama T., Tanabe, K., Eds.), Kodansha-Elsevier, Tokyo-Amsterdam, 1980, 1086.

Oyama, S. T., Desikan, A. N., Hightower, J. W., In: *Catalytic Selective Oxidation,* (Oyama S. T., Hightower, J. W., Eds.), ACS Symposium Series 523, Chapter 1, American Chemical Society, Washington, 1993, 1.

Oyama, S. T., In: *Heterogeneous Hydrocarbon Oxidation,* (Warren, B. K., Oyama S. T., Eds.), ACS Symposium Series 638, Chapter 1, American Chemical Society, Washington, 1996, 2.

Peacock, J. M., Parker, A. J., Ashmore, P. G., Hockey, T. A., J. Catal., **15**, 1969, 398.

Pietsch, E. H. E., In: *Gmelins Handbuch der Anorganischen Chemie, Antimon B,* System-Nummer 18, Gmelin Verlag, Clausthal-Zellerfeld, 1949.

Portefaix, J. L., Figueras, F., Forissier, M., J. Catal., **63**, 1980, 307.

Press, W. H., Flannery, B. P., Teukolsky, S. A., Vetterling, W. T., Numerical Recipies in Pascal, Chapter 10, Cambridge University Press, Cambridge, 1989.

Reid, R. C., Prausnitz, J. M., Poling, B. E., The Properties of Gases and Liquids, Fourth edition, McGraw-Hill, New York, 1987.

Robertson, S. D., McNicol, B. D., de Baas, J. H., Kloet, S. C., Jenkins, J. W., J. Catal., **37**, 1975, 424.

Sachtler, W. M. H., de Boer, N. K., In*: Proceedings of the 3rd International Congress on Catalysis, Amsterdam, 1964,* (Sachtler, W. M. H., Schuit, G. C. A., Zwietering, P., Eds.), North Holland Publishing Company, Amsterdam, **1**, 1965, 252.

Sala, F., Trifirò, F., J. Catal., **41**, 1976, 1.

Saleh-Alhamed, Y. A., Hudgins, R.R., Silveston, P. L., In: *New Frontiers in Catalysis, Proceedings of the 10th International Congress on Catalysis, 1992,* (Guczi, L., Solymosi, F., Tétényi, P., Eds.), Budapest, Hungary, Elsevier, Amsterdam, 1993, 2019.

Table 1 Response factors for hydrogen flame ionisation detector (Dietz, 1967)

Compound	Response factor
Methane (reference)	1.03
Propane	1.02
n-Butane	0.92
2,2,4-Trimethylpentane (iso-Octane, reference)	1.00
Cyclohexane (reference)	0.99
Benzene	0.89
Ethene	0.98
1-Hexene	1.01
1-Octene	0.97

Except for benzene the values are all approximately 1.0. For oxygenates the response factors were determined according to the method of Kaiser (1969). According to Kaiser (1969) is the signal of a CH_3- and of a CH_2-group equal to 1.0, while the signal of an aldehyd group is equal to 0. The response factors of the detected oxygenates were calculated using this method and are summarised in Table 2.

Table 2 Response factors for aldehydes calculated using the method of Kaiser (1969)

Aldehyde	Response factor f_i
Acrolein (Propenal)	1.5
Crotonaldehyde (2-Butenal)	1.33
2-methyl-Furan	1.25

The products CO and CO_2 were not detected by the FID and therefore Equation 5 cannot be applied for those products. The IR photometer measured the concentrations of CO and CO_2 in the effluent in vol-%, this reading was converted into the molar fraction x_i by dividing through 100. The molar flow of CO and CO_2 in the effluent were calculated using the ideal gas law:

CALCULATION OF CONVERSION, YIELD AND SELECTIVITY

The following formulas were used to calculate the yields Y_i, conversions X_i and selectivities S_i. All calculations were done on a carbon basis.

$$X_i = \frac{\dot{n}_{feed,in} - \dot{n}_{feed,out}}{\dot{n}_{feed,in}} \tag{1}$$

$$Y_i = \frac{\dot{n}_{i,out}}{\dot{n}_{feed,in}} \tag{2}$$

$$S_i = \frac{Y_i}{X_i} \tag{3}$$

The molar flows were determined using the ratios of the area A_i of the peaks for each component i to the area A_{ref} of the peak for the internal standard from the GC analysis. Equations 1 and 2 change to:

$$X_i = \frac{\left(\frac{A_{feed} \cdot f_{feed}}{A_{ref} \cdot f_{ref}}\right)_{in} - \left(\frac{A_{feed} \cdot f_{feed}}{A_{ref} \cdot f_{ref}}\right)_{out}}{\left(\frac{A_{feed} \cdot f_{feed}}{A_{ref} \cdot f_{ref}}\right)_{in}} \tag{4}$$

$$Y_i = \frac{\left(\frac{A_i \cdot f_i}{A_{ref} \cdot f_{ref}}\right)_{out}}{\left(\frac{A_{feed} \cdot f_{feed}}{A_{ref} \cdot f_{ref}}\right)_{in}} \tag{5}$$

with f_i being the response factor for the component i for the flame ionisation detector (FID) of the GC. The response factors for the olefins and paraffins used in the experiments were taken from Dietz (1967) and are summarised in Table 1. The response factors are based on the response of n-heptane, which is defined as 1.0.

$$\dot{n} = \frac{p \cdot F}{R \cdot T} \cdot x_i \qquad \text{i = CO, } CO_2 \tag{6}$$

The flow F was measured using a soap bubble meter and the flow was corrected to standard conditions (T = 25°C, p=1,013 mbar).

In order to evaluate the experimental run, a carbon balance for each run was calculated using Equation 7:

$$C\text{-}balance = \frac{\left(\frac{A_{feed} \cdot f_{feed}}{A_{ref} \cdot f_{ref}}\right)_{out} + \sum_{i-1}^{n}\left(\frac{A_i \cdot f_i}{A_{ref} \cdot f_{ref}}\right)_{out} + \frac{\frac{p \cdot F}{R \cdot T} \cdot (x_{CO} + x_{CO_2})}{\dot{n}_{ref}}}{\left(\frac{A_{feed} \cdot f_{feed}}{A_{ref} \cdot f_{ref}}\right)_{in}} \tag{7}$$

with n being the number of products.

Calculation of kinetic data

The reaction rate for the consumption of feed was calculated as follows:

$$-r_{feed} = \frac{\dot{n}_{feed,in} - \dot{n}_{feed,out}}{m_{cat}} \tag{8}$$

which can also be written using Equation (1) as

$$-r_{feed} = \frac{X_{feed} \cdot \dot{n}_{feed,in}}{m_{cat}} \tag{9}$$

The rate of formation of the hydrocarbons in the product was calculated as follows:

$$r_{Hydrocarbon,product} = \frac{\dot{n}_{i,out}}{m_{cat}} \tag{10}$$

which can be written using Equation (2) as

$$r_{Hydrocarbon,product} = \frac{Y_i \cdot \dot{n}_{feed,in}}{m_{cat}} \tag{11}$$

APPENDIX III

X-RAY DIFFRACTION OF IRON ANTIMONY OXIDE

Influence of calcination temperature on crystal structure as determined by X-ray diffraction for different Sb:Fe ratios:

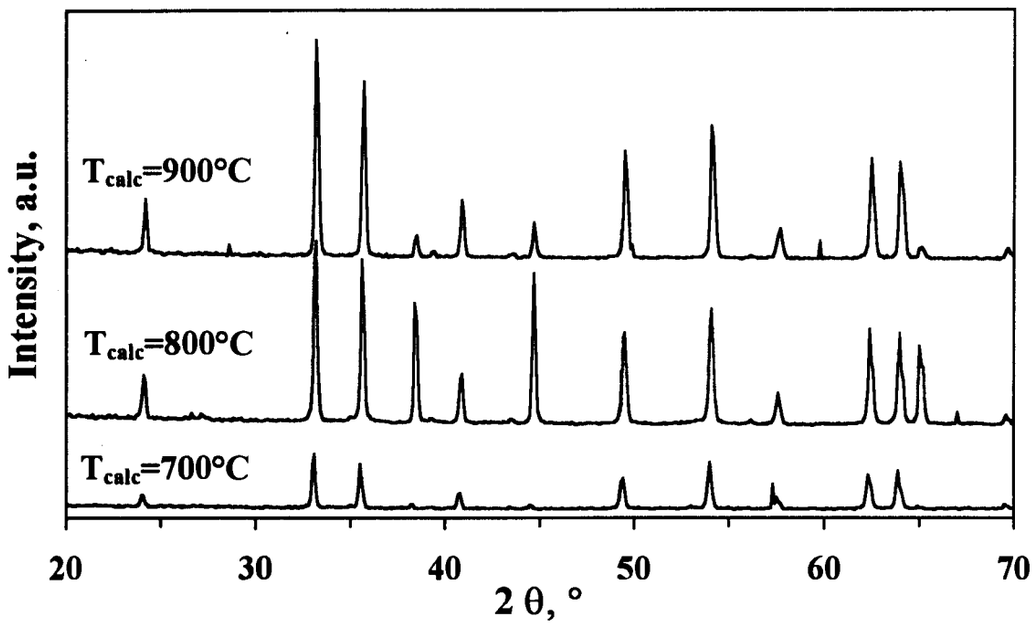

XRD pattern for sample Fe_2O_3

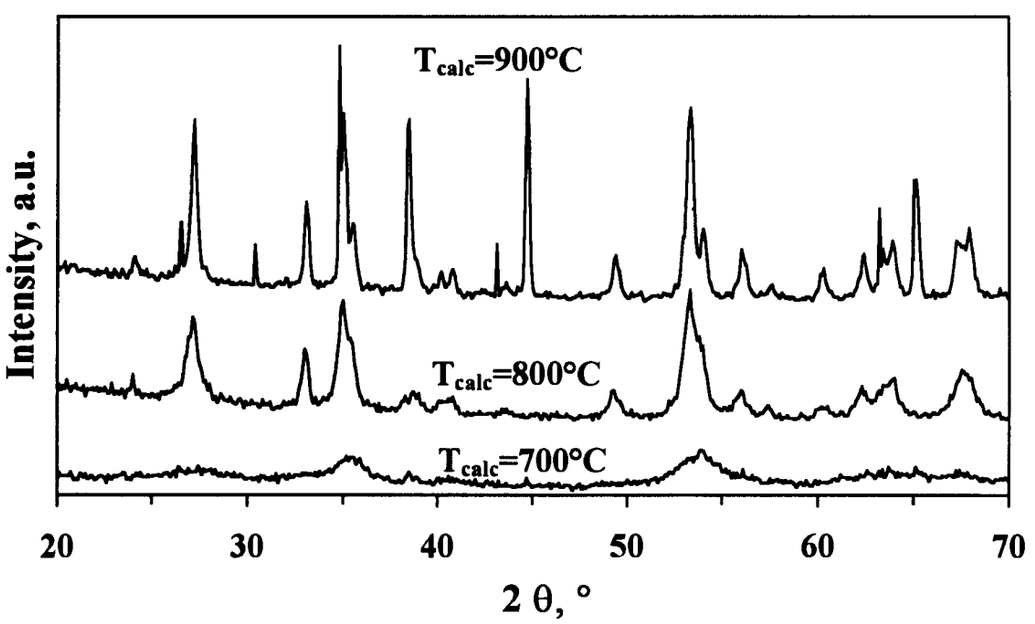

XRD pattern for sample SbFe025

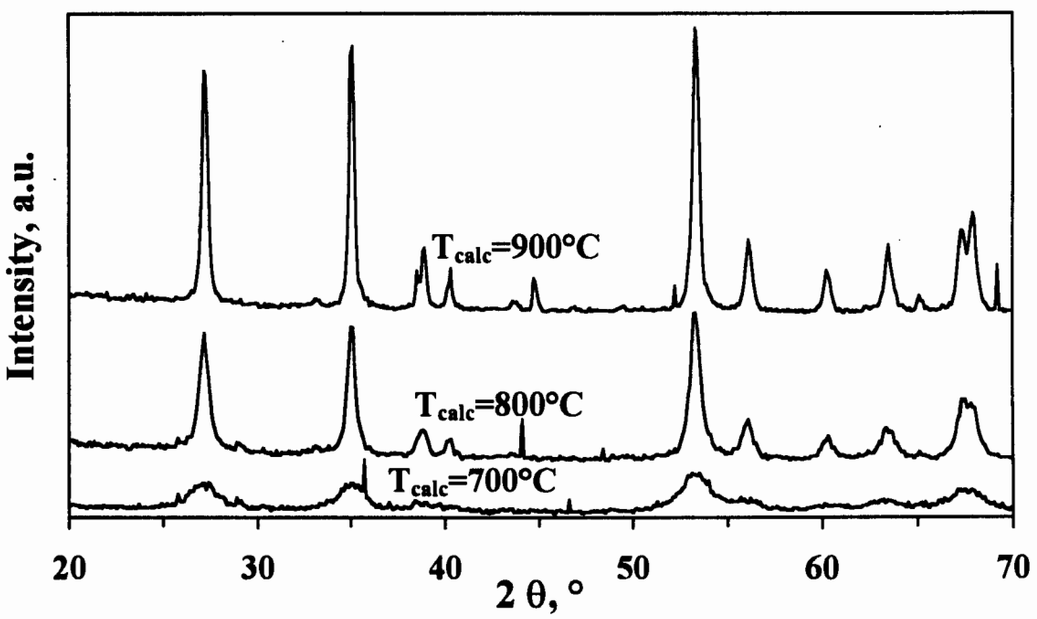

XRD pattern for sample SbFe075

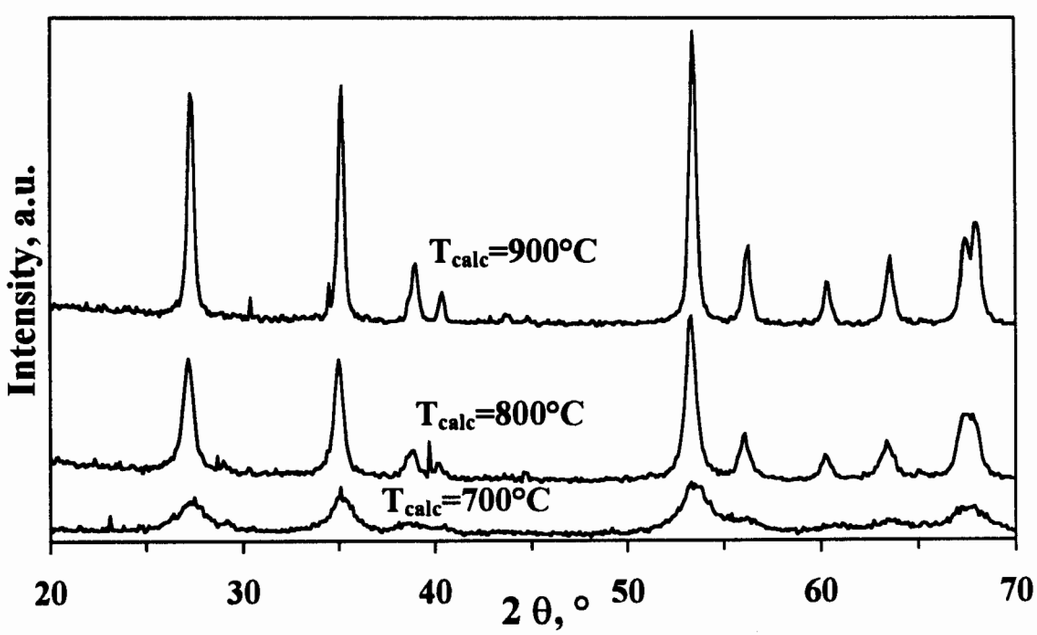

XRD pattern for sample SbFe09

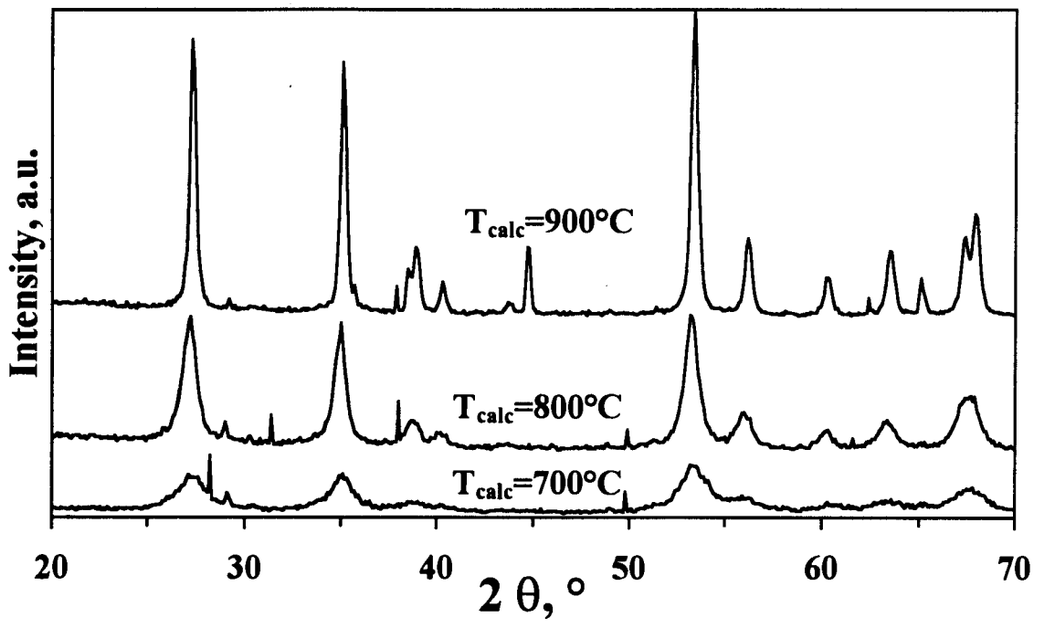

XRD pattern for sample SbFe125

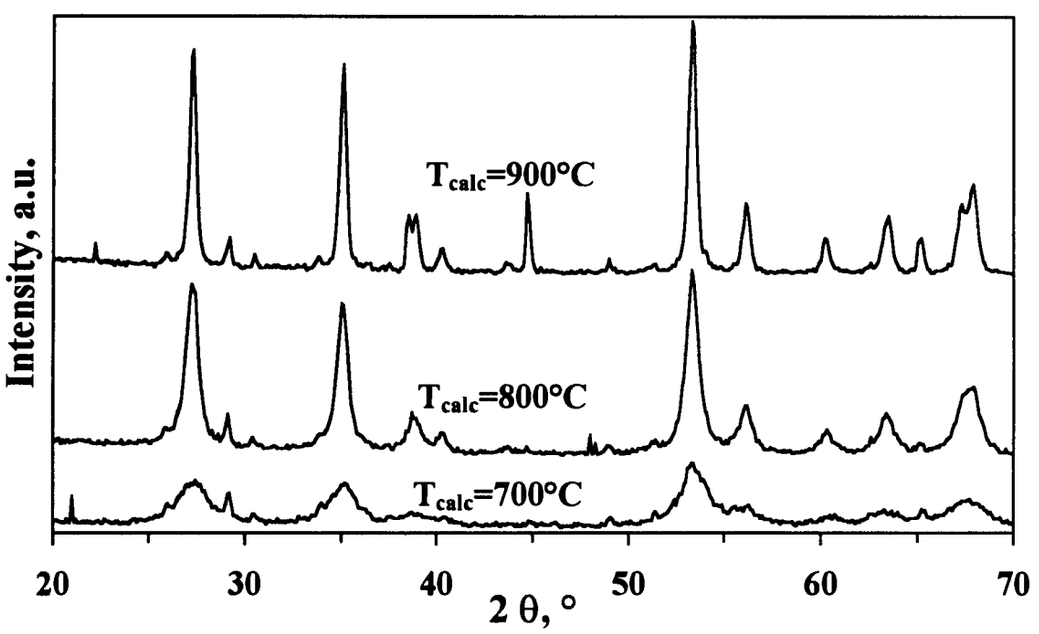

XRD pattern for sample SbFe15

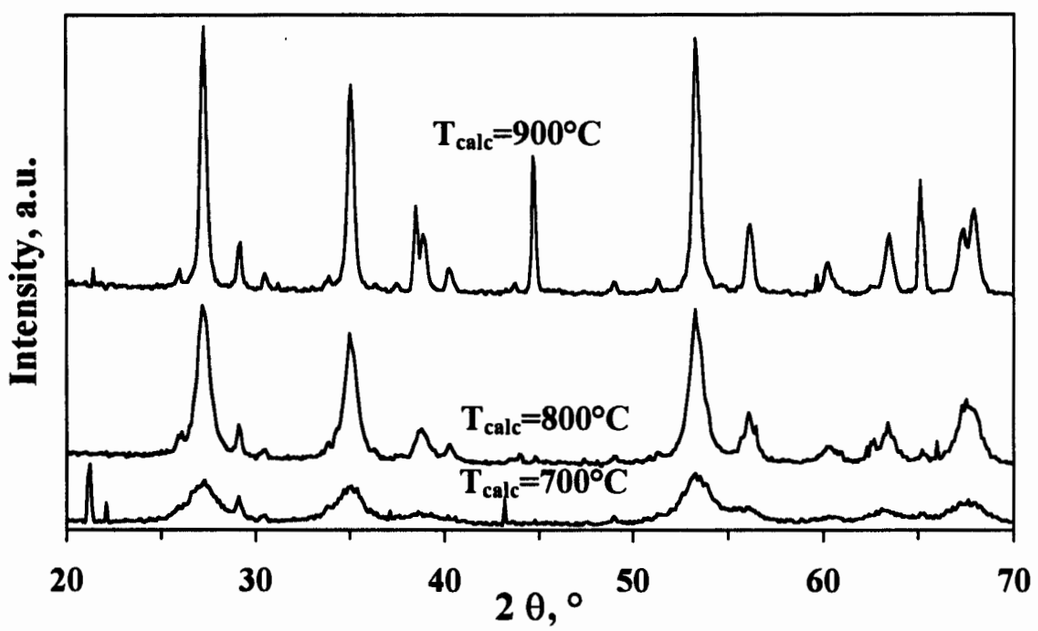

XRD pattern for sample SbFe175

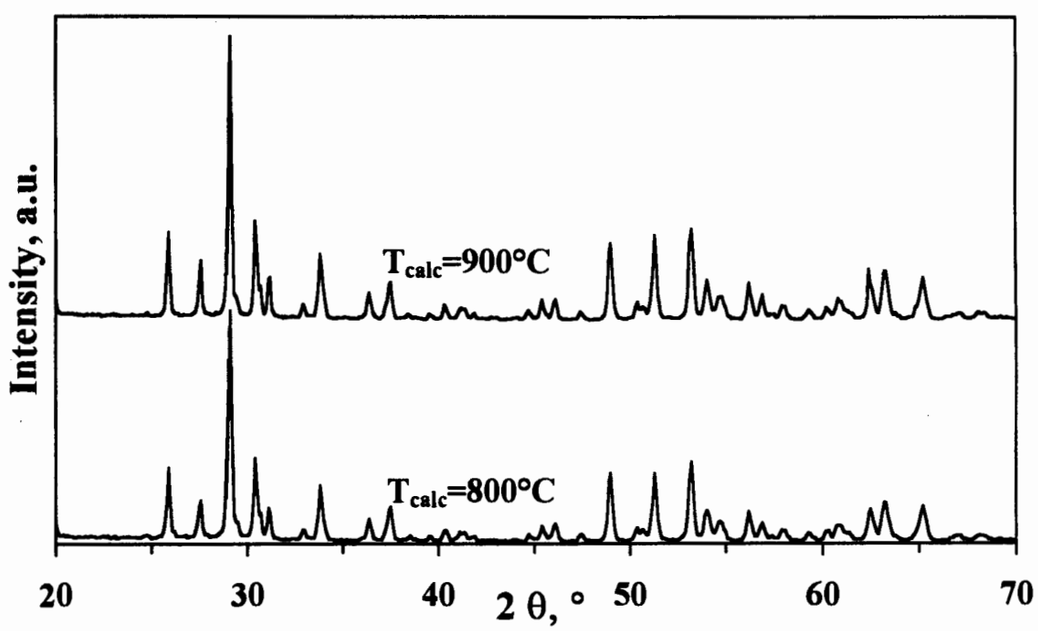

XRD pattern for sample Sb_2O_4

APPENDIX IV

TEM IMAGES OF IRON ANTIMONY OXIDES AND FREQUENCY DISTRIBUTION OF CRYSTALLITE DIAMETERS

TEM images for iron antimony oxides:

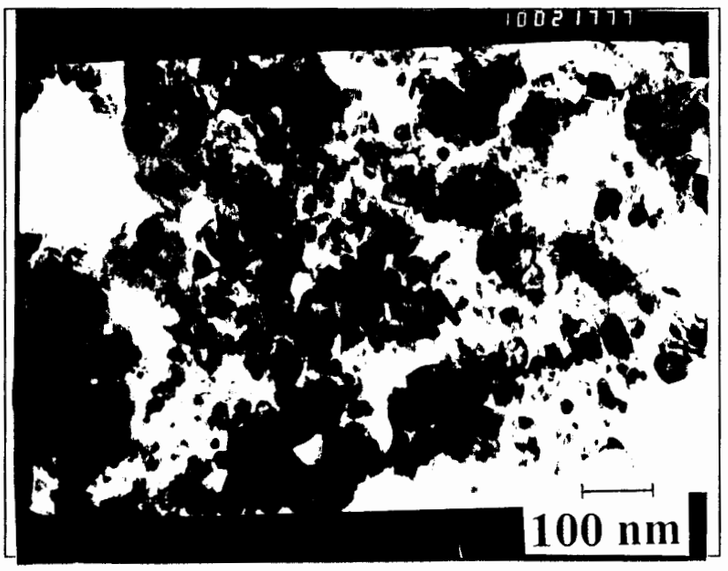

T_{calc}=900°C, Sb:Fe=0.25
magnification: 100 000

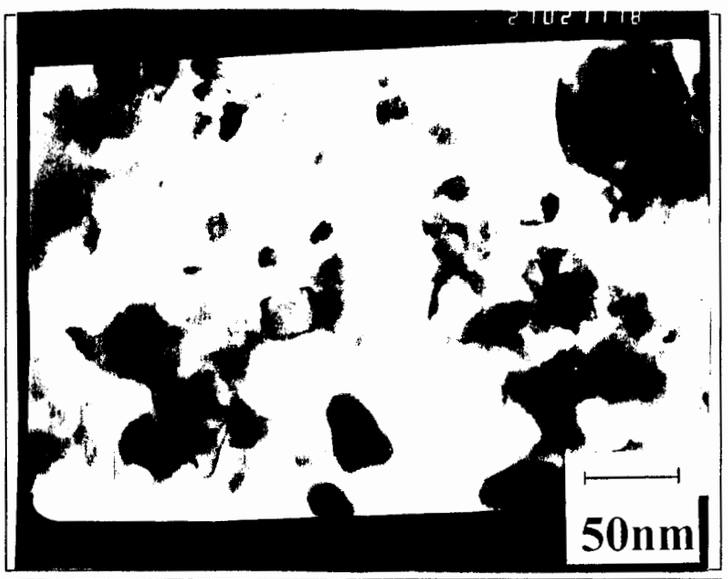

T_{calc}=900°C, Sb:Fe=0.25
magnification: 270 000

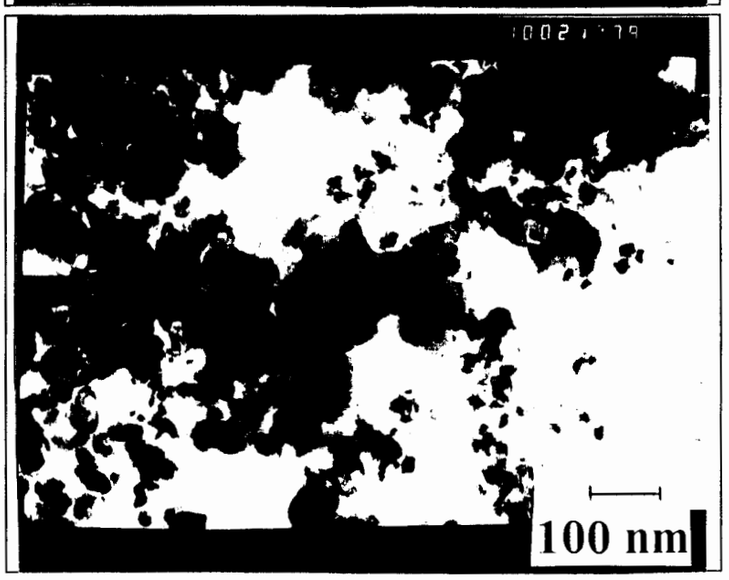

T_{calc}=900°C, Sb:Fe=0.5
magnification: 100 000

T_{calc}=900°C, Sb:Fe=0.75

magnification: 270 000

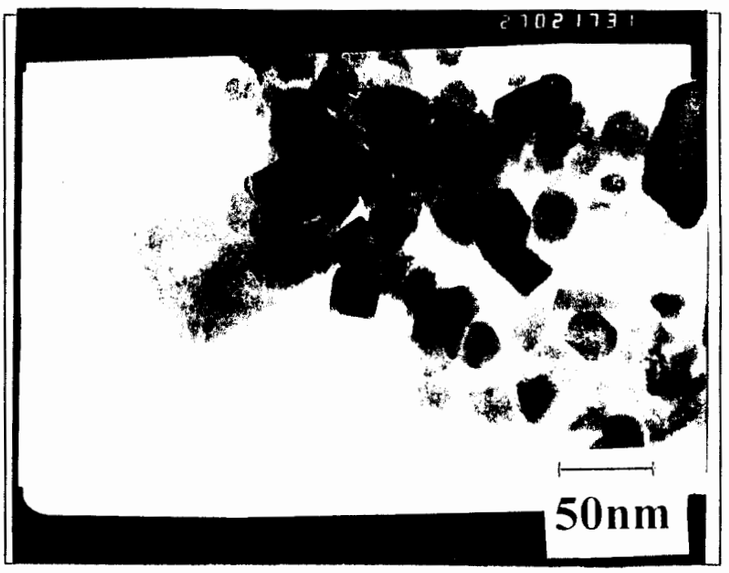

T_{calc}=900°C, Sb:Fe=1.0

magnification: 100 000

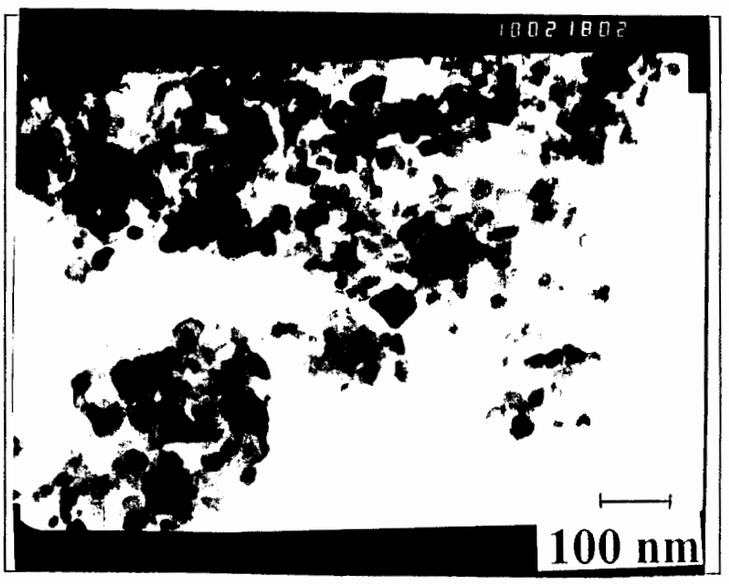

T_{calc}=900°C, Sb:Fe=2.0

magnification: 270 000

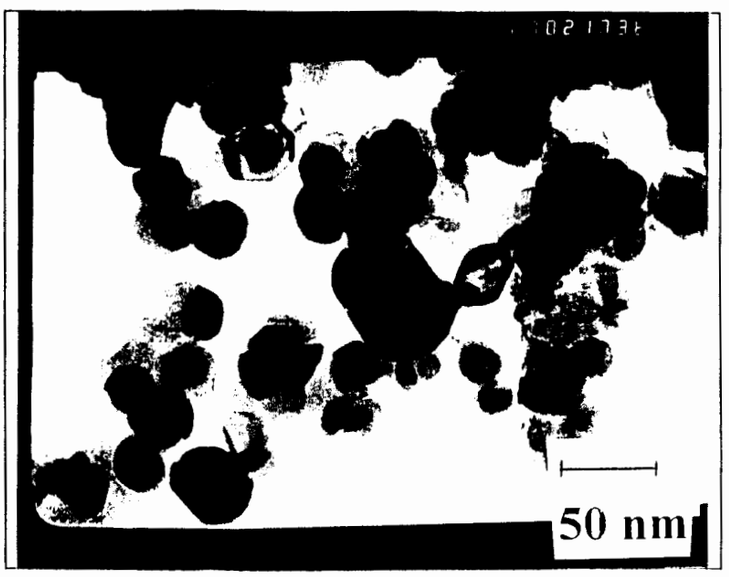

T_{calc}=800°C, Sb:Fe=0.5

magnification: 270 000

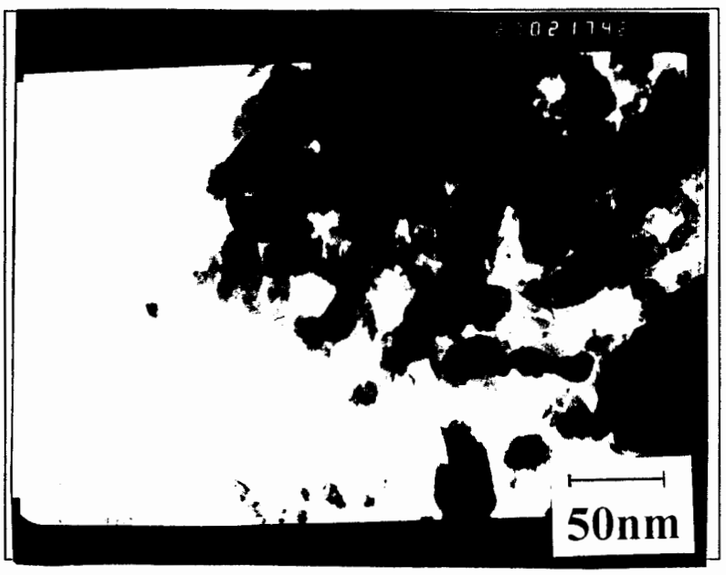

T_{calc}=800°C, Sb:Fe=1.0

magnification: 100 000

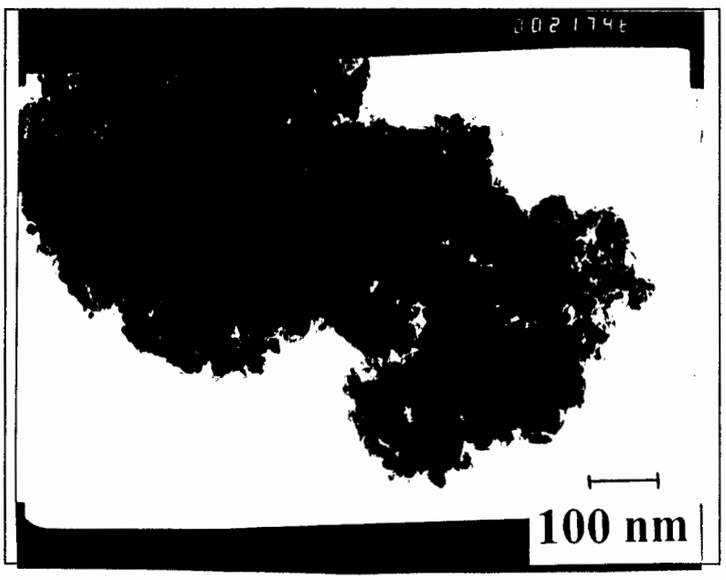

T_{calc}=800°C, Sb:Fe=1.75

magnification: 100 000

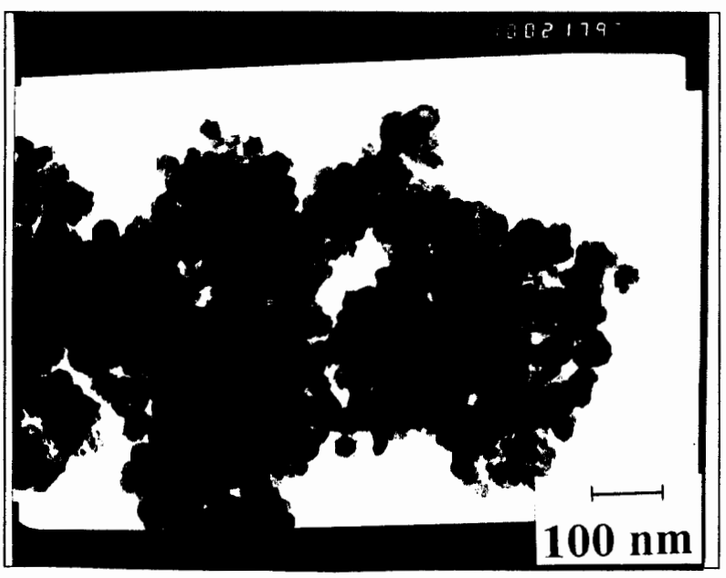

T_{calc}=800°C, Sb:Fe=1.75

magnification: 270 000

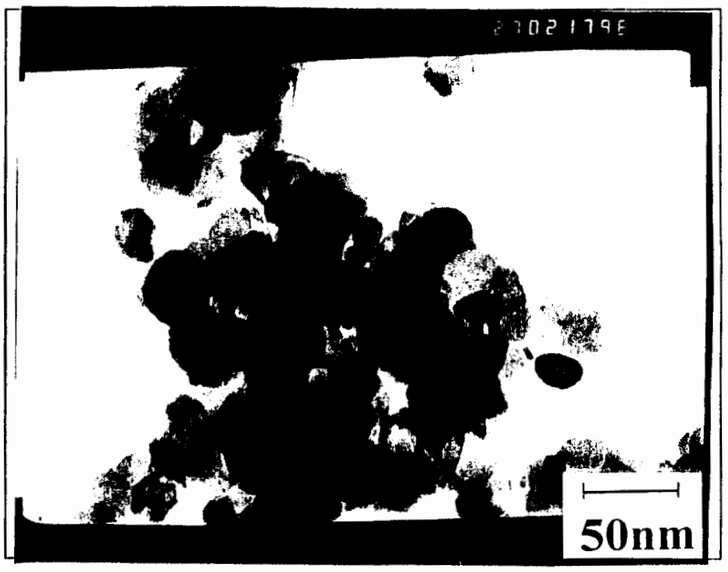

T_{calc}=700°C, Sb:Fe=0.9

magnification: 270 000

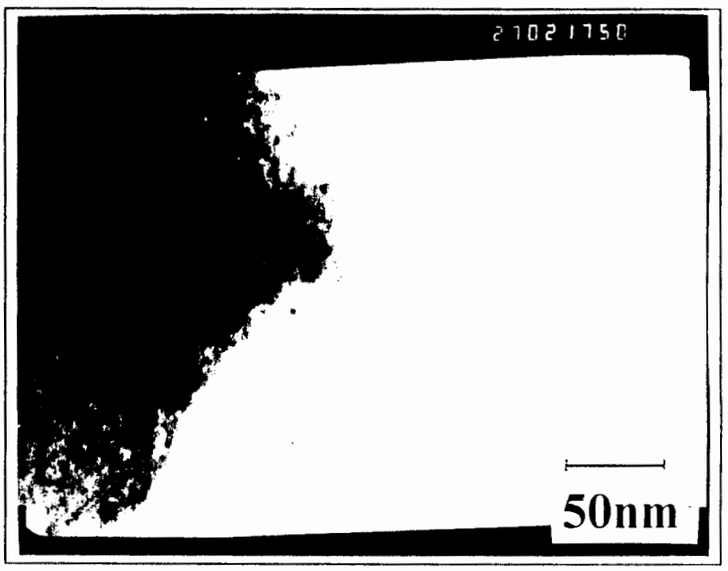

T_{calc}=700°C, Sb:Fe=1.0

magnification: 100 000

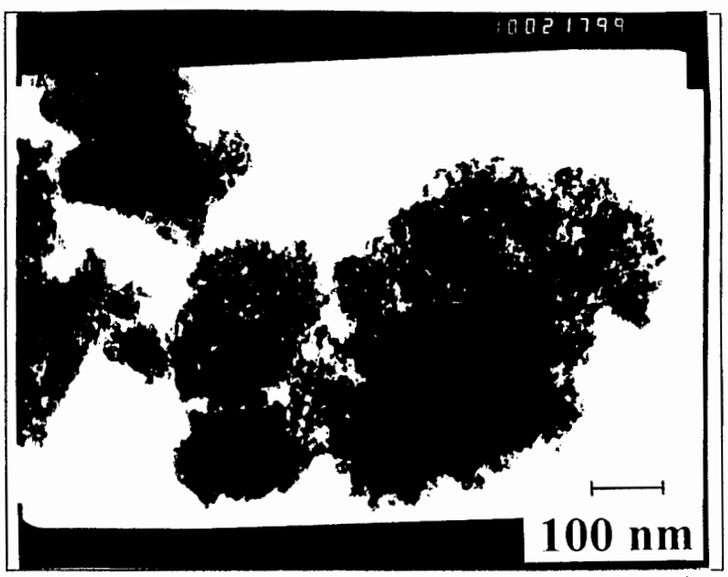

T_{calc}=700°C, Sb:Fe=1.1

magnification: 270 000

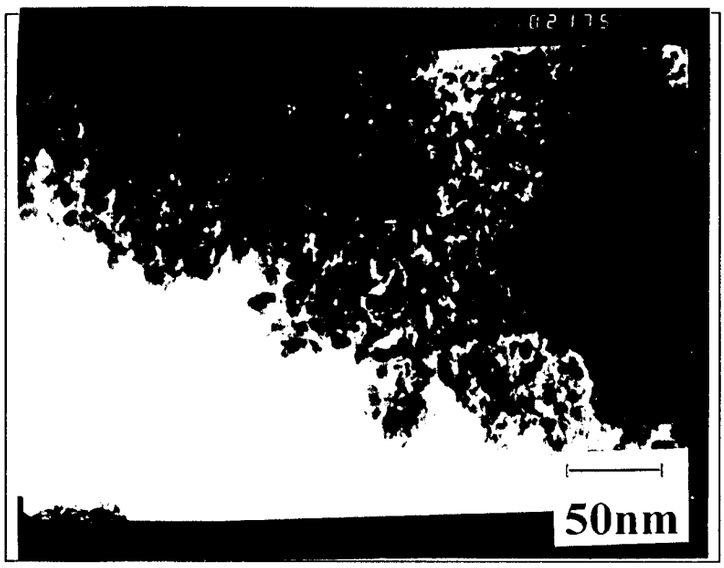

Distribution of the crystallite size for iron antimony oxides:

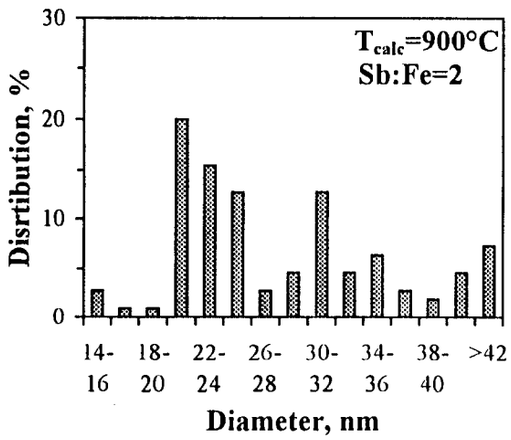

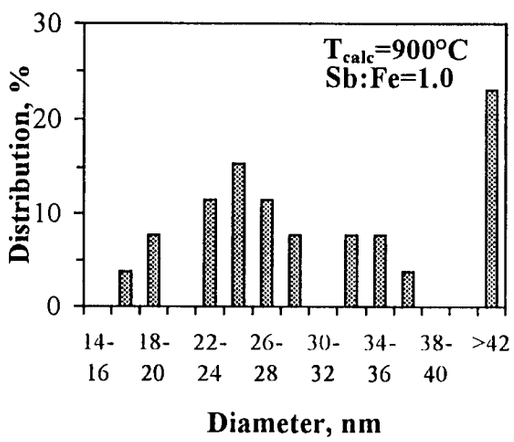

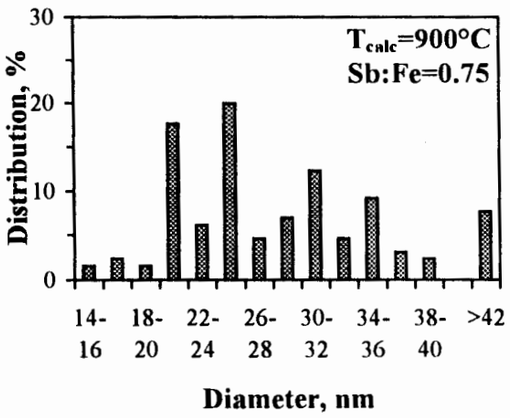
T_{calc}=900°C
Sb:Fe=0.75
Distribution, %
0
10
20
30
14-16
18-20
22-24
26-28
30-32
34-36
38-40
>42
Diameter, nm

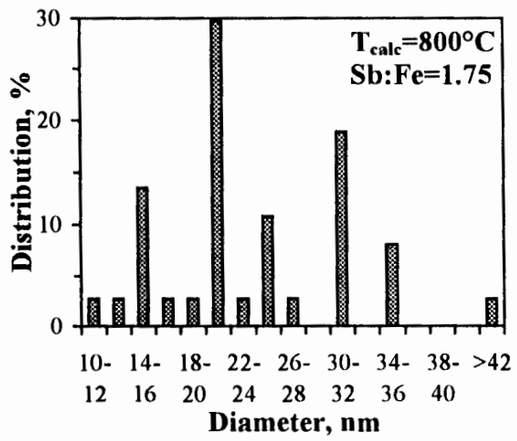
T_{calc}=800°C
Sb:Fe=1.75
Distribution, %
0
10
20
30
10-12
14-16
18-20
22-24
26-28
30-32
34-36
38-40
>42
Diameter, nm

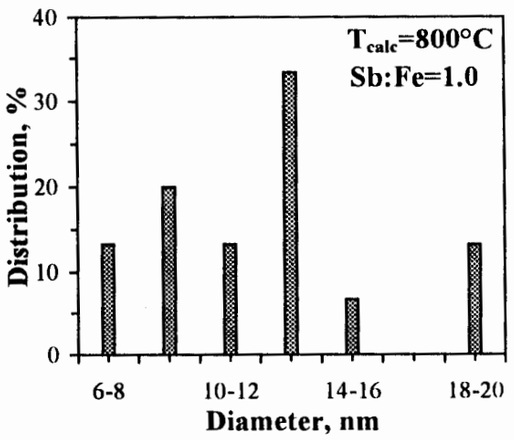
T_{calc}=800°C
Sb:Fe=1.0
Distribution, %
0
10
20
30
40
6-8
10-12
14-16
18-20
Diameter, nm

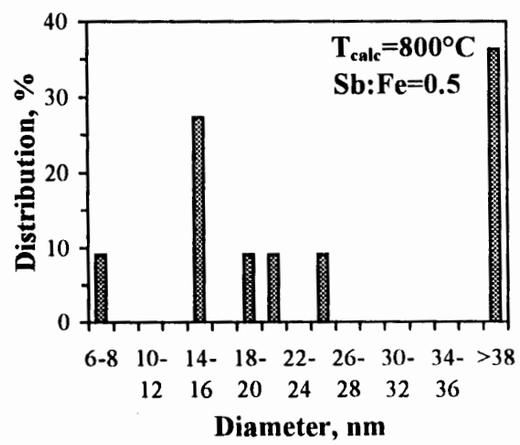
T_{calc}=800°C
Sb:Fe=0.5
Distribution, %
0
10
20
30
40
6-8
10-12
14-16
18-20
22-24
26-28
30-32
34-36
>38
Diameter, nm

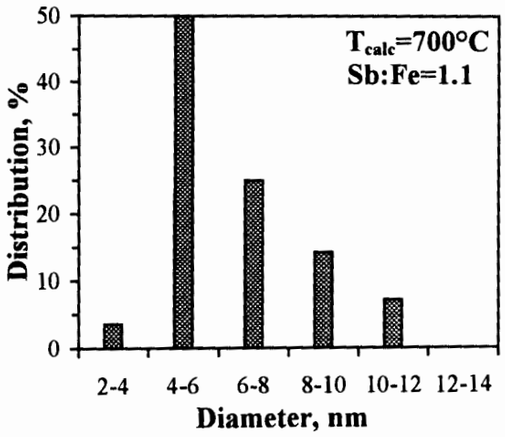
T_{calc}=700°C
Sb:Fe=1.1
Distribution, %
0
10
20
30
40
50
2-4
4-6
6-8
8-10
10-12
12-14
Diameter, nm

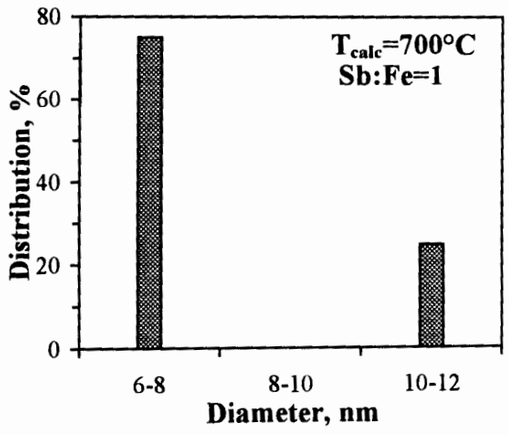
T_{calc}=700°C
Sb:Fe=1
Distribution, %
0
20
40
60
80
6-8
8-10
10-12
Diameter, nm

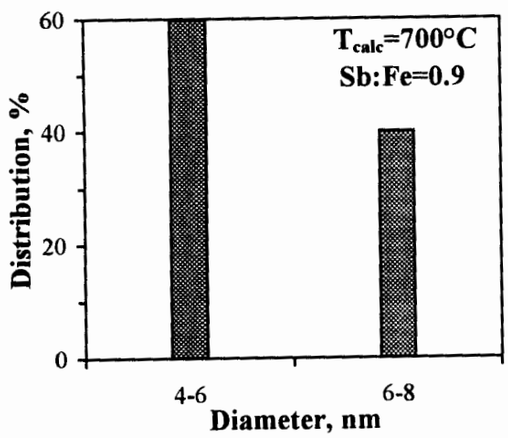
T_{calc}=700°C
Sb:Fe=0.9
Distribution, %
0
20
40
60
4-6
6-8
Diameter, nm

APPENDIX V

GC PRINT OUTS

GC print outs

An overview of the GC setup conditions and of the temperature programs of the GC oven is given in Section 2.3.2.2.

Feed: Ethene:

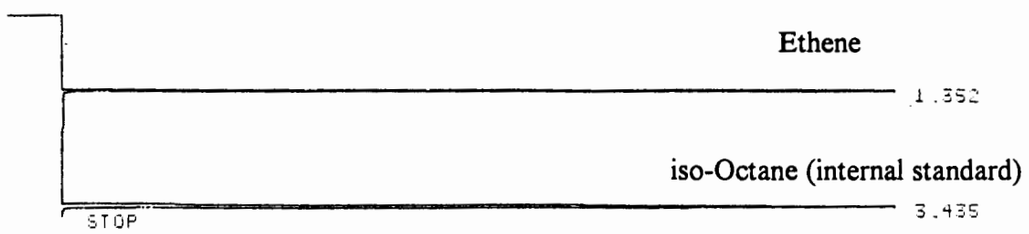

Feed: Propene:

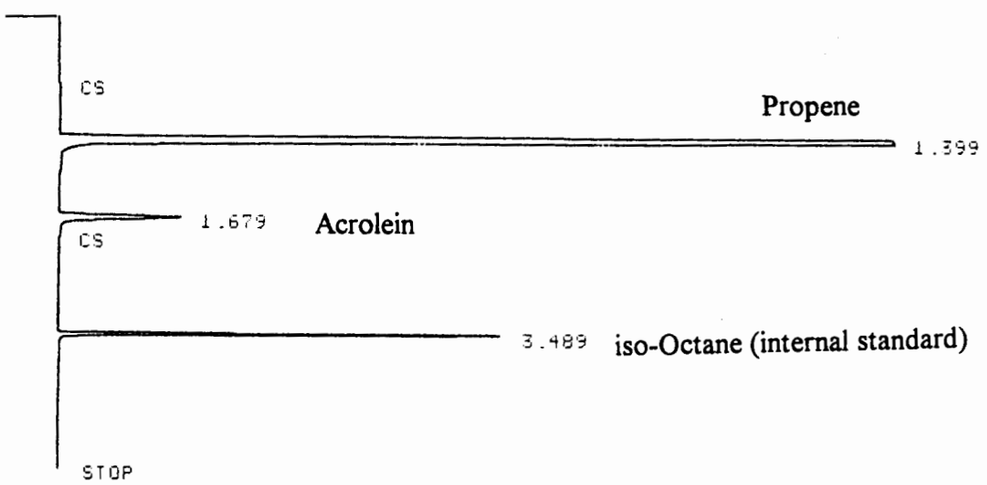

Feed: 1-Butene:

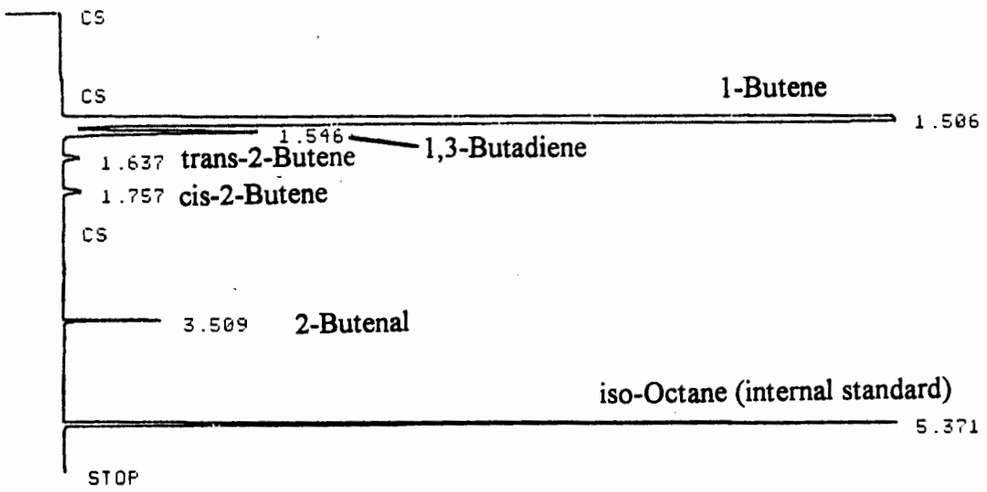

Feed: 1-Pentene:

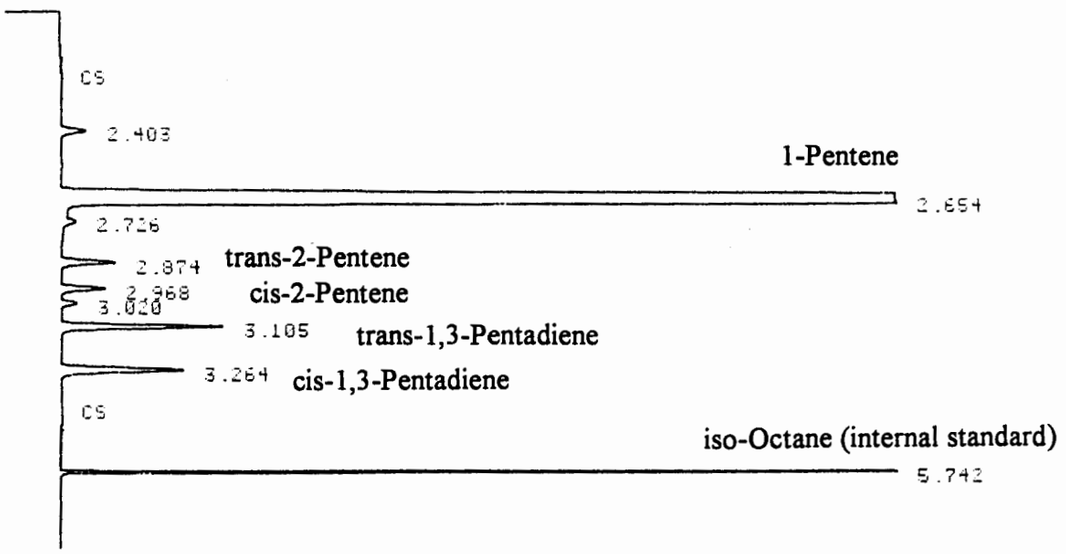

Feed: 1-Hexene:

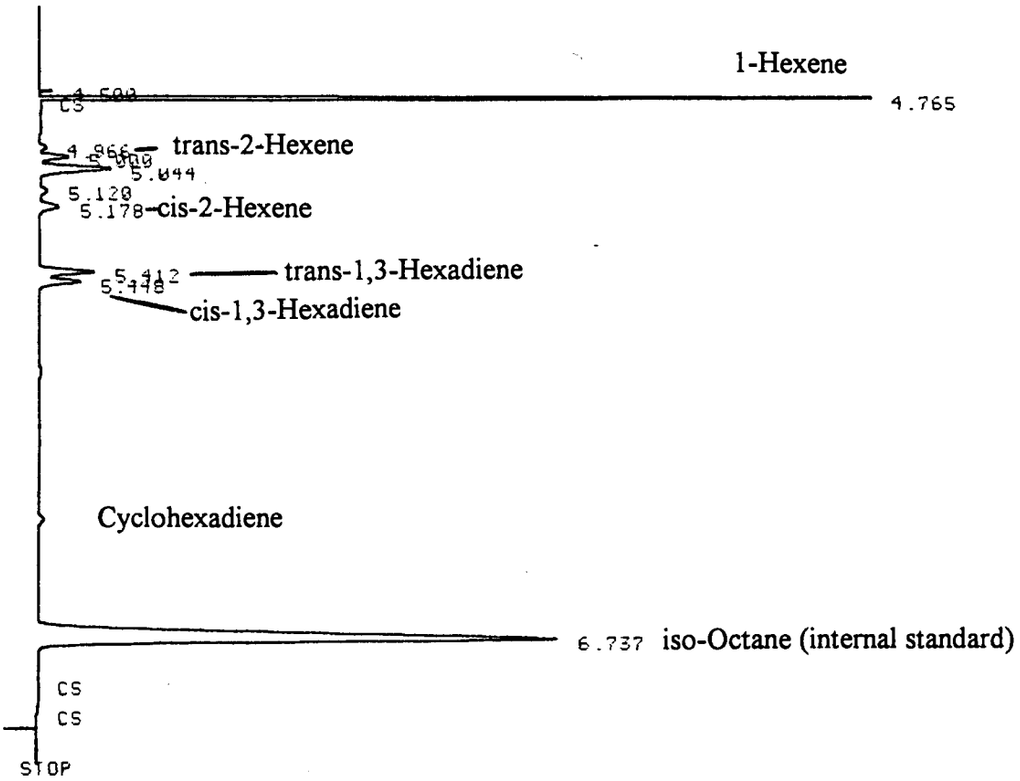

Feed: 1-Heptene:

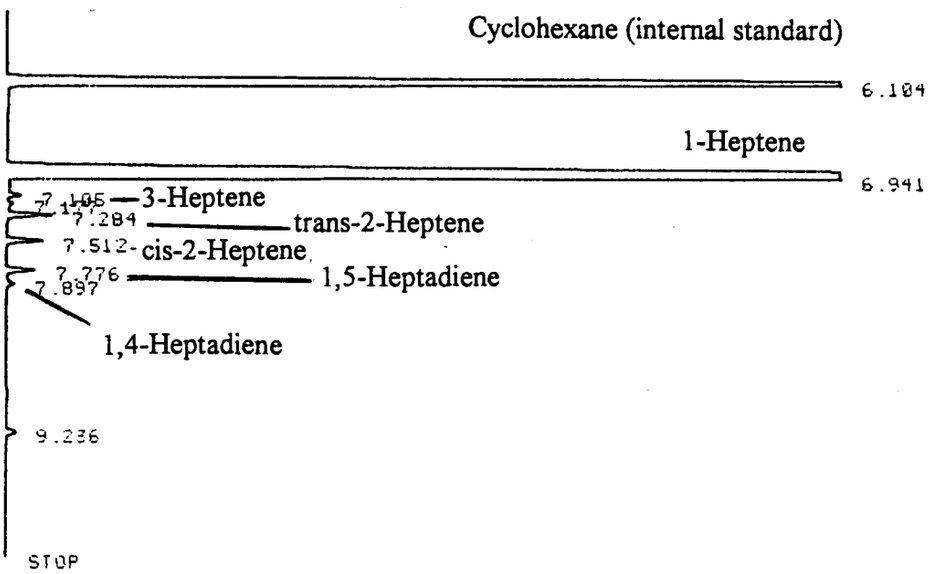

Feed: 1-Octene:

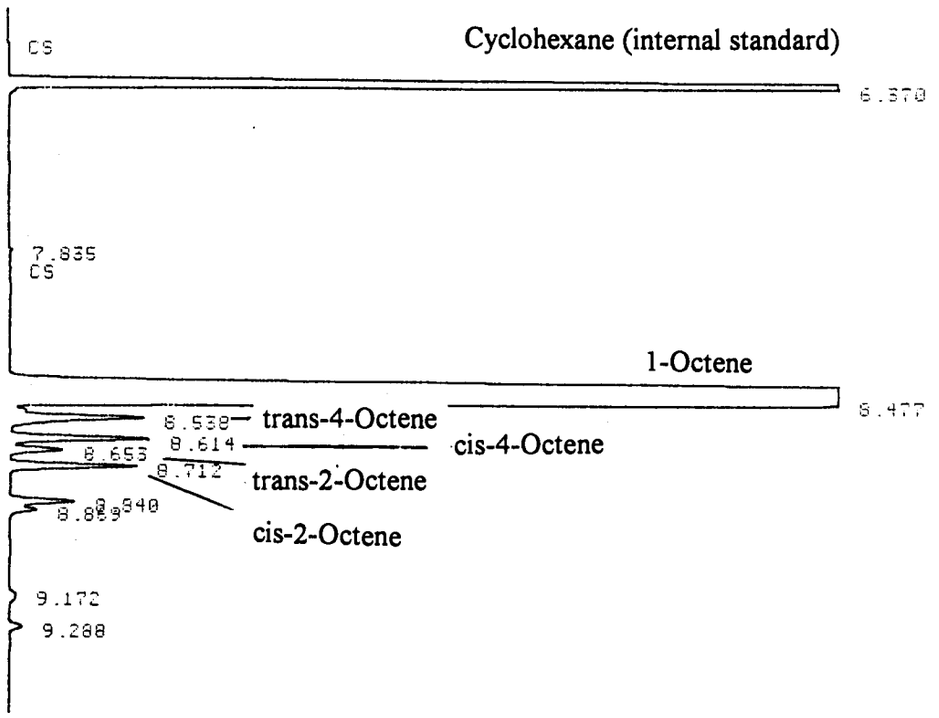

Feed: 1-Nonene:

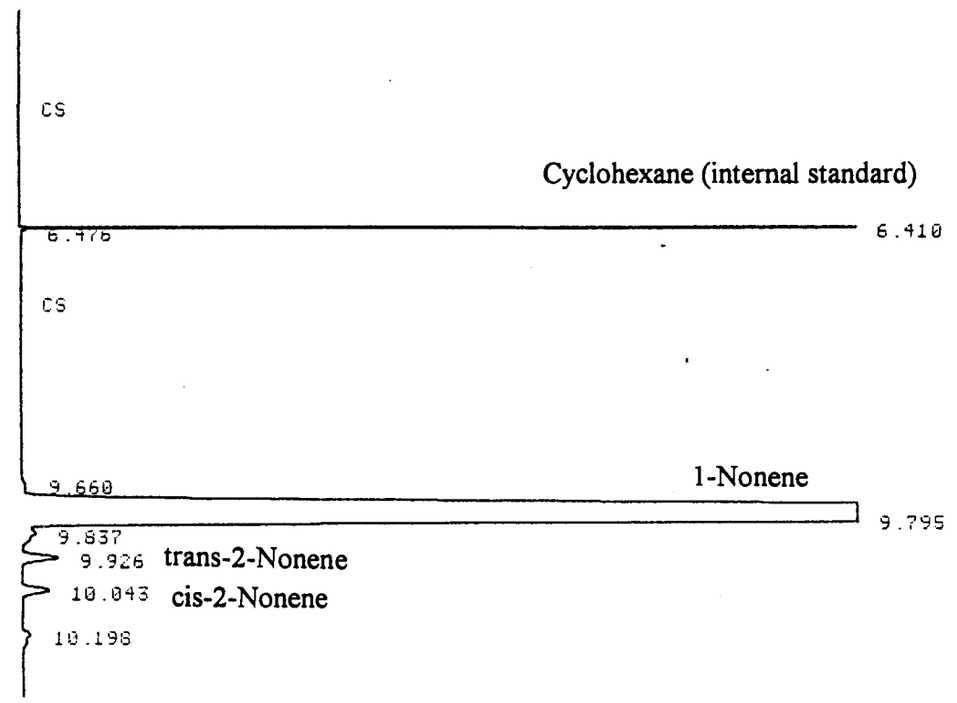

APPENDIX VI

DENSITY OF IRON ANTIMONY OXIDE CATALYSTS

Density of iron antimony oxides calcined at 800°C:

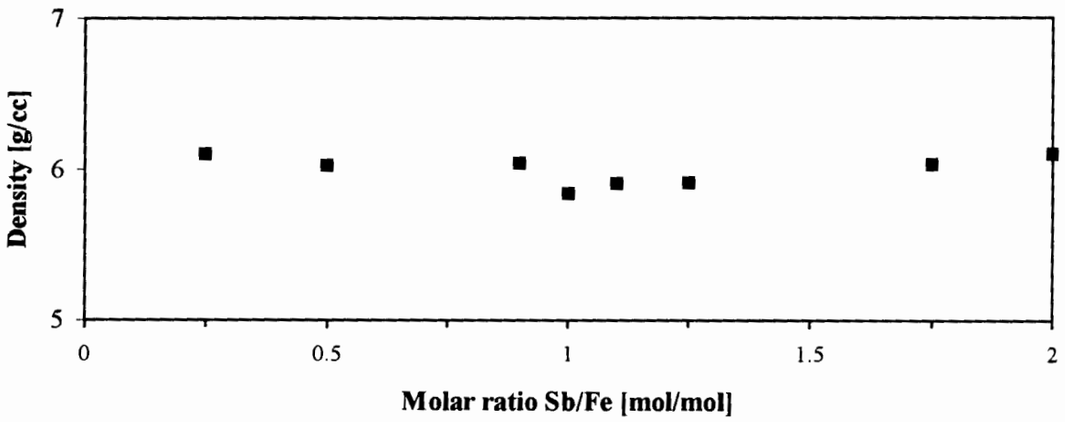

APPENDIX VII

INFLUENCE OF PARTIAL PRESSURE OF OLEFIN AND OXYGEN ON CONVERSION AND SELECTIVITY

Influence of partial pressures on conversion and selectivities

Feed: Ethene:

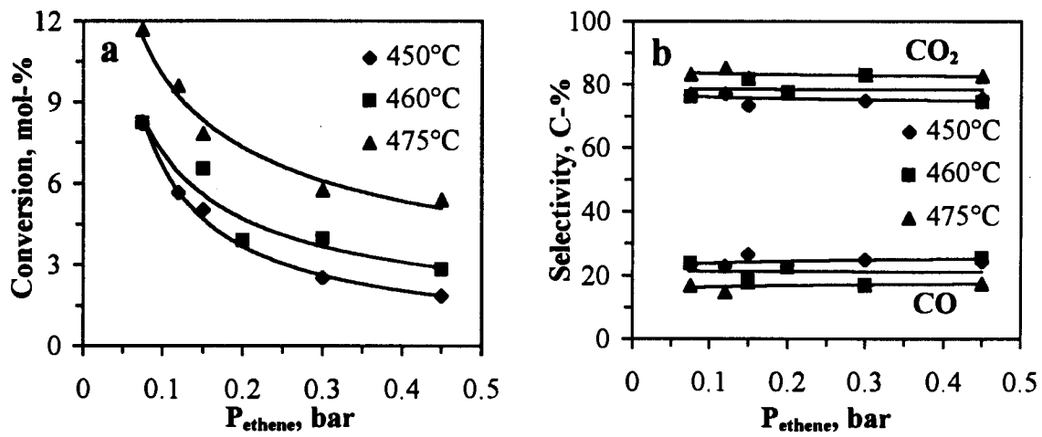

Influence of partial pressure of ethene on conversion (a) and selectivity to carbon oxides (b) in the partial oxidation of ethene over iron antimony oxide at different reaction temperatures; Sb:Fe=1.5, T_{calc} = 900°C, t_{calc} = 7h, p = 1.2 bar, p_{O2}=0.525 bar, F=115 ml(NPT)/ min, $m_{catalyst}$ = 0.5 g.

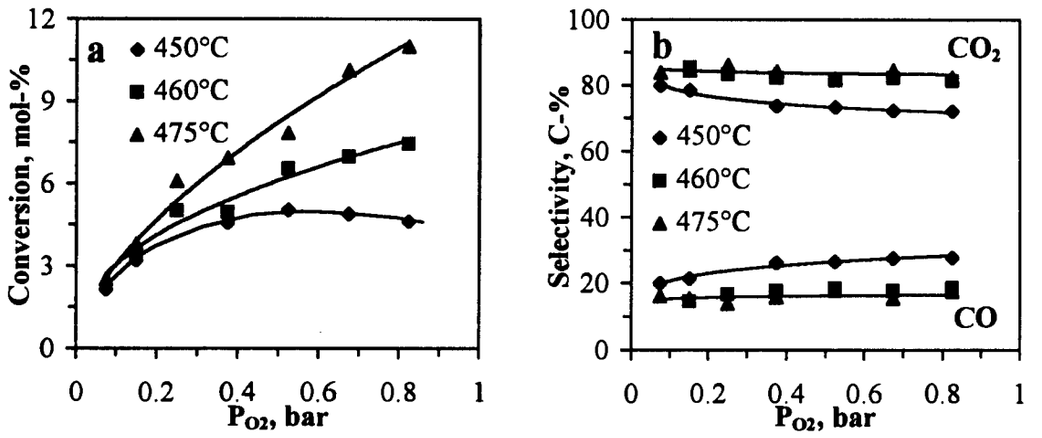

Influence of partial pressure of oxygen on conversion (a) and selectivities to carbon oxides (b) in the partial oxidation of ethene over iron antimony oxide at different reaction temperatures; Sb:Fe=1.5, T_{calc} = 900°C, t_{calc} = 7h, p = 1.2 bar, p_{ethene}=0.15 bar, F=115 ml(NPT)/ min, $m_{catalyst}$ = 0.5 g.

Feed: Propene:

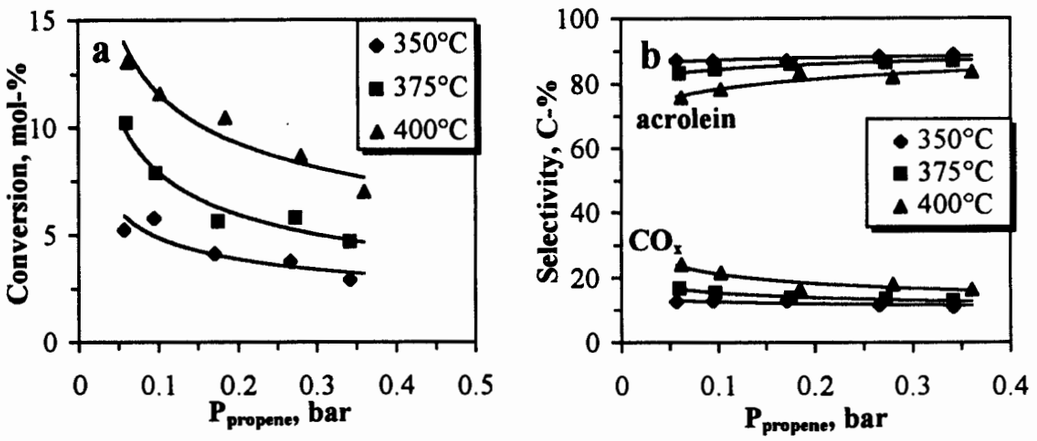

Influence of partial pressure of propene on conversion (a) and on selectivities to acrolein and CO_x (b) in the partial oxidation of propene over iron antimonate at different reaction temperatures; Sb:Fe=1.5, T_{calc} = 900°C, t_{calc} = 7h, p = 1.2 bar, p_{O2}=0.34 bar, τ=0.38s, $m_{catalyst}$ = 0.5 g.

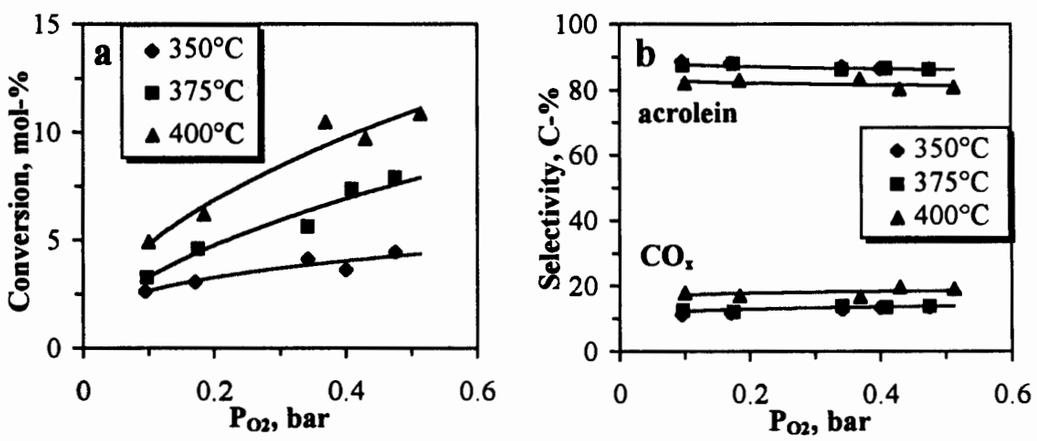

Influence of partial pressure of oxygen on conversion (a) and on selectivities to acrolein and CO_x (b) in the partial oxidation of propene over iron antimonate at different reaction temperatures; Sb:Fe=1.5, T_{calc} = 900°C, t_{calc} = 7h, p = 1.2 bar, $p_{propene}$=0.17 bar, τ=0.38s, $m_{catalyst}$ = 0.5 g.

Feed: 1-Butene:

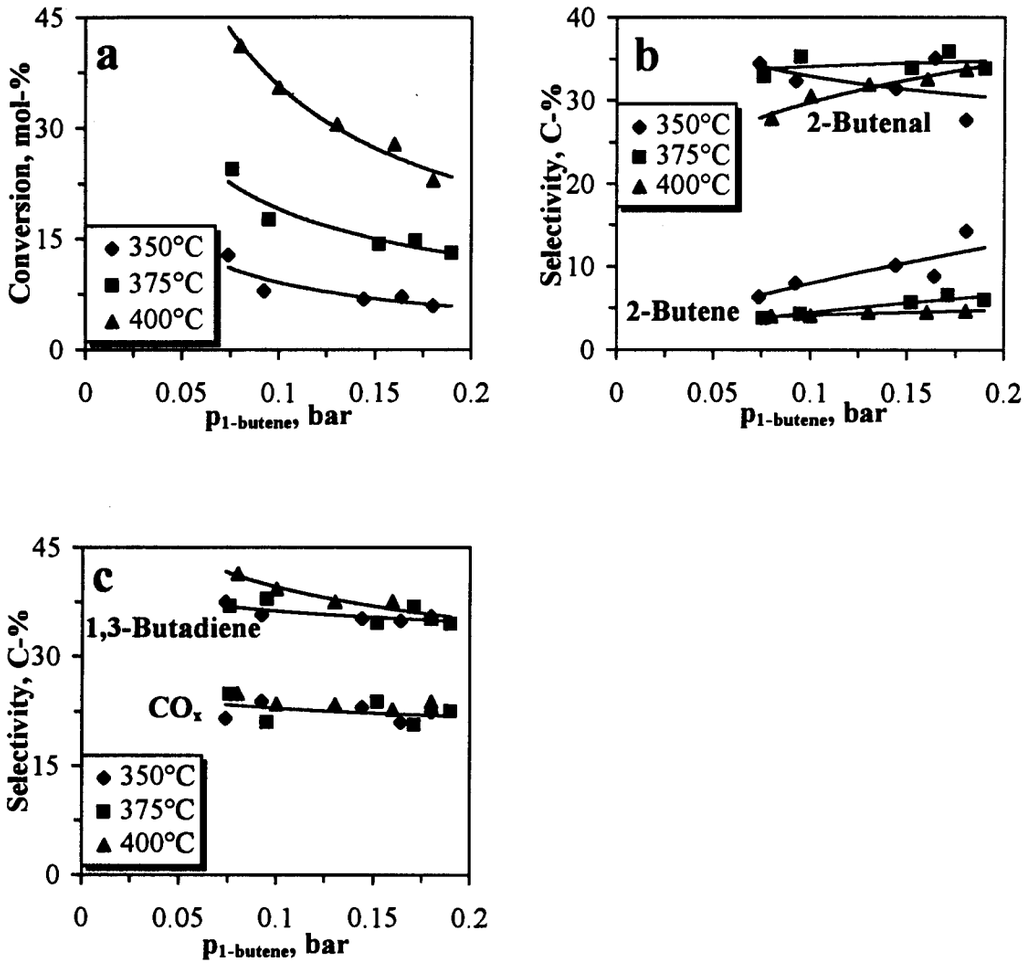

Influence of partial pressure of butene on conversion (a) and selectivities to 2-butenal and 2-butene (b) and selectivities to 1,3-butadiene and carbon oxides (c) in the partial oxidation of butene over iron antimonate at different reaction temperatures (Sb:Fe=1.5, T_{calc} = 900°C, t_{calc} = 7h; p = 1.2 bar, p_{O2}=0.34 bar, F=175 ml(NPT)/ min, $m_{catalyst}$ = 0.5 g)

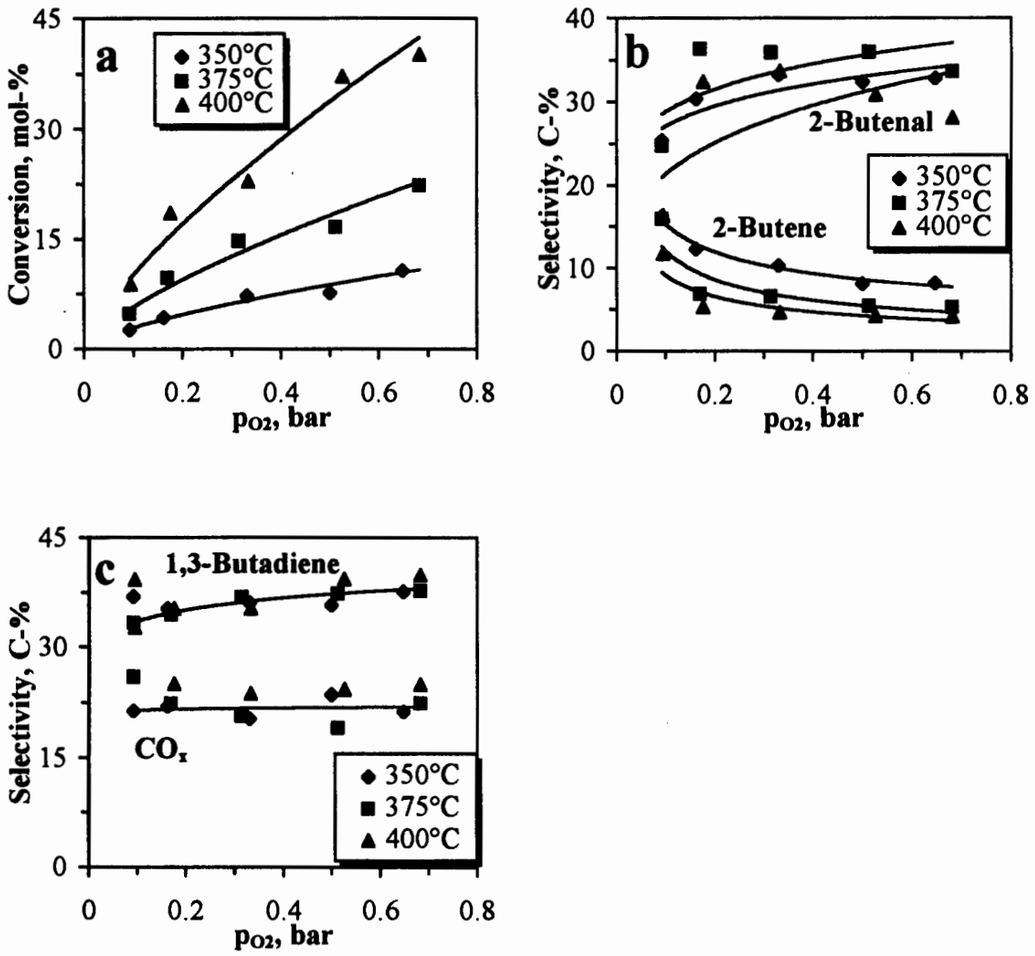

Influence of partial pressure of oxygen on conversion (a) and selectivities to 2-butenal and 2-butene (b) and selectivities to 1,3-butadiene and carbon oxides (c) in the partial oxidation of butene over iron antimonate at different reaction temperatures (Sb:Fe=1.5, T_{calc} = 900°C, t_{calc} = 7h; p = 1.2 bar, p_{butene}=0.17 bar, F=175 ml(NPT)/ min, $m_{catalyst}$ = 0.5 g)

APPENDIX VIII

PASCAL COMPUTER PROGRAMMES

Feed: 1-Pentene:

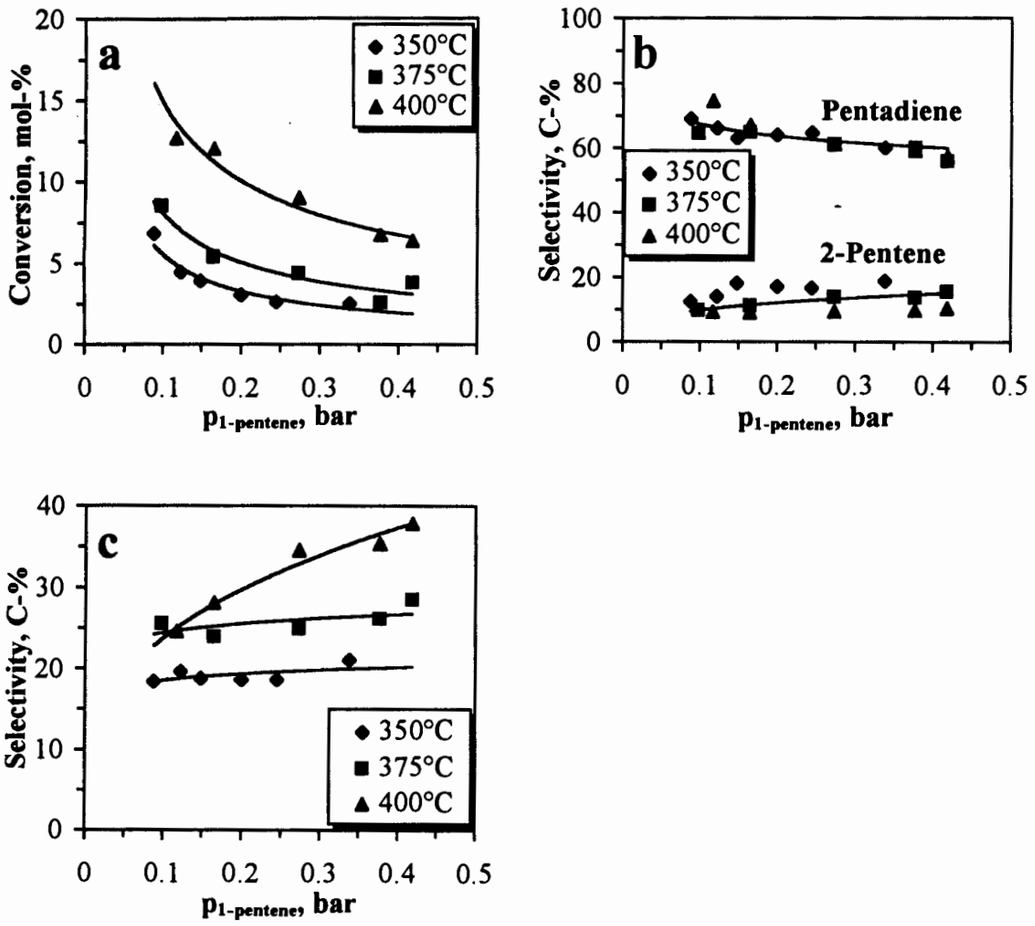

Influence of partial pressure of pentene on the conversion (a) and the selectivities to pentadiene and 2-pentene (b) and the selectivity to carbon oxides (c) in the partial oxidation of pentene over iron antimonate at different reaction temperatures (Sb:Fe=1.5, T_{calc} = 900°C, t_{calc} = 7h; p = 1.2 bar, p_{O2}=0.34 bar, τ=0.47s, $m_{catalyst}$ = 0.5 g)

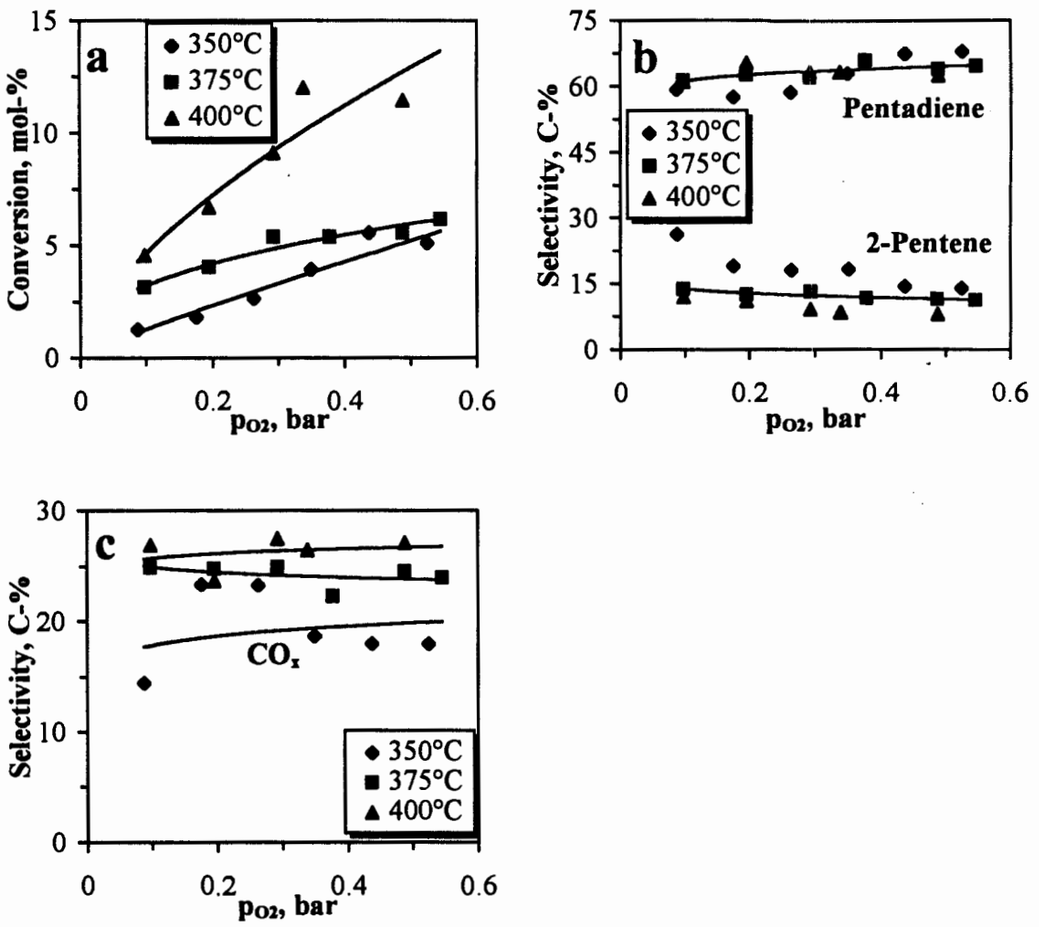

Influence of partial pressure of oxygen on the conversion (a) and the selectivities to pentadiene and 2-pentene (b) and the selectivity to carbon oxides (c) in the partial oxidation of pentene over iron antimonate at different reaction temperatures (Sb:Fe=1.5, T_{calc} = 900°C, t_{calc} = 7h; p = 1.2 bar, $p_{pentene}$=0.17 bar, τ=0.47s , $m_{catalyst}$ = 0.5 g)

Feed: 1-hexene:

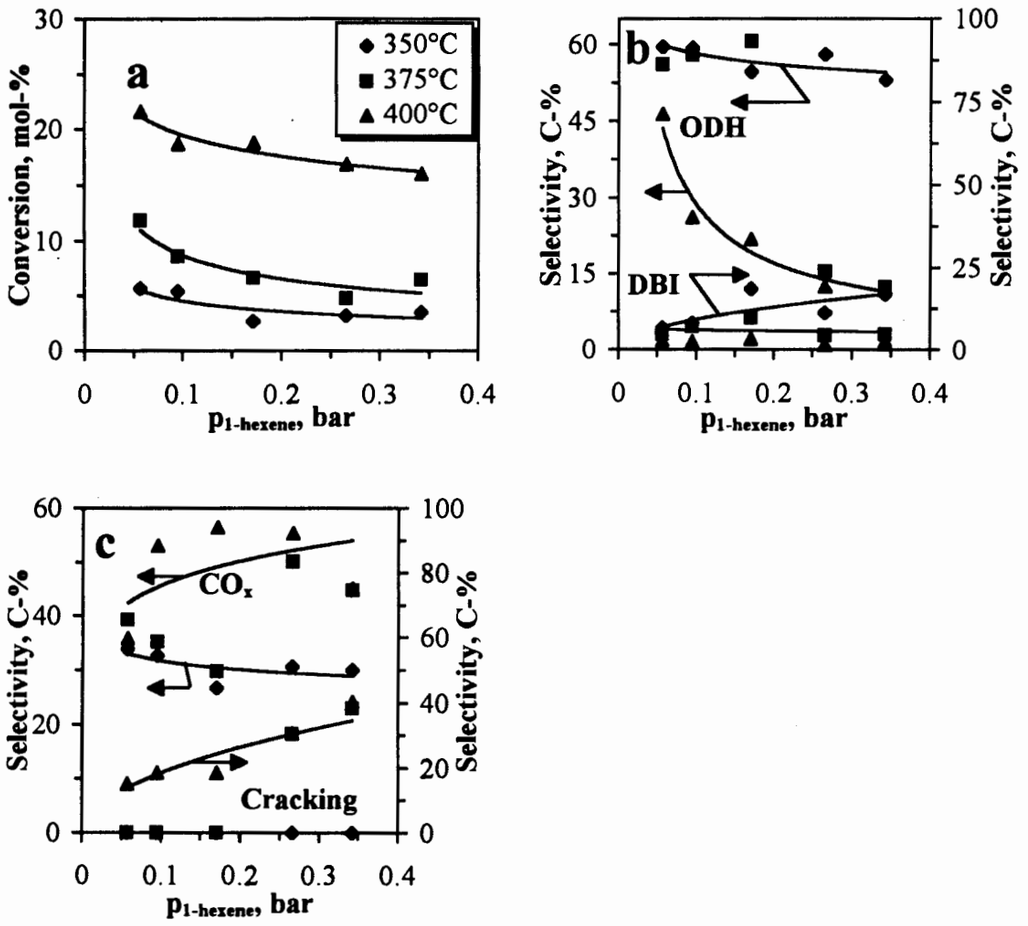

Influence of partial pressure of hexene on conversion (a), selectivities to oxidative dehydrogenation (ODH) products and double bond isomerisation (DBI) products (b) and selectivities to carbon oxides and cracking products (c) in the partial oxidation of hexene over iron antimonate at different reaction temperatures (Sb:Fe=1.5, T_{calc} = 900°C, t_{calc} = 7h; p = 1.2 bar, p_{O2}=0.34 bar, τ=0.43s, $m_{catalyst}$ = 0.5 g)

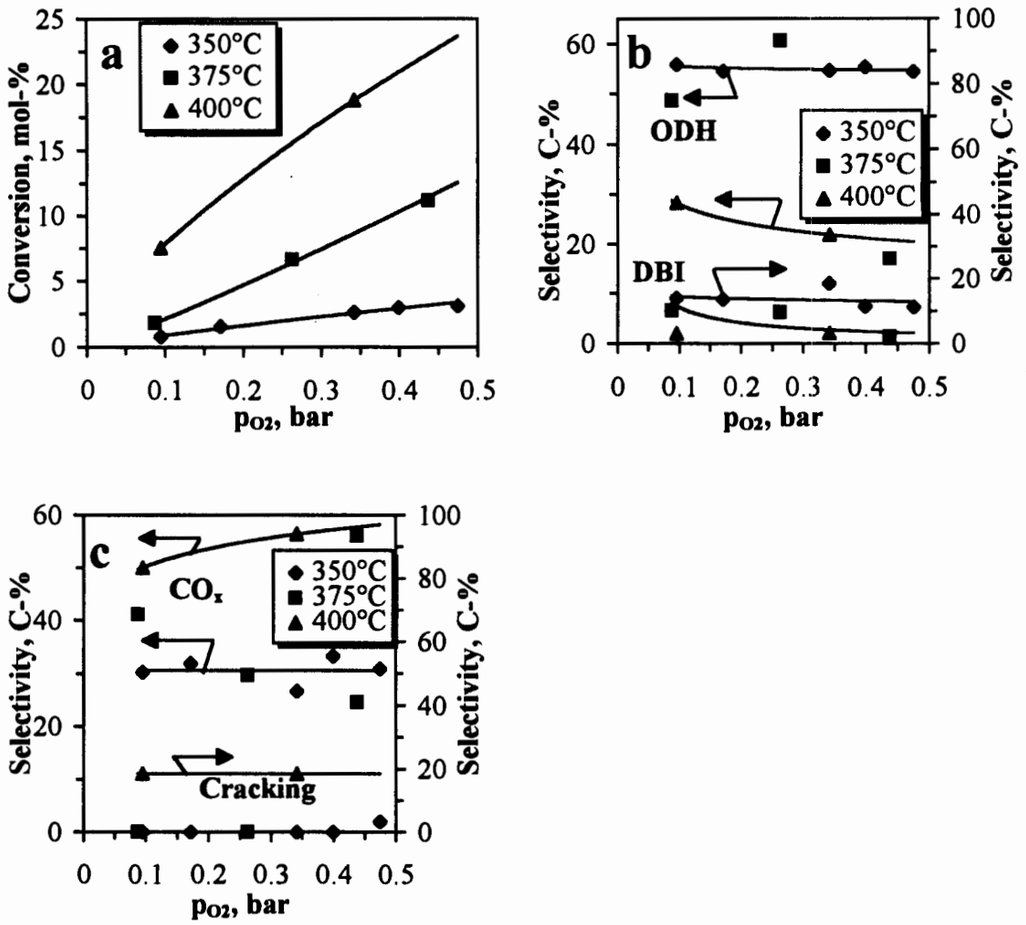

Influence of partial pressure of oxygen on conversion (a), selectivities to oxidative dehydrogenation (ODH) products and double bond isomerisation (DBI) products (b) and selectivities to carbon oxides and cracking products (c) in the partial oxidation of hexene over iron antimonate at different reaction temperatures (Sb:Fe=1.5, T_{calc} = 900°C, t_{calc} = 7h; p = 1.2 bar, p_{hexene}=0.17 bar, τ=0.43s, $m_{catalyst}$ = 0.5 g)

PASCAL program to optimise parameters of rate equations using the simplex algorithm:

```
{Program using the simplex algorithm
(unconstrained)}
 program optim1 (input,output);

 USES crt;

 CONST
  np = 3;
  mp = 4;
  ab = 11;

 TYPE
   DoubleArrayMpbyNp = array [1..mp, 1..np]
OF double;
   DoubleArrayMP = array [1..mp] OF double;
   DoubleArrayNP = array [1..np] OF double;
   DoubleArrayN  = array [1..ab] OF double;

 VAR
  j,i,ndim,n,nfunc,l : INTEGER;
    p: DoubleArrayMpbyNp;
    polef: DoubleArrayN;
    pox: DoubleArrayN;
    rmeas: DoubleArrayN;
    rate: DoubleArrayN;
    y: DoubleArrayMp;
    z: DoubleArrayNp;
    f,ftol: Double;
    ratefile: text;
    pmatrixfile: text;
    rateinfile: string[80];
    pmatrixinfile: string[80];

 FUNCTION func(VAR pr: DoubleArrayNP;
n:integer): Double;

{n is the number of experiments performed}
   BEGIN
   f:= 0.0;
   FOR l := 1 TO n DO
     BEGIN
      rate[l]:= (pr[1]*pr[2]*polef[l]*

SQRT(pox[l]))/SQR(1+pr[3]*polef[l]);
          f:= f+SQR(rmeas[l]-rate[l]);
      end;
    func:=f
   end; { FUNCTION func}

 PROCEDURE amoeba (VAR p:
DoubleArrayMpbyNp;
              VAR y: DoubleArrayMP;
               ndim: INTEGER;
               n:integer;
               ftol: Double;
            VAR nfunc: INTEGER);

 LABEL 99;
 CONST
  alpha = 1.0;
  beta = 0.5;
  gamma = 1.5;
  nfuncmax = 50000000;
 VAR
  mpts,j,inhi,ilo,ihi,i : INTEGER;
  ytry,ysave,sum,rtol : Double;
  psum : ^DoubleArrayNP;

 FUNCTION amotry(VAR p:
DoubleArrayMPbyNP;
             VAR y: DoubleArrayMP;
             VAR sum: DoubleArrayNP;
             ndim,ihi,n: integer;
             VAR nfunc: integer;
             fac: double):double;

 VAR
   j: integer;
   fac1,fac2,ytry: double;
   ptry: ^DoubleArrayNP;
 BEGIN
     new(ptry);
     fac1 := (1.0-fac)/ndim;
     fac2 := fac1-fac;
     FOR j := 1 TO ndim DO
        ptry^[j] := sum[j]*fac1-p[ihi,j]*fac2;
     ytry := func(ptry^,n);
     nfunc := nfunc+1;
     IF ytry < y[ihi] THEN BEGIN
       y[ihi] := ytry;
       FOR j := 1 TO ndim DO BEGIN
          sum[j] := sum[j]+ptry^[j]-p[ihi,j];
          p[ihi,j] := ptry^[j]
       END
     END;
     amotry := ytry;
     dispose(ptry)
 END; {FUNCTION amotry}

 BEGIN {amoeba}
```

```
 new(psum);
 mpts := ndim+1;
 nfunc := 0;
 FOR j := 1 TO ndim DO BEGIN
   sum := 0.0;
   FOR i := 1 TO mpts DO
     sum := sum+p[i,j];
   psum^[j] := sum
 END;
 WHILE true DO BEGIN
  ilo := 1;
  IF y[1] > y[2] THEN
   BEGIN
    ihi := 1;
    inhi := 2;
   END
  ELSE
   BEGIN
    ihi := 2;
    inhi := 1;
   END;
  FOR i := 1 TO mpts DO
   BEGIN
    IF y[i] < y[ilo] THEN ilo := i;
    IF y[i] > y[ihi] THEN
     BEGIN
      inhi := ihi;
      ihi := i
     END
    ELSE
     IF y[i] > y[inhi] THEN
      IF i <> ihi THEN inhi := i
   END;
   {Compute the fractional range from highest
to lowest}


  rtol := 2.0*ABS(y[ihi]-
y[ilo])/(ABS(y[ihi])+ABS(y[ilo]));
  IF rtol < ftol THEN GOTO 99;
  IF  nfunc >= nfuncmax THEN
   BEGIN
    WRITELN ('Pause in routine AMOEBA -
too many iterations');
    READLN
   END;
   {Begin a new iteration. First extrapolate by a
factor alpha through the face of the simplex
across from the high point,
    i.e., reflect the simplex from the high point.}

   ytry :=amotry(p,y,psum^,ndim,ihi,n,nfunc,-
alpha);
   IF ytry <= y[ilo] THEN
   {gives a result better than the best point, so
try  an additional extrapolation by a factor
gamma}
      ytry :=
amotry(p,y,psum^,ndim,ihi,n,nfunc,gamma)
   ELSE IF ytry >= y[inhi] THEN
   BEGIN
   {the reflected point is worse than the second
highest, so look for an intermediate lower point,
   i.e. do an one-dimensional contraction}
     ysave := y[ihi];
     ytry :=
amotry(p,y,psum^,ndim,ihi,n,nfunc,beta);
      IF ytry >= ysave THEN BEGIN


       {Can't seem to get rid of that high point.
Better contract around the lowest (best) point.}
        FOR i := 1 TO mpts DO
          IF i <> ilo THEN
          BEGIN
           FOR j := 1 TO ndim DO
            BEGIN
            psum^[j] := 0.5*(p[i,j]+p[ilo,j]);
            p[i,j] := psum^[j]
           END;
           y[i] := func(psum^,n)
          END;
        nfunc := nfunc+ndim; {keep track of
function evaluations.}
        FOR j := 1 TO ndim DO BEGIN
          sum := 0.0;
          FOR i := 1 TO mpts DO
            sum := sum+p[i,j];
          psum^[j] := sum
        END
       END
      END
     END;
 99:
 dispose(psum)
END;{amoeba}

BEGIN {program optim1}

{input of filename}

 writeln('Please enter the name of the input file,
which contains');
 writeln('number of experiments n,
P(olefin),P(oxygen) and rmeas');
 readln(rateinfile);
 assign(ratefile,rateinfile);
 reset(ratefile);
```

APPENDIX IX

DERIVATION OF RATE EQUATIONS FOR THE OXIDATION MODEL

Modelling the kinetics of the oxidation of α-olefins according to the oxidation model:

Elementary reactions:

Sb	+	O_2	$\xleftrightarrow{K_1}$	Sb-O-O				(1)
Sb-O-O	+	*	$\xleftrightarrow{K_2}$	Sb=O	+	O*		(2)
Sb=O	+	*	$\xleftrightarrow{K_3}$	Sb	+	O*		(3)
Sb-O-O	+	olefin	$\longrightarrow$	Sb-O-O-olefin				(4)
Sb-O-O-olefin	+	*	$\longrightarrow$	$CO+CO_2$				(4a)
Sb=O	+	olefin	$\xleftrightarrow{K_5}$	Sb-O-olefin				(5)
Sb-O-olefin	+	O*	$\longrightarrow$	Part. oxidation/ox. dehydrogenation				(5a)
Sb-O-olefin	+	O*	$\longrightarrow$	Double bond isomers				(5b)
Sb	+	olefin	$\xleftrightarrow{K_6}$	Sb-olefin				(6)
Sb-olefin	+	O*	$\longrightarrow$	CO+CO2				(6a)
Sb-olefin	+	O*	$\longrightarrow$	Double bond isomers				(6b)

with * and O* being the bridging positions between two metal atoms in the crystallite lattice surface. The number of vacancies and the number of oxygen atoms are assumed to be at steady state, i. e. there is no flux of lattice oxygen to the surface of the catalyst.

The formation of the various products can be thought to arise from the various olefin surface species:

It can be assumed, that the reactions (1), (2), (3), (5) and (6) are at equilibrium and reactions (4), (4a), (5a) and (6a) are irreversible. A balance equation for the surface antimony leads to:

$$n_{Sb,\,total} = n_{Sb} + n_{Sb\text{-}O\text{-}O} + n_{Sb=O} + n_{Sb\text{-}O\text{-}O\text{-}olefin} + n_{Sb\text{-}O\text{-}olefin} + n_{Sb\text{-}olefin}$$

If reaction (1) is at equilibrium then

$$n_{Sb\text{-}O\text{-}O} = K_1 \cdot n_{Sb} \cdot p_{O2}$$

If reaction (2) is at equilibrium then

$$n_{Sb=O} = K_2 \cdot n_{Sb\text{-}O\text{-}O} \cdot \frac{\theta_V}{\theta_O} = K_1 \cdot K_2 \cdot n_{Sb} \cdot p_{O2} \cdot \frac{\theta_V}{\theta_O}$$

with θ_V and θ_O being the vacant and the oxidised bridging position, respectively.

If reaction (3) is at equilibrium then

$$n_{Sb=O} = K_3 \cdot n_{Sb} \cdot \frac{\theta_O}{\theta_V}$$

From these equilibria it can be derived that:

$$\theta_O = K_1^{\frac{1}{2}} \cdot K_2^{\frac{1}{2}} \cdot K_3^{\frac{1}{2}} \cdot p_{O2}^{\frac{1}{2}} \cdot \theta_v$$

Since the total number of bridging positions is constant, i.e.

$$\theta_O + \theta_v = 1$$

and

$$\theta_v = \frac{1}{1 + K_1^{\frac{1}{2}} \cdot K_2^{\frac{1}{2}} \cdot K_3^{\frac{1}{2}} \cdot p_{O2}^{\frac{1}{2}}}$$

$$\theta_O = \frac{K_1^{\frac{1}{2}} \cdot K_2^{\frac{1}{2}} \cdot K_3^{\frac{1}{2}} \cdot p_{O2}^{\frac{1}{2}}}{1 + K_1^{\frac{1}{2}} \cdot K_2^{\frac{1}{2}} \cdot K_3^{\frac{1}{2}} \cdot p_{O2}^{\frac{1}{2}}}$$

Applying the steady state approximation for the Sb - O - O - Olefin species in conjunction with the equilibrium of reaction (1) yields:

$$n_{Sb-O-O-olefin} = K_1 \cdot \frac{k_4}{k_{4a}} \cdot n_{Sb} \cdot p_{O_2} \cdot p_{olefin} \cdot (1 + K_1^{\frac{1}{2}} \cdot K_2^{\frac{1}{2}} \cdot K_3^{\frac{1}{2}} \cdot p_{O2}^{\frac{1}{2}})$$

Considering reaction (5) to be in equilibrium in conjunction with the above derived dependencies yields:

$$n_{Sb-O-olefin} = K_1^{\frac{1}{2}} \cdot K_2^{\frac{1}{2}} \cdot K_3^{-\frac{1}{2}} \cdot K_5 \cdot n_{Sb} \cdot p_{O_2}^{\frac{1}{2}} \cdot p_{olefin}$$

Considering reaction (6) to be in equilibrium, yields:

$$n_{Sb\text{-}olefin} = K_6 \cdot n_{Sb} \cdot p_{olefin}$$

The rate of formation of the various product groups can then be derived to be:

<u>rate of formation of the partial oxidation plus oxidative dehydrogenation products:</u>

$$r_{POX+OXD} = \frac{k_{5a} \cdot K_5 \cdot n_{Sb,total} \cdot p_{olefin} \cdot p_{O_2}^{\frac{1}{2}} \cdot \frac{K_1^{\frac{1}{2}} \cdot K_2^{\frac{1}{2}} \cdot K_3^{-\frac{1}{2}}}{1 + K_1^{\frac{1}{2}} \cdot K_2^{\frac{1}{2}} \cdot K_3^{-\frac{1}{2}} \cdot p_{O_2}^{\frac{1}{2}}}}{1 + K_1 \cdot p_{O_2} + K_1^{\frac{1}{2}} \cdot K_2^{\frac{1}{2}} \cdot K_3^{-\frac{1}{2}} \cdot p_{O_2}^{\frac{1}{2}} + \frac{k_4}{k_{4a}} \cdot K_1 \cdot p_{O_2} \cdot p_{olefin} (1 + K_1^{\frac{1}{2}} \cdot K_2^{\frac{1}{2}} \cdot K_3^{-\frac{1}{2}} \cdot p_{O_2}^{\frac{1}{2}}) + K_1^{\frac{1}{2}} \cdot K_2^{\frac{1}{2}} \cdot K_3^{-\frac{1}{2}} \cdot K_5 \cdot p_{O_2}^{\frac{1}{2}} \cdot p_{olefin} + K_6 \cdot p_{olefin}}$$

rate of formation of the cracking products plus combustion products CO and CO_2:

$$r_{TOX+C} = \frac{K_1 \cdot k_4 \cdot n_{Sb,total} \cdot p_{olefin} \cdot p_{O_2} + K_6 \cdot k_{6a} \cdot n_{Sb,total} \cdot p_{olefin} \cdot \frac{K_1^{\frac{1}{2}} \cdot K_2^{\frac{1}{2}} \cdot K_3^{\frac{1}{2}} \cdot p_{O2}^{\frac{1}{2}}}{1 + K_1^{\frac{1}{2}} \cdot K_2^{\frac{1}{2}} \cdot K_3^{\frac{1}{2}} \cdot p_{O2}^{\frac{1}{2}}}}{1 + K_1 \cdot p_{O_2} + K_1^{\frac{1}{2}} \cdot K_2^{\frac{1}{2}} \cdot K_3^{-\frac{1}{2}} \cdot p_{O_2}^{\frac{1}{2}} + \frac{k_4}{k_{4a}} \cdot K_1 \cdot p_{O_2} \cdot p_{olefin} (1 + K_1^{\frac{1}{2}} \cdot K_2^{\frac{1}{2}} \cdot K_3^{-\frac{1}{2}} \cdot p_{O_2}^{\frac{1}{2}}) + K_1^{\frac{1}{2}} \cdot K_2^{\frac{1}{2}} \cdot K_3^{-\frac{1}{2}} \cdot K_5 \cdot p_{O_2}^{\frac{1}{2}} \cdot p_{olefin} + K_6 \cdot p_{olefin}}$$

rate of formation of the double bond isomers:

$$r_{DBI} = \frac{K_5 \cdot k_{5b} \cdot n_{Sb,total} \cdot p_{olefin} \cdot p_{O_2}^{\frac{1}{2}} \cdot \frac{K_1^{\frac{1}{2}} \cdot K_2^{\frac{1}{2}} \cdot K_3^{-\frac{1}{2}}}{1 + K_1^{\frac{1}{2}} \cdot K_2^{\frac{1}{2}} \cdot K_3^{-\frac{1}{2}} \cdot p_{O_2}^{\frac{1}{2}}} + k_{6b} \cdot K_6 \cdot n_{Sb,total} \cdot p_{olefin}}{1 + K_1 \cdot p_{O_2} + K_1^{\frac{1}{2}} \cdot K_2^{\frac{1}{2}} \cdot K_3^{-\frac{1}{2}} \cdot p_{O_2}^{\frac{1}{2}} + \frac{k_4}{k_{4a}} \cdot K_1 \cdot p_{O_2} \cdot p_{olefin} (1 + K_1^{\frac{1}{2}} \cdot K_2^{\frac{1}{2}} \cdot K_3^{-\frac{1}{2}} \cdot p_{O_2}^{\frac{1}{2}}) + K_1^{\frac{1}{2}} \cdot K_2^{\frac{1}{2}} \cdot K_3^{-\frac{1}{2}} \cdot K_5 \cdot p_{O_2}^{\frac{1}{2}} \cdot p_{olefin} + K_6 \cdot p_{olefin}}$$

Following simplifying assumptions can now be made:

a) The transformation of the oxygen species in Sb=O to the bridging positions is not favoured, i.e. $K_3 <<$

b) The total oxidation reaction (4a) is much faster than the adsorption of the olefin on the peroxo-group

c) The total oxidation reaction (4a) is much faster than the total oxidation reaction (6a) via a π-allylic cation.

Then the rate of formation of partial oxidation plus oxidative dehydrogenation products can be simplified to:

$$r_i = \frac{a_i \cdot p_{olefin} \cdot p_{O_2}^{\frac{1}{2}}}{1 + K_1 \cdot p_{O_2} + K_1^{\frac{1}{2}} \cdot K_2^{\frac{1}{2}} \cdot K_3^{-\frac{1}{2}} \cdot p_{O_2}^{\frac{1}{2}} + \frac{k_4}{k_{4a}} \cdot K_1 \cdot p_{O_2} \cdot p_{olefin} + K_1^{\frac{1}{2}} \cdot K_2^{\frac{1}{2}} \cdot K_3^{-\frac{1}{2}} \cdot K_5 \cdot p_{O_2}^{\frac{1}{2}} \cdot p_{olefin} + K_6 \cdot p_{olefin}}$$

with $a_i = k_{5a} \cdot K_5 \cdot n_{Sb,total} \cdot K_1^{\frac{1}{2}} \cdot K_2^{\frac{1}{2}} \cdot K_3^{-\frac{1}{2}}$.

The rate of formation of double bond isomerisation becomes:

$$r_i = \frac{p_{olefin} \cdot (a_i \cdot p_{O_2}^{\frac{1}{2}} + b_i)}{1 + K_1 \cdot p_{O_2} + K_1^{\frac{1}{2}} \cdot K_2^{\frac{1}{2}} \cdot K_3^{-\frac{1}{2}} \cdot p_{O_2}^{\frac{1}{2}} + \frac{k_4}{k_{4a}} \cdot K_1 \cdot p_{O_2} \cdot p_{olefin} + K_1^{\frac{1}{2}} \cdot K_2^{\frac{1}{2}} \cdot K_3^{-\frac{1}{2}} \cdot K_5 \cdot p_{O_2}^{\frac{1}{2}} \cdot p_{olefin} + K_6 \cdot p_{olefin}}$$

with $a_i = k_{5b} \cdot K_5 \cdot n_{Sb,total} \cdot K_1^{\frac{1}{2}} \cdot K_2^{\frac{1}{2}} \cdot K_3^{-\frac{1}{2}}$,

and $b_i = k_{6b} \cdot K_6 \cdot n_{Sb,total}$.

The rate of formation of cracking and total oxidation products becomes:

$$r_i = \frac{p_{olefin} \cdot (a_i \cdot p_{O_2}^{\frac{1}{2}} + b_i \cdot p_{olefin})}{1 + K_1 \cdot p_{O_2} + K_1^{\frac{1}{2}} \cdot K_2^{\frac{1}{2}} \cdot K_3^{-\frac{1}{2}} \cdot p_{O_2}^{\frac{1}{2}} + \frac{k_4}{k_{4a}} \cdot K_1 \cdot p_{O_2} \cdot p_{olefin} + K_1^{\frac{1}{2}} \cdot K_2^{\frac{1}{2}} \cdot K_3^{-\frac{1}{2}} \cdot K_5 \cdot p_{O_2}^{\frac{1}{2}} \cdot p_{olefin} + K_6 \cdot p_{olefin}}$$

with $a_i = k_{6b} \cdot K_6 \cdot n_{Sb,total} \cdot K_1^{\frac{1}{2}} \cdot K_2^{\frac{1}{2}} \cdot K_3^{-\frac{1}{2}}$,

and $b_i = k_4 \cdot K_1 \cdot n_{Sb,total}$.

```
{input of number of experiments n from file
rateinfile}
readln (ratefile, n);

FOR i := 1 TO n DO
 BEGIN

   readln(ratefile, polef[i], pox[i], rmeas[i]);
{input of experimental data}
 end;
close(ratefile);

{input of ndim}
writeln('what is the dimension of the function? ');
readln(ndim);

{input of data of matrix p for starting simplex}
   writeln ('enter filename of the file, which
contains');
   writeln ('the matrix p for starting simplex');
   readln(pmatrixinfile);
   assign(pmatrixfile,pmatrixinfile);
   reset(pmatrixfile);

FOR i:=1 TO ndim+1 DO
 BEGIN
   FOR j:=1 TO ndim DO
   readln(pmatrixfile, p[i,j]);
 end;

writeln ('Please enter value for the convergence
tolerance');
readln (ftol);

{input of vector y, whose components are pre-
initialized to the values
of func}

FOR i:=1 TO ndim+1 DO
 BEGIN
 FOR j:=1 TO ndim DO
  z[j] := p[i,j];
  y[i] := func(z,n);
  end;

amoeba(p,y,ndim,n,ftol,nfunc);

{output of data of matrix p on screen}

     writeln('output of matrix p: ');
     FOR i := 1 TO ndim+1 DO
      BEGIN
       writeln;
       FOR j := 1 to ndim DO
        BEGIN
        write(p[i,j]:12:8);
        end;
      end;
      writeln;

writeln('output of vector y: ');
FOR i:= 1 TO ndim+1 DO
 BEGIN
 writeln('y[',i,'] = ', y[i]:12:8);
 end;

{number of function evaluations taken}

writeln('number of function evaluations:
',nfunc:12);
readln;


end. {program opti1}
```

PASCAL program for the calculation of the 95% confidence limits:

```
{program calculates the 95% confidence limits
of the parameters from a
nonlinear rate equation. The formulas are
derived from "Draper, Smith:
Applied Regression Analysis, p.487". The
procedures for the LU Decomposition
are from 'Numerical Recipes in Pascal' Chapter
2.3}
{PROGRAM SPECIFICALLY FOR RATE
EQUATION OF SINGLE SITE MODEL}

program conflim (input, output);

USES crt;

CONST
  np = 2;
  nr =15;
TYPE
  IntegerArrayNP = ARRAY [1..np] OF integer;
  DoubleArrayNP = ARRAY [1..np] OF double;
  DoubleArrayNE = ARRAY [1..nr] OF double;
  DoubleArrayNPbyNP = ARRAY [1..np,1..np]
OF double;
  DoubleArrayNEbyNP = ARRAY [1..nr,1..np]
OF double;
```

```
  DoubleArrayNPbyNE = ARRAY [1..np,1..nr]
OF double;

VAR
  n,i,j,ne,k:integer;
  d,ssr,clrk,clak,f,rk,ak:double;
  indx:IntegerArrayNP;
  col,b:DoubleArrayNP;
  x1,x2,komp:DoubleArrayNE;
  a,y:DoubleArrayNPbyNP;
   z:DoubleArrayNEbyNP;
  zt:DoubleArrayNPbyNE;
  rateinfile:string[90];
  ratefile:text;

FUNCTION f1 (VAR rk:Double; ak:Double;
x1:Double; x2:Double):Double;
BEGIN
  f:=ak*sqrt(x1)*x2/SQR(1+ak*x2);
  f1:=f;
  {write('f1=', f:8:4);
  writeln;
  readln;}
end;


FUNCTION f2 (VAR rk:Double; ak:Double;
x1:Double; x2:Double):Double;
BEGIN
  f:=(rk*sqrt(x1)*x2*(1+ak*x2)-
2*rk*ak*sqrt(x1)*sqr(x2))/
  (sqr(1+ak*x2)*(1+ak*x2));
  f2:=f;
  {write('f2=', f:8:4);
  writeln;
  readln;}
end;


PROCEDURE ludcmp (VAR a:
DoubleArrayNPbyNP;
                n: integer;
          VAR indx: IntegerArrayNP;
            VAR d: double);

CONST
   tiny = 1.0e-20;
VAR
   k,j,imax,i: integer;
   sum,dum,big: double;
   vv: ^DoubleArrayNP;
BEGIN {LU decomposition}
   new(vv);
   d:= 1.0;
   FOR i:=1 TO np DO BEGIN
     big:=0.0;
     FOR j:=1 TO np DO
       IF abs(a[i,j]) > big THEN big:=abs(a[i,j]);
     IF big = 0.0 THEN BEGIN  {no nonzero
largest element}
       writeln('pause in LUDCMP - singular
matrix');
       readln
     END;
     vv^[i] := 1.0/big
   END;
   FOR j:=1 TO np DO BEGIN
     FOR i:= 1 TO j-1 DO BEGIN
       sum:= a[i,j];
       FOR k:= 1 to i-1 DO
         sum:=sum-a[i,k]*a[k,j];
       a[i,j]:=sum
     END;
     big :=0.0; {initialize for the search for
largest pivot element}
     FOR i:=j TO np DO BEGIN
       sum:= a[i,j];
       FOR k:=1 to j-1 DO
         sum:=sum-a[i,k]*a[k,j];
       a[i,j]:=sum;
       dum:=vv^[i]*abs(sum);
       IF dum >=big THEN BEGIN
         big:=dum;
         imax:=i
       END
     END;
     IF j<> imax THEN BEGIN
       FOR k:=1 TO np DO BEGIN
         dum:=a[imax,k];
         a[imax,k]:=a[j,k];
         a[j,k]:=dum
       END;
       d:=-d;
       vv^[imax]:=vv^[j]
     END;
     indx[j]:=imax;
     IF a[j,j] = 0.0 THEN a[j,j]:=tiny;
{substituting tiny for zero}
     IF j<> n THEN BEGIN
      dum:=1.0/a[j,j];
      FOR i:=j+1 TO np DO
        a[i,j]:=a[i,j]*dum
     END
   END;
   dispose(vv);
END; {ludcmp}

PROCEDURE lubksb (VAR a:
DoubleArrayNPbyNP;
                n: integer;
          VAR indx: IntegerArrayNP;
            VAR b: DoubleArrayNP);
```

```
VAR
  j,ip,ii,i: integer;
  sum: double;
BEGIN
 ii:=0;
 FOR i:=1 TO np DO BEGIN
   ip:=indx[i];
   sum:=b[ip];
   b[ip]:=b[i];
     IF ii <> 0 THEN
       FOR j:=ii TO i-1 DO
       sum:=sum-a[i,j]*b[j]
     ELSE IF sum <> 0.0 THEN
       ii:=i;
       b[i]:=sum
 END;
 FOR i:= np DOWNTO 1 DO BEGIN
   sum:=b[i];
   FOR j:=i+1 TO np DO
     sum:=sum-a[i,j]*b[j];
   b[i]:=sum/a[i,i]
 END
END; {lubksb}

BEGIN {program conflim}
{input of filename}
writeln('Please enter the values of k and K1 for
which you would');
writeln('like to determine the 95% confidence
limits');
writeln('k =  ');
readln(rk);
writeln('K1 =  ');
readln(ak);
writeln('Please enter the name of the input file,
which contains');
writeln('number of experiments l, P(olefin),
P(oxygen) and rmeas');
readln(rateinfile);
assign(ratefile,rateinfile);
reset(ratefile);

{input of number of experiments ne from file
rateinfile}
readln(ratefile,ne);
{input of vector x1(pox) and x2(polef) from
input file}

FOR i:=1 TO ne DO
  readln(ratefile, x1[i],x2[i]);
{check if x1 and x2 are right}
{writeln('the vector x1 has the values:');
For i:=1 TO ne DO
write(x1[i]:8:4);
writeln;
writeln('vector x2 has the values:');
For i:=1 TO ne DO
write(x2[i]:8:4);
writeln;}

{calculation of matrix Z}
FOR i:=1 TO ne DO
BEGIN

  z[i,1]:=f1(rk,ak,x1[i],x2[i]);
  z[i,2]:=f2(rk,ak,x1[i],x2[i]);
end;

{calculation of transposed matrix Zt}

FOR i:=1 TO ne DO BEGIN
  zt[1,i]:=z[i,1];
  zt[2,i]:=z[i,2];
end;


{matrix multiplication Zt x Z}
FOR i:=1 TO np DO
 FOR k:=1 TO np DO
  a[i,k]:=0.0;
  FOR i:=1 TO 2 DO BEGIN
    FOR k:=1 TO 2 DO BEGIN
      FOR j:= 1 TO ne DO BEGIN
        komp[j]:=zt[i,j]*z[j,k];
        a[i,k]:=komp[j]+a[i,k];
        end;
      writeln('a[',i, k,']=', a[i,k]:8:7);
  end;
end;

{calculation of the inverse matrix A^-1}

ludcmp(a,np,indx,d);
  FOR j:=1 TO np DO BEGIN
    FOR i:=1 TO np DO
    col[i]:=0.0;
    col[j]:=1.0;
    lubksb(a,np,indx,col);
    FOR i:=1 TO np DO BEGIN
    y[i,j]:=col[i]
    end;
    writeln('y[1 1]=',y[1,1]:10:6);
    writeln('y[2 2]=',y[2,2]:10:6);
  END;

writeln('Please enter the value for the sum of
squares of residuals');
readln(ssr);
{calculation of confidence limits}
{for reaction rate constant k}
clrk:=2*sqrt(abs(y[1,1])*ssr/(ne-2));
{for adsorption equilibrium constant}
```

```
clak:=2*sqrt(abs(y[2,2])*ssr/(ne-2));
{output of 95% confidence limits}
writeln('the 95% confidence limits for the rate
constant are');
writeln('+/-  ',clrk);
writeln('the 95% confidence limits for the
adsorption equilibrium');
writeln('konstant are +/-  ',clak);
readln;

END. {conflim}
```